Real-time single-molecule observations of proteins at the solid-liquid interface

by

Blake Brianna Langdon

B.A. & B.S., University of Chicago, 2008

A thesis submitted to the Faculty of the Graduate School of the University of Colorado in partial fulfillment of the requirement for the degree of Doctor of Philosophy

Department of Chemical and Biological Engineering

2014

This thesis entitled:

'Real-time single-molecule observations of proteins at the solid-liquid interface'

written by Blake Brianna Langdon

has been approved for the Department of Chemical and Biological Engineering

_____

Daniel K. Schwartz

_____

Ted Randolph

Date _____

The final copy of this thesis has been examined by the signatories, and we find that both the content and the form meet acceptable presentation standards of scholarly work in the above mentioned disciple.

Abstract

Langdon, Blake Brianna (Ph.D., Department of Chemical and Biological Engineering)

Real-time single-molecule observations of proteins at the solid-liquid interface

Thesis directed by Professor Daniel K. Schwartz

Non-specific protein adsorption to solid surfaces is pervasive and observed across a broad spectrum of applications including biomaterials, separations, pharmaceuticals, and biosensing. Despite great interest in and considerable literature dedicated to the phenomena, a mechanistic understanding of this complex phenomena is lacking and remains controversial, partially due to the limits of ensemble-averaging techniques used to study it. Single-molecule tracking (SMT) methods allow us to study distinct protein dynamics (e.g. adsorption, desorption, diffusion, and intermolecular associations) on a molecule-by-molecule basis revealing the protein population and spatial heterogeneity inherent in protein interfacial behavior. By employing single-molecule total internal reflection fluorescence microscopy (SM-TIRFM), we have developed SMT methods to directly observe protein interfacial dynamics at the solid-liquid interface to build a better mechanistic understanding of protein adsorption. First, we examined the effects of surface chemistry (e.g. hydrophobicity, hydrogen-bonding capacity), temperature, and electrostatics on isolated protein desorption and interfacial diffusion for fibrinogen (Fg) and bovine serum albumin (BSA). Next, we directly and indirectly probed the effects of protein-protein interactions on interfacial desorption, diffusion, aggregation, and surface spatial heterogeneity on model and polymeric thin films.

These studies provided many useful insights into interfacial protein dynamics including the following observations. First, protein adsorption was reversible, with the majority of proteins desorbing from all surface chemistries within seconds. Isolated protein-surface interactions were relatively weak on both hydrophobic and hydrophilic surfaces (apparent desorption activation energies of only a few k_BT). However, proteins could dynamically and reversibly

associate at the interface, and these interfacial associations led to proteins remaining on the surface for longer time intervals. Surface chemistry and surface spatial heterogeneity (i.e. surface sites with different binding strengths) were shown to influence adsorption, desorption, and interfacial protein-protein associations. For example, faster protein diffusion on hydrophobic surfaces increased protein-protein associations and, at higher protein surface coverage, led to proteins remaining on hydrophobic surfaces longer than on hydrophilic surfaces. Ultimately these studies suggested that surface properties (chemistry, heterogeneity) influence not only protein-surface interactions but also interfacial mobility and protein-protein associations, implying that surfaces that better control protein adsorption can be designed by accounting for these processes.

Acknowledgements

First, I would like to acknowledge and thank the funding sources that have supported me throughout my graduate career. This has included support from the National Science Foundation Industry/University Cooperative Research Center for Membrane Science, Engineering and Technology (IIP1034720), National Institutes of Health (NIH) Pharmaceutical Biotechnology Training Fellowship, and Pall Corporation. The oral and written reporting requirements for each funding source also allowed for great collaborations and wonderful interactions with scientists from industry and fellow colleagues at CU Boulder. In particular, I greatly appreciated the interesting conversations and research discussions I had with Ajay Lajmi and Irv Joffrey of Pall Corp.

Through the NIH Pharmaceutical Biotech Training Fellowship, I was able to intern with the Medical Pharmaceutical Systems Analytical Technologies Group at Becton Dickinson (BD) in Grenoble France. I would like to thank Ted Randolph and Paolo Mangiagalli for helping set up the internship as well as Jean-Bernard Hamel, Tzvety Chevolleau, Flora Felsovalyi, Stephanie Blampignon and everyone else on the team for making it a scientifically stimulating, productive, and incredibly fun experience.

Next, I would like to thank all of the wonderful scientists and engineers I've had the pleasure of interacting with these past few years at CU. The department has provided a collaborative community that encourages discovery and great research. In particular, Dominique deVangel does an amazing job as the department's graduate advisor. The experiences and education that I have gained over the years has come from talented teachers inside and outside of the classroom, who are both passionate about their research and about helping students learn and succeed. In particular, I'd like to thank my committee members Ted Randolph, John Carpenter, Joel Kaar, Arthi Jayaraman, and Stephanie Bryant for their support, guidance, and helpful insights.

I'd also like to thank my fellow Schwartz lab members and co-adivsed members of the Kaar, Medlin, and Randolph labs, both past and present. Our group meetings, social gatherings, and everyday discussions have greatly contributed to making me a better thinker and scientist. In particular I want to thank the individuals I've worked closely, including the talented, fun, and incredibly knowledgeable post-docs Robert Walder, Indira Sriram, and Mark Kastantin (now Assistant Research Professor); fellow graduate student Josh Mabry, for many long, pleasantly distracting, helpful, and research-focusing conversations (thanks Kate Macri and Pat Noonan for jumping in too on occasion); and undergraduate student Roya Mirhossani, a very talented, compassionate, and hard-working doctor in the making.

My family and friends, both near and far, helped me keep perspective with their support. I'd like to thank the good friends I've made while in Boulder; the happy hours, barbecues, dessert competitions, outdoor adventures, and multitude of soccer games made life in Colorado splendid. I'd also like to thank the Vagt and Langdon clans for their love and encouragement. In particular, I'd like to thank my mom, dad, and sister for all of the visits, phone calls, emails, and snail mail, and for sending positive brainwaves my way over the years. This dissertation would not be possible without their encouragement. Finally, I'd like to thank my boyfriend, Jason Kephart, for making every day a lovely with his humor, fun, and companionship.

I'd finally like to thank my advisor, Dan Schwartz, for providing an incredible learning experience. Dan has indulged my many distractions from research such as getting my graduate energy certificate, participating in student clubs, and leaving for 6 months for an internship in France. These distractions positively impacted my time in grad school and broadened my perspective on my own research. I am also thankful for Dan selflessly giving his time, energy, and wisdom to my research pursuits. He has made me a more resourceful and thoughtful researcher by inspiring critical thinking, encouraging persistent problem-solving, and demanding compelling and quality work. Thank you Dan for making this dissertation possible.

Table of Contents

List of Tables

List of Figures

Chapter 1: Introduction

Non-specific protein adsorption at the solid-liquid interface is fundamental to many applications, including biocompatible materials, biosensing, pharmaceutical protein stability, and membrane filtration.[1–5] The breadth of applications for this very common but complex phenomenon has led to diverse and abundant research.[6,7] The goal of this research has been to directly relate environmental factors (e.g. surface physio-chemical properties, pH, temperature, salt concentration) to protein surface coverage and interfacial dynamic properties (e.g. desorption, adsorption, lateral diffusion, aggregation). Yet to date there remains a considerable lack of understanding about the underlying mechanisms that result in macroscopically observed protein interfacial behavior and protein layer formation.[2,8]

In many applications a full mechanistic understanding of how proteins adsorb to, change conformation or orientation on, and associate with other proteins on the surface is essential for designing and evaluating advanced, protein-compatible materials.[2,9] Chromatographic separations seek to tune the affinity of the interface to reversibly bind different protein species.[10] The efficiency of membrane filtration processes can be greatly reduced by protein adsorption that leads to pore-blocking and decreased filtration rates.[11] For many biosensors, non-specific protein adsorption to the sensor surface can obscure the desired signal from specific protein interactions.[12] For therapeutic protein products, protein-surface interactions (ubiquitous in manufacturing, storage, and handling), resulting in protein denaturation, aggregation, and particle formation, can lead to loss of drug efficacy and decreased safety.[13] Surfaces coated with extracellular matrix proteins like collagen and fibronectin, rather than other pathological proteins, can promote cell adhesion and spreading in tissue engineering applications.[14,15]

From this cursory examination of applications impacted by protein adsorption, it is clear that many different environmental factors and protein interfacial dynamics may be important in each of these systems. In the following sections I describe important factors that influence

interfacial dynamics (e.g. surface chemistry, solution conditions, protein composition, protein surface coverage), proposed mechanisms of protein adsorption, and the various microscopic processes (adsorption, desorption, diffusion, conformational changes, aggregation, etc) involved in protein interfacial dynamics. Further complicating this field, many different methods and surface sensitive techniques have been developed to study non-specific protein adsorption.[2] These techniques typically measure either the amount of protein present on the surface or protein conformations at the surface (discussed in detail below). Many of these techniques measure only the ensemble-averaged protein behavior and cannot directly capture distinct microscopic processes. Single-molecule (SM) techniques provide a more microscopic picture of protein interfacial dynamics and allow us to investigate heterogeneous protein behaviors. Some of the advantages and limitations of SM techniques are also outlined below.

1.1 Factors Influencing Protein Adsorption

Below we discuss the factors that influence interfacial protein dynamics including protein, surface, and aqueous environment properties. Importantly, the role of water should not be neglected when considering protein-surface interactions. Table 1.1 provides a useful reference for this discussion.

1.1.1 Protein Properties

Proteins are essentially complex amphiphilic polymers of varying lengths, comprised of 20 natural occurring amino acids monomeric units that vary in hydrophobicity and charge.[16] Much like languages are populated with millions of words composed of strings of letters, the diversity of proteins is vast, with each protein possessing a “unique molecular personality” and specific function.[17] Therefore, one can imagine that generalizing any particular surface behavior to all proteins (e.g. proteins stick to hydrophobic surfaces better) would be foolish. However, by considering specific protein properties (e.g. size, composition, structure, and stability) we can better understand how certain classes of proteins may behave at interfaces. For example,

protein composition (i.e. amino acids and post translation modifications) influences protein structures that range from large, rod-like proteins like fibrinogen, to Y-shaped immunoglobulin, and sphere-shaped lysozyme, each with multiple possible orientations on surfaces and in protein oligomers. In general, very stable "hard" proteins (e.g. fibrinogen, lysozyme) have been shown to be more sensitive to electrostatic driving forces (e.g. they do not adsorb to like-charged surfaces) while less stable "soft" proteins (e.g. serum albumin) adsorb to all surfaces, and are more likely to undergo conformation reorientations at the interface.[16]

The concentration of protein in solution and protein surface coverage have also been shown to influence interfacial protein dynamics both through lateral interfacial interactions and interactions in solution. For example, due to longer range protein-protein repulsions, protein layers formed at a pH far away a protein's isoelectric point (pI, pH where a protein's net charge is zero) were less dense than at the protein's pI.[18] Attractive protein-protein interactions (e.g. due to hydrophobic effects, van der Waals interactions, and hydrogen bonding) can also result in protein-protein associations and the formation of protein clusters and lead to greater protein adsorption (as described in Section 3.3).[19]

1.1.2 Surface Properties

As mentioned, the goal of many researchers studying these phenomena is to understand how surface properties (e.g. hydrophobicity, charge, and structure) influence protein adsorption and ultimately to finely control protein adsorption. Self-assembled monolayer formation and silanization of surface hydroxyl groups are popular and facile ways to modify surface chemistry by attaching the desired surface chemistries to the moiety reacting with the surface.[20] For example, in work done in our group we have extensively used silanes with hydrocarbon chains, oligoethylene glycol polymers, and amine moieties to modify bare fused silica.[21] These methods have been very effective at producing surfaces with different hydrophobicity and charge profiles and in changing how molecules interact with the surface.

Much of our understanding of how surface chemistry influences protein adsorption comes from empirical observations. For example, protein adsorption to hydrophobic surfaces is generally observed to be greater than on hydrophilic surfaces.[22] These empirical observations have led to several "rules of thumb" for designing protein resistant surfaces: surface should be (1) hydrophilic, (2) electrically neutral, (3) contain hydrogen bond acceptors, and (4) not contain hydrogen bond donors.[23] Beyond these general design principles there is little mechanistic understanding or consensus as to why we observe these behaviors.

A surface's structure and topography can also influence how proteins adsorb to surfaces, specifically how proteins orient and diffusive on surfaces. Several studies have patterned surfaces and created nanostructured materials that influenced the orientation and diffusive behavior of molecules on these interfaces.[24,25] For example, periodic diffusive steps were observed on a surface that exhibited periodic chemical patterns.[25]

1.1.3 Aqueous Properties

The vast majority of proteins have specifically evolved over millennia to be stable in water. Indeed, the spectrum of amino acid affinities for water determines the structure of a protein. Surface chemistry – of both proteins and materials – influences how water molecules interact with and order near the surface. A major driving force to protein adsorption is an entropy gain from the release of water molecules at the protein and material surface when proteins partition to the solid interface.[2,26] Therefore it is important to consider protein-water and surface-water interactions when trying to understand interfacial protein dynamics.

The composition of the aqueous solution (e.g. pH, ionic strength, and additives) also influences protein adsorption. The net charge of a protein as well as surface charge depends on the solution pH. At pH below the protein's pI the protein is positively charged while above the pI the protein is negatively charged. As discussed previously, at the pI, electrostatically repulsive protein-protein interactions are minimized, which leads to higher surface packing

densities.[18] Electrostatic forces can also be dampened at higher ionic strengths through salt charge screening. At high salt concentrations, the type of salt used can also influence the extent of protein precipitation and theoretically follows the 'Hofmeister-series'. Finally additives, such as surface-active surfactants, sugars, and urea, can influence protein stability and its propensity to partition to the surface.

Table 1.1: Factors influencing interfacial protein dynamics (adapted from Vogler)[2]

Variables	Property	Impact
Protein	Size	Larger proteins can interact with more surface area and potentially displace smaller proteins (Vroman effect)[27]
	Hydrophobicity	The content of hydrophobic amino acids on the interior and exterior of a protein can influence protein-surface interactions (e.g. protein denaturation on hydrophobic surfaces) [28]
	Charge	Protein-surface and protein-protein electrostatic attraction or repulsion can change kinetics
	Structure	Determines protein orientations and conformations at the surface as well as protein-protein association orientations
	Internal stability	Less stable "soft" proteins tend to adsorb to both hydrophilic and hydrophobic surfaces more readily than "hard" proteins[28]
	Solution concentration	Protein-protein interactions become dominant in solution and on the surface at higher concentrations[29–31]
Surface	Hydrophobicity	Influences the water structure near the surface and more hydrophobic surface may dehydrate proteins[23,32]
	Charge	Protein-surface electrostatic attraction or repulsion can increase of decrease adsorption
	Structure	Surface patterning and the conformation and density of grafted polymer brushes can influence protein adsorption and diffusion[33,34]
	Topography	Surface roughness or topographic features can influence interfacial diffusion[25]
Aqueous	pH	Surface charge and net protein charge vary with pH[35,36]
	Ionic strength	Higher ionic strength solutions can shield electrostatic interactions, particular ions can promote or reduce protein adsorption (Hofmiester series)[35,37]
	Excipients	Excipients can displace proteins from the surface (e.g. surfactants), drive proteins to the surface (e.g. sugars) or change the stability of a protein (e.g. urea, surfactants)
	Temperature	Temperature can change kinetics and non-monotonically influences water structure and the hydrophobic effect

1.2 Basic Models of Protein Monolayer Formation

The goal of this section is to outline the macroscopic approach to understanding protein monolayer formation, using a Langmuir model to demonstrate how parameters describing microscopic dynamic processes are extracted from transient and steady-state measurements of protein surface coverage. The Langmuir model has been widely criticized for deficiencies in describing protein adsorption and more complicated alternative models have been proposed that better describe experimental data.[7] However, the Langmuir model is easy to understand, with a simple mathematical form that is derived in many of the cited references, and is therefore used as a representative of the broad class of macroscopic models that make ad hoc assumptions about microscopic protein dynamics in order to predict the macroscopic behavior.

When attempting to model the macroscopic surface coverage as a function of time after exposure to protein solution of constant concentration, at minimum one must consider the possibility that proteins can adsorb to and desorb from the surface as well as the fact that an interface has a finite area available for direct protein-surface contact. If interactions between different proteins are neglected, both adsorption and desorption are generally considered to be homogeneous first-order processes, each characterized by a single rate constant. The assumption of finite surface area is important because accumulation of protein on the surface decreases the area available for subsequent protein adsorption. For modeling purposes, a reasonable ad hoc assumption is that the surface can be decomposed into a lattice of adsorption sites that are completely filled by an adsorbed protein, with no interactions between sites. With the further assumption that adsorption and desorption are not rate-limited by diffusion to and from the interface, protein surface coverage (θ) as a function of time (*t*) is given by the Langmuir model (equation 1).[38]

$$\theta(t) = \frac{c}{c + k_d/k_a}\left(1 - e^{-(k_a c + k_d)t}\right) \quad (1)$$

where c is the concentration of protein in solution and k_a and k_d are the first-order adsorption and desorption rate constants, respectively.

Qualitatively, equation 1 captures the fact that increasing protein concentration in bulk solution increases interfacial surface coverage and that the rate of net accumulation decreases as surface coverage increases. When fitting this model to experimental data to determine k_a and k_d, the steady-state surface coverage is the best indicator of the ratio k_d/k_a. While kinetic behavior at short times is most sensitive to k_a (where $\theta << 1$), in practice this value can be highly error-prone due to the fact that techniques for measuring macroscopic surface coverage are often least accurate at low surface coverage. The corresponding desorption experiment, in which a surface at steady-state coverage is exposed to a solution with $c = 0$, can be used as an independent measure of k_d. In this case, desorption kinetics are expected to follow equation 1, which is valid only if readsorption of protein to the interface can be neglected. However, in practice, even if the bulk solution is presented with a large volume per area of interface such that the average protein concentration is negligible after desorption,[39] a significant concentration boundary layer will be established that permits readsorption and alters the apparent desorption kinetics. The effect of the concentration boundary layer can be minimized using flow to remove desorbed protein. However, high shear rates at the interface invite questions whether shear is contributing to the observed desorption behavior.

Although experimental data of proteins desorbing from solid-liquid interfaces often appear to exhibit a distribution of characteristic decay constants[40–43] (i.e. are not well-described by a single exponential decay constant) the use of equation 2 is required in order to compare k_d between adsorption and desorption experiments.

$$\theta(t) = \frac{c}{c + k_d/k_a} e^{-k_d t} \qquad (2)$$

Furthermore, surface coverage in desorption experiments generally reaches a non-zero value at long times rather than decaying to zero as predicted by equation 2. This behavior indicates the

presence of an irreversibly bound fraction. For modeling within the Langmuir framework, however, an ad hoc correction can be made by adding a constant to equation 2 to represent the irreversible population.

The final step in the macroscopic approach is to vary environmental factors in order to determine their effects on the adsorption and desorption rates. For example, variation of k_a with temperature would yield an apparent activation energy barrier for adsorption (i.e. an Arrhenius analysis) that could be compared to predictions based on different intermolecular forces between protein and surface. It should be noted that, strictly speaking, an Arrhenius analysis is only correctly applied to parameters derived from the Langmuir model described above. Whereas both the Langmuir and Arrhenius models assume that desorption is an elementary process, characterized by a single energy barrier, many variants on the Langmuir model assume a distribution of energy barriers. A distribution of energy barriers would create a distribution of rate constants, each with different temperature-dependent behavior. Although this situation is not accounted for in the Arrhenius model of rate constants, the Arrhenius model is still used to interpret non-elementary protein adsorption kinetics.

The steady-state form of equation 1, $\theta(c) = c/(c + k_d/k_a)$, is often called the Langmuir isotherm. Although the Langmuir isotherm predicts that $\theta \rightarrow 1$ for $c >> k_d/k_a$, it is often observed that $\theta(c)$ levels off at values significantly less than unity at high c. This phenomenon can be explained by a random sequential adsorption model (RSA), which does not assume regularly-spaced adsorption sites.[44–47] Rather, adsorption occurs at random (i.e. off-lattice in the context of the Langmuir model) locations on the surface, leaving gaps between neighboring proteins that are too small to permit adsorption of a new protein. The maximum surface coverage in the RSA, often called the 'jamming' limit, depends on the assumed geometric footprint of the protein, with 2D circles or squares both expected to reach maximum area coverage between 0.54-0.56.[48] However, protein mobility, specifically desorption and diffusion, would allow molecular rearrangements that eventually lead to a close-packed state with significantly higher

surface coverage (e.g. 2D close packed circles yield θ ≈ 0.91, squares yield θ = 1). In practice, maximum surface coverage often falls somewhere between the close-packed and jamming limits.[49] Perhaps more importantly, the neglect of desorption in the RSA model leads to significantly different kinetic predictions than the Langmuir model. In previous work we have demonstrated that both desorption and interfacial diffusion play an important role in protein layer formation.[50,24] Consequently, the kinetic behavior predicted by RSA is almost certianly wrong despite the fact that it partially explains the observation of a steady-state surface coverage below that of a close-packed monolayer. In practice, it is common to include the idea of imperfect packing into the Langmuir model by multiplying equation 1 by a constant, θ_{max}, such that

$$\theta(t) = \theta_{max} \frac{c}{c+k_d/k_a}\left(1 - e^{-(k_a c + k_d)t}\right) \quad (3)$$

An ad hoc rationale for this additional parameter involves the notion that even in mobile systems, an object may exclude an interfacial area (due to molecular motions or repulsive enthalpic pairwise interactions) greater than its physical size. An important consequence of introducing a third parameter into equation 3 is that the determination of k_d/k_a is made with greater uncertainty and it becomes more important to determine k_d independently, as described above. Alternatively, coarse-grained structural models have led to statistical-thermodynamic theories that can provide semi-quantitative predictions of excluded volume effects and place reasonable bounds on θ_{max}.[51]

The Langmuir and RSA models are not the only available descriptions of protein adsorption. For example, the Temkin[52] and Elovich[53] models postulate that the surface contains different types of sites for possible adsorption, with a uniform distribution of site-protein binding energies. Proteins first adsorb to sites that are most strongly binding, followed by subsequent adsorption to weaker sites. The macroscopic net adsorption rate appears to decrease over time because proteins are forced to find progressively weaker adsorption sites. This model was a

better description of histidine-containing proteins onto copper-chelating surfaces than the Langmuir isotherm.[54] In contrast, the Langmuir−Freundlich[55] and Tóth[56] models assume a Gaussian-shaped distribution of binding energies. Still other models assume the presence of discrete 'states', which may arise from different protein orientations or conformations, and allow for interconversion between these states on the surface.[57,58] There are many such alternative ad hoc models that have advantages in describing specific subsets of protein-surface combinations and have been reviewed elsewhere.[7] Like the Langmuir model, their common characteristic is that they all seek to extract unknown parameters, representing unobservable microscopic protein behavior, from the macroscopically observable surface coverage. Thus, given just the one observable property of surface coverage, a many-parameter model would risk over-fitting the data, and certainly it is very difficult to claim that a given model provides a unique description of the data, compared to the vast number of alternative models.

1.3 Protein Dynamics

Numerous experimental studies highlight the fact that interfacial protein behavior is both more dynamic and more complex than assumed in models described in the previous section. This section will review some of this work and discuss its implications in the context of protein layer formation.

1.3.1 Adsorption and Desorption

Even at the macroscopic level, both adsorption and desorption are readily apparent using surface plasmon resonance,[59,60] optical waveguide lightmode spectroscopy,[61,62] quartz crystal microbalance,[62–64] ellipsometry,[62,65] and total internal reflection fluorescence (TIRF) spectroscopy (discussed further in Section 4.1).[58] However, new perspectives on these processes have been provided by single-molecule tracking (SMT) experiments that are based on TIRF microscopy.[66,67] In SMT, fluorescently-labeled proteins are observed, one-by-one, to adsorb, diffuse in the interfacial plane, and desorb. The time between adsorption and desorption

is a direct measure of a protein's surface residence time, and large numbers of these observations can be used to construct a probability distribution of surface residence times.

In one set of SMT studies, Yeung and co-workers analyzed total BSA coverage as a function of time with a Langmuir model and found apparent desorption rate constants between 10^{-3}-10^{-2} s^{-1}.[68,69] In contrast, apparent desorption rate constants extracted from macroscopic measurements varied between 10^{-7}-10^{-2} s^{-1} on different hydrophilic and hydrophobic surfaces for these same proteins.[70] It is clear that desorption appears many orders of magnitude faster when observed at the single-molecule level than at the macroscopic level. Because SMT is a direct measurement of the elementary process of desorption, it must be concluded that the apparent, macroscopic desorption rate represents contributions from multiple desorption pathways that are characterized by different rate constants. Thus, it seems reasonable to conclude that there is a significant population of adsorbed protein that is in rapid dynamic equilibrium with the bulk solution as well as a population with much slower dynamic behavior. In fact, multiple populations are often observed in SMT experiments on proteins, peptides, and DNA, and the shorter-lived populations are generally found to represent a much greater fraction of the full ensemble.[66,68,71–73]

1.3.2 Diffusion

Diffusion is often neglected in models of protein dynamics at solid-liquid interfaces. This choice can be rationalized in terms of the Stokes-Einstein relationship for the diffusion coefficient (*D*) of a disk straddling an interface:

$$D = 3k_BT/[16R(\eta_1 + \eta_2)] \quad (4)$$

Here, k_B is the Boltzmann constant, T is absolute temperature, R is the disk radius and η_1 and η_2 are the viscosities of the media on the different sides of the interface. As the interface in contact with water becomes more viscous, D should decrease and a solid interface, with infinite viscosity, will have D=0. However, Sriram et al. found that D deviates from predictions of

equation 4 at high viscosities of the non-aqueous phase.[74] Physically, this is because protein mobility is no longer dominated by Brownian motion but instead is believed to move through a series of partial or complete detachments from the solid surface that permit lateral translation.[75] In this case, diffusion behavior is not governed by hydrodynamic effects but rather by energetics of interfacial interactions that determine the rate of detachment.

Macroscopic measurements of interfacial diffusion coefficients, using fluorescence recovery after photobleaching (FRAP)[76] illustrate why it is tempting to neglect diffusion at the solid-liquid interface. These measurements show that protein diffusion coefficients at air-water interfaces ($D \sim 10^1$-10^2 $\mu m^2/s$),[77] or on model lipid bilayers in aqueous media ($D \sim 10^0$-10^1 $\mu m^2/s$)[78] are much larger than at solid-liquid interfaces ($D \sim 10^{-3}$-10^{-2} $\mu m^2/s$).[79] Importantly, however, interfacial diffusion at solid-liquid interfaces is non-zero. Therefore, in the context of protein layer formation, interfacial diffusion is expected to facilitate protein-protein interactions and the significance of interfacial diffusion will depend on the average separation between proteins.

1.3.3 The Role of Protein-Protein Interactions and Surface Relaxation in Long-Lived Species

Macroscopic studies of protein adsorption commonly observe a fraction of molecules that appear 'irreversibly' bound whereby excessive rinsing of the surface simply does not remove all protein from the interface.[80,81] However, there is still a question of whether adsorption is truly irreversible (i.e. leading to non-equilibrium behavior) or whether this population simply has a characteristic timescale for desorption that is much longer than the experimental observation.[58,82,83] Although for most practical purposes the distinction is inconsequential, as will be discussed below, it is possible that protein denaturation and/or clustering phenomena may be responsible for long-lived protein species. Desorption of denatured protein in monomeric or cluster form could nucleate denaturation and/or aggregation of proteins in solution.[5,84] For

convenience, this work will hereafter refer to this phenomenon as irreversible adsorption with the understanding that this may not strictly be true.

Mechanistically, irreversible binding is often attributed to interfacial 'relaxation', which is a general term that may include protein unfolding and/or reorientation of protein relative to the interface. There is ample experimental evidence that the *average* structure of an adsorbed protein population often becomes increasingly denatured over time.[85,86] Hydrophobic interactions are generally believed to drive interfacial denaturation, as the Gibbs free energy of unfolding is often related to the ability of an unfolded protein to sequester hydrophobic amino acid side chains away from contact with water.[87,88] However, hydrophobically-driven denaturation is not always the dominant factor, as Baugh et al. observed a greater degree of spreading of fibronectin (Fn) on hydrophilic, as opposed to hydrophobic, surfaces.[89] In this case, the 'spread' Fn conformation was better able to support cell adhesion and growth, presumably because this conformation presented important peptide sequences in the proper orientation for recognition by integrins on the cell surface. Other studies have also noted an increase in the size of the protein footprint after adsorption,[90,91] which may correlate with changes in protein conformation but may also be due to conversion between end-on and side-on configurations in macromolecules with high aspect ratios.[92] The consequence of protein spreading is that total surface coverage at apparent saturation often depends on the rate of adsorption relative to spreading; slower adsorption allows more time for spreading, which decreases the available area for subsequent adsorption.

There is increasing evidence from experiment, simulation, and theory that protein-protein attractions are important and may also explain irreversible binding behavior. Atomic force, electron, and fluorescence microscopy have been able to visualize cluster formation in different proteins at solid interfaces[81,93–96] while simulations[97,16] and theory[96,19,98] highlight that attractive interactions between proteins, combined with interfacial diffusion and/or the ability of a protein to adsorb directly into a cluster, are responsible for the appearance of clusters. Although a

repulsive component of a protein-protein interaction is expected from the steric interactions combined with the fact that proteins often carry net charges of the same sign, a low Debye length in physiological environments can screen electrostatic repulsion and allow attractive interactions to overcome steric repulsion. Protein-protein attractions may stem from a combination of van der Waals, hydrogen bonding, and hydrophobic interactions between amino acid side chains as well as the peptide backbones of separate proteins. Additionally, the local distribution of positively and negatively charged amino acids may cause strong attraction despite the fact that the net protein charge would suggest repulsion. In addition, strong protein-protein attractions may be inherent in the structure of the protein, as is the case for proteins that form ordered, stable networks (i.e. S-layers) on solid or lipid-coated surfaces and are of increasing interest in nanotechnology applications.[99]

We expect that surfaces that promote more frequent protein-protein interactions to lead to clustering and potentially more irreversibly bound protein (Figure 1.1A, B). More frequent protein-protein collisions result both from faster interfacial diffusion and from slower desorption and/or faster adsorption of irreversibly bound protein that increases the transient surface coverage. Perhaps less appreciated is the potential for the surface to influence the 'productivity' of protein-protein collisions (Figure 1.1C, D). In other words, the collision between two proteins may be more likely to result in a long-lasting association on one surface relative to another. For example, nanostructured polymer surfaces with anisotropic nanoscale topography[100] are believed to pre-orient Fg monomers and promote the formation of stable clusters.[24] Another mechanistic hypothesis is that surface interactions may 'soften' protein structure without completely denaturing the protein, thereby increasing the propensity for hydrophobically-driven aggregation.

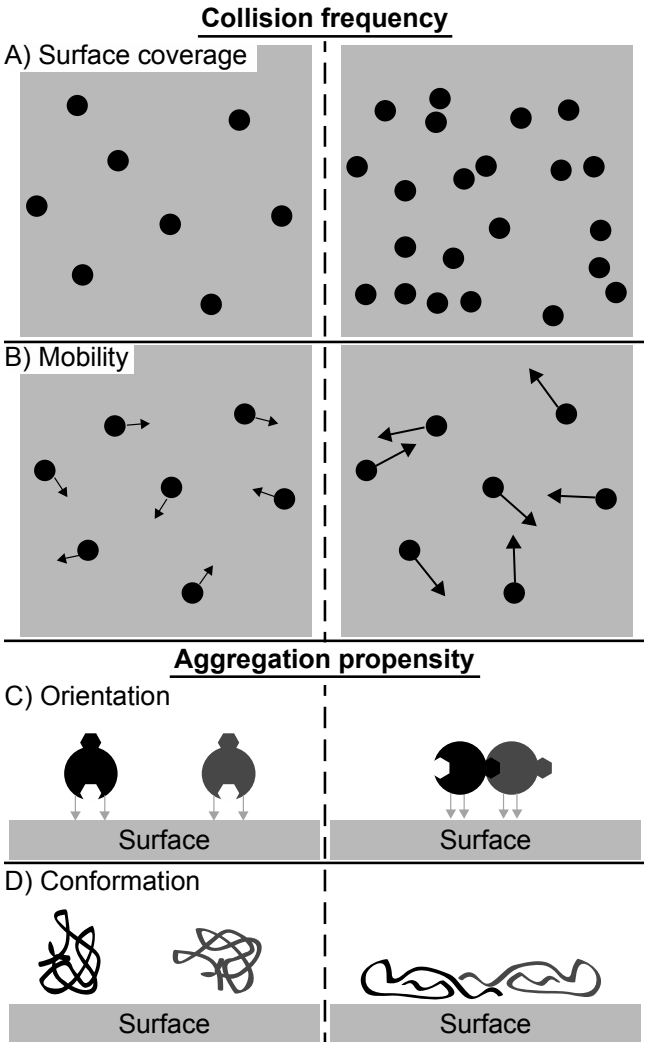

Figure 1.1: Indirect effects of environmental conditions on protein-protein interactions. In each example, protein-protein interactions are more important in the scenario shown to the right of the dashed line. The environment can increase the frequency of protein-protein interactions by higher surface coverage due to faster adsorption and/or slower desorption (A) or faster diffusion caused by smaller corrugations in the surface interaction potential (B). The tendency of a protein-protein interaction to result in aggregation can depend on orientation bias due to anisotropic protein-surface interactions (C) or protein denaturation due to strong protein-surface interactions (D).[9]

1.4. Techniques for Studying Protein Adsorption

Because protein adsorption to surfaces is such a common phenomenon with many applications, it has been studied using a variety of techniques. These techniques historically have measured macroscopic, ensemble-averaged properties of protein surface phenomena. As discussed in Section 2, many mechanistic, top-down models have been proposed based on these macroscopic measurements, relying mainly on measuring the amount of protein adsorbed with time. These techniques have provided valuable, but often highly empirical, observations and insights. They have also led to a large and conflicting body of literature on protein interfacial phenomena.[2] More recently, microscopic, SM techniques (as well as molecular dynamics simulations) have helped provide information that is obscured by macroscopic measurements involving a large number molecules, such as rare but significant protein interfacial behaviors. Below I discuss some of the macroscopic techniques widely used in literature (summarized in Table 1.2). I then discuss the advantages of and challenges with microscopic SM fluorescence techniques used in this work.

1.4.1 Macroscopic Surface Techniques

In general, ensemble-averaged, macroscopic techniques provide information about either (1) the amount of protein at an interface or (2) the conformation of protein at the interface.[1] Table 1.2 details some of the most commonly used macroscopic techniques for studying protein adsorption. Techniques that measure protein conformational changes are often used to further investigate adsorbed protein layers and connect surface coverage measurements with conformational changes. For example, Sethuraman and coworkers found that the extent of slow, surface-induced conformational changes of lysozyme were considerably reduced when higher protein concentrations were present in solution and at the interface.[101,102]

Table 1.2: Protein adsorption surface-sensitive techniques (adapted from Nakanishi et al.)[1]

Technique	Measures	Principle	References
Depletion	Amount of protein adsorbed	The amount of protein remaining in solution after incubation with a surface with UV absorbance	106,31
Surface plasmon resonance (SPR)	*in situ* amount of protein adsorbed	Change in surface plasmon resonance reflectivity, excited by an evanescent wave and sensitive to near surface environment	59,60,80,107
Optical waveguide lightmode spectroscopy (OWLS)	*in situ* amount of protein adsorbed	Changes in constructive interference angle in waveguide due to protein adsorption	61,62
Quartz crystal microbalance (QCM) with dissipation (QCM-D)	*in situ* amount of protein adsorbed, viscoelastic properties of the layer	Change in oscillating frequency of piezoelectric device upon adsorption	62,63,85,108, 109
Ellipsometry	Amount or thickness of protein adsorbed	change in state of polarized light upon reflection due to protein adsorption	62,65
Total internal reflection fluorescence (TIRF) spectroscopy	*in situ* amount of protein adsorbed, conformation of adsorbed protein	Change in fluorescence at the interface by exciting fluorescent moieties (fluorophores or amino acid side chains) with an evanescent field	58,110
Circular dichroism (CD)	Conformation of adsorbed protein	Change in ellipticity and adsorbance of light due to protein secondary structure	30,111
Fourier transform infrared spectroscopy (FTIR)	Conformation of adsorbed protein	Change in infrared adsorption spectrum of protein on adsorption, sensitive to secondary structure	86,112
Atomic force microscopy (AFM)	Surface and adsorbed protein topography, protein-surface adhesion forces	Measures interactions between surface and scanniny probe, records surface forces	97,107,113,114

Some of the techniques are limited to *ex situ* application (i.e. often requiring rinsing and/or drying before analysis). Such techniques are often more flexible in the types of surface-solution systems examined. For example, depletion techniques, where the amount of protein remaining in solution after incubation with a surface is quantified, can be applied to many different surface geometries including filtration membranes and curved vials.[103,104] However sample preparation for such techniques can often damage adsorbed proteins (especially drying) and often do not capture reversibly adsorbed proteins that are removed in rinsing steps.[2] This makes it challenging to compare results from such experiments, where generally only strongly-

bound protein remains, to measurements of the amount of protein adsorbed made in real time by *in situ* techniques.

Techniques such as surface plasmon resonance and quartz crystal microbalance can capture both weakly and strongly bound protein species, as confirmed by solution exchanges.[105] Such techniques have been used to measure net protein adsorption and desorption rates (usually on the order of minutes to hours).[70] However, by measuring only mean behaviors and *net* rates such techniques cannot resolve the dynamic exchange of proteins at the interface (e.g. adsorption and desorption rates, as discussed in Section 3.1) and heterogeneous protein behavior due to surface spatial and protein population heterogeneity. Microscopic techniques, such as SM fluorescence techniques, overcome some of these limitations.

1.4.2 Single-Molecule Fluorescence Techniques

SM fluorescence techniques and applications have exploded in the last two decade as instruments have become more sophisticated (e.g. CCD cameras can now detect fewer photons and faster, laser pulse speed and intensity increased, more stable fluorophores are available, more sophisticated SMT programs have been developed).[115,116] Such advances and wider application of SM techniques resulted in the 2014 Nobel Prize in chemistry being awarded for the development of super-resolution fluorescence microscopy.[117–122] It has particularly found great acceptance in biological systems[123] where it has been used to determine mechanistic information about protein folding dynamics[124,125], enzyme conformation changes[126], peptide aggregation[127], vesicle fusion[128], DNA-protein specific binding[129]. It has also been used to elucidate fundamental interfacial dynamics such as diffusion[130–136] and adsorption.[137–139]

One of the major advantages of SM techniques is the ability observe the variations, or heterogeneity, of molecular behavior that is often lost in ensemble-averaging techniques.[140] By recording the interfacial properties of a single object's trajectory – time of adsorption, amount of time at the interface, spatial positions, and fluorescent intensity and color – one can correlate

these properties on a molecule by molecule bases. For example, SM observations of proteins at the oil-water and solid-water interface identified multiple protein populations (e.g. monomer, dimer, and trimer) using fluorescent intensity and surface residence time.[68,69,73] At the oil-water interface, Walder and co-workers observed that larger protein oligomers (dimers and trimers) could switch between two modes of interfacial diffusion over the course of their surface trajectory.[73] By accumulating molecular dynamic information of many molecules at the same position, we can also "map" surfaces using dynamic properties. For example, Mabry et al. identified adsorption "hot spots" (i.e. discrete surface sites were more molecules adsorbed to and resided longer on) at aqueous – trimethylsilane-modified interfaces.[141] Therefore, SM techniques are a powerful tool for elucidating population, dynamic, and spatial heterogeneity.

A second advantage of SM techniques is their ability to separate elementary mechanistic steps. In the case of interfacial protein dynamics this can simply mean measuring adsorption and desorption separately, rather than a net adsorption or desorption rate captured by ensemble-averaging techniques (further discussed in Section 3.1). For example, SM studies of diffusion at the solid-liquid interface suggest that, unlike random walk diffusion in solution, surface mobility proceeds through intermittent hopping.[131,132] More fundamentally, SM studies reveal that molecules at surfaces desorb and readsorb to the surface much more frequently than had been previously captured with macroscopic techniques.[68,69]

In the work described in this dissertation, SM total internal reflections fluorescent microscopy (TIRFM) was used to observe fluorescently-labeled proteins at the solid-liquid interface. Below I describe TIRFM, resonance energy transfer (RET), and fluorescence considerations relevant in this work.

1.4.2.1 Total Internal Reflection Fluorescence Microscopy (TIRFM)

Schematically depicted in Figure 1.2, TIRFM can be used to observe fluorescently labeled molecules at solid-liquid or liquid-liquid interfaces. The technique takes advantage of

Snell's law and the optical phenomenon of total internal reflection which occurs when light waves (in this case a light wave at a specific wavelength, created by a laser) propagating through a medium (e.g. glass) is incident at an interface with another medium that has a lower refractive index (e.g. water), above some critical angle such that the light is total internally reflected.[142,143] At this interface, an evanescent wave is created in the second medium exciting fluorophores very near this interface. The intensity of the evanescent wave decays exponentially with distance from the interface, as a function of the angle of incidence and light wavelength. In our experimental setup this evanescent wave can excite fluorophore up to 100 nm away from the interface. Therefore, fluorophores in the bulk solution at further distance from the interface are not excited, greatly reducing the background that is present in other fluorescent microscopy techniques such as wide-field epi-fluorescence. Further theoretical and technical aspects have been widely reviewed[144], for example by Wazawa and Ueda and references within.[142] TIRFM's reduction in background and surface sensitivity makes it an ideal technique for observing single molecules with fluorescent labels at the solid-liquid interface.

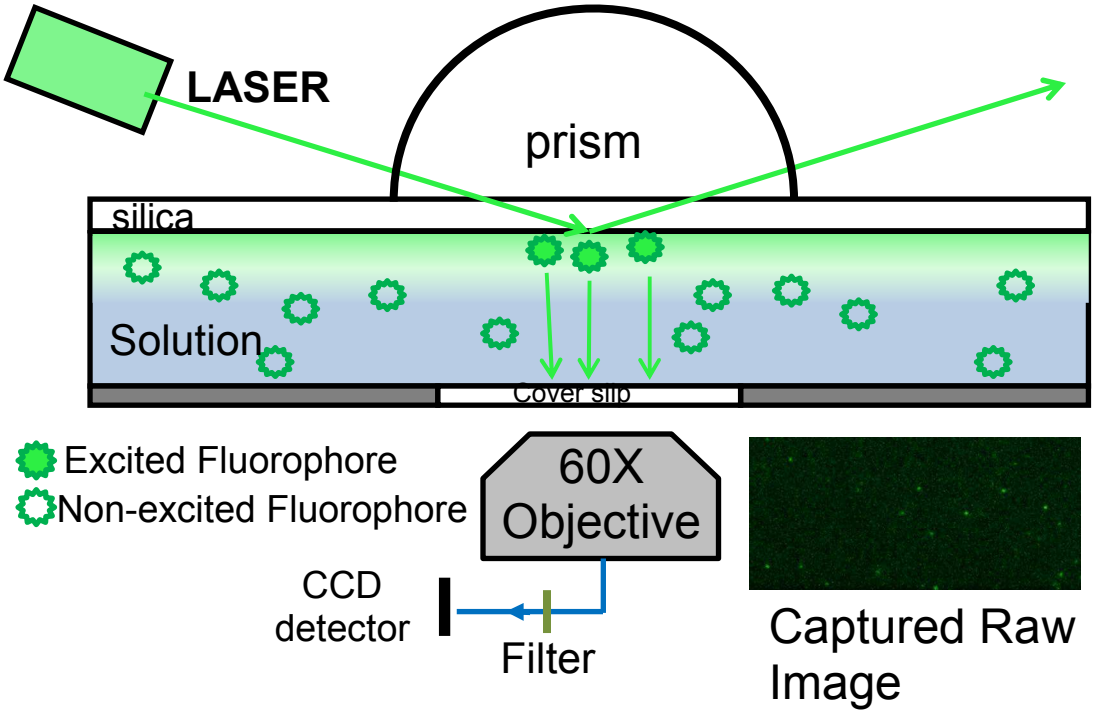

Figure 1.2: Prism-based TIRFM setup.

1.4.2.2 Fluorescence

Fluorescence occurs when photons are emitted from a substance due to the relaxation of excited electrons to ground states. This is shown schematically by in Figure 1.3A with a Jablonski diagram. An electron in the ground state (S_0) can be excited to an excited state (first ground states shown, S_1) by light irradiation (hv_A) with energy greater than the difference in energy between S_0 and S_1 ($hv_A > hv_F$). At each of these electronic states (e.g. S_0, S_1, S_2) the electron can exist in several vibration states, shown as the light gray lines; electrons populate the lowest vibration state via internal conversion following adsorption of hv_A. From the lowest vibrational state excited electron can either undergo:

1. Fluorescence: relaxation to ground state and emission of light (hv_F),
2. Intersystem crossing: transition to a triplet state and ultimately relaxation to ground state (not shown here, results in phosphorescence),
3. Quenching: non-radiative loss of energy, often due to collisions with certain solution species (Q, e.g. oxygen, halogens, and amines), or
4. Resonance energy transfer (RET or FRET): non-radiative 'donation' of energy to an 'acceptor' fluorescent molecule, which results in the acceptor molecule's fluorescence (hv_{acc}).

The process of fluorescence is characterized by several phenomena. Because fluorescence typically occurs from the lowest excited vibrational state, photon emission occurs at lower energies or longer wavelengths than those used for excitation. This phenomenon is known as the Stokes shift, demonstrated by the offset of the excitation and emission spectra of Alexa Fluor 555 shown in Figure 1.3B. The emission spectrum (filled in dark green) is generally independent of the wavelength used for excitation due to the fast transition to the lowest vibrational state in the excited electronic state. A given fluorophore can be further characterized by its fluorescence lifetime and quantum yield. The fluorescence lifetime is the average time a molecule spends in the excited state prior to relaxation and is generally on the time scale of 10

ns. A continuous fluorescent signal is the result of millions of fluorescent events per second. A fluorophore's quantum yield represents the number of photons emitted (rather than energy losses due to non-radiative processes) to the number of photons adsorbed and is always less than one. Generally speaking, molecules with higher quantum yields make better fluorescent dyes.

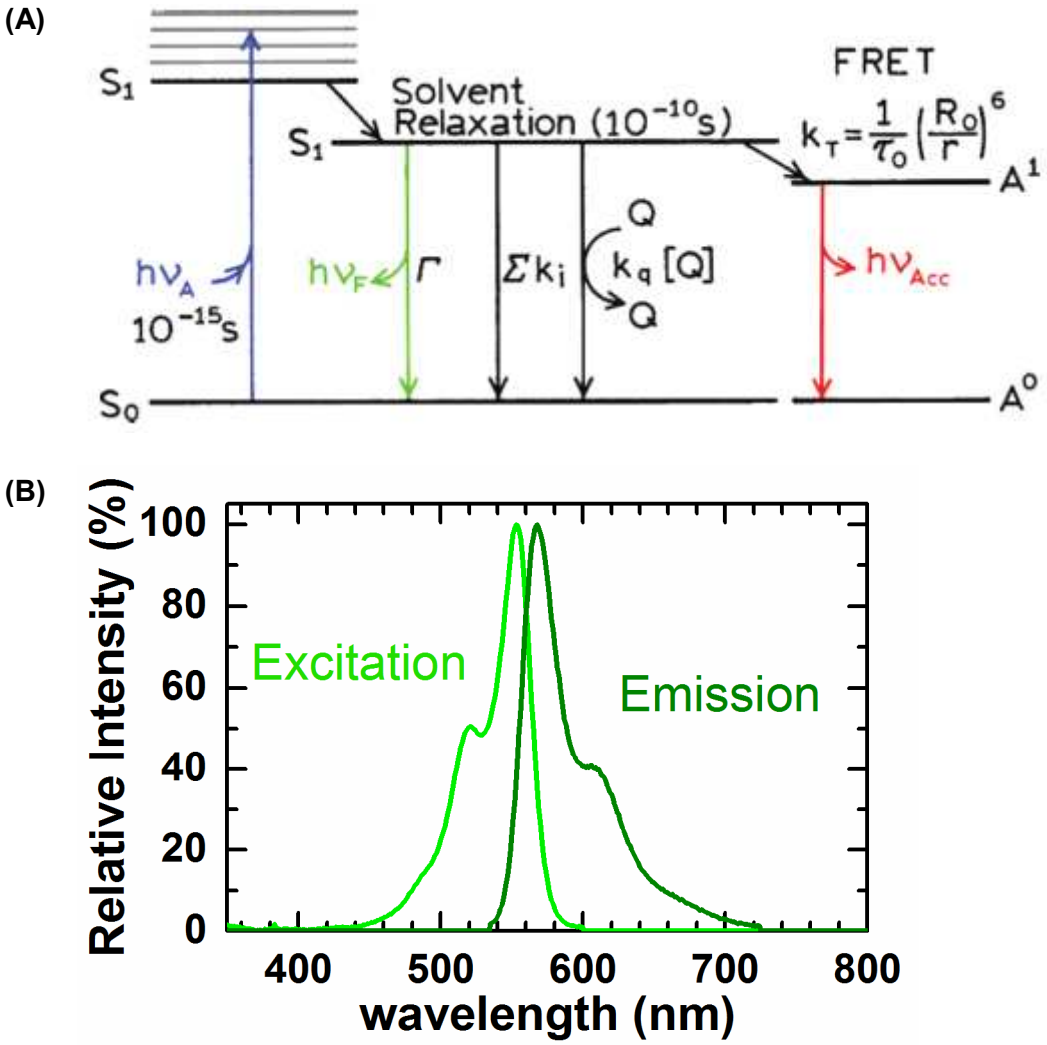

Figure 1.3: (A) Jablonski diagram with collisional quenching and fluorescence resonance energy transfer (RET). The summation term represents non-radiative paths to the ground state other than quenching and RET (from Lakowicz).[145] (B) Excitation and emission spectra of Alexa Fluor 555.

Intersystem crossing, while a much rarer process and molecule dependent, can have serious negative consequence in the resulting fluorescence signal including photobleaching and photoblinking. Photoblinking processes – dark state periods, frequently due to triplet states with lifetimes of microseconds to milliseconds up to seconds – can result in temporal fluctuations of the fluorescence intensity.[146] In SMT experiments, photoblinking can lead to object identification losses and shortened trajectories.[147] When employing RET systems, it can also result in erroneous RET efficiency calculations and incorrect RET state identification.[148] Photobleaching is an irreversible process whereby fluorescence is inactivated due to chemical damage or other chemical reactions, caused by from photon-excitation and long-lived excited triplet states.[149] Photobleaching reduces our ability to observe slow interfacial processes and accurately measure residence times of long-lived surface species. Photoblinking and photobleaching processes can be mitigated by using more photo-stable dyes (e.g. quantum dots, Alexa Fluors, etc.), labeling molecules of interest with multiple labels when possible, reducing excitation power (often at the expense of temporal resolution), and adding triplet state quenchers to solution.[150,151] Also, several post-experiment processing methods can be employed to connect trajectories where photoblinking occurs mid-trajectory (e.g. two maximum likelihood estimation).[147,148]

Quenching broadly describes any process by which fluorescent intensity is decreased and can occur by many different mechanisms. One potential mechanism, shown in Figure 1.3A, is collisional quenching where a fluorophore returns to the ground state simply by colliding with a quencher molecule, without undergoing any chemical reaction. Similar strategies to those used to reduce photoblinking and photobleaching can also be employed to reduce quenching (e.g. adding antioxidants, oxygen scavenging systems to solution).[150]

In RET, or Förster resonance energy transfer (FRET), a fluorophore that fluoresces at a low wavelength (e.g. 488, 532) is directly excited and can non-fluorescently transfer energy to the ground state of a fluorophore which fluoresces at a higher wavelength (e.g. 594, 647). RET

is schematically shown in Figure 1.4A. This energy transfer results in reduced fluorescence of the low wavelength fluorophore, referred to as the donor, and fluorescence of the high wavelength fluorophore, referred to as the acceptor.[152] Importantly, acceptors only significantly fluoresce in the presence of a donor and this energy transfer is distance dependent.

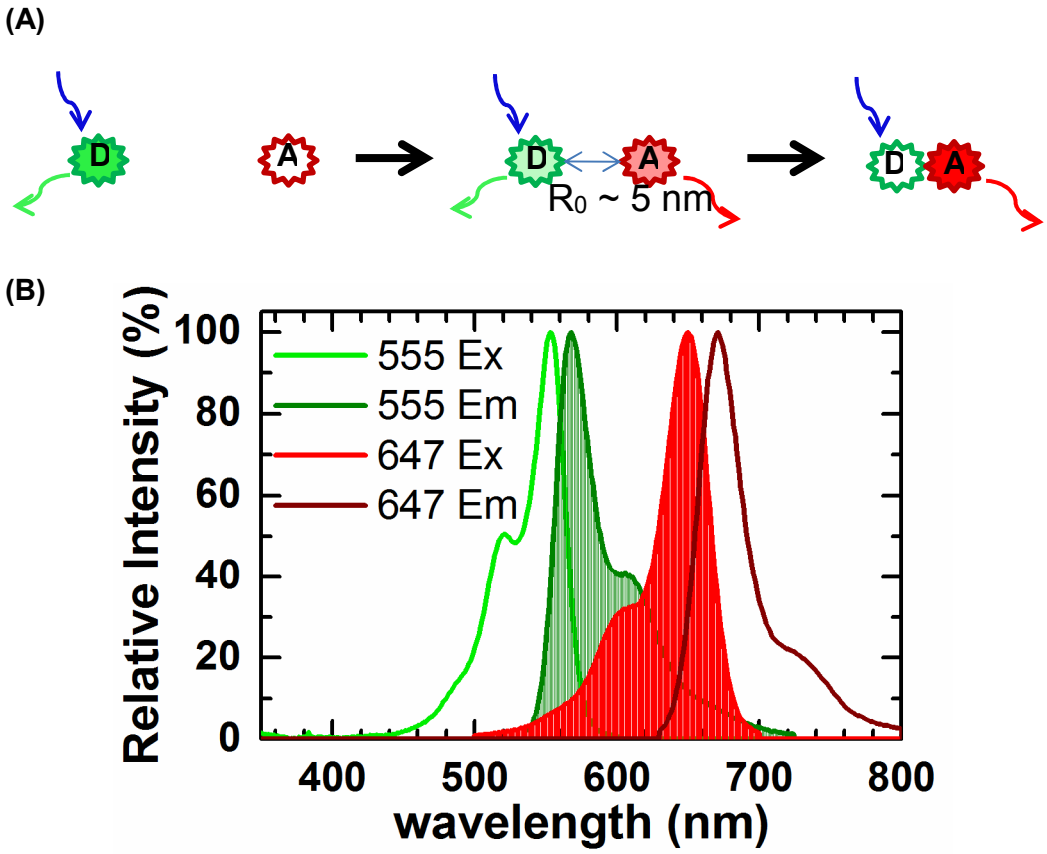

Figure 1.4: (A) Schematic of resonance energy transfer between a donor fluorophore *D* and acceptor fluorophore *A* as a function of distance. 50% RET efficiency is achieved around 5 nm for most *D-A* pairs. (B) Excitation and emission spectra of Alexa fluor 555 (green) and Alexa fluor 647 (red). The filled spectra help illustrate the spectral overlap between donor emission (dark green) and acceptor excitation (red), which ultimately determines the Förster radius.

The energy transfer from donor to acceptor depends on the overlap of the donor emission spectra and the acceptor adsorption spectra, the quantum yield of the donor, and the distance and orientation between fluorophores. For a given donor-acceptor pair, the distance at which RET is 50% efficient, called the Förster distance, R_0, depends primarily on the spectral properties of the fluorophores (e.g. spectra overlap and quantum yield) and typically ranges

from 2-9 nm, as shown in Figure 1.4B. RET depends strongly on distance and is proportional to the distance, r, between fluorophores to the one sixth, $F_D/F_A \sim r^6$, where F_A and F_D are acceptor and donor fluorescent intensity, respectively.

RET is a powerful "spectroscopic ruler" for understanding protein-protein associations[153], conformational changes[126,154,155], and specific protein-molecule interactions.[156] While TIRFM is limited to a spatial resolution of ~50 nm, RET allows us to visualize molecular interactions on the nanometer scale.

1.4.2.3 Labeling Proteins with Fluorescent Molecules

There are many ways to attach a fluorophores to proteins including natural amino acid amine, thiol, and carbohydrate covalent binding chemistries and non-native click chemistries. In labeling proteins, amine conjugation chemistries are most commonly used due to their simplicity, low cost, and ability to reach high dye/protein ratios due to the relative abundance of amine moieties on proteins.[157] In this chemistry scheme protein side chains containing amine moieties (e.g. lysine, arginine, and histidine) as well as the amine terminus (N-terminus) of a protein can react with a fluorescent molecule containing a succinimidyl ester. Due to their hydrophilicity, these groups are usually abundantly present on the outer surface of a protein (e.g. BSA has up to 20 lysine residues present on its surface). This conjugation reaction proceeds at room temperature in an aqueous solution at pH 9. This method is nonspecific and stochastic with each protein being labeled at different amine moieties present on a protein and on average at a dye to protein ratio that can be measured with variance of the square-root of the dye to molecule ratio (i.e. follows Poisson statistics).

There are several advantages and considerations to labeling protein with fluorophores. Obviously fluorescently labeled proteins allow us to monitor protein dynamics at the single-molecule level with high signal to noise ratios with existing technology. In addition, a high dye to molecule ratio (greater than one) can enhance a single molecule's fluorescent signal and

reduces the effects of photoblinking and photobleaching (discussed in Section 4.2.2). However multiple dyes per molecule can result in dye self-quenching. This is especially a problem for fluorescein.[158,159] However Alexa Fluor dyes – used extensively here – are less prone to self-quenching. The nonspecific nature of amine labeling has the potential to effect a protein's interactions with other molecules (e.g. dimerization), its activity (in the case of enzymes), or propensity to specifically bind (in the case of antibodies). Therefore this type of labeling becomes most important when studying specific protein interactions or events and can be quantified by enzyme activity assays or binding assays. In the case of nonspecific interactions – which we are concerned with here – one can compare the behavior of unlabeled protein to that of fluorescently labeled protein. For example, a protein's propensity to aggregate can be measured via size exclusion chromatography or analytical ultracentrifugation and a protein's partitioning to an interface can be measured by surface sensitive techniques and different ratios of labeled to unlabeled protein can be compared. In preliminary studies, we compared the residence times on a hydrophobic surface of BSA labeled with different fluorophores (Alexa fluor 555, 488, or 647) and saw no difference in residence times suggesting at least that the identity of the fluorophore does not significantly change BSA-surface interactions.

In many cases commonly used proteins (e.g. fibrinogen, serum albumin, and secondary antibodies used in many microbiology techniques) can be purchased with multiple covalently-linked fluorescent labels (3-15 dyes/molecule). Proteins unique to a particular experiment can also be labeled efficiently and easily using amine conjugation. Alexa Fluor labeled proteins were extensively used in this work.

1.5 The Ability of Single-Molecule Tracking to Resolve Microscopic Protein Dynamics

In recent years, SMT measurements have been increasingly used to observe microscopic interfacial protein dynamics. Below we will discuss the strengths and limitations of the technique for providing mechanistic information.

1) Sample size has long been a concern in SMT, as each molecule must be observed and tracked separately from all others; this can require significant computational effort. Recent advances in high throughput tracking methods have increased typical sample sizes by several orders of magnitude to 10^4-10^6 molecular trajectories, allowing relatively rare behaviors to be characterized with statistical significance.[160] However, even a sample size of 10^6 is still several orders of magnitude below the number of molecules that contribute to macroscopic measurements, making it inevitable that SMT will neglect some rare behaviors. Neglected rare events may or may not be important to the system in question, but this bias should be considered in conclusions drawn from SMT experiments.

2) A common expectation of SMT is that, because the point spread functions of fluorescent objects may not overlap, these experiments are done at ultralow surface coverage such that results are not applicable to higher coverage. While it is true that most SMT experiments are done at low surface coverage, arbitrarily high surface coverage may be studied so long as the surface density of fluorescently labeled objects is low.[24,161] In other words, objects tracked in SMT can be used as representative probes of their local environment.

3) It is now relatively straightforward to use SMT to make direct observations of heterogeneous behavior in diffusion or desorption processes. However, artifacts in these data can result from finite temporal and spatial resolution. Temporally, SMT will neglect processes

with characteristic time scales much faster than the minimum required time to observe interfacial positions. Very slow processes, on the other hand, may either exceed the practically observable time window and be neglected or may be very rare, as discussed above. Regarding diffusion, uncertainty in determining instantaneous object position, due both to motion blur and to noise in signal collection, leads to apparent diffusion that is faster than the true diffusion.[162] While this effect becomes increasingly important at higher temporal resolution, data analysis methods have been proposed to extract the true diffusive behavior.[163] The significance of the artifacts discussed above should be considered on a case-by-case basis when drawing conclusions from SMT data.

4) Quantifying adsorption at the molecular level is not as straightforward as it is for desorption, which is characterized by a surface residence time distribution. For adsorption, the challenge is to distinguish between a 'collision' with the surface and the point at which a molecule crosses a free energy barrier to become 'adsorbed', and to quantity the fraction of collisions that result in adsorption. One might imagine doing this by setting a minimum surface residence time for a molecule to be considered adsorbed (often limited by the time resolution of the instrument), but this is an arbitrary criterion. In practice, the best strategy might be to extrapolate the measured surface residence time distribution back to zero time in order to determine the theoretical number of adsorbed objects. Furthermore, quantifying the number of protein-surface collisions will require high temporal resolution due to the high diffusion coefficients of proteins in solution (30-80 $\mu m^2/s$). During typical observation periods (10^{-2}-10^{-1} s) necessary to measure object position in SMT, many objects that collide with the surface and diffuse back into bulk solution will appear to be background noise.

5) The use of single-molecule resonance energy transfer (RET) provides an orthogonal signal to distinguish protein structural changes or protein-protein associations from observations

of molecular adsorption, diffusion, and desorption. Measuring the distance between two points on a single protein can provide information about secondary and tertiary structure while the nanoscale distance between two proteins can be used to identify protein-protein associations such as nonspecific clustering or specific receptor-ligand binding. Indeed, SMT incorporating intramolecular RET has been demonstrated in freely-adsorbing, diffusing, and desorbing DNA molecules.[164,165] The challenge for translating these methods to the study of interfacial protein behavior is the ability to place fluorescent labels in appropriate places on the protein. Although protein engineering techniques facilitate site-specific labeling, experimental design depends critically on a priori knowledge of the conformational states in question in order to correlate the donor-acceptor distance with conformational change. Such an approach was recently demonstrated in which site-specific fluorescence labeling allowed a conformational change in freely-adsorbing organophosphorous hydrolase to be measured at the single-molecule level.[154] Regarding protein-protein associations, labeling donors and acceptors at random sites on separate proteins creates a RET signature that can distinguish unassociated from associated states. Rabe et al. used such a strategy to observe slow spreading kinetics (over several hours) of large BSA clusters on hydrophilic and hydrophobic surfaces.[153]

1.6 Objective

The objective of this research was to develop a molecule-level mechanistic understanding of nonspecific protein interactions that lead to protein layer formation, and other macroscopically observed protein adsorption phenomena, at the solid-liquid interface. Of specific interest were the effects of protein-surface interactions versus protein-protein interactions on protein interfacial dynamics (e.g. adsorption, desorption, diffusion, aggregation). SMT, based on TIRFM techniques, were uniquely suited for this study because they allowed us to directly observe protein adsorption, desorption, interfacial diffusion, and intermolecular associations on a molecule-by-molecule basis. By varying several environmental conditions

(e.g. surface chemistry, pH, ionic strength, temperature, protein concentration) and directly observing protein interfacial dynamics with SM-TIRFM, we have built a mechanistic understanding of protein adsorption that has led to a more meaningful understanding of macroscopically observed phenomena. In order to address this objective, four specific aims were addressed:

1. Develop SMT methods to study the dynamic behavior of isolated proteins interacting with surfaces of contrasting physico-chemical properties (e.g. hydrophobicity and hydrogen-bonding capacity).
2. Determine the effects of surface chemistry and solution electrostatics on isolated protein-surface interactions.
3. Develop methods to study protein-protein interactions on surfaces.
4. Determine the effects of surface chemistry and the relative roles of protein-surface and protein-protein interactions on protein surface layer formation, relevant to membrane fouling and biomaterial protein adsorption.

The insights gained by these aims led to a mechanistic understanding of how surface chemistry, surface heterogeneity, and solution conditions affect macroscopic protein behavior, thereby informing the rational design of materials that promote desirable protein behaviors.

In the following chapters, the above aims will be addressed. In chapter 1, we developed and used SMT methods to study fibrinogen interfacial dynamics on hydrophilic bare fused silica (FS), hydrophobic trimethyl silane modified (TMS), and 'protein-resistant' polyethylene glycol (PEG) modified surfaces, addressing aim 1. Chapters 2 and 3 address aim 2 by investigating the apparent activation energies of surface diffusion and desorption of isolated BSA and fibrinogen molecules on FS and TMS (chapter 2) and the role of electrostatics in isolated BSA molecule adsorption, desorption, and diffusion at FS interfaces (chapter 3). We develop methods to directly measure BSA-BSA associations at a PEG-modified surface – aqueous interface using intermolecular RET in chapter 5, addressing aim 3. Finally, aim 4 is addressed

in chapters 6 and 7 by directly and indirectly observing the effects of protein-protein interactions on surfaces with different surface chemistries. In chapter 6 we investigate the roles of protein population and spatial heterogeneity in protein surface dynamics at extremely dilute and high protein solution concentrations on FS and TMS as well as on surface composed of materials relevant to ultrafiltration. Chapter 7 describes how interfacial fibrinogen-fibrinogen association dynamics differ on oligo-ethylene glycol (OEG) and TMS surfaces. Throughout, a mechanistic picture of protein adsorption phenomena and interfacial dynamics emerges.

1.7 References

(1) Nakanishi, K.; Sakiyama, T.; Imamura, K. On the Adsorption of Proteins on Solid Surfaces, a Common but Very Complicated Phenomenon. *J. Biosci. Bioeng.* **2001**, *91*, 233–244.

(2) Vogler, E. A. Protein Adsorption in Three Dimensions. *Biomaterials* **2012**, *33*, 1201–1237.

(3) Ratner, B. D.; Bryant, S. J. Biomaterials: Where We Have Been and Where We Are Going. *Annu. Rev. Biomed. Eng.* **2004**, *6*, 41–75.

(4) Mansouri, J.; Harrisson, S.; Chen, V. Strategies for Controlling Biofouling in Membrane Filtration Systems: Challenges and Opportunities. *J. Mater. Chem.* **2010**, *20*, 4567–4586.

(5) Bee, J. S.; Chiu, D.; Sawicki, S.; Stevenson, J. L.; Chatterjee, K.; Freund, E.; Carpenter, J. F.; Randolph, T. W. Monoclonal Antibody Interactions with Micro-and Nanoparticles: Adsorption, Aggregation, and Accelerated Stress Studies. *J. Pharm. Sci.* **2009**, *98*, 3218–3238.

(6) Norde, W. My Voyage of Discovery to Proteins in Flatland ...and beyond. *Colloids Surf. B. Biointerfaces* **2008**, *61*, 1–9.

(7) Rabe, M.; Verdes, D.; Seeger, S. Understanding Protein Adsorption Phenomena at Solid Surfaces. *Adv. Colloid Interface Sci.* **2011**, *162*, 87–106.

(8) Gray, J. J. The Interaction of Proteins with Solid Surfaces. *Curr. Opin. Struct. Biol.* **2004**, *14*, 110–115.

(9) Kastantin, M.; Langdon, B. B.; Schwartz, D. K. A Bottom-up Approach to Understanding Protein Layer Formation at Solid-Liquid Interfaces. *Adv. Colloid Interface Sci.* **2014**, *207*, 240–252.

(10) McCue, J. T.; Engel, P.; Ng, A.; Macniven, R.; Thömmes, J. Modeling of Protein Monomer/aggregate Purification and Separation Using Hydrophobic Interaction Chromatography. *Bioprocess Biosyst. Eng.* **2008**, *31*, 261–275.

(11) Van Reis, R.; Zydney, A. Bioprocess Membrane Technology. *J. Memb. Sci.* **2007**, *297*, 16–50.

(12) Choi, S.; Goryll, M.; Sin, L. Y. M.; Wong, P. K.; Chae, J. Microfluidic-Based Biosensors toward Point-of-Care Detection of Nucleic Acids and Proteins. *Microfluid. Nanofluidics* **2010**, *10*, 231–247.

(13) Bee, J. S.; Randolph, T. W.; Carpenter, J. F.; Bishop, S. M.; Dimitrova, M. N. Effects of Surfaces and Leachables on the Stability of Biopharmaceuticals. *J. Pharm. Sci.* **2011**, *100*, 4158–4170.

(14) Diener, A.; Nebe, B.; Lüthen, F.; Becker, P.; Beck, U.; Neumann, H. G.; Rychly, J. Control of Focal Adhesion Dynamics by Material Surface Characteristics. *Biomaterials* **2005**, *26*, 383–392.

(15) Keselowsky, B. G.; Collard, D. M.; García, A. J. Surface Chemistry Modulates Focal Adhesion Composition and Signaling through Changes in Integrin Binding. *Biomaterials* **2004**, *25*, 5947–5954.

(16) Rabe, M.; Verdes, D.; Seeger, S. Understanding Cooperative Protein Adsorption Events at the Microscopic Scale: A Comparison between Experimental Data and Monte Carlo Simulations. *J. Phys. Chem. B* **2010**, *114*, 5862–5869.

(17) Andrade, J. D.; Hlady, V.; Wei, A. P. Adsorption of Complex Proteins at Interfaces. *Pure Appl. Chem.* **1992**, *64*, 1777–1781.

(18) Norde, W.; Lyklema, J. Why Proteins Prefer Interfaces. *J. Biomater. Sci. Polym. Ed.* **1991**, *2*, 183–202.

(19) Minton, A. P. Effects of Excluded Surface Area and Adsorbate Clustering on Surface Adsorption of Proteins I. Equilibrium Models. *Biophys. Chem.* **2000**, *86*, 239–247.

(20) Prime, K. L. K.; Whitesides, G. M. G. Self-Assembled Organic Monolayers: Model Systems for Studying Adsorption of Proteins at Surfaces. *Science (80-.).* **1991**, *252*, 1164–1167.

(21) Walder, R.; Nelson, N.; Schwartz, D. K. Super-Resolution Surface Mapping Using the Trajectories of Molecular Probes. *Nat. Commun.* **2011**, *2*, 515.

(22) Andrade, J. D.; Hlady, V. Protein Adsorption and Materials Biocompatibility: A Tutorial Review and Suggested Hypotheses. *Adv. Polym. Sci.* **1986**, *79*, 1–63.

(23) Ostuni, E.; Chapman, R. G.; Holmlin, R. E.; Takayama, S.; Whitesides, G. M. A Survey of Structure-Property Relationships of Surfaces That Resist the Adsorption of Protein. *Langmuir* **2001**, *17*, 5605–5620.

(24) Kastantin, M.; Keller, T. F.; Jandt, K. D.; Schwartz, D. K. Single-Molecule Tracking of Fibrinogen Dynamics on Nanostructured Poly(ethylene) Films. *Adv. Funct. Mater.* **2012**, *22*, 2617–2623.

(25) Skaug, M. J.; Lacasta, A. M.; Ramirez-Piscina, L.; Sancho, J. M.; Lindenberg, K.; Schwartz, D. K. Single-Molecule Diffusion in a Periodic Potential at a Solid-Liquid Interface. *Soft Matter* **2014**, *10*, 753–759.

(26) Sethuraman, A.; Han, M.; Kane, R. S.; Belfort, G. Effect of Surface Wettability on the Adhesion of Proteins. *Langmuir* **2004**, *20*, 7779–7788.

(27) Wertz, C. F.; Santore, M. M. Adsorption and Relaxation Kinetics of Albumin and Fibrinogen on Hydrophobic Surfaces: Single-Species and Competitive Behavior. *Langmuir* **1999**, *15*, 8884–8894.

(28) Arai, T.; Norde, W. The Behavior of Some Model Proteins at Solid-Liquid Interfaces 1. Adsorption from Single Protein Solutions. *Colloids and Surfaces* **1990**, *51*, 1–15.

(29) Treuheit, M. J.; Kosky, A. a; Brems, D. N. Inverse Relationship of Protein Concentration and Aggregation. *Pharm. Res.* **2002**, *19*, 511–516.

(30) Sivaraman, B.; Fears, K. P.; Latour, R. A. Investigation of the Effects of Surface Chemistry and Solution Concentration on the Conformation of Adsorbed Proteins Using an Improved Circular Dichroism Method. *Langmuir* **2009**, *25*, 3050–3056.

(31) Kao, P.; Parhi, P.; Krishnan, A.; Noh, H.; Haider, W.; Tadigadapa, S.; Allara, D. L.; Vogler, E. A. Volumetric Interpretation of Protein Adsorption: Interfacial Packing of Protein Adsorbed to Hydrophobic Surfaces from Surface-Saturating Solution Concentrations. *Biomaterials* **2011**, *32*, 969–978.

(32) Chapman, R.; Ostuni, E.; Takayama, S.; Holmlin, R. E.; Yan, L.; Whitesides, G. M. Surveying for Surfaces That Resist the Adsorption of Proteins. *J. Am. Chem. Soc.* **2000**, *122*, 8303–8304.

(33) Currie, E. P. K.; Norde, W.; Cohen Stuart, M. a. *Tethered Polymer Chains: Surface Chemistry and Their Impact on Colloidal and Surface Properties.*; 2003; Vol. 100-102, pp. 205–265.

(34) Sofia, S.; Premnath, V.; Merrill, E. Poly(ethylene Oxide) Grafted to Silicon Surfaces: Grafting Density and Protein Adsorption. *Macromolecules* **1998**, *31*, 5059–5070.

(35) Mathes, J.; Friess, W. Influence of pH and Ionic Strength on IgG Adsorption to Vials. *Eur. J. Pharm. Biopharm.* **2011**, *78*, 239–247.

(36) Su, T. J.; Lu, J. R.; Thomas, R. K.; Cui, Z. F. Effect of pH on the Adsorption of Bovine Serum Albumin at the Silica/Water Interface Studied by Neutron Reflection. *J. Phys. Chem. B* **1999**, *103*, 3727–3736.

(37) Kisley, L.; Chen, J.; Mansur, A. P.; Dominguez-Medina, S.; Kulla, E.; Kang, M. K.; Shuang, B.; Kourentzi, K.; Poongavanam, M.-V.; Dhamane, S.; et al. High Ionic Strength Narrows the Population of Sites Participating in Protein Ion-Exchange Adsorption: A Single-Molecule Study. *J. Chromatogr. A* **2014**, *1343*, 135–142.

(38) Karpovich, D. S.; Blanchard, G. J. Direct Measurement of the Adsorption Kinetics of Alkanethiolate Self-Assembled Monolayers on a Microcrystalline Gold Surface. *Langmuir* **1994**, *10*, 3315–3322.

(39) Sarkar, D.; Chattoraj, D. Kinetics of Desorption of Proteins from the Surface of Protein-Coated Alumina by Various Desorbing Reagents. *J. Colloid Interface Sci.* **1996**, *178*, 606–613.

(40) Asanov, A. N.; Delucas, L. J.; Oldham, P. B.; Wilson, W. W. Heteroenergetics of Bovine Serum Albumin Adsorption from Good Solvents Related to Crystallization Conditions. *J. Colloid Interface Sci.* **1997**, *191*, 222–235.

(41) Ostuni, E.; Grzybowski, B.; Mrksich, M. Adsorption of Proteins to Hydrophobic Sites on Mixed Self-Assembled Monolayers. *Langmuir* **2003**, *19*, 1861–1872.

(42) Van der Veen, M.; Stuart, M. C.; Norde, W. Spreading of Proteins and Its Effect on Adsorption and Desorption Kinetics. *Colloids Surf. B. Biointerfaces* **2007**, *54*, 136–142.

(43) Vasina, E. N.; Déjardin, P. Kinetics of Adsorption, Desorption, and Exchange of A-Chymotrypsin and Lysozyme on Poly (ethyleneterephthalate) Tracked Film and Track-Etched Membrane. *Biomacromolecules* **2003**, *4*, 304–313.

(44) Adamczyk, Z.; Weroński, P.; Musiał, E. Particle Adsorption under Irreversible Conditions: Kinetics and Jamming Coverage. *Colloids Surfaces A Physicochem. Eng. Asp.* **2002**, *208*, 29–40.

(45) Schaaf, P.; Voegel, J. C.; Senger, B. From Random Sequential Adsorption to Ballistic Deposition: A General View of Irreversible Deposition Processes. *J. Phys. Chem. B* **2000**, *104*, 2204–2214.

(46) Schaaf, P.; Talbot, J. Kinetics of Random Sequential Adsorption. *Phys. Rev. Lett.* **1989**, *62*, 175–178.

(47) Schaaf, P.; Talbot, J. Surface Exclusion Effects in Adsorption Processes. *J. Chem. Phys.* **1989**, *91*, 4401.

(48) Cadilhe, A.; Araújo, N. A. M.; Privman, V. Random Sequential Adsorption: From Continuum to Lattice and Pre-Patterned Substrates. *J. Phys. Condens. Matter* **2007**, *19*, 065124.

(49) Norde, W. Adsorption of Proteins at Solid-Liquid Interfaces. *Cells Mater.* **1995**, *5*, 97–112.

(50) Kastantin, M.; Langdon, B. B.; Chang, E. L.; Schwartz, D. K. Single-Molecule Resolution of Interfacial Fibrinogen Behavior: Effects of Oligomer Populations and Surface Chemistry. *J. Am. Chem. Soc.* **2011**, *133*, 4975–4983.

(51) Zhou, H.-X.; Rivas, G.; Minton, A. P. Macromolecular Crowding and Confinement: Biochemical, Biophysical, and Potential Physiological Consequences. *Annu. Rev. Biophys.* **2008**, *37*, 375–397.

(52) Sips, R. On the Structure of a Catalyst Surface. II. *J. Chem. Phys.* **1950**, *18*, 1024.

(53) Low, M. J. D. Kinetics of Chemisorption of Gases on Solids. *Chem. Rev.* **1960**, *60*, 267–312.

(54) Johnson, R. D.; Arnold, F. H. The Temkin Isotherm Describes Heterogeneous Protein Adsorption. *Biochim. Biophys. Acta* **1995**, *1247*, 293–297.

(55) Sips, R. On the Structure of a Catalyst Surface. *J. Chem. Phys.* **1948**, *16*, 490.

(56) Tóth, J. Uniform Interpretation of Gas/solid Adsorption. *Adv. Colloid Interface Sci.* **1995**, *55*, 1–239.

(57) Rabe, M.; Verdes, D.; Rankl, M.; Artus, G. R. J.; Seeger, S. A Comprehensive Study of Concepts and Phenomena of the Nonspecific Adsorption of Beta-Lactoglobulin. *ChemPhysChem* **2007**, *8*, 862–872.

(58) Wertz, C. F.; Santore, M. M. Fibrinogen Adsorption on Hydrophilic and Hydrophobic Surfaces: Geometrical and Energetic Aspects of Interfacial Relaxations. *Langmuir* **2002**, *18*, 706–715.

(59) Green, R. J.; Davies, J.; Davies, M. C.; Roberts, C. J.; Tendler, S. J. B. Surface Plasmon Resonance for Real Time in Situ Analysis of Protein Adsorption to Polymer Surfaces. *Biomaterials* **1997**, *18*, 405–413.

(60) Snopok, B. a; Kostyukevich, E. V. Kinetic Studies of Protein-Surface Interactions: A Two-Stage Model of Surface-Induced Protein Transitions in Adsorbed Biofilms. *Anal. Biochem.* **2006**, *348*, 222–231.

(61) Calonder, C.; Tie, Y.; Van Tassel, P. R. History Dependence of Protein Adsorption Kinetics. *Proc. Natl. Acad. Sci. U. S. A.* **2001**, *98*, 10664–10669.

(62) Höök, F.; Vörös, J.; Rodahl, M.; Kurrat, R.; Böni, P.; Ramsden, J. J.; Textor, M.; Spencer, N. D.; Tengvall, P.; Gold, J.; et al. A Comparative Study of Protein Adsorption on Titanium Oxide Surfaces Using in Situ Ellipsometry, Optical Waveguide Lightmode Spectroscopy, and Quartz Crystal Microbalance/dissipation. *Colloids Surfaces B Biointerfaces* **2002**, *24*, 155–170.

(63) Jin, J.; Jiang, W.; Yin, J.; Ji, X.; Stagnaro, P. Plasma Proteins Adsorption Mechanism on Polyethylene-Grafted Poly(ethylene Glycol) Surface by Quartz Crystal Microbalance with Dissipation. *Langmuir* **2013**, *29*, 6624–6633.

(64) Berglin, M.; Pinori, E.; Sellborn, A.; Andersson, M.; Hulander, M.; Elwing, H. Fibrinogen Adsorption and Conformational Change on Model Polymers: Novel Aspects of Mutual Molecular Rearrangement. *Langmuir* **2009**, *25*, 5602–5608.

(65) Jönsson, U.; Malmqvist, M.; Ronnberg, I. Adsorption of Immunoglobulin G, Protein A, and Fibronectin in the Submonolayer Region Evaluated by a Combined Study of Ellipsometry and Radiotracer Techniques. *J. colloid interface …* **1985**, *103*, 360–372.

(66) Myers, G. A.; Gacek, D. A.; Peterson, E. M.; Fox, C. B.; Harris, J. M. Microscopic Rates of Peptide-Phospholipid Bilayer Interactions from Single-Molecule Residence Times. *J. Am. Chem. Soc.* **2012**, *134*, 19652–19660.

(67) Langdon, B. B.; Kastantin, M.; Schwartz, D. K. Apparent Activation Energies Associated with Protein Dynamics on Hydrophobic and Hydrophilic Surfaces. *Biophys. J.* **2012**, *102*, 2625–2633.

(68) Kwok, K. C.; Yeung, K. M.; Cheung, N. H. Adsorption Kinetics of Bovine Serum Albumin on Fused Silica: Population Heterogeneities Revealed by Single-Molecule Fluorescence Microscopy. *Langmuir* **2007**, *23*, 1948–1952.

(69) Yeung, K. M.; Lu, Z. J.; Cheung, N. H. Adsorption of Bovine Serum Albumin on Fused Silica: Elucidation of Protein-Protein Interactions by Single-Molecule Fluorescence Microscopy. *Colloids Surf. B. Biointerfaces* **2009**, *69*, 246–250.

(70) Pandey, L. M.; Pattanayek, S. K.; Delabouglise, D. Properties of Adsorbed Bovine Serum Albumin and Fibrinogen on Self-Assembled Monolayers. *J. Phys. Chem. C* **2013**, *117*, 6151–6160.

(71) Monserud, J. H.; Schwartz, D. K. Effects of Molecular Size and Surface Hydrophobicity on Oligonucleotide Interfacial Dynamics. *Biomacromolecules* **2012**, *13*, 4002–4011.

(72) Nelson, N.; Walder, R.; Schwartz, D. K. Single Molecule Dynamics on Hydrophobic Self-Assembled Monolayers. *Langmuir* **2012**, *28*, 12108–12113.

(73) Walder, R.; Schwartz, D. K. Single Molecule Observations of Multiple Protein Populations at the Oil-Water Interface. *Langmuir* **2010**, *26*, 13364–13367.

(74) Sriram, I.; Walder, R.; Schwartz, D. K. Stokes–Einstein and Desorption-Mediated Diffusion of Protein Molecules at the Oil–water Interface. *Soft Matter* **2012**, *8*, 6000.

(75) Dobbs, K. D.; Doren, D. J. Dynamics of Molecular Surface Diffusion: Origins and Consequences of Long Jumps. *J. Chem. Phys.* **1992**, *97*, 3722.

(76) Axelrod, D.; Koppel, D. E.; Schlessinger, J.; Elson, E.; Webb, W. W. Mobility Measurement by Analysis of Fluorescence Photobleaching Recovery Kinetics. *Biophys. J.* **1976**, *16*, 1055–1069.

(77) Krägel, J.; Wüstneck, R.; Husband, F.; Wilde, P. J.; Makievski, A. V; Grigoriev, D. O.; Li, J. B. Properties of Mixed Protein/surfactant Adsorption Layers. *Colloids surfaces B …* **1999**, *12*, 399–407.

(78) Gambin, Y.; Lopez-Esparza, R.; Reffay, M.; Sierecki, E.; Gov, N. S.; Genest, M.; Hodges, R. S.; Urbach, W. Lateral Mobility of Proteins in Liquid Membranes Revisited. *Proc. Natl. Acad. Sci. U. S. A.* **2006**, *103*, 2098–2102.

(79) Vieira, E. P.; Rocha, S.; Carmo Pereira, M.; Möhwald, H.; Coelho, M. A. N. Adsorption and Diffusion of Plasma Proteins on Hydrophilic and Hydrophobic Surfaces: Effect of Trifluoroethanol on Protein Structure. *Langmuir* **2009**, *25*, 9879–9886.

(80) Mrksich, M.; Sigal, G. B.; Whitesides, G. M. Surface Plasmon Resonance Permits in Situ Measurement of Protein Adsorption on Self-Assembled Monolayers of Alkanethiolates on Gold. *Langmuir* **1995**, *11*, 4383–4385.

(81) Kim, D. T.; Blanch, H. W.; Radke, C. J. Direct Imaging of Lysozyme Adsorption onto Mica by Atomic Force Microscopy. *Langmuir* **2002**, *18*, 5841–5850.

(82) Fainerman, V. B.; Miller, R.; Ferri, J. K.; Watzke, H.; Leser, M. E.; Michel, M. Reversibility and Irreversibility of Adsorption of Surfactants and Proteins at Liquid Interfaces. *Adv. Colloid Interface Sci.* **2006**, *123-126*, 163–171.

(83) Dijt, J. C.; Stuart, M. A. C.; Fleer, G. J. Kinetics of Polymer Adsorption and Desorption in Capillary Flow. *Macromolecules* **1992**, *25*, 5416–5423.

(84) Bee, J. S.; Schwartz, D. K.; Trabelsi, S.; Freund, E.; Stevenson, J. L.; Carpenter, J. F.; Randolph, T. W. Production of Particles of Therapeutic Proteins at the Air–water Interface during Compression/dilation Cycles. *Soft Matter* **2012**, *8*, 10329.

(85) Höök, F.; Rodahl, M.; Kasemo, B.; Brzezinski, P. Structural Changes in Hemoglobin during Adsorption to Solid Surfaces: Effects of pH, Ionic Strength, and Ligand Binding. *Proc. Natl. Acad. Sci.* **1998**, *95*, 12271–12276.

(86) Tunc, S.; Maitz, M. F.; Steiner, G.; Vázquez, L.; Pham, M. T.; Salzer, R. In Situ Conformational Analysis of Fibrinogen Adsorbed on Si Surfaces. *Colloids Surf. B. Biointerfaces* **2005**, *42*, 219–225.

(87) Baldwin, R. L. Temperature Dependence of the Hydrophobic Interaction in Protein Folding. *Proc. Natl. Acad. Sci.* **1986**, *83*, 8069–8072.

(88) Dill, K. A. Dominant Forces in Protein Folding. *Biochemistry* **1990**, *29*, 7133–7155.

(89) Baugh, L.; Vogel, V. Structural Changes of Fibronectin Adsorbed to Model Surfaces Probed by Fluorescence Resonance Energy Transfer. *J. Biomed. Mater. Res. A* **2004**, *69*, 525–534.

(90) Brynda, E.; Hlady, V.; Andrade, J. D. Protein Packing in Adsorbed Layers Studied by Excitation Energy Transfer. *J. Colloid Interface Sci.* **1990**, *139*, 374–380.

(91) Wertz, C. F.; Santore, M. M. Effect of Surface Hydrophobicity on Adsorption and Relaxation Kinetics of Albumin and Fibrinogen: Single-Species and Competitive Behavior. *Langmuir* **2001**, *17*, 3006–3016.

(92) Daly, S.; Przybycien, T.; Tilton, R. Coverage-Dependent Orientation of Lysozyme Adsorbed on Silica. *Langmuir* **2003**, 3848–3857.

(93) Nygren, H. Attractive Adsorbate Interaction in Biological Surface Reactions. *Biophys. Chem.* **1996**, *61*, 73–84.

(94) Nygren, H.; Stenberg, M. Surface-Induced Aggregation of Ferritin. Kinetics of Adsorption to a Hydrophobic Surface. *Biophys. Chem.* **1990**, *38*, 67–75.

(95) Mulheran, P.; Pellenc, D.; Bennett, R. A.; Green, R. J.; Sperrin, M. Mechanisms and Dynamics of Protein Clustering on a Solid Surface. *Phys. Rev. Lett.* **2008**, *100*, 068102.

(96) Rabe, M.; Verdes, D.; Zimmermann, J.; Seeger, S. Surface Organization and Cooperativity during Nonspecific Protein Adsorption Events. *J. Phys. Chem. B* **2008**, *112*, 13971–13980.

(97) Siegismund, D.; Keller, T. F.; Jandt, K. D.; Rettenmayr, M. Fibrinogen Adsorption on Biomaterials--a Numerical Study. *Macromol. Biosci.* **2010**, *10*, 1216–1223.

(98) Minton, A. P. Adsorption of Globular Proteins on Locally Planar Surfaces. II. Models for the Effect of Multiple Adsorbate Conformations on Adsorption Equilibria and Kinetics. *Biophys. J.* **1999**, *76*, 176–187.

(99) Lopez, A. E.; Moreno-Flores, S.; Pum, D.; Sleytr, U. B.; Toca-Herrera, J. L. Surface Dependence of Protein Nanocrystal Formation. *Small* **2010**, *6*, 396–403.

(100) Keller, T. F.; Schönfelder, J.; Reichert, J.; Tuccitto, N.; Licciardello, A.; Messina, G. M. L. M.; Marletta, G.; Jandt, K. D. How the Surface Nanostructure of Polyethylene Affects Protein Assembly and Orientation. *ACS Nano* **2011**, *5*, 3120–3131.

(101) Sethuraman, A.; Vedantham, G.; Imoto, T.; Przybycien, T.; Belfort, G. Protein Unfolding at Interfaces: Slow Dynamics of Alpha-Helix to Beta-Sheet Transition. *Proteins* **2004**, *56*, 669–678.

(102) Sethuraman, A.; Belfort, G. Protein Structural Perturbation and Aggregation on Homogeneous Surfaces. *Biophys. J.* **2005**, *88*, 1322–1333.

(103) Robertson, B. C.; Zydney, A. L. Protein Adsorption in Asymmetric Ultrafiltration Membranes with Highly Constricted Pores. *J. Colloid Interface Sci.* **1990**, *134*, 563–575.

(104) Gerhardt, A.; Mcgraw, N. R.; Schwartz, D. K.; Bee, J. S.; Carpenter, J. F.; Randolph, T. W. Protein Aggregation and Particle Formation in Prefilled Glass Syringes. *J. Pharm. Sci.* **2014**, *103*, 1601–1612.

(105) Silin, V.; Weetall, H.; Vanderah, D. SPR Studies of the Nonspecific Adsorption Kinetics of Human IgG and BSA on Gold Surfaces Modified by Self-Assembled Monolayers (SAMs). *J. Colloid Interface Sci.* **1997**, *185*, 94–103.

(106) Noh, H.; Vogler, E. A. Volumetric Interpretation of Protein Adsorption: Partition Coefficients, Interphase Volumes, and Free Energies of Adsorption to Hydrophobic Surfaces. *Biomaterials* **2006**, *27*, 5780–5793.

(107) Servoli, E.; Maniglio, D.; Aguilar, M. R.; Motta, A.; San Roman, J.; Belfiore, L. a; Migliaresi, C. Quantitative Analysis of Protein Adsorption via Atomic Force Microscopy and Surface Plasmon Resonance. *Macromol. Biosci.* **2008**, *8*, 1126–1134.

(108) Pegueroles, M.; Tonda-Turo, C.; Planell, J. a; Gil, F.-J.; Aparicio, C. Adsorption of Fibronectin, Fibrinogen, and Albumin on TiO2: Time-Resolved Kinetics, Structural Changes, and Competition Study. *Biointerphases* **2012**, *7*, 48.

(109) Jiang, J.; Zhu, L.; Zhu, L.; Zhang, H.; Zhu, B.; Xu, Y. Antifouling and Antimicrobial Polymer Membranes Based on Bioinspired Polydopamine and Strong Hydrogen-Bonded poly(N-Vinyl Pyrrolidone). *ACS Appl. Mater. Interfaces* **2013**, *5*, 12895–12904.

(110) Andrade, J. D.; Hlady, V. L.; Van Wagenen, R. A. Effects of Plasma Protein Adsorption on Protein Conformation and Activity. *Pure Appl. Chem.* **1984**, *56*, 1345–1350.

(111) Maste, M. C. L.; Norde, W.; Visser, A. J. W. G. Adsorption-Induced Conformational Changes in the Serine Proteinase Savinase: A Tryptophan Fluorescence and Circular Dichroism Study. *J. Colloid Interface Sci.* **1997**, *196*, 224–230.

(112) Schwinté, P.; Ball, V.; Szalontai, B.; Haikel, Y.; Voegel, J.-C.; Schaaf, P. Secondary Structure of Proteins Adsorbed onto or Embedded in Polyelectrolyte Multilayers. *Biomacromolecules* **2002**, *3*, 1135–1143.

(113) Xu, L.-C.; Siedlecki, C. a. Atomic Force Microscopy Studies of the Initial Interactions between Fibrinogen and Surfaces. *Langmuir* **2009**, *25*, 3675–3681.

(114) Agnihotri, A.; Siedlecki, C. a. Time-Dependent Conformational Changes in Fibrinogen Measured by Atomic Force Microscopy. *Langmuir* **2004**, *20*, 8846–8852.

(115) Holzmeister, P.; Acuna, G. P.; Grohmann, D.; Tinnefeld, P. Breaking the Concentration Limit of Optical Single-Molecule Detection. *Chem. Soc. Rev.* **2014**, *43*, 1014–1028.

(116) Deniz, A. a; Mukhopadhyay, S.; Lemke, E. a. Single-Molecule Biophysics: At the Interface of Biology, Physics and Chemistry. *J. R. Soc. Interface* **2008**, *5*, 15–45.

(117) The Nobel Prize in Chemistry 2013 http://www.degruyter.com/view/j/ci.2014.36.issue-2/ci.2014.36.2.2/ci.2014.36.2.2.xml.

(118) Moerner, W. E. Illuminating Single Molecules in Condensed Matter. *Science (80-.).* **1999**, *283*, 1670–1676.

(119) Betzig, E.; Chichester, R. J. Single Molecules Observed by near-Field Scanning Optical Microscopy. *Science (80-.).* **1993**, *262*, 1422–1425.

(120) Hell, S. W. Far-Field Optical Nanoscopy. *Science (80-.).* **2007**, *316*, 1153–1158.

(121) Hell, S. W.; Wichmann, J. Breaking the Diffraction Resolution Limit by Stimulated Emission: Stimulated-Emission-Depletion Fluorescence Microscopy. *Opt. Lett.* **1994**, *19*, 780–782.

(122) Betzig, E.; Patterson, G. H.; Sougrat, R.; Lindwasser, O. W.; Olenych, S.; Bonifacino, J. S.; Davidson, M. W.; Lippincott-Schwartz, J.; Hess, H. F. Imaging Intracellular Fluorescent Proteins at Nanometer Resolution. *Science (80-.).* **2006**, *313*, 1642–1645.

(123) Leake, M. The Physics of Life: One Molecule at a Time. *Philos. Trans. R. Soc. B* **2012**, *368*.

(124) Pirchi, M.; Ziv, G.; Riven, I.; Cohen, S. S.; Zohar, N.; Barak, Y.; Haran, G. Single-Molecule Fluorescence Spectroscopy Maps the Folding Landscape of a Large Protein. *Nat. Commun.* **2011**, *2*, 493.

(125) Stigler, J.; Ziegler, F.; Gieseke, A.; Gebhardt, J. C. M.; Rief, M. The Complex Folding Network of Single Calmodulin Molecules. *Science (80-.).* **2011**, *334*, 512–516.

(126) Zarrabi, N.; Ernst, S.; Verhalen, B.; Wilkens, S.; Börsch, M. Analyzing Conformational Dynamics of Single P-Glycoprotein Transporters by Förster Resonance Energy Transfer Using Hidden Markov Models. *Methods* **2014**, *66*, 168–179.

(127) Chang, C.; Althaus, J. C.; Carruthers, C. J. L.; Sutton, M. A.; Steel, D. G.; Gafni, A. Synergistic Interactions between Alzheimer's Aβ40 and Aβ42 on the Surface of Primary Neurons Revealed by Single Molecule Microscopy. *PLoS One* **2013**, *8*, 1–8.

(128) Bowen, M. E.; Weninger, K.; Ernst, J.; Chu, S.; Brunger, A. T. Single-Molecule Studies of Synaptotagmin and Complexin Binding to the SNARE Complex. *Biophys. J.* **2005**, *89*, 690–702.

(129) Levy-Sakin, M.; Grunwald, A.; Kim, S.; Gassman, N. R.; Gottfried, A.; Antelman, J.; Kim, Y.; Ho, S. O.; Samuel, R.; Michalet, X.; et al. Toward Single-Molecule Optical Mapping of the Epigenome. *ACS Nano* **2014**, *8*, 14–26.

(130) Wang, B.; Kuo, J.; Bae, S. C.; Granick, S. When Brownian Diffusion Is Not Gaussian. *Nat. Mater.* **2012**, *11*, 481–485.

(131) Yu, C.; Guan, J.; Chen, K.; Bae, S. C.; Granick, S. Single-Molecule Observation of Long Jumps in Polymer Adsorption. *ACS Nano* **2013**, *7*, 9735–9742.

(132) Skaug, M. J.; Mabry, J.; Schwartz, D. K. Intermittent Molecular Hopping at the Solid-Liquid Interface. *Phys. Rev. Lett.* **2013**, *110*, 256101.

(133) Walder, R.; Honciuc, A.; Schwartz, D. K. Phospholipid Diffusion at the Oil-Water Interface. *J. Phys. Chem. B* **2010**, *114*, 11484–11488.

(134) Elliott, L. C. C.; Barhoum, M.; Harris, J. M.; Bohn, P. W. Trajectory Analysis of Single Molecules Exhibiting Non-Brownian Motion. *Phys. Chem. Chem. Phys.* **2011**, *13*, 4326–4334.

(135) McCain, K. S.; Hanley, D. C.; Harris, J. M. Single-Molecule Fluorescence Trajectories for Investigating Molecular Transport in Thin Silica Sol-Gel Films. *Anal. Chem.* **2003**, *75*, 4351–4359.

(136) Schmidt, T.; Schütz, G. J.; Baumgartner, W.; Gruber, H. J.; Schindler, H. Characterization of Photophysics and Mobility of Single Molecules in a Fluid Lipid Membrane. *J. Phys. Chem.* **1995**, *99*, 17662–17668.

(137) Wirth, M. J.; Legg, M. A. Single-Molecule Probing of Adsorption and Diffusion on Silica Surfaces. *Annu. Rev. Phys. Chem.* **2007**, *58*, 489–510.

(138) Peterson, E. M.; Harris, J. M. Single-Molecule Fluorescence Imaging of DNA at a Potential-Controlled Interface. *Langmuir* **2013**, *29*, 8292–8301.

(139) Zareh, S. K.; Wang, Y. M. Single-Molecule Imaging of Protein Adsorption Mechanisms to Surfaces. *Microsc. Res. Tech.* **2011**, *74*, 682–687.

(140) Weiss, S. Fluorescence Spectroscopy of Single Biomolecules. *Science (80-.).* **1999**, *283*, 1676–1683.

(141) Mabry, J. N.; Skaug, M. J.; Schwartz, D. K. Single-Molecule Insights into Retention at a Reversed-Phase Chromatographic Interface. *Anal. Chem.* **2014**, *86*, 9451–9458.

(142) Wazawa, T.; Ueda, M. Total Internal Reflection Fluorescence Microscopy in Single Molecule Nanobioscience. *Adv. Biochem. Eng. Biotechnol.* **2005**, *95*, 77–106.

(143) Lok, B. K.; Cheng, Y.-L.; Robertson, C. R. Total Internal Reflection Fluorescence: A Technique for Examining Interactions of Macromolecules with Solid Surfaces. *J. Colloid Interface Sci.* **1983**, *91*, 87–103.

(144) Axelrod, D. Total Internal Reflection Fluorescence Microscopy in Cell Biology. *Methods Enzymol.* **2003**, *361*, 1–33.

(145) Lakowicz, J. R. Introduction to Fluorescence. In *Principles of fluorescence spectroscopy*; 2006; pp. 1–26.

(146) Schuster, J.; Brabandt, J.; von Borczyskowski, C. Discrimination of Photoblinking and Photobleaching on the Single Molecule Level. *J. Lumin.* **2007**, *127*, 224–229.

(147) Shuang, B.; Byers, C. P.; Kisley, L.; Wang, L.-Y.; Zhao, J.; Morimura, H.; Link, S.; Landes, C. F. Improved Analysis for Determining Diffusion Coefficients from Short, Single-Molecule Trajectories with Photoblinking. *Langmuir* **2013**, *29*, 228–234.

(148) Jung, S.; Dickson, R. M. Hidden Markov Analysis of Short Single Molecule Intensity Trajectories. *J. Phys. Chem. B* **2009**, *113*, 13886–13890.

(149) Eggeling, C.; Widengren, J.; Rigler, R.; Seidel, C. A. M. Photobleaching of Fluorescent Dyes under Conditions Used for Single-Molecule Detection: Evidence of Two-Step Photolysis. *Anal. Chem.* **1998**, *70*, 2651–2659.

(150) Widengren, J.; Chmyrov, A.; Eggeling, C.; Löfdahl, P.-A.; Seidel, C. A. M. Strategies to Improve Photostabilities in Ultrasensitive Fluorescence Spectroscopy. *J. Phys. Chem. A* **2007**, *111*, 429–440.

(151) Rasnik, I.; McKinney, S. a; Ha, T. Nonblinking and Long-Lasting Single-Molecule Fluorescence Imaging. *Nat. Methods* **2006**, *3*, 891–893.

(152) Lakowicz, J. R. Energy Transfer. In *Principles of Fluorescence Spectroscopy*; Lakowicz, J. R., Ed.; Springer New York, 2006; pp. 443–475.

(153) Rabe, M.; Verdes, D.; Seeger, S. Surface-Induced Spreading Phenomenon of Protein Clusters. *Soft Matter* **2009**, *5*, 1039–1047.

(154) McLoughlin, S. Y.; Kastantin, M.; Schwartz, D. K.; Kaar, J. L. Single-Molecule Resolution of Protein Structure and Interfacial Dynamics on Biomaterial Surfaces. *Proc. Natl. Acad. Sci.* **2013**, *110*, 19396–19401.

(155) Fox, C. B.; Wayment, J. R.; Myers, G. A.; Endicott, S. K.; Harris, J. M. Single-Molecule Fluorescence Imaging of Peptide Binding to Supported Lipid Bilayers. *Anal. Chem.* **2009**, *81*, 5130–5138.

(156) Truong, K.; Ikura, M. The Use of FRET Imaging Microscopy to Detect Protein–protein Interactions and Protein Conformational Changes in Vivo. *Curr. Opin. Struct. Biol.* **2001**, *11*, 573–578.

(157) Shrestha, D.; Bagosi, A.; Szöllősi, J.; Jenei, A. Comparative Study of the Three Different Fluorophore Antibody Conjugation Strategies. *Anal. Bioanal. Chem.* **2012**, *404*, 1449–1463.

(158) McDonagh, P.; Williams, S. The Preparation and Use of Fluorescent-Protein Conjugates for Microvascular Research. *Microvasc. Res.* **1984**, *27*, 14–27.

(159) Gajraj, A.; Ofoli, R. Effect of Extrinsic Fluorescent Labels on Diffusion and Adsorption Kinetics of Proteins at the Liquid-Liquid Interface. *Langmuir* **2000**, *16*, 8085–8094.

(160) Walder, R.; Kastantin, M.; Schwartz, D. K. High Throughput Single Molecule Tracking for Analysis of Rare Populations and Events. *Analyst* **2012**, *137*, 2987–2996.

(161) Walder, R.; Schwartz, D. K. Dynamics of Protein Aggregation at the Oil–water Interface Characterized by Single Molecule TIRF Microscopy. *Soft Matter* **2011**, *7*, 7616–7622.

(162) Savin, T.; Doyle, P. S. Static and Dynamic Errors in Particle Tracking Microrheology. *Biophys. J.* **2005**, *88*, 623–638.

(163) Kastantin, M.; Schwartz, D. K. Distinguishing Positional Uncertainty from True Mobility in Single-Molecule Trajectories That Exhibit Multiple Diffusive Modes. *Microsc. Microanal.* **2012**, *18*, 793–797.

(164) Kastantin, M.; Schwartz, D. K. DNA Hairpin Stabilization on a Hydrophobic Surface. *Small* **2013**, *9*, 933–941.

(165) Kastantin, M.; Schwartz, D. K. Connecting Rare DNA Conformations and Surface Dynamics Using Single-Molecule Resonance Energy Transfer. *ACS Nano* **2011**, *5*, 9861–9869.

Chapter 2: Single-Molecule Resolution of Interfacial Fibrinogen Behavior: Effects of Oligomer Population and Surface Chemistry

Mark Kastantin, Blake B. Langdon, Erin L. Chang, and Daniel K. Schwartz

(Published April, 2011: JACS 2011, 133 (13), 4975-4983.)

Abstract

Through the use of single-molecule total internal reflection fluorescence microscopy, the dynamic behavior of fibrinogen was observed at the interface between aqueous solution and various solid surfaces. Multiple populations of objects were observed, as characterized by surface residence times, interfacial diffusion, and fluorescence intensity. On all surfaces, populations exhibited direct links between surface residence time, rate of diffusion, and fluorescence intensity. In particular, longer-lived populations diffused more slowly and exhibited greater fluorescence intensity, leading to the conclusion that the objects represented fibrinogen monomers and discrete oligomer populations (dimers, trimers, etc.), and that these oligomer populations play an important role in the protein–surface interaction because of their long surface residence times. Two or three diffusive modes were observed for most populations, indicating that protein aggregates have multiple mechanisms for interaction with solid substrates. In addition, the fastest diffusive mode is believed to represent a hopping mode that often precedes desorption events. Surprisingly, a monolayer of 5000 Da poly(ethylene glycol) (PEG5000) increased surface residence time and slowed diffusion of fibrinogen relative to bare fused silica or hydrophobically modified fused silica, suggesting that the mechanism of PEG resistance to protein adhesion is more sophisticated than the simple repulsion of individual proteins.

2.1 Introduction

Biomaterials used for in vivo applications are often chemically inert with respect to specific interactions with cells and proteins. Nonspecific protein adsorption at the solid–liquid interface is problematic, however, as proteins may functionalize the inert biomaterial surface to support more pathological processes such as inflammation and thrombosis. In particular, fibrinogen adsorption is of primary concern due to its abundance in plasma. Fibrinogen is a 340 kDa glycoprotein that consists of two identical subunits that each contain three unique chains (α, β, and γ).[1,2] Two sequences on the γ chain ($\gamma_{190-202}$ and $\gamma_{377-395}$) are recognized synergistically by the phagocyte integrin, Mac-1, and can lead to inflammatory and wound-healing responses.[3,4] These sequences were found to be inaccessible to Mac-1 in native fibrinogen but are presented upon fibrinogen denaturation or polymerization to fibrin.[3,5] Additionally, the platelet integrin, GPIIa-IIIb, binds to both an RGD (Arg-Gly-Asp) sequence on the α-chain and a 12 amino acid sequence on the C-terminus of the γ chain.[2,6,7] Aggregation of activated platelets at the biomaterial surface can lead to thrombosis due to increased thrombin production and conversion of solution-phase fibrinogen to fibrin.[8]

Due to its importance for the biocompatibility of surfaces in contact with blood, fibrinogen adsorption at solid–liquid interfaces has been extensively studied.[9-15] A qualitative picture has emerged suggesting that some protein molecules in an adsorbed fibrinogen monolayer exhibit reversible binding at the interface while others remain adsorbed for longer than experimentally accessible time scales. Early studies explained this observation by assuming a single adsorbing fibrinogen species that either desorbs or converts to an irreversibly bound state through unfolding or other relaxation processes.[10,11,14] Subsequent work allowed for a single adsorbing species to assume a distribution of protein "footprints" on the surface that correlated with the reversibility of binding.[15] From this later work, it was concluded that the fraction of reversibly

bound proteins increased with protein flux, as increased flux decreased the available area for any one protein to spread and relax on the surface.

Surface chemistry has also been shown to affect the behavior of adsorbed fibrinogen. In the work of Hu et al.,[3] poly(ethylene terephthalate), poly(vinyl chloride), and low-density polyethylene were effective at exposing Mac-1 binding sequences, while fibrinogen on poly(ether urethane) or poly(dimethylsiloxane) was substantially less immunoreactive. In the work of Wertz and Santore,[15] surface chemistry was found to affect the relaxation rates and maximum observable footprint of fibrinogen. Fibrinogen relaxation on hydrophobic surfaces was attributed to slow unfolding events, while proteins on hydrophilic surfaces increased their binding strength via reorientations on time scales shorter than those for unfolding.

While protein denaturation and spreading on a surface seems to be an important factor in determining the irreversibility and pathology of adsorbed fibrinogen, the role of heterogeneity in the adsorbing population has received less attention. Light scattering data have shown that monomeric bovine fibrinogen cannot be the only species in solution, as the average weight of soluble species is twice that of the monomer.[16] Here and throughout this work, the term monomer refers to the entire 340 kDa protein, rather than one of its two identical subunits mentioned in the introductory paragraph. Although there is disagreement on the exact fractions of monomers and aggregates, size-exclusion chromatographic data have also shown the presence of soluble aggregates in bovine fibrinogen solutions.[17] This work will test the idea that soluble protein aggregates, small oligomers in particular, with more ways to interact favorably with a surface, have longer residence times than monomers and predispose its constituent proteins to spread and become irreversibly bound.

Experimental studies of the role of aggregation in fibrinogen monolayer formation are possibly absent from the literature because it is difficult to determine the properties of an adsorbing or desorbing species via the ensemble-averaged techniques that have been employed previously (i.e., studying net adsorption or desorption). In the present work, total

internal reflectance fluorescence microscopy (TIRFM) is used at very low surface coverage to track individual species as they adsorb to, diffuse along, and desorb from the solid–liquid interface. This allows a direct measurement of a protein object's surface residence time, independent of transport phenomena in solution. When this method is combined with analysis of that object's diffusive behavior and fluorescence intensity, an accurate and direct assessment of protein–surface interactions for oligomeric proteins is possible. This detailed picture of the initial stages of fibrinogen monolayer formation demonstrates that heterogeneity in the adsorbing fibrinogen population leads to diversity in protein–surface interactions.

The role of surface chemistry in this process is also studied due to its importance for biomaterial design. Model hydrophilic and hydrophobic surfaces will be compared along with a protein-resistant poly(ethylene glycol) (PEG) layer due to the ubiquity of PEG in drug-delivery and biomaterial applications.[18-20] It is generally accepted that a densely grafted PEG layer inhibits recognition of PEGylated surfaces by proteins and cells, although this inhibition is often incomplete.[21-23] Commonly cited mechanisms for this protein resistance are that stable water layers near the PEG surface or the steric barrier presented by the flexible polymer chain makes protein adsorption thermodynamically unfavorable.[24,25] This work will further explore the PEG–fibrinogen interaction as it pertains to initially adsorbing proteins.

2.2 Materials and Methods

2.2.1 Fibrinogen Solution

Human fibrinogen labeled with AlexaFluor ® 488 was purchased from Molecular Probes, Inc. The manufacturer specified degree of labeling was approximately 15 dye molecules per fibrinogen. Phosphate-buffered saline (PBS) was purchased from Invitrogen (calcium- and magnesium-free). Fibrinogen solutions were prepared at concentrations in the range 0.5×10^{-13} to 0.5×10^{-12} M in order to achieve low surface densities for single-molecule experiments.

2.2.2 Surface Preparation

Fused silica (FS) wafers were washed with cationic detergent (Micro 90, International Product Corp.) and thoroughly rinsed with water purified to 18 MΩ cm^{-1}. Wafers were then immersed in warm piranha solution for 1 h followed by UV-ozone treatment for 1 h. Following this treatment, FS wafers were either used without further treatment or were coated with monolayers of trimethylsilane (TMS) or methoxy-terminated PEG5000 silane. To form TMS monolayers, wafers were exposed to hexamethyldisilazine (Sigma) vapors for 18 h at room temperature. PEG5000 silane monolayers were formed via a 2 h solution deposition in which PEG5000 triethoxysilane (Nanocs) was dissolved in toluene at a concentration of 0.1 mg/mL.

2.2.3 Surface Characterization

Contact-Angle Measurements. Static contact angles of functionalized surfaces were measured with a custom-built contact-angle goniometer. A 1 μL drop of deionized water was deposited on the surface and at least six drops on three independent samples were averaged for reported values here. Almost complete wetting was observed on bare fused silica to the point that contact angles could not be measured. The static contact angle of the TMS substrate was 94º ± 4º. This value is consistent with a hydrophobic surface and with previous characterization of TMS-coated surfaces but is smaller than the ~110º contact angle typical of highly ordered, long-chain self-assembled monolayers.[26,27] The static contact angle of the PEG5000 monolayer was found to be 35º ±1º.[28,29] This value is in good agreement with contact angles of methoxy-terminated PEG (MW = 460–590) monolayers (36º ± 1º) and methoxy-terminated PEG5000 monolayers (33º ± 3º).[30]

Ellipsometry for PEG Monolayers. A single wavelength (632.8 nm), variable-angle, null ellipsometer (Multiskop, Optrel, Sinzing, Germany) was used to measure surface density of PEG chains in air. For ellipsometry experiments, PEG5000 surfaces were prepared on silicon wafers (2-in. intrinsic,Wafer Reclaim Services, San Jose, CA) as previously described for fused

silica substrates. A three-layer planar model of the solid surface, considering air and its refractive index (n = 1.003), PEG (n = 1.45), native silicon dioxide (n = 1.457), and silicon (n = 3.881), was used to simultaneously fit the amplitude ratios, tan Ψ, and phase shifts, Δ, measured at angles between 45º and 70º.[31] The thickness of the native oxide layer was measured by ellipsometry prior to PEG5000 functionalization. This technique gave a PEG5000 layer thickness of 2.4 ± 0.3 nm. At a density of 1 g/cm^3, this leads to a grafting density of 0.28 ± 0.04 chains/nm^2 or 31 ± 4 monomer units/nm^2. This monomer density is believed to confer protein resistance in human blood serum.[32] Higher monomer densities, resulting in an extended brush in which the methoxy terminus of the PEG chain is forced to the PEG–water interface, have been shown to support protein adsorption.[22]

2.2.4 Image Acquisition

TIRFM measurements were performed on a custom-built prism-based illumination system, flow cell, Nikon TE-2000 microscope with 60x objective, and 488 nm Ar ion laser that have been described previously.[33] The flow cell was maintained at 37±0.1ºC, and flow was stopped after introduction of the fibrinogen solution. The intensity of the laser illumination was high enough to resolve individual objects in sequential images with a 2 s acquisition time but low enough to permit continuous observation of objects for several minutes without photobleaching.

The evanescent wave created by total internal reflection has a penetration depth of less than 100 nm and consequently only objects near the surface are excited. While any object within this penetration depth may be excited and fluoresce, those that are not adsorbed to the surface are typically not observed. This is because diffusion coefficients in solution are 2–3 orders of magnitude higher than even the fastest surface diffusion coefficients observed in these experiments and the residence time of any one molecule in the capture region of a single imaging pixel is negligible unless it is adsorbed to the surface. Consequently, objects in solution contribute to higher background levels but are not identified as objects themselves.

Diffraction-limited objects were identified in each frame via convolution with a disk matrix and thresholding.[34] Object positions were calculated as the centroid of intensity. Object tracking was accomplished by identifying the closest objects in sequential frames while requiring the distance between closest objects to be less than 3 pixels (810 nm). Surface residence times were calculated as the number of frames on which the object was identified, multiplied by the exposure time of each frame. The error in this measurement was assumed to be the exposure time divided by √2 due to the fact that an object is not necessarily present for the entire first and last frames in which it is observed. Objects that were not observed to both adsorb and desorb were ignored due to the uncertainty in assigning their residence time. The intensity of an object in each frame was determined by integration of all pixels assigned to that object by the disk convolution and thresholding algorithm, and local background subtraction was also performed.

2.2.5 Data Analysis

Residence Times. The surface residence time of a given fibrinogen population is assumed to follow first-order desorption kinetics, and consequently the integrated or cumulative residence time distribution can be described as the sum of all such populations:

$$p(t) = \sum_{i=1} f_i \, e^{-t/\tau_i} \tag{1}$$

where $p(t)$ is the probability that a given object will have a residence time greater than or equal to time t. Each population is denoted with the subscript i, and τ_i is the inverse of the first-order desorption rate constant for that population (i.e., that population's mean surface residence time). The relative fraction of all analyzed objects represented by population i is f_i. In this work, cumulative distributions are preferable to raw desorption probability distributions because experimental data can be displayed and modeled without artifacts from binning into discrete residence time groups (for residence time data) or squared-displacement groups (for diffusion data).

The experimental residence time distribution was constructed by first accounting for the finite length of a movie whereby the adsorption and desorption of an object has a lower a priori probability of being observed for longer residence times because there are fewer opportunities to observe both events in a finite window. The number of objects observed to have a given residence time (n_t) was multiplied by a correction factor, $c(t)$, given by

$$c(t) = \left[H(T-t)\left(1-\frac{t}{T}\right)\right]^{-1}$$

where T is the length of the movie and H is the Heaviside step function. After correction for finite movie length, the cumulative residence time distribution was therefore given by

$$p(t) = \sum_{t'>t} n_{t'}c(t') / \sum_{t'} n_{t'}c(t')$$

Counting the number of objects with a given residence time (n_t) is assumed to follow Poisson statistics, and the error shown for each data point in the cumulative distribution represents 68% confidence intervals for a Poisson distribution with a mean of $\sum_{t'>t} n_{t'}$ scaled with the appropriate correction factor. Cumulative residence time distributions from multiple movies were averaged with a relative weight of the number of objects observed in that movie.

Diffusion. By default, one expects interfacial diffusion to follow two-dimensional Gaussian random-walk statistics where the probability of finding an object at a distance, r, away from its initial position after a time interval of Δt is given by

$$p(r,\Delta t) = (2D\Delta t)^{-1} r e^{-r^2/4D\Delta t}$$

where D is the diffusion coefficient. Often it is more convenient to view this probability distribution in its integrated form (the so-called cumulative squared-displacement distribution):

$$C(R^2,\Delta t) = e^{-R^2/4D\Delta t}$$

which represents the probability that an object will diffuse a distance ≥ R in a time interval Δt.

If a diffusing object is capable of multiple modes of diffusion each characterized by a diffusion coefficient D_j, its cumulative squared-displacement distribution is simply the sum of the

cumulative distributions for each mode weighted by the fraction of observed steps, x_j, corresponding to that mode

$$C(R^2, \Delta t) = \sum_j x_j e^{-R^2/4D_j\Delta t} \quad (2)$$

and the average diffusion coefficient is taken to be the fraction-weighted average of each mode:

$$\overline{D} = \sum_j x_j D_j$$

The experimental cumulative squared-displacement distribution is calculated as described previously33 by sorting the squared displacement data in ascending order and ranking each data point. Thus, $C\left({R_k}^2, \Delta t\right)$ is given by

$$C\left({R_k}^2, \Delta t\right) = 1 - k/N$$

where k is the rank in the sorted order and N is the total number of sorted data points. The error shown for each data point in the cumulative distribution represents 68% confidence intervals for a Poisson distribution with a mean of $N + \ 1 - k$.

Data Fitting. The experimental cumulative distribution of either residence time data or squared-displacement data was fit to eq 1 or 2 by minimizing the variance weighted by the squared error for each data point. For a given data set, the number of populations used for the fit was increased until populations were found with either characteristic residence time constants or diffusion coefficients that were not statistically different from each other as determined by a t-test to 90% confidence. This modest confidence value was generally found to exclude models with characteristic residence time constants or diffusion coefficients that had the same first significant digit.

2.3 Results and Discussion

2.3.1 Heterogeneity in Adsorbing Fibrinogen

Each object observed in these experiments was characterized by its residence time, median intensity, and surface trajectory. Of these, residence time distributions were examined

first in order to identify unique populations of adsorbed fibrinogen. The experimental cumulative residence time distributions on FS, TMS, and PEG5000 surfaces are shown in Figure 2.1 along with experimental fits to eq 2 and parameters given in Table 2.1. These data represent observations of more than 35 000 fibrinogen objects on each type of surface chemistry. Numbers given in parentheses following each value represent uncertainty in the last significant figure given.

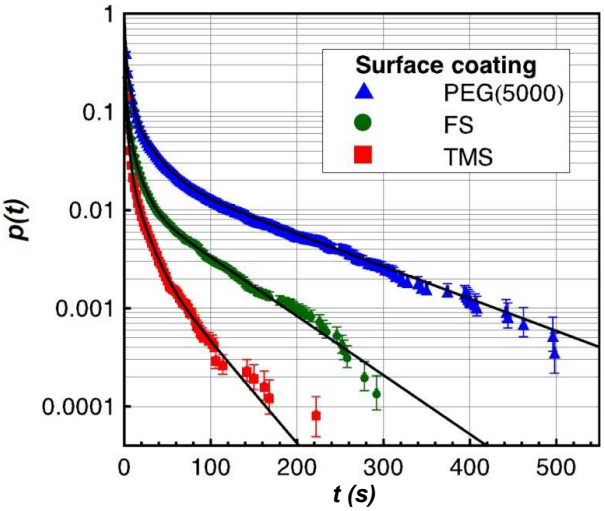

Figure 2.1: Semilog plot of the cumulative residence time distribution of fibrinogen on fused silica that has been functionalized with PEG5000 or TMS or left unfunctionalized after acid treatment. Quadruple-exponential fits to the data (parameters given in Table 2.1) are shown by solid lines.

Table 2.1: Parameters used to fit eq 1 to the cumulative residence time distribution accounting for 4 subpopulations.

population	fused silica		TMS		PEG5000	
	f_i	τ_i (s)	f_i	τ_i (s)	f_i	τ_i (s)
A	0.73(3)	0.59(5)	0.81(2)	0.65(3)	0.54(2)	1.18(4)
B	0.19(3)	2.6(3)	0.16(2)	2.9(2)	0.31(1)	5.0(3)
C	0.069(7)	10.6(6)	0.028(3)	13(2)	0.104(6)	20.4(9)
D	0.0135(5)	69(2)	0.004(2)	45(8)	0.0437(8)	109(1)

Data from a homogeneous fibrinogen population with a single characteristic residence time would appear as a straight line on the log–linear scale used for Figure 2.1. This is clearly not the case for any surface chemistry, and this effect is quantified by use of the parameters in

Table 2.1, where four populations were identified with distinct characteristic residence times. Although population A typically has a characteristic residence time that is shorter than one frame (2 s), the assignment of this parameter comes from the tail of the distribution that extends to longer residence times. On all surfaces, there is an inverse relationship between characteristic residence time and the relative fraction of that population, suggesting that proteins with more favorable surface interactions are increasingly rare compared to those with weaker surface affinity. An obvious explanation for this phenomenon is that larger fibrinogen aggregates have greater surface affinity and are also increasingly rare in solution due to their larger aggregation numbers. Alternatively, one could argue that aggregation is unimportant in the determination of residence time and this phenomenon is caused by preferential adsorption to anomalous “defect” sites. This latter hypothesis is ruled out, however, by the direct correlation between intensity and residence time that is presented in Figure 2.2 and discussed in the following section. That is, objects with longer residence times appear brighter and the intensity of populations A–D increases in roughly integer multiples moving from A to D.

With regard to the population fractions f_i in Table 2.1, little significance should be placed in the comparison of values between different surfaces. Because fibrinogen aggregation in solution may be a kinetic phenomenon, with the protein aggregating over time, details of solution preparation can affect the solution fractions of each aggregate. This means that slight variations in solution preparation could lead to different oligomer fractions that impinge on the surface. Alternatively, one might imagine that surface chemistry somehow affects the observed relative fractions of oligomeric species. This latter hypothesis is ruled out by the observation that experiments done on the same type of surface but on different days frequently had different relative fractions of populations A–D but gave the same characteristic residence times, relative intensity values, and diffusion coefficients.

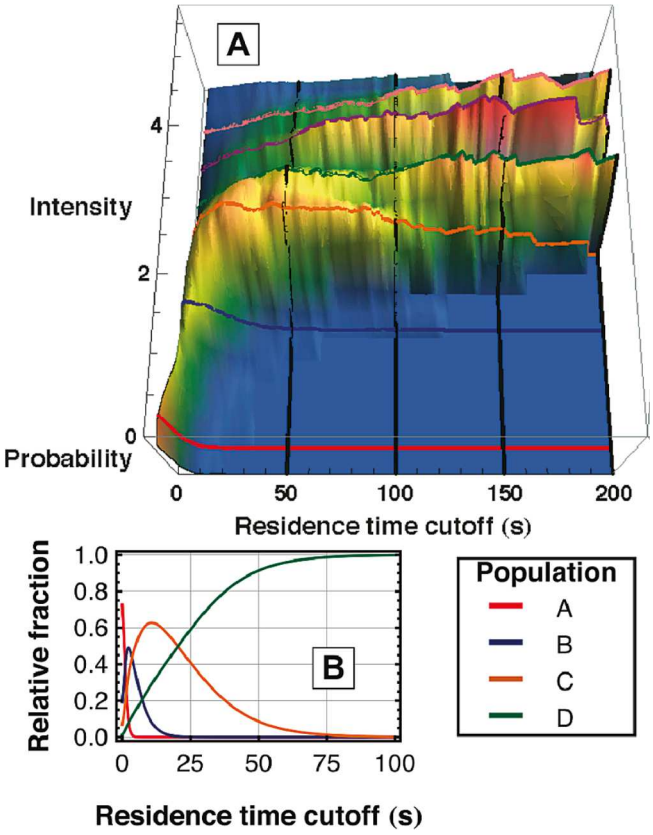

Figure 2.2: Characteristic intensities exist for fibrinogen populations, indicating different aggregation states. (A) Probability distribution of intensities on fused silica, shown as a function of the lowest residence time included in the distribution. Distinct ridges appear in the direction of increasing residence time cutoff that correspond to the values given in Table 2.2. (B) From the fit parameters to residence time data given in Table 2.1, relative fractions of populations A-D are shown as a function of residence time cutoff. This helps to explain the growth and disappearance of the first four ridges in panel A.

2.3.2 Fibrinogen Aggregates Are Responsible for Heterogeneous Behavior

The intensity data for each object provides direct evidence that aggregation is responsible for the heterogeneous behavior observed in the residence time data. In particular, objects with longer surface residence times were observed to have systematically greater fluorescence intensities. In the subsequent analysis, objects were collected that had a residence time greater than a given cutoff value. The probability distribution of fluorescence intensity for these objects was then calculated and normalized. Figure 2.2A shows these intensity distributions as a function of residence time cutoff for the fused silica surface. It is clear that the distributions associated with longer residence time cutoffs are dominated by objects with greater fluorescence intensity. Notably, ridges of approximately constant intensity are visible, suggesting the presence of discrete populations with unique characteristic intensities. Of course, larger fluorescence intensities are likely to be associated with aggregates containing a greater number of protein molecules and therefore more fluorescent labels. At the relatively low

level of fluorophore loading used in these experiments, intraprotein fluorophore quenching is expected to be negligible and interprotein quenching in oligomeric species is expected to be a minor effect. These assumptions predict a linear relationship between intensity and aggregate size to a first approximation.

A direct connection can be made between the populations identified via surface residence time (shown in Table 2.1) and the populations associated with specific fluorescence intensities. Figure 2.2B shows the fractional contribution of each population to the total object distribution as a function of residence time cutoff, calculated from the residence time parameters in Table 2.1. The result is the appearance and disappearance of populations as a function of the residence time cutoff axis, which allows identification of characteristic intensities for these populations (as the intensity coordinate of each ridge backbone) by direct comparison with the visible ridges in Figure 2.2A. Variation in the number of fluorophores per protein in addition to uncertainty in the intensity measurement results in broadening of each ridge but does not shift the intensity value of the ridgeline.

Prominent intensity ridges were observed at approximate positions of 2, 3, 4, and 5 intensity units, where 1 unit is believed to represent the intensity of a monomer. Units were arbitrarily chosen so the ridge with the smallest width in the residence time direction and lowest intensity was assigned a value of 2 units. When the residence time cutoff was 2 s (i.e., all objects were included), an additional peak existed in the probability distribution at approximately 0.5 intensity unit, which is believed to represent the intensity of the large number of objects with a residence time less than the frame acquisition time that consequently appear to be less intense. Although four populations were identified in analysis of residence time data, a fifth, and occasionally a sixth, ridge was also observed in the intensity analysis. They have been identified in Figure 2.2A but not considered in other analyses (e.g., residence time, diffusion) because there were typically not enough of these objects for sufficient statistical significance. The exact values for intensity determinations are given in Table 2.2. It should be noted that the

characteristic intensity values of species C,D, and E are all slightly less than the assumed aggregation numbers for these species. This is likely due to a combination of the following effects: self-quenching between nearby fluorophores on different proteins (as was previously discussed), increased bleaching in objects with longer residence times, and saturation of the CCD camera (primarily with population E). The fact that the intensity ratios are in good agreement with the integer series 2:3:4:5 in many experiments on three different surfaces strongly suggests that the heterogeneity in the residence time data is due to the presence of discrete fibrinogen oligomers, specifically dimers, trimers, and tetramers.

Table 2.2 Relative fluorescence intensity values for populations.[a]

population	fused silica	TMS	PEG5000
A	0.4(1)	0.4(1)	0.6(1)
B	2	2	2
C	2.9(2)	2.8(2)	2.9(2)
D	3.8(2)	3.7(2)	3.9(2)
E	4.7(2)	4.5(3)	5.0(4)

[a] The intensity of population B is defined as 2. Population E was not seen in residence time data and is ignored in analysis of diffusive modes.

To confirm that protein aggregates were present in bulk solution, both analytical centrifugation and size-exclusion chromatography were performed on the labeled human fibrinogen solutions used in this work (see Supporting Information in Appendix B, Figures B1 and B2). Consistent with results from the present residence time analysis and previous experiments on bovine fibrinogen,[16,17] these results showed a large monomer fraction coexisting with a smaller fraction of larger aggregates of dimer size or greater. The fact that oligomers were observed in both labeled fibrinogen studied here and unlabeled fibrinogen studied previously demonstrates that labeling is not the cause of the observed aggregation and that preexisting aggregates in solution are likely in physiological environments.

The idea that fibrinogen oligomers in solution result in interfacial objects with different characteristic residence times sheds new light on the discussion of fibrinogen–surface

interactions. In particular, Wertz and Santore[15] found that relaxation to an irreversibly bound state was slow, on the order of 103 s for hydrophilic and hydrophobic surfaces. This work provides strong evidence that the vast majority of fibrinogen aggregates with aggregation numbers less than 4 do not remain on the surface long enough to relax. As larger aggregates may have exponentially increasing characteristic residence times, these may be the proteins that are more likely to relax to irreversibly bound states. Furthermore, oligomers observed in these experiments must preexist in solution as it is nearly impossible for two proteins to aggregate on the surface, given the extremely low surface coverage used in these experiments and the relatively slow observed diffusion coefficients.

While the work of Wertz and Santore used higher solution concentrations and surface densities than in this work, AFM experiments have also observed slow fibrinogen relaxation of individual proteins.[35] Given the results in this work, it seems likely that monomeric fibrinogen observed by AFM over hour-long time scales represents a vanishingly small fraction of the total number of monomers that interact with the surface. These monomers may have long residence times because they adsorbed to anomalous defect sites, because there is something inherently different about these monomers (e.g., partial denaturation), or because they merely represent the extreme tail end of the monomer population A described in this work. It is worth further study to identify which of these explanations is most likely and the subsequent implications for the interpretation of previous studies on fibrinogen–surface interactions.

In the above-mentioned AFM study and in several others, there is seemingly evidence of a small fraction of fibrinogen aggregates.[35-37] Potential aggregates may appear as individual proteins that are extremely close to each other or as groups where individual proteins cannot be distinguished. Given the results in this work, it may be worthwhile for future AFM studies to compare the properties of these aggregates to those of the monomers. Finally, the work of Siegismund et al.[38] considers the importance of cluster formation due to surface diffusion in the growth of a fibrinogen protein layer. Although their modeling technique considers fibrinogen at

higher solution concentrations and surface densities than in this work, it may be important, in light of the present results, to include the possibility that small clusters may also originate in solution.

The present work has demonstrated the presence of fibrinogen aggregates at low concentrations, and the previous work discussed above suggests that these species are also present at higher concentrations. It therefore seems appropriate to consider the possible effects of fibrinogen aggregates in the interpretation of in vitro adsorption experiments despite the fact that quantitative modeling is obscured by uncertainty in f_i. It is also interesting to consider the possibility that fibrinogen aggregates might exist in blood. In particular, a small fraction of oligomers would be virtually unseen by aggregate-detecting techniques like scattering, centrifugation, or chromatography in such a heterogeneous environment. In light of the present demonstration of the importance of fibrinogen aggregates, this work hopes to motivate further exploration of these aggregates in blood.

2.3.3 Influence of Surface Functionalization

Surface functionalization also influences the behavior of fibrinogen at the interface. Table 2.1 shows that the characteristic residence times are comparable for fibrinogen on fused silica and TMS but that the residence times of fibrinogen on PEG5000 were longer for each population by about a factor of 2. This result is surprising because it is generally believed that PEGylated surfaces resist the adsorption of individual protein molecules as discussed in the Introduction. One possible theory for this observation is that partial insertion of fibrinogen into the PEG layer may increase van der Waals attractions and possibly even permit entanglements between PEG and protein, overwhelming the repulsive forces of steric repulsion and water layer formation. However, this work presents no direct mechanistic evidence for the attraction between PEG and fibrinogen, and further study is necessary on this front. Although the mechanism remains unknown, it is important to note that this observation is believed to be the

first of its kind because the single-molecule techniques employed here directly assess protein–surface interactions, independent of protein–protein interactions, through residence time measurements at extremely low surface coverage.

The broad conclusion that should be drawn from the observation of increased residence times on PEG is that PEG does not appear to decrease protein adsorption at the level of direct protein–surface repulsion or attraction. This is not to cast doubt on the well-established fact that PEG is protein-resistant but rather to suggest that protein–protein interactions may be important in determining ultimate surface coverage and that surface chemistry may indirectly affect these interactions. Surface chemistry may play an indirect but nevertheless important role at this level by influencing the orientation of proteins relative to the surface as well as their secondary, tertiary, or quaternary structures and their subsequent propensity to form a stable protein layer. However, this is not the same as saying that PEG decreases the residence time of individual proteins, a statement that the present work does not support. This is an important distinction because while PEG's protein resistance in physiological environments is well-documented, it is also known that some protein still does adsorb to most PEG-coated surfaces.[23] A more sophisticated understanding of the ability of PEG to permit protein adsorption but prevent protein layer formation may lead to surface coatings with improved biocompatibility.

2.3.4 Diffusion Provides an Independent Assessment of Protein-Surface Interactions

Like residence time analysis, diffusive behavior provides another way to assess fibrinogen–surface interactions. This stems from the fact that an object must detach partially or completely from a solid surface in order to change its lateral position at the interface, as was suggested in previous work on surfactant molecules by Honciuc and Schwartz.[26] Therefore, one might expect some correlation between trends in desorption kinetics and interfacial diffusion coefficients. In order to make a direct comparison, the diffusive behavior of each population A–D was determined. Given the characteristic intensities and residence times of each population

determined previously, both properties were used to assess the population to which a given trajectory belonged. Although, in principle, populations can be identified solely by intensity, in practice the intensity distribution is broad due to heterogeneity in labeling and photophysical effects like blinking and intraprotein self-quenching. As a result, binning by residence time and intensity helps to increase the accuracy of population identification (details of the intensity and residence time ranges used to define populations are given in the Supporting Information in Appendix B, Tables B1–B3). Figure 2.3 shows a direct comparison of mean surface residence time and mean interfacial diffusion coefficient for the four populations on the three types of surfaces studied in this work. There is a dramatic similarity in the trends of these two dynamic properties with population. Notably, on all three surfaces, the mean surface residence time increases by a factor of 4.6 ± 0.9 and the mean diffusion coefficient decreases by a factor of 1.8 ± 0.3 as the aggregation state increases by one protein monomer (i.e., from population A to B to C to D). The fact that these quantities scale so similarly suggests a deep mechanistic connection associated with the energy barriers for full and partial detachment. Future temperature-dependent studies will directly probe these energy barriers.

Interestingly, the diffusion of an individual population was not typically described by simple two-dimensional Brownian motion. For example, Figure 2.4 shows the cumulative squared-displacement distribution for each population on a fused silica surface. Parameter values used in fitting the data with eq 2 are shown in Figure 2.5A. This analysis was repeated for the TMS and PEG5000 surfaces and these parameters are shown in Figure 2.5 panels B and C, respectively. The tabulated values of these parameters are given in the Supporting Information Appendix B, Tables B1–B3.

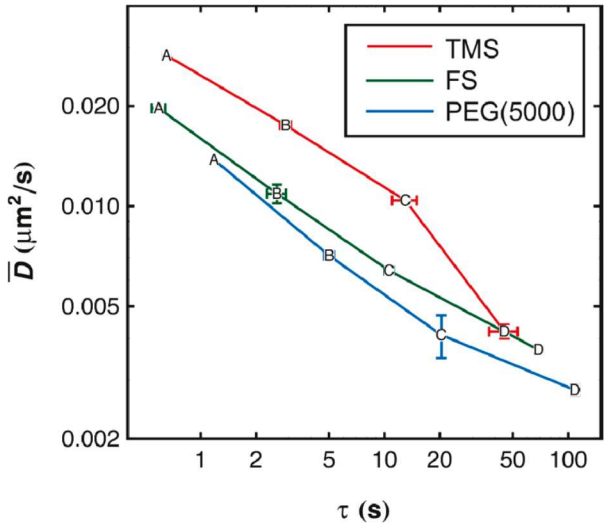

Figure 2.3: Average diffusion coefficient, plotted on a log log scale as a function of characteristic residence time for each population (labeled A–D) on each surface. Error bars represent uncertainty in each coordinate where this value is larger than the data marker. Lines are drawn as a visual guide.

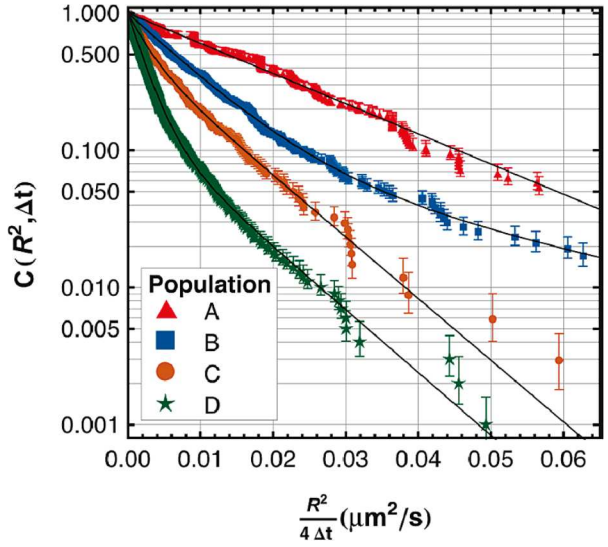

Figure 2.4: Cumulative squared-displacement distribution on fused silica for trajectories that have been binned by intensity and residence time. From top to bottom (moving from A to D), brighter objects with longer residence times diffuse more slowly.

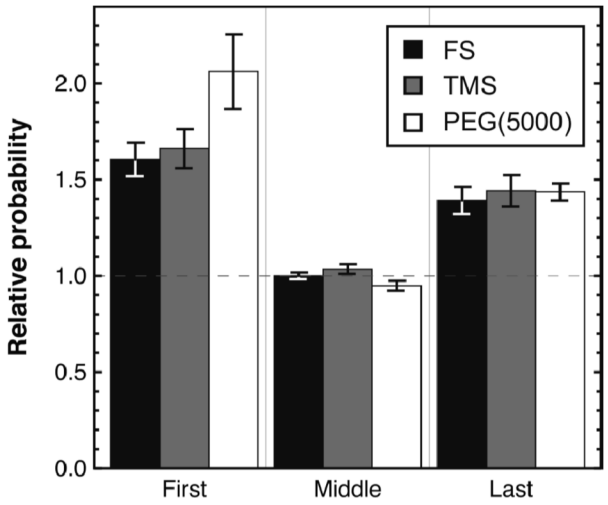

Figure 2.5: Relative probabilities of a "large" step for the first, middle, and last steps in a trajectory on FS, TMS, and PEG5000. Probabilities are relative to the distribution of all observed steps, and error bars represent the error introduced by choosing an arbitrary cutoff for a "large" step.

Multiple diffusive modes are necessary to explain the diffusive behavior of all populations except A. This means that the correlation time for diffusive motion must be at least as long as the frame acquisition time. If diffusive motion were uncorrelated on this time scale, all steps from each diffusive mode would be averaged in a single frame, leading to a single apparent diffusion coefficient. The presence of multiple diffusive modes has previously been linked to different types of association between adsorbate molecule and the surface. For example, a pancake-shaped molecule might associate with the surface in an edge-on or a face-on geometry and might switch between the two on a characteristic time scale.[39] During periods of edge-on association, the barrier to partial detachment would be relatively small, and so the molecule would diffuse more rapidly than during periods of face-on association. Given this picture, multiple diffusive modes are expected for increasingly large aggregates, as there are more ways for a larger protein to interact favorably with a surface than a smaller one.

Although the diffusive behavior as shown in Figure 2.5 is complicated, one can make some generalizations. For example, in all cases there appears to be a “fast” mode with a diffusion coefficient in the range 0.01–0.03 $\mu m^2/s$. Oligomers of all sizes exhibit this mode to some extent, and the diffusion coefficient associated with this mode changes only modestly with aggregation number on a given surface. However, while monomers exhibit this fast mode exclusively, the fast mode represents a systematically smaller fraction of trajectories for progressively larger aggregates. This suggests that while oligomers may occasionally visit configurations where they are weakly bound (and therefore diffuse rapidly), these configurations are increasingly rare for larger aggregates.

Figure 2.5 also exhibits a second cluster of “slow” diffusive modes in the range 0.002–0.006 $\mu m^2/s$, and sometimes a third set of even slower modes for the larger aggregates. Again, the diffusion coefficients within a given set decrease modestly with aggregate size, but there is a clear trend suggesting that the trajectories of larger aggregates systematically exhibit a greater fraction of steps associated with the slower modes. Roughly speaking, it is possible to say that

while monomers and oligomers of all sizes exhibit both fast and slow diffusive modes, the dominant mechanism for the slower interfacial diffusion of larger aggregates is associated with the fact that their trajectories are increasingly dominated by the slower modes. It is also worth mentioning that aggregates were found on TMS surfaces that exhibited diffusive behavior that was anomalous for their aggregation number. While this observation is not important for the discussion at hand, further discussion on these populations is provided in the Supporting Information in Appendix B.

If the various diffusive modes truly correspond to different types of molecule–surface associations, one might expect to see a direct correlation between the diffusive mode and the processes of adsorption and desorption. For example, if faster diffusion corresponds to a weaker binding mode, molecules should be more likely to desorb while executing fast diffusion than slow diffusion. Since the correlation time for diffusive motion is at least as long as the frame acquisition time, it is possible to directly probe this question by looking at the characteristic diffusive behavior immediately prior to desorption. Specifically, objects with a residence time of at least 10 s were collected. Their diffusion steps were divided into four groups: (1) the first step after adsorption, (2) the middle step of the trajectory (as a control), (3) the last step prior to desorption, and (4) a weighted average of all steps. Trajectories for group 4 were weighted so that each trajectory contributed an equal number of statistical steps to the observed diffusive behavior, regardless of the actual length of the trajectory. This was done to mimic the statistical bias induced by taking one step from each trajectory in groups 1–3 but to take advantage of the greater statistics provided by including all observed steps in a trajectory. Diffusive steps for these groups were analyzed by arbitrarily choosing a cutoff value for R^2 to denote a “large” step. The probability of observing this value of R^2 or greater was determined for groups 1–3 and normalized by that of group 4 to get the relative probability of a large step. The results of this analysis are shown in Figure 2.6, where the error bars represent the standard deviation in the calculated relative probability when the large-step cutoff value is varied over a

reasonable range. Here, a reasonable range was determined by identifying the values of R^2 that gave a probability of a large step in group 4 between 0.01 and 0.05. The cumulative squared-displacement distributions for groups 1–4 are shown in the Supporting Information Appendix B, Figure B3. The analogous graph to Figure 2.6, giving the relative probabilities of "small" steps, is not shown, as all probabilities are within statistical error of unity.

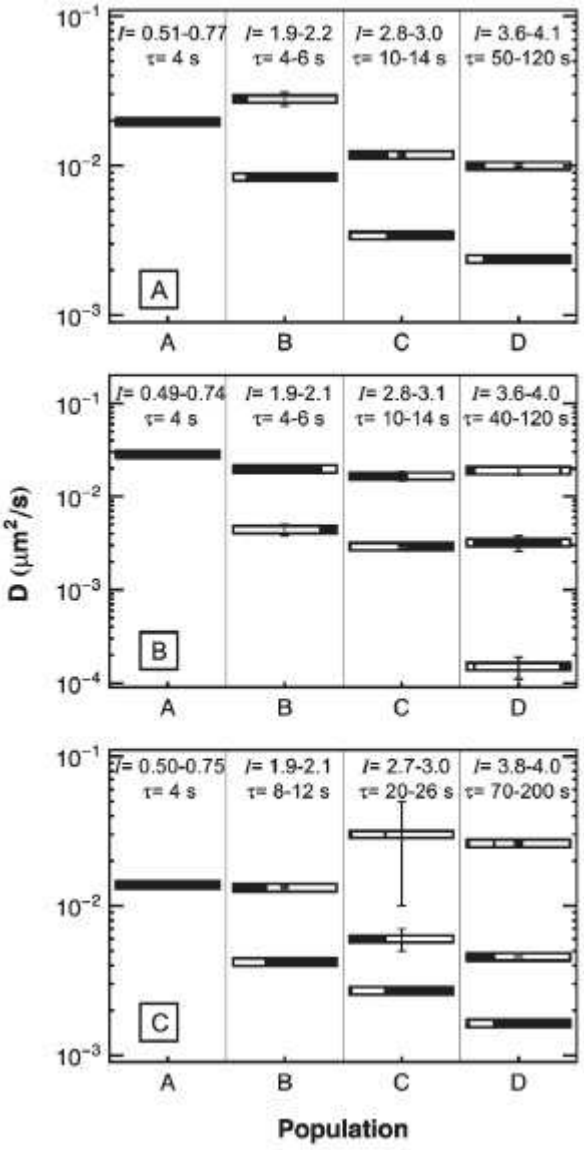

Figure 2.6: Diffusion coefficients for the multiple diffusive modes of populations A–D on different surfaces: (A) FS, (B) TMS, and (C) PEG5000. The black area of each bar represents the fraction of steps observed with the diffusion coefficient given by the bar's position on the vertical axis. The intensity and residence time binning criteria used to define each population are shown along the top of each panel.

From Figure 2.6, it is evident that the first and last steps in a trajectory are more likely to be "large" than all other steps in the trajectory. This is true for all surfaces studied. The fact that the diffusion immediately prior to desorption is fast suggests that desorption is more likely to

occur during periods of fast diffusion and is consistent with the notion that fast diffusion corresponds to relatively weak surface association. The fact that diffusion immediately following adsorption is also fast suggests that an adsorbing molecule does not immediately adopt a favorable orientation on the surface. It may be that favorable surface orientations are easier to come by in larger aggregates, and consequently larger aggregates that interact with the surface are more likely to stick before they diffuse back into solution. These observations also provide an explanation for the data in Figure 2.5, which show that the trajectories of monomers (population A) are dominated by the fast diffusive mode; since the surface residence time of these molecules is small, their diffusion does not have time to become uncorrelated from the fast diffusion that follows adsorption and precedes desorption. In contrast, population D typically has time to settle on the surface and explore slower modes of diffusion.

As discussed above, a comparison of the average diffusion coefficient for each population shows a consistent trend whereby diffusion on TMS is faster than on FS, which is faster than on PEG5000. It is expected that diffusion on the PEG5000 surface would be slowest from both the residence time data and the earlier discussion on the similarity between the fast diffusion mode and desorption, and this is observed in the data. Residence time data also lead to the expectation that fibrinogen should diffuse similarly on TMS and FS, but this prediction is not supported by the data. This discrepancy suggests that protein–surface interactions on TMS and FS surfaces are fundamentally different types of interaction and that it is mere coincidence that their residence times are similar. It is possible that the sum of interactions between fused silica and fibrinogen (such as hydrogen bonding) equals the sum of a different type of interactions between TMS and the protein (such as hydrophobic effects), leading to comparable probabilities for desorption. However, these two fundamentally different types of interactions may allow fibrinogen to diffuse more quickly on TMS than on FS because of the length scales involved in each type of interaction. More specifically, if a hydrophobic patch on fibrinogen can feel an attractive force toward a hydrophobic TMS surface from a distance of several water

molecules (e.g., via water depletion effects), it will diffuse quickly through the near-surface liquid (i.e., parallel to the surface) but long-range attractions will keep it from leaving the near-surface region completely. In contrast, on a hydrogen-bonding surface like fused silica, once fibrinogen is no longer close enough to hydrogen-bond to the surface, it is free to desorb. It should be noted that this is only one possible explanation for the observed results, and further work is necessary to clarify the mechanism of fibrinogen diffusion on each surface. However, this type of analysis illustrates the power of comparing residence time data with diffusion data. While a simplistic view of protein–surface interactions predicts an inverse relationship between residence time and diffusion coefficient, instances where this does not hold true are evidence of more sophisticated interactions that would merit further study through the use of temperature variation to determine activation barriers for diffusion and desorption.

2.4 Conclusions

Single-molecule resolution of fibrinogen-surface interactions illustrates the ability of this technique to unravel complex behavior involving multiple populations with a variety of surface residence times and diffusive modes. In particular, fibrinogen behavior is much more complicated than the conventional picture of a single protein molecule adsorbing to the surface, exhibiting a simple Brownian random walk at the interface, and either desorbing (with a single characteristic residence time) or relaxing to an irreversibly bound state. The single-molecule approach permits strong connections between observable behavior, and the physical significance attributed to these observations is provided by the correlation between different types of information.

Analysis of protein residence times, fluorescence intensities, and diffusive motion has identified soluble fibrinogen aggregates/oligomers with the propensity for varied behavior at the interface. Oligomers with increasing aggregation number were found to have longer surface residence times and to diffuse more slowly. Multiple modes of diffusion were observed for many

of the aggregated populations, indicating that a large protein oligomer has multiple ways to interact with a solid surface. The inclusion of fibrinogen aggregates into the analysis of other types of experiments and models of fibrinogen–surface interactions may help to clarify mechanisms of protein layer formation on biomaterial surfaces.

This work studied proteins that had surface residence times typically less than 600 seconds and therefore cannot provide direct information on long-lived species that may also be important for protein-layer formation. However, these experiments were able to directly assess protein–surface interactions through residence time and diffusion data. The results showed that a monolayer of PEG5000 actually extended the surface residence time and slowed diffusion of fibrinogen relative to a bare fused silica surface (or to a hydrophobically modified surface). This contrast with conventional wisdom regarding the protein resistance of PEG monolayers suggests that PEG's biocompatibility is not primarily a product of its ability to decrease the mean residence time of isolated fibrinogen molecules. We speculate that an important factor in the protein resistance of PEG layers may involve their ability to mediate post-adsorption protein behavior, perhaps by influencing fibrinogen orientation and its propensity to form a stable layer with other proteins via protein–protein interactions in the near-surface environment.

A comparison of fused silica and TMS surfaces indicated that the two chemistries lead to similar surface residence times. However, diffusive data indicated that this was merely a coincidence because fibrinogen exhibited significantly faster diffusion on TMS monolayers than on fused silica, indicating fundamentally different types of interactions on each. Further studies will seek to elucidate the mechanisms of interaction with each type of surface chemistry.

Acknowledgement

This work was supported by the National Science Foundation (Award CHE-0841116) and the National Institute of General Medical Sciences (Grant 1F32GM091777-01). In addition, we gratefully acknowledge support for this research from the NSF Industry/University

Cooperative Research Center for Membrane Science, Engineering and Technology that has been supported via NSF Award IIP1034720. E.L.C. acknowledges support from a National Science Foundation Research Experience for Undergraduates award (EEC-0851849). We also thank Dr. Robert Walder for his efforts in developing the software packages used for data analysis and Professors John Carpenter and David Bain at the University of Colorado at Denver for their help in SEC and AUC experiments, respectively.

2.5 References

(1) Doolittle, R.F. Annu. Rev. Biochem. 1984, 53, 195–229.

(2) Mosesson, M.W. J. Thromb. Haemostasis 2005, 3 (8), 1894–1904.

(3) Hu,W. J.; Eaton, J.W.;Tang, L.P. Blood 2001, 98 (4), 1231–1238.

(4) Tang, L.P.; Eaton, J.W. J. Exp. Med. 1993, 178 (6), 2147–2156.

(5) Sivaraman, B.; Latour, R.A. Biomaterials 2010, 31 (5), 832–839.

(6) Phillips, D.R.; Charo, I.F.; Parise, L.V.; Fitzgerald, L.A. Blood 1988, 71 (4), 831–843.

(7) Watt, K.W.K.; Cottrell, B.A.; Strong, D.D.; Doolittle, R.F. Biochemistry 1979, 18 (24), 5410–5416.

(8) Packham, M.A. Can. J. Physiol. Pharmacol. 1994, 72 (3), 278–284.

(9) Bosco, M.C.; Chan, C.; Brash, J.L. J. Colloid Interface Sci. 1981, 82 (1), 217–225.

(10) Retzinger, G.S.; Cook, B.C.; Deanglis, A.P. J. Colloid Interface Sci. 1994, 168 (2), 514–521.

(11) Schmitt, A.; Varoqui, R.; Uniyal, S.; Brash, J.L.; Pusineri, C. J. Colloid Interface Sci. 1983, 92 (1), 25–34.

(12) Weathersby, P.K.; Horbett, T.A.; Hoffman, A. S. J. Bioeng. 1977, 1 (4), 395–410.

(13) Wertz, C.F.; Santore, M.M. Langmuir 1999, 15 (26), 8884–8894.

(14) Wertz, C.F.; Santore, M.M. Langmuir 2001, 17 (10), 3006–3016.

(15) Wertz, C.F.; Santore, M.M. Langmuir 2002, 18 (3), 706–715.

(16) Kim, S.H.; Haimovich-Caspi, L.; Omer, L.; Yu, C.M.; Talmon, Y.; Wang, N.H.L.; Franses, E.I. Langmuir 2007, 23 (10), 5657–5664.

(17) Okubo, M.; Azuma, I.; Hattori, H. J. Appl. Polym. Sci. 1992, 45 (2), 245–251.

(18) Gref, R.; Luck, M.; Quellec, P.; Marchand, M.; Dellacherie, E.; Harnisch, S.; Blunk, T.; Muller, R.H. Colloids Surf., B 2000, 18 (3-4), 301–313.

(19) Ratner, B.D.; Bryant, S.J. Annu. Rev. Biomed. Eng. 2004, 6, 41–75.

(20) Woodle,M.C. Adv. DrugDelivery Rev. 1995, 16 (2-3), 249–265.

(21) Hamilton-Brown, P.; Gengebach, T.; Griesser, H.J.; Meagher, L. Langmuir 2009, 25 (16), 9149–9156.

(22) Unsworth, L.D.; Sheardown, H.; Brash, J.L. Langmuir 2008, 24 (5), 1924–1929.

(23) Kingshott, P.; McArthur, S.; Thissen, H.; Castner, D.G.; Griesser, H. J. Biomaterials 2002, 23 (24), 4775–4785.

(24) Jeon, S.I.; Lee, J.H.; Andrade, J.D.; de Gennes, P.G. J. Colloid Interface Sci. 1991, 142 (1), 149–158.

(25) Wang, R.L.C.; Kreuzer, H.J.; Grunze, M. J. Phys. Chem. B 1997, 101 (47), 9767–9773.

(26) Honciuc, A.; Schwartz, D.K. J. Am. Chem. Soc. 2009, 131 (16), 5973–5979.

(27) Peanasky, J.; Schneider, H.M.; Granick, S.; Kessel, C.R. Langmuir 1995, 11 (3), 953–962.

(28) Janssen, D.; De Palma, R.; Verlaak, S.; Heremans, P.; Dehaen, W. Thin Solid Films 2006, 515 (4), 1433–1438.

(29) Papra, A.; Gadegaard, N.; Larsen, N.B. Langmuir 2001, 17 (5), 1457–1460.

(30) Sorribas, H.; Padeste, C.; Tiefenauer, L. Biomaterials 2002, 23 (3), 893–900.

(31) Tompkins, H.G. A User's Guide to Ellipsometry, 1st ed.; Academic Press: Boston, 1993; p xv.

(32) Pasche, S.; De Paul, S.M.; Voros, J.; Spencer, N.D.; Textor, M. Langmuir 2003, 19 (22), 9216–9225.

(33) Honciuc, A.; Harant, A.W.; Schwartz, D.K. Langmuir 2008, 24 (13), 6562–6566.

(34) Walder, R.; Schwartz, D.K. Langmuir 2010, 26 (16), 13364–13367.

(35) Agnihotri, A.; Siedlecki, C.A. Langmuir 2004, 20 (20), 8846–8852.

(36) Abou-Saleh, R.H.; Connell, S.D.; Harrand, R.; Ajjan, R.A.; Mosesson, M.W.; Smith, D.A.M.; Grant, P.J.; Ariens, R.A.S. Biophys. J. 2009, 96 (6), 2415–2427.

(37) Cacciafesta, P.; Humphris, A.D.L.; Jandt, K.D.; Miles, M.J. Langmuir 2000, 16 (21), 8167–8175.

(38) Siegismund, D.; Keller, T.F.; Jandt, K.D.; Rettenmayr, M. Macromol. Biosci. 2010, 10 (10), 1216–1223.

(39) Jamadagni, S.N.; Godawat, R.; Garde, S. Langmuir 2009, 25 (22), 13092–13099.

Chapter 3: Apparent Activation Energies Associated With Protein Dynamics on Hydrophobic and Hydrophilic Surfaces

Blake B. Langdon, Mark Kastantin, and Daniel K. Schwartz

(Published April, 2012: Biophys. J 2012, 102 (11), 2625-2633.)

Abstract

Using single-molecule total internal reflection fluorescence microscopy, the dynamics of bovine serum albumin (BSA) and human fibrinogen (Fg), at low concentrations, were observed at the solid-aqueous interface as a function of temperature on hydrophobic trimethylsilane (TMS) and hydrophilic fused silica (FS) surfaces. Multiple dynamic modes and populations were observed and characterized by their surface residence times and squared-displacement distributions (surface diffusion). Characteristic desorption and diffusion rates for each population/mode were generally found to increase with temperature, and apparent activation energies were determined from Arrhenius analyses. Apparent activation energies of desorption and diffusion were typically higher on FS than on TMS surfaces, suggesting that protein desorption and mobility were hindered on hydrophilic surfaces due to favorable protein-surface and solvent-surface interactions. The diffusion of BSA on TMS was apparently activation-less for several populations, while diffusion on FS always exhibited an apparent activation energy. All activation energies were small in absolute terms (generally only a few k_BT) suggesting that most adsorbed protein molecules are weakly-bound and move and desorb readily under ambient conditions.

3.1 Introduction

Protein adsorption at the solid-liquid interface is fundamental to many applications including biocompatible materials, biofilm fouling, biosensing, and protein separations (1, 2). The breadth of applications for this very common yet complex phenomenon has spurred diverse and abundant research (3, 4), yet a complete mechanistic understanding of dynamic surface behaviors is lacking. Fundamentally, interfacial protein dynamics can involve adsorption, surface diffusion, conformational changes, protein-protein aggregation, and desorption. These dynamics are influenced by four types of binary interactions: protein-solvent and surface-solvent (relative to solvent-solvent), protein-surface and protein-protein interactions (2, 5).

Hydrophobic effects are commonly believed to play a prominent role in protein-surface interactions by influencing the reversibility of binding. For example, both the extent of protein adsorption and the degree of protein unfolding are thought to correlate directly with the surface hydrophobicity (4, 6, 7). Recent studies have led to a more nuanced view of this assertion, demonstrating the effects of protein concentration on protein unfolding (e.g. lower surface coverage allows easier surface reorientation and greater unfolding) (8-11). Other studies have specifically focused on the behavior of strongly bound protein populations (i.e. protein that is not removed by rinsing) (12, 13). For example, Fainerman et al. calculated the activation energy for protein desorption from the air-water interface and concluded that protein adsorption is thermodynamically reversible, but may appear kinetically irreversible due to slow desorption rates (12).

Conventional methods widely-used to study interfacial protein behavior include solution depletion (14), surface plasmon resonance (15, 16), quartz crystal microbalance (2), ellipsometry/reflectometry (17, 18), fluorescence recovery after photobleaching (13) etc. These techniques are limited in their ability to provide direct mechanistic insights (19). For example, these methods measure only the *net effects* (e.g. total coverage) associated with multi-step

mechanisms, so interpretations based on these methods are highly model-dependent (20). Also, they measure only the *ensemble average* behavior under conditions that are recognized to be heterogeneous, e.g. proteins exist in a range of states associated with conformation, orientation, and/or aggregation. These experimental limitations (and the desire to infer molecular mechanisms from these data) have unfortunately led to a field that is fraught with examples of over-interpretation and a 'conventional wisdom' that is often unsupported by empirical data. For example, it is often said that certain types of surfaces (e.g. hydrophobic) 'cause' protein unfolding and irreversible adsorption, while other surfaces (e.g. PEG brushes) are 'protein-resistant'. However, several alternate hypotheses are consistent with the *net ensemble-average* behavior that has been measured on these surfaces. For example, it is equally possible that hydrophobic surfaces act as 'collectors' of rare unfolded/aggregated populations that exist in solution. Similarly, there is little evidence that PEG surfaces actually resist adsorption of individual proteins; alternatively they may influence protein-protein associations in a way that inhibits interfacial aggregation.

Previous work in our lab and in other labs employing total internal reflection fluorescence microscopy (TIRFM) has imaged single-molecule dynamics at the solid-liquid interface (20-28). Using a single-molecule approach, one can directly observe an individual protein adsorbing, diffusing, and desorbing from the interface. Single-molecule methods are uniquely able to identify and characterize heterogeneous behavior and populations (21-23). For example, Kwok and coworkers identified two populations of bovine serum albumin (BSA) adsorbing to quartz surfaces based on surface residence times; the majority population (99.3% of objects) resided on the surface for less than 1 min, while the second population exhibited much longer residence times (21). In this work, we separate protein-surface dynamics into distinct populations and elementary modes. Each population or mode is analyzed separately to better elucidate

important surface-protein interactions and behaviors that may lead to protein unfolding, aggregation, and surface fouling surfaces.

To address protein-surface interactions on a mechanistic level, previous work has used ensemble-averaged methods to measure free energies associated with protein adsorption/desorption on hydrophobic and hydrophilic surfaces (12, 14, 29, 30). Figure 3.1 illustrates the conventional view of energies associated with adsorbate-surface interactions. Although dramatically oversimplified, this view provides a useful context to frame a discussion of the phenomena presented below. In particular, this diagram suggests that the activation energy associated with desorption can be greater than the free energy of adsorption (ΔE), and that both adsorption and desorption are activated processes. Figure 3.1 also illustrates the difference between the activation energy for desorption and the activation energy for surface diffusion, where the latter is associated with the corrugation of the surface interaction potential.

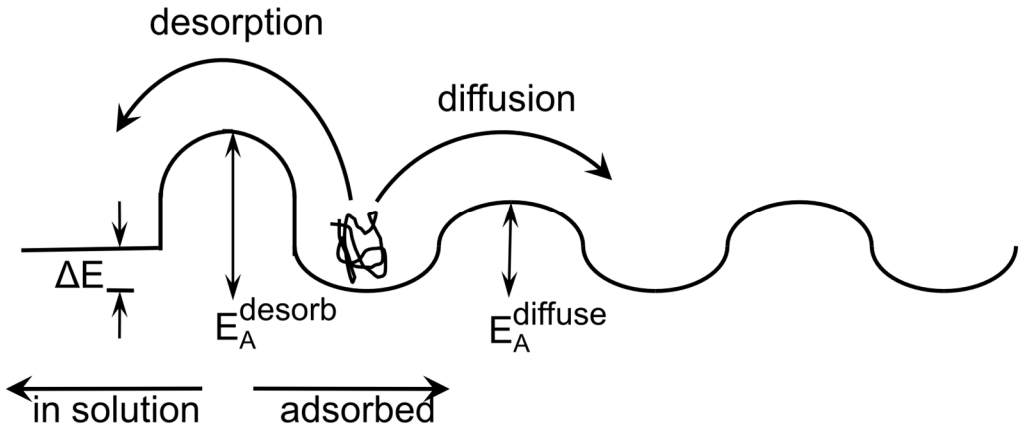

Figure 3.1: Schematic energy diagram illustrating the (simplified) conventional picture of surface adsorption, desorption, and diffusion.

We show here that the true situation is even more complex. Multiple populations and modes are omnipresent in studies of proteins at interfaces, and one must isolate these populations/modes if quantitative measurements of energies are to be mechanistically meaningful. Here, single-molecule TIRFM is employed in order to measure apparent activation

energies associated with specific dynamic mechanisms. Two common proteins, BSA and fibrinogen (Fg) are studied on both hydrophilic FS and hydrophobic, TMS-coated FS. These experiments were done at very low adsorbed protein coverage, much like initial protein adsorption before surface fouling occurs. Under these conditions, protein-protein interactions on the surface are insignificant, allowing us to probe *direct* effects of surface chemistry on protein binding and mobility.

3.2 Materials and Methods

3.2.1 Protein Sample and Surface Preparation

Fg labeled with AlexaFluor 488 and BSA labeled with AlexaFluor 555 were purchased from Molecular Probes, Inc. (Eugene, OR). Fg was labeled on average with 15 fluorophores per protein molecule while BSA was labeled on average with 5 fluorophores per molecule, as specified by the manufacturer. Phosphate-buffered saline (PBS) at pH 7.2 was purchased from Gibco (Carlsbad, CA). Low surface densities required for single-molecule experiments were achieved using protein solutions at concentrations of 10^{-14} and 10^{-12} M on TMS and FS surfaces, respectively. FS wafers were purchased from Mark Optics, Inc (Santa Ana, CA). Cleaning and surface functionalization procedures have previously been described and are available in the Supporting Material. Surface hydrophobicity of TMS was verified by measuring the static contact angle (e.g. TMS contact angle of 95° ± 3°).

3.2.2 Data Acquisition

Protein samples were injected into a temperature controlled flow cell. Observations at the solid-liquid interface were made under static conditions using TIRFM. Several movies were acquired of each sample using acquisition times for individual frames of 200 ms. An object-recognition algorithm involving disk matrix convolution followed by thresholding was used to identify diffraction-limited objects (described previously (26)). The position of an object was determined by its centroid of intensity. Object tracking between movie frames was accomplished

by identifying the closest objects within a 4 pixel (908 nm) distance in sequential frames. Surface residence times were calculated by multiplying the number of frames in which an object was identified by the exposure time of each frame. Further experimental considerations and details are available in the Supporting Information in Appendix C.

3.2.3 Data Analysis

Cumulative residence time distributions were constructed by calculating the probability of objects residing on the surface for a time *t* or greater. Objects with residence times of a single frame were ignored due to sensitivity of object identification for a single frame to noise. The number of objects with a given residence time were assumed to follow Poisson statistics. Desorption kinetics were assumed to be first-order processes such that cumulative residence time distributions can be described by Eq. 1

$$p(t) = \sum_{i=1} f_i e^{-t/\tau_i} \quad (1)$$

where *p(t)* is the probability that a given object has a residence time greater than or equal to *t* and f_i is the relative fraction of all objects represented by population *i*. Each population had a characteristic surface residence time of τ_i, which is the inverse of that population's effective desorption rate constant ($k_{des,i} = 1/\tau_i$). Orthogonal fitting using the distributed maximum entropy method (MEM) and discrete maximum likelihood (ML) algorithm with MemExp program (31) confirmed the number of populations used in the above fitting.

Cumulative square-displacement distributions were constructed by sorting displacement data in ascending order and ranking each data point. Interfacial diffusion was assumed to follow 2D random walks with Gaussian statistics. Accounting for positional uncertainty (due to instrument noise) by methods in ref (32), the cumulative squared-displacement distribution can be described by Eq. 2

$$C(R^2, \Delta t) = \sum_{j=1} x_j e^{-R^2/4(D_j \Delta t + \sigma^2)} \quad (2)$$

where R^2 is the square-displacement radius given Δt, the time window between observations, x_j is the fraction of observed steps in mode j, D_j is the characteristic diffusion coefficient of mode j, and σ is the positional uncertainty.

Eq. 1 and Eq. 2 were used to fit experimental cumulative distributions of residence time and squared-displacement data, respectively, by minimizing the variance weighted by the data point divided by the squared error for the data point.

In order to determine the apparent activation energy (E_a), the desorption rate constant (k_{des}) or diffusion coefficient (k_{diff}) for a given population/mode was calculated at various temperatures. These data were then fit using the Arrhenius relationship:

$$\ln(k) = \frac{-E_a}{R}\frac{1}{T} + \ln(A) \qquad (3)$$

where k is the rate constant for diffusion or desorption, R is the universal gas constant, and A is the (variable) pre-exponential factor. Further details of data analysis can be found in the Supporting Material.

3.3 Results and Discussion

3.3.1 Surface Dynamics Reveals Heterogeneous Populations and Modes

For each protein-surface combination at least three single-molecule movies (frame time: 200ms, length: 1500 frames) were obtained at 6°C, 10°C, 15°C, 20°C, 25°C, 30°C, 35°C, and 40°C respectively. Each object observed in these experiments was characterized by its residence time, mean intensity, and surface trajectory. These data represented more than 40,000 (BSA on FS), 12,000 (BSA on TMS), 7,000 (Fg on FS), and 5,000 (Fg on TMS) identified objects respectively.

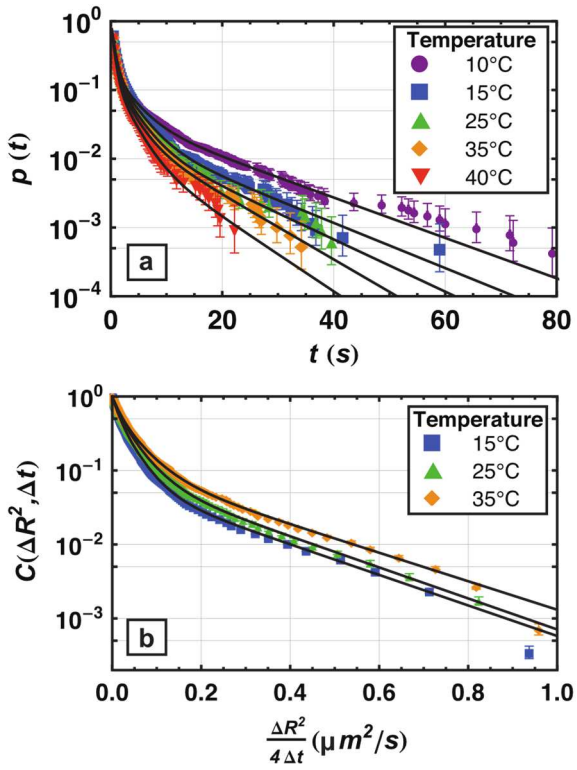

Figure 3.2: Semilog plot of cumulative distribution associated with Fg adsorbed on FS: (a) surface residence times probability distributions, and (b) squared-displacement distributions. Each data series represents protein dynamics at a different temperature of 10, 15, 25, 35, or 40°C. Experimental cumulative distributions are assumed to follow Poisson statistics. The error of each data point represents 68% confidence intervals for a Poisson distribution with mean of the data point.

Figure 3.2*A* shows typical cumulative surface residence time distributions for several temperatures. Assuming an exponential decay of residence time probabilities (as would be observed for first-order desorption kinetics), a homogeneous protein population would appear as a linear relationship with a single characteristic residence time (τ) on the log-linear scaled graph in Figure 3.2*A*. The nonlinearity of the data indicated the presence of multiple populations. This is consistent with previous studies that also found and characterized multiple protein populations (21, 22, 26, 27). At least three exponentials were required to fit each cumulative distribution. The number of distinct populations identified by this method was verified using a convolution of the maximum entropy method and maximum likelihood fitting (described in Supporting Information Appendix C) for the same cumulative residence time fit (Figure C1 in Appendix C) (31). These independent analyses identified the same number of populations for the same cumulative distributions (e.g. four populations for BSA and three for Fg).

As a general rule, the populations identified by surface residence times had certain qualitatively similar characteristics regardless of protein or surface chemistry. Importantly, the

fraction of objects observed in the shortest-lived population (characteristic residence time of 0.4-0.7s) accounted for the majority of objects (~70-80%) and an order of magnitude more objects than was observed in longest lived population (characteristic residence time of 9-75s, 2-9% of objects). The detailed results of fits to cumulative residence time distributions are shown in Table C1 in Appendix C. Using intensity data for each population, we previously demonstrated that each residence-time population roughly corresponded to a different oligomeric state for Fg on TMS or FS and for BSA at the silicone oil-water interface (26, 27). Similar connections between residence time populations and oligomers were explicitly made here for BSA on TMS and FS (Figure C2).

Due to the statistical distribution of fluorescent labels on a given molecule, some variation is expected in the fluorescence intensity within a given oligomer population. However, this variation is not so large as to preclude identification of monomers, dimers, and trimers. Using the expected Poisson statistics, for example, Fg was labeled with 15±4 fluorophores; dimers and trimers would therefore be expected to have 30±5 and 45±7 fluorophores respectively, permitting robust resolution of these species. For BSA, which was labeled with 5±2 fluorophores, the separation from dimers (10±3 fluorophores) or trimers (15±4 fluorophores) was not as complete, but it was still possible to identify ranges of intensity corresponding to each species.

Analyses of surface residence times provide important insights into the mechanisms that can lead to protein film formation or surface fouling. For example, regardless of protein identity or the nature of the surface, isolated monomeric proteins have extremely short residence times and are unlikely to lead to surface fouling in the absence of productive collisions that can lead to larger oligomers/aggregates with systematically longer surface residence times. This suggests that it is important to understand how collisions/aggregation may occur on surfaces, leading naturally to a discussion of interfacial mobility.

Figure 3.2*B* shows typical cumulative squared-displacement distributions, i.e. the probability of finding the observed molecule beyond a circle of radius *R* after some time interval, Δt. On this log-linear scaled graph, where cumulative probability is plotted against $R^2/4\Delta t$, diffusion corresponding to a simple 2D random walk would appear as a straight line. These data, which do not appear linear, indicated the presence of multiple interspersed diffusive modes. For most protein-surface combinations, three Gaussian modes were used to fit each movie's cumulative distribution.

Each system exhibited a very fast diffusive mode (M1) with effective diffusion coefficients of 0.23–0.32 $\mu m^2/s$. Generally speaking, the large 'flights' associated with this fast mode were uncommon (5-10%); with the exception being Fg on TMS surfaces where this mode represented nearly 35% of the diffusive steps. The other modes were much slower (effective diffusion coefficients of 0.03–0.05 $\mu m^2/s$ and 0.007–0.014 $\mu m^2/s$ for M2 and M3 respectively). Typically M2 and M3 both represented substantial fractions of the overall diffusive steps. The detailed results of fits to cumulative squared-displacement distributions are shown in Table C2.

The direct observation, and quantitative analysis, of protein mobility at the solid-liquid interface represents direct counter-evidence to the notion that proteins are immobilized upon adsorption. While the measured diffusion coefficients are much smaller than those observed in solution, they still represent significant mobility. Given the measured diffusion coefficients and residence times, a rough calculation shows that a typical protein object explores an area of ~0.01-0.10 μm^2 between adsorption and desorption, an area that is thousands of times larger than the molecular footprint of the protein itself. This suggests that even at a very low surface coverage of 10–100 molecules/μm^2, multiple protein molecules will simultaneously be exploring the same region of surface leading to possible collisions. Thus one should not think of proteins as being irreversibly immobilized upon adsorption; similarly random sequential adsorption would appear to be an inappropriate model for protein adsorption. Instead, protein objects remain mobile upon adsorption and can explore significant surface areas prior to desorption. Some

previous reports have also emphasized the mobility of adsorbed proteins (13, 33-35). These new observations should further dispel the misconception of protein immobilization upon adsorption.

In contrast with residence time populations, the heterogeneity of the diffusive modes did not correspond directly to protein oligomer populations. In particular, an individual oligomer population often exhibited more than one diffusive modes identified in the total cumulative squared-displacement distribution (Figure C3 in Appendix C). For example, BSA monomers on TMS experienced two diffusive modes with diffusion coefficients 0.048 $\mu m^2/s$ and 0.24 $\mu m^2/s$. The trajectories of brighter objects (i.e. oligomers) were dominated by multiple slow diffusive modes. These observations were similar for both proteins on both types of surface. We speculate that these multiple diffusive modes for a given oligomerization state result from different types of protein associations with the surface, explored further below.

3.3.2 Rates Associated with Individual Populations/Modes Increase with Temperature

The pervasive heterogeneity described above for both residence time populations and diffusive modes emphasizes the importance of identifying and analyzing each of these individual elementary mechanisms separately. For example, if one were to analyze the ensemble-averaged desorption rate (or the mean diffusion coefficient) using transition state theory (12, 29), one could extract an effective activation energy; however, this energy would be physically meaningless since it would not correspond to the actual energy of any particular transition state. The temperature-dependence of an averaged quantity depends both on changes in the rates of individual modes as well as changes in the relative fractions of various modes. However, only the temperature-dependence of rates associated with individual modes has real physical meaning. For example, in previous work it was shown that diffusion coefficients associated with distinct diffusive modes of surfactants may have different characteristic activation barriers (24).

Figure 3.2*A* shows that the overall residence time distribution shifted to shorter times as temperature was increased. Similarly, as shown in Figure 3.2*B*, the cumulative squared-displacement distribution shifted to larger displacements with increasing temperature. These changes with temperature could result from two different trends: (1) the fraction of objects associated with each population/mode may change such that the fraction of objects in the shortest lived population or fastest diffusing mode increases with temperature, or (2) the characteristic residence times and diffusion coefficients change systematically with temperature. Only the latter effect would indicate that surface dynamics are activated processes. Our observations found that the population and mode fractions did not vary over the temperature range within statistical significance. Instead, the characteristic residence times (i.e. inverse desorption rates) and diffusion coefficients changed systematically with temperature for each population/mode.

Figure 3.3 shows Arrhenius plots (i.e. the natural log of the rate constant versus the reciprocal absolute temperature) for the characteristic desorption rate constants of all populations calculated for each protein-surface combination. Again, P1 corresponds to the shortest lived population (fastest desorption rate), and P2, P3, and P4 correspond to the populations with progressively slower desorption rates. Figure 3.4 shows the Arrhenius plots for the diffusion coefficients of diffusive modes associated with each protein-surface combination. These Arrhenius plots show that diffusion also followed Arrhenius behavior (with the exception of M2 for BSA on TMS, which exhibited negligible changes with temperature and will be discussed below in greater detail).

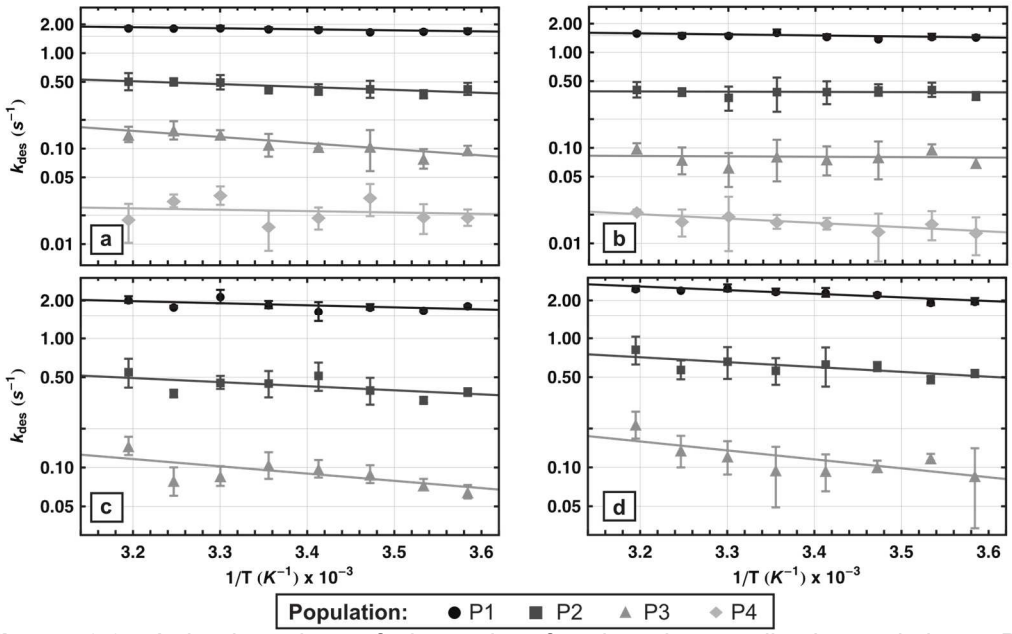

Figure 3.3: Arrhenius plots of desorption for the shortest lived populations, P1; intermediate P2 and P3; and longest lived P4 as annotated. (a) BSA on FS, (b) BSA on TMS, (c) Fg on FS, and (d) Fg on TMS. Error bars correspond to the standard deviation of multiple measurements of $k_{des,i}$.

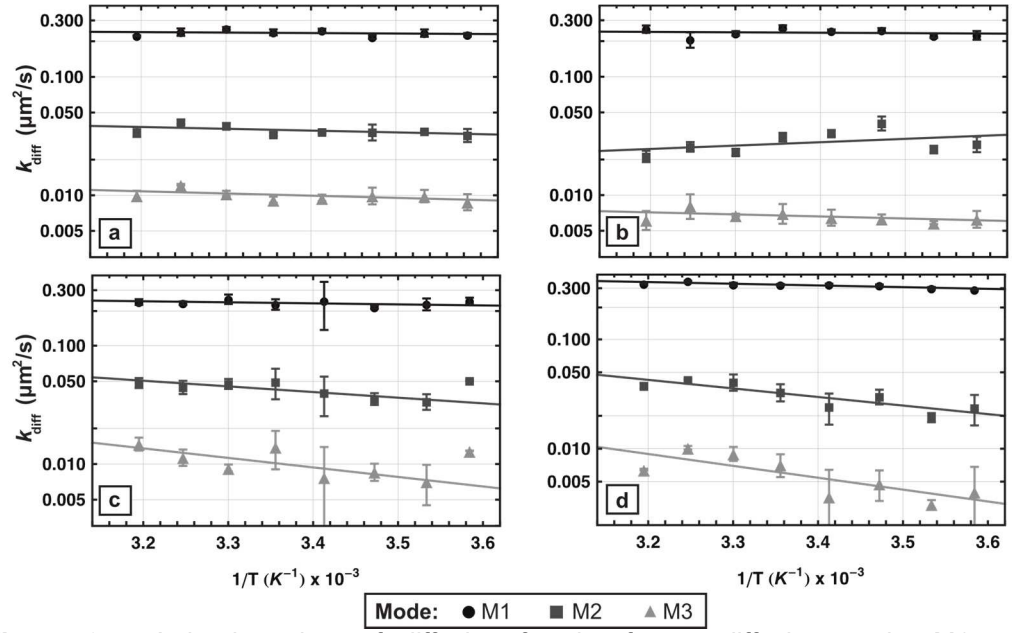

Figure 3.4: Arrhenius plots of diffusion for the fastest diffusion mode, M1, and successively slower M2, and M3 modes as annotated. (a) BSA on FS, (b) BSA on TMS, (c) Fg on FS, and (d) Fg on TMS. Error bars correspond to the standard deviation of multiple measurements of $k_{diff,j}$.

3.3.3 Apparent Activation Energies of Protein-Surface Dynamics

As described above, an analysis of the temperature-dependence for each dynamic mode, population, and protein-surface combination found agreement with Arrhenius behavior for the vast majority of populations/modes. Figure 3.5 and Figure 3.6 depict the apparent activation energies, calculated from this analysis, associated with desorption and diffusion respectively. In the sections below apparent activation energy trends and their mechanistic implications are discussed.

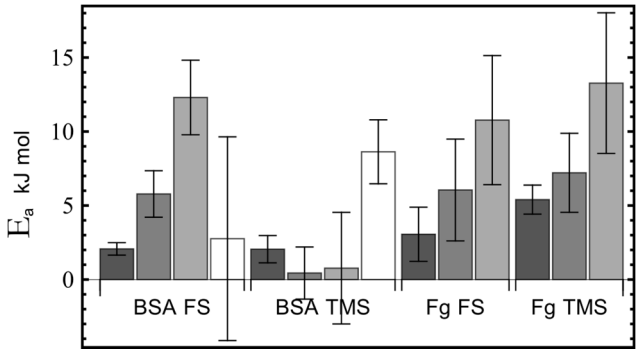

Figure 3.5: Apparent activation energies of desorption for P1 (dark gray), P2 (gray), P3 (light gray), and P4 (white). Error bars represent standard errors associated with fitting Arrhenius temperature trends.

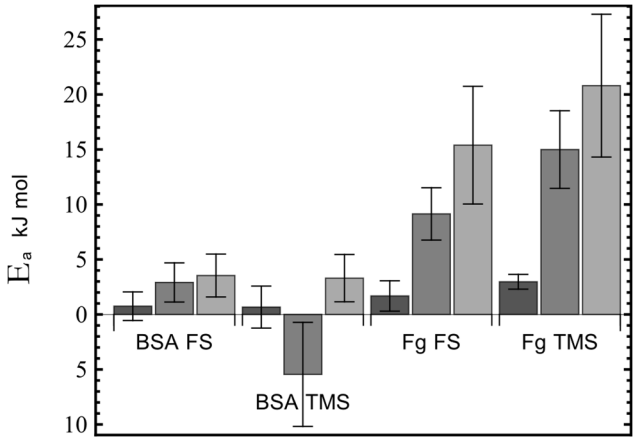

Figure 3.6: Apparent activation energies of diffusion for the fastest mode (M1, dark gray), and progressively slower modes (M2, gray; M3, light gray). Error bars represent standard errors associated with fitting Arrhenius temperature trends.

Apparent activation energy of desorption

Figure 3.5 shows the calculated apparent activation energies of desorption for each population and protein-surface combination. It is important to recognize that the shortest-lived population, P1, represents the vast majority of all objects, and that virtually all monomeric protein objects fall within the P1 population. For all protein-surface combinations, the apparent

activation energy associated with P1 was in the range 2–4 kJ/mol, or <2 $k_B T$. This is a major conclusion for this work; the energy barrier for removal of an isolated protein is extremely weak, regardless of the protein identity or surface hydrophobicity. In general, however, the apparent activation barriers associated with longer-lived populations P2, P3, and P4 (ranging from 2–12 kJ/mol), associated with protein oligomers, increased systematically from P1. Intuitively, larger oligomers are expected to occupy a greater surface area and therefore have stronger overall protein-surface interactions. This would facilitate more opportunities for favorable interactions (e.g. hydrogen bonding, van der Waals attractions) with a greater activation energy required for surface dissociation. These observations were consistent with the notion that monomers and dimers are typically very weakly-bound, and that, therefore, surface fouling relies on the creation of larger oligomeric states.

For BSA the apparent activation energies for desorption from hydrophobic TMS were lower than those for hydrophilic FS and were similar for Fg on both surfaces. This would appear to be in contradiction to the literature observations that the *net ensemble-averaged* protein adsorption increases with increasing surface hydrophobicity, and that on average proteins tend to adhere more strongly to hydrophobic surfaces (3, 4, 36). A previously-proposed rationale for this observation is that proteins more readily unfold and spread on hydrophobic surfaces (3, 37). Wertz and coworkers observed that Fg relaxation to an irreversibly bound state on hydrophobic surfaces was extremely slow (characteristic spreading time of 1425s) (10). However, the residence times observed in this work are much shorter for all protein-surface combinations than this proposed spreading time, so there would appear to be insufficient time for isolated proteins (or small oligomers) to ‘spread’ or unfold before desorption. The small activation energies for desorption from TMS would, therefore, appear to be consistent with the expected weak interactions between the hydrophobic surface and the native protein with predominantly hydrophilic exposure. This explanation also accounts for the observation that differences between BSA and Fg were fairly minimal on both hydrophilic and hydrophobic surfaces. While

BSA is a softer, globular protein that more readily undergoes conformational changes (4), the short surface residence times observed here suggest that unfolding does not occur extensively for short lived species.

We suggest that the apparent inconsistency between previous bulk ensemble-averaged measurements (e.g. extremely slow relaxation, enhanced fouling of hydrophobic surfaces) and the data presented here provides valuable new insights into the mechanisms for protein layer formation. For example, our results show conclusively that, in the absence of protein-protein interactions, direct protein-surface interactions do not typically lead to irreversible adsorption and/or spreading or unfolding of monomers, dimers, etc. Instead, our results suggest that oligomers and aggregates are the long-lived species that ultimately lead to surface fouling. This is consistent with previous observations that protein surface behavior varies greatly with protein concentration (10, 11).

It is therefore critical to focus on the ways in which surface chemistry may influence protein-protein interactions by promoting or inhibiting aggregation on the surface. For example, three different interactions are important in determining the mechanism and progression of layer formation: (1) direct protein-surface interactions in the absence of protein-protein interactions; (2) pairwise protein-protein interactions in the absence of protein-surface interactions; and (3) protein-surface interactions in the presence of protein-protein interactions (a three-body interaction). In this work we have carefully studied the first type of interaction (isolated protein-surface interactions) and found that alone it is incapable of explaining layer formation phenomena, indicating that the second and third types of interactions must be important. Future work will address quantifying these effects indirectly (examining surface dynamics at higher bulk concentrations) and directly (visualizing protein-protein collisions and associations).

Apparent activation energy of diffusion

Diffusive modes have been linked to multiple types of surface associations, molecular surface footprints, and the extent of molecule-surface associations (26, 38). In the context of Figure 3.1, these different types of associations lead hypothetically to different corrugations in the potential energy experienced by the adsorbate molecule as a function of position and orientation on the interfacial plane. For example, for ellipsoidal proteins (or protein oligomers) end-on and side-on associations have been proposed (8, 10, 26). Proteins can potentially switch between the two associations on a characteristic time scale leading to motion characterized by multiple interspersed modes for a single object.

For small molecules, we previously found that mobile surface molecules exhibit two distinct mechanisms of diffusion: (1) a 'sliding' or crawling mode where a molecule stays in direct contact with the surface, or (2) a 'flying' or partial-detachment mode where a molecule briefly detaches from the surface during motion (24, 28). These modes were characterized for fatty acid molecules on TMS, where a single hydrophobic tail-surface interaction, and the associated surface-water interactions, were believed to dictate the mode(s) of diffusion. When considering large protein molecules, a larger number of surface contacts and a more diverse variety of protein-surface interactions presumably lead to the more complex behavior observed here. We therefore hypothesize that heterogeneity associated with protein surface diffusion results from multiple surface association configurations and mechanisms.

Figure 3.6 shows the measured apparent activation energies for diffusion. As with the activation energies associated with desorption of monomers (P1 in Figure 3.5), the activation energies for the diffusion of the fastest mode M1 (often associated with protein monomers and presumably weaker interactions) were again very small in magnitude, typically in the range 0–2 $k_B T$. Thus our data consistently showed that regardless of the protein identity or the surface chemistry, the energy barriers associated with removal and/or mobility weakly-bound protein monomers or oligomers were extremely small.

The activation energies for slower modes M2 and M3, however, exhibited different trends for each surface-protein combination. For Fg on FS, the activation energies associated with diffusion and desorption were similar in magnitude. One might expect that populations/modes with similar activation energies correspond to similar protein-surface interactions. However, as discussed above, a given desorption activation energy is not necessarily correlated to a particular diffusion activation energy. The fact that these energy barriers did correspond (for Fg on FS) suggests that partial-desorption represents the more likely type of diffusion on FS for Fg. Due to the potential for hydrogen bonding with hydrophilic surfaces, stronger surface-solution interactions on hydrophilic surfaces would make displacement of surface-bound water molecules less favorable for hypothetical sliding/crawling modes. Thus, partial-desorption diffusive modes may be more energetically favorable, compared to sliding/crawling modes, on H-bonding surfaces.

The large discrepancy between BSA and Fg diffusion energies on TMS suggests that diffusion on hydrophobic surfaces is highly protein dependent. For BSA the diffusive modes for nearly all modes were activationless (within experimental error) while the diffusive modes for Fg exhibited relatively large activation barriers. These differences suggest that different diffusive modes can result from qualitatively different mechanisms and that the relative favorability of these diffusion mechanisms is protein-dependent. For example, we propose that BSA primarily diffuses on TMS via a sliding mode while Fg motion is dominated by the flying mode. This hypothesis is supported not only by the trends in the activation energies but also in the proportion of steps associated with the various modes. In particular, BSA motion on TMS is strongly dominated by the slowest M3 mode; Fg motion was more balanced between modes, but the fastest M1 mode was the most populated. Sliding modes would appear to be favored on homogeneous hydrophobic surfaces because of the absence of specific short-range interactions, like H-bonding, and this should lead to very small corrugations in the surface

energy. This might explain the low apparent activation energies of BSA on TMS and the prevalence of fast moving Fg on TMS.

Activation barriers are small in absolute terms

The measured activation energies over the 6-40°C temperature range were found to be relatively small for all protein-surface combination and types of dynamics. Previous work in our lab measured activation energies of 5–20 kJ/mol associated with the dynamics of small fatty acid probe molecules (i.e. for adsorption on FS and diffusion on TMS) (24, 25). Multiple protein-surface interactions as well as multiple surface-solvent interactions are expected to contribute to the energy required to move or desorb a protein from the interface. Nevertheless, virtually all of the apparent activation barriers for BSA and Fg were similar or smaller than the barriers for a single fatty acid molecule, or even that of a single hydrogen bond (~15–20 kJ/mol) (39, 40).

This finding is puzzling yet not unprecedented. Protein-surface interaction free energies have been previously quantified using solution depletion (12, 14, 29, 30, 41), molecular dynamics simulations (5), and other methods (12, 42). Many of these studies have indicated small free energies associated with protein adsorption, on the order of 10-18 kJ/mol. Latour and coworkers theoretically and experimentally calculated the free energy of adsorption of lysozyme and Fg to be smaller or equal to a single hydrogen bond for the entire protein at low surface coverage (42, 43). Similarly Noh and Vogler's study of several types of proteins (a range of 10-100 kDa) found all to have a low apparent free energy of adsorption on hydrophobic surfaces similarly on the order of 10-15 kJ/mol (14, 30). This reinforces the idea that isolated protein-surface interactions are relatively weak and therefore that protein-protein interactions must be important in explaining protein-resistant surface mechanisms. Other work in our lab, incorporating higher concentrations of unlabeled protein, provided insight into the role of protein-protein interactions on the layer formation of BSA at the oil-water interface (44). In these experiments, the distribution of diffusion coefficients was observed to broaden, and the spatial

distribution of adsorption rates became more heterogeneous with time, indicating aggregation at the interface (44). It is possible that these phenomena may also be relevant with other proteins and at other interfaces.

3.4 Conclusions

The ability to observe single-molecule protein-surface interactions over a wide temperature range demonstrates the power of single-molecule tracking to isolate complicated protein-surface behaviors into elementary component mechanisms, as well as to determine the effective energies associated with protein interfacial dynamics. The omnipresent proof of heterogeneity in every aspect of these experiments highlights the need for more sophisticated analysis of protein-surface interactions, and calls into question many mechanistic interpretations that are made on the basis of ensemble-averaged methods.

Regardless of the protein identity or surface chemistry, the vast majority of individual protein objects exhibited short residence times (<1s), relatively fast motion, and weak surface binding at low protein concentrations where protein-protein interactions are insignificant. While this is consistent with a growing literature on protein-surface interactions, it stands in strong contrast with previous literature interpretations that often regarded adsorbed proteins as irreversibly bound and immobilized. In contrast, our observations directly showed that isolated protein molecules quickly desorb from the surface in the absence of protein-protein interactions, and that the formation of larger oligomers/clusters is necessary to achieve the longer residence times that ultimately lead to surface fouling. This suggests that isolated native protein-surface interactions, while playing some role in protein adsorption at the interface, are not the dominant drivers for surface protein fouling. Thus it is critically important to consider the effects associated with populations of pre-formed oligomers in solution as well as dynamic formation of oligomers on the surface, especially when considering higher protein solution concentrations necessary for protein fouling. In particular, interactions between proteins within the surface layer may be

strongly influenced by the physicochemical properties of the surface, representing a complex 'three-body' problem.

While surface residence times were relatively insensitive to the details of the protein-surface interaction, the mechanisms of surface mobility exhibited a complex dependence on these interactions. We speculate that these details of surface mobility may play a critical role in defining the process of protein aggregation on the surface. For example, proteins that engage primarily in sliding/crawling diffusion (and surfaces that encourage this mode of diffusion) are more likely to lead to protein-protein collisions that can lead to the formation of surface aggregates. Nevertheless, we suggest that the effects of surface chemistry on protein surface mobility, and more generally on protein-protein clustering, may be a critical determinant of protein layer formation and surface fouling.

Acknowledgements

We acknowledge support by the National Science Foundation (NSF) award CHE-0841116, NSF Industry/University Cooperative Research Center for Membrane Science, Engineering and Technology (NSF Award IIP1034720), the US Department of Energy (DE-SC0001854), and the National Institute of General Medical Sciences (award # 1F32GM091777-02).

3.5 References

1. Wisniewski, N., and M. Reichert. 2000. Methods for reducing biosensor membrane biofouling. Colloids Surf., B 18:197-219.

2. Roach, P., D. Farrar, and C. C. Perry. 2005. Interpretation of protein adsorption: Surface-induced conformational changes. J. Am. Chem. Soc. 127:8168-8173.

3. Rabe, M., D. Verdes, and S. Seeger. 2011. Understanding protein adsorption phenomena at solid surfaces. Adv. Colloid Interface Sci. 162:87-106.

4. Nakanishi, K., T. Sakiyama, and K. Imamura. 2001. On the adsorption of proteins on solid surfaces, a common but very complicated phenomenon. J. Biosci. Bioeng. 91:233-244.

5. Jamadagni, S. N., R. Godawat, and S. Garde. 2011. Hydrophobicity of proteins and interfaces: Insights from density fluctuations. Annu. Rev. Chem. Biomol. Eng. 2:147-171.

6. Ostuni, E., B. A. Grzybowski, M. Mrksich, C. S. Roberts, and G. M. Whitesides. 2003. Adsorption of proteins to hydrophobic sites on mixed self-assembled monolayers. Langmuir 19:1861-1872.

7. Gray, J. J. 2004. The interaction of proteins with solid surfaces. Curr. Opin. Struct. Biol. 14:110-115.

8. Daly, S. M., T. M. Przybycien, and R. D. Tilton. 2003. Coverage-dependent orientation of lysozyme adsorbed on silica. Langmuir 19:3848-3857.

9. Wertz, C. F., and M. M. Santore. 1999. Adsorption and relaxation kinetics of albumin and fibrinogen on hydrophobic surfaces: Single-species and competitive behavior. Langmuir 15:8884-8894.

10. Wertz, C. F., and M. M. Santore. 2002. Fibrinogen adsorption on hydrophilic and hydrophobic surfaces: Geometrical and energetic aspects of interfacial relaxations. Langmuir 18:706-715.

11. Seigel, R. R., P. Harder, R. Dahint, M. Grunze, F. Josse, M. Mrksich, and G. M. Whitesides. 1997. On-line detection of nonspecific protein adsorption at artificial surfaces. Anal. Chem. 69:3321-3328.

12. Fainerman, V. B., R. Miller, J. K. Ferri, H. Watzke, M. E. Leser, and M. Michel. 2006. Reversibility and irreversibility of adsorption of surfactants and proteins at liquid interfaces. Adv. Colloid Interface Sci. 123:163-171.

13. Vieira, E. P., S. Rocha, M. C. Pereira, H. Mohwald, and M. A. N. Coelho. 2009. Adsorption and diffusion of plasma proteins on hydrophilic and hydrophobic surfaces: Effect of trifluoroethanol on protein structure. Langmuir 25:9879-9886.

14. Noh, H., S. T. Yohe, and E. A. Vogler. 2008. Volumetric interpretation of protein adsorption: Ion-exchange adsorbent capacity, protein pI, and interaction energetics. Biomaterials 29:2033-2048.

15. Ostuni, E., R. G. Chapman, R. E. Holmlin, S. Takayama, and G. M. Whitesides. 2001. A survey of structure-property relationships of surfaces that resist the adsorption of protein. Langmuir 17:5605-5620.

16. Sigal, G. B., M. Mrksich, and G. M. Whitesides. 1998. Effect of surface wettability on the adsorption of proteins and detergents. J. Am. Chem. Soc. 120:3464-3473.

17. Prime, K. L., and G. M. Whitesides. 1991. Self-assembled organic monolayers: Model systems for studying adsorption of proteins at surfaces. Science 252:1164-1167.

18. Jackler, G., R. Steitz, and C. Czeslik. 2002. Effect of temperature on the adsorption of lysozyme at the silica/water interface studied by optical and neutron reflectometry. Langmuir 18:6565-6570.

19. Vogler, E. A. 2012. Protein adsorption in three dimensions. Biomaterials 33:1201-1237.

20. Honciuc, A., D. J. Baptiste, I. P. Campbell, and D. K. Schwartz. 2009. Solvent dependence of the activation energy of attachment determined by single molecule observations of surfactant adsorption. Langmuir 25:7389-7392.

21. Kwok, K. C., K. M. Yeung, and N. H. Cheung. 2007. Adsorption kinetics of bovine serum albumin on fused silica: Population heterogeneities revealed by single-molecule fluorescence microscopy. Langmuir 23:1948-1952.

22. Yeung, K. M., Z. J. Lu, and N. H. Cheung. 2009. Adsorption of bovine serum albumin on fused silica: Elucidation of protein-protein interactions by single-molecule fluorescence microscopy. Colloids Surf., B 69:246-250.

23. Honciuc, A., A. W. Harant, and D. K. Schwartz. 2008. Single-molecule observations of surfactant diffusion at the solution-solid interface. Langmuir 24:6562-6566.

24. Honciuc, A., and D. K. Schwartz. 2009. Probing hydrophobic interactions using trajectories of amphiphilic molecules at a hydrophobic/water interface. J. Am. Chem. Soc. 131:5973-5979.

25. Honciuc, A., A. L. Howard, and D. K. Schwartz. 2009. Single molecule observations of fatty acid adsorption at the silica/water interface: Activation energy of attachment. J. Phys. Chem. C 113:2078-2081.

26. Walder, R., and D. K. Schwartz. 2010. Single molecule observations of multiple protein populations at the oil-water interface. Langmuir 26:13364-13367.

27. Kastantin, M., B. B. Langdon, E. L. Chang, and D. K. Schwartz. 2011. Single-molecule resolution of interfacial fibrinogen behavior: Effects of oligomer populations and surface chemistry. J. Am. Chem. Soc. 133:4975-4983.

28. Walder, R., N. Nelson, and D. K. Schwartz. 2011. Single molecule observations of desorption-mediated diffusion at the solid-liquid interface. Phys. Rev. Lett. 107.

29. Sarkar, D., and D. K. Chattoraj. 1996. Kinetics of desorption of proteins from the surface of protein-coated alumina by various desorbing reagents. J. Colloid Interface Sci. 178:606-613.

30. Vogler, E. A., and H. Noh. 2006. Volumetric interpretation of protein adsorption: Mass and energy balance for albumin adsorption to particulate adsorbents with incrementally increasing hydrophilicity. Biomaterials 27:5801-5812.

31. Steinbach, P. J., R. Ionescu, and C. R. Matthews. 2002. Analysis of kinetics using a hybrid maximum-entropy/nonlinear-least-squares method: Application to protein folding. Biophys. J. 82:2244-2255.

32. Kastantin, M., and D. K. Schwartz. 2012. Distinguishing positional uncertainty from true mobility in single-molecule trajectories that exhibit multiple diffusive modes. Microsc Microanal. In press.

33. Tilton, R. D., A. P. Gast, and C. R. Robertson. 1990. Surface diffusion of interacting proteins: Effect of concentration on the lateral mobility of adsorbed bovine serum albumin. Biophys. J. 58:1321-1326.

34. Tilton, R. D., C. R. Robertson, and A. P. Gast. 1990. Lateral diffusion of bovine serum albumin adsorbed at the solid-liquid interface. J. Colloid Interface Sci. 137:192-203.

35. Nygren, H., S. Alaeddin, I. Lundstrom, and K. E. Magnusson. 1994. Effect of surface wettability on protein adsorption and lateral diffusion. Analysis of data and a statistical model. Biophys. Chem. 49:263-272.

36. Ostuni, E., L. Yan, and G. M. Whitesides. 1999. The interaction of proteins and cells with self-assembled monolayers of alkanethiolates on gold and silver. Colloids Surf., B 15:3-30.

37. Wertz, C. F., and M. M. Santore. 2001. Effect of surface hydrophobicity on adsorption and relaxation kinetics of albumin and fibrinogen: Single-species and competitive behavior. Langmuir 17:3006-3016.

38. Jamadagni, S. N., R. Godawat, and S. Garde. 2009. How surface wettability affects the binding, folding, and dynamics of hydrophobic polymers at interfaces. Langmuir 25:13092-13099.

39. Curtiss, L. A., D. J. Frurip, and M. Blander. 1979. Studies of molecular association in H2O and D2O vapors by measurement of thermal-conductivity. J. Chem. Phys. 71:2703-2711.

40. Feyereisen, M. W., D. Feller, and D. A. Dixon. 1996. Hydrogen bond energy of the water dimer. J. Phys. Chem. 100:2993-2997.

41. Vogler, E. A., and H. Noh. 2006. Volumetric interpretation of protein adsorption: Partition coefficients, interphase volumes, and free energies of adsorption to hydrophobic surfaces. Biomaterials 27:5780-5793.

42. Wei, Y., and R. A. Latour. 2010. Correlation between desorption force measured by atomic force microscopy and adsorption free energy measured by surface plasmon resonance spectroscopy for peptide-surface interactions. Langmuir 26:18852-18861.

43. Latour, R. A. 2006. Thermodynamic perspectives on the molecular mechanisms providing protein adsorption resistance that include protein-surface interactions. J. Biomed. Mater. Res., Part A 78A:843-854.

44. Walder, R., and D. K. Schwartz. 2011. Dynamics of protein aggregation at the oil-water interface characterized by single molecule TIRF microscopy. Soft Matter 7:7616-7622.

Chapter 4: Interfacial Protein-Protein Associations

Blake B. Langdon, Mark Kastantin, Robert Walder, Daniel K. Schwartz

(Published November, 2013: *Biomacromol.* 2014, 15 (1), 66-74.)

Abstract

While traditional models of protein adsorption focus primarily on direct protein-surface interactions, recent findings suggest that protein-protein interactions may play a central role. Using high-throughput intermolecular resonance energy transfer (RET) tracking, we directly observed dynamic, protein-protein associations of bovine serum albumin on poly(ethylene glycol) modified surfaces. The associations were heterogeneous and reversible, and associating molecules resided on the surface for longer times. The appearance of three distinct RET states suggested a spatially heterogeneous surface – with areas of high protein density (i.e. strongly-interacting clusters) coexisting with mobile monomers. Distinct association states exhibited characteristic behavior, i.e. partial-RET (monomer-monomer) associations were shorter-lived than complete-RET (protein-cluster) associations. While the fractional surface area covered by regions with high protein density (i.e. clusters) increased with increasing concentration, the distribution of contact times between monomers and clusters was independent of solution concentration, suggesting that associations were a local phenomenon, and independent of the global surface coverage.

4.1 Introduction

Non-specific protein adsorption and deposition at the liquid-solid interface is an important, often problematic, phenomenon in a wide variety of technological applications including biomaterials, food science, pharmaceutical protein stability, membrane filtration, etc.[1–5] Precise control of protein adsorption is necessary in applications involving separation and purification (e.g. chromatography, filtration) and identification (e.g. biosensors, immunological assays). While dynamic protein behavior at interfaces (e.g. adsorption, diffusion, desorption, and aggregation) has been studied extensively for the last few decades, little consensus has developed regarding the role of protein-protein interactions with respect to protein layer deposition.[2,6,7] Although protein clusters have been observed and modeled for some protein-surface systems,[8–14] many models of protein adsorption do not specifically consider protein-protein associations, and little information exists about the dynamics of these associations.

In previous work, single-molecule total internal reflection fluorescence microscopy (SM-TIRFM) was used to directly examine the dynamic behavior of isolated proteins at interfaces (e.g. adsorption, desorption, surface diffusion at ultra-low surface coverage).[15–17] By studying the behavior of "probe" proteins in crowded environments, SM-TIRFM also provided indirect information about protein-protein interactions that lead to protein layer formation.[18,19] These studies have shown that protein behavior under extremely dilute conditions (where protein-protein interactions are negligible) is significantly different than at higher protein concentrations, highlighting the importance of protein-protein interactions for protein layer formation and interfacial aggregation. For example, fibrinogen and bovine serum albumin (BSA) oligomers or aggregates were found to reside on the surface for orders of magnitude longer than protein monomers.[15,17] On nanostructured high-density polyethylene, under conditions of high surface coverage, particularly strong protein-protein interactions between fibrinogen molecules led to extraordinarily long residence times and anisotropic lateral diffusion.[19,20]

Traditional experimental methods have also suggested that protein-protein interactions and aggregation affects the arrangement of adsorbed protein at the interface.[14,21] For example, protein clustering has been observed in atomic force microscopy images.[9–13,22] However, these methods cannot directly observe dynamic protein-protein interactions and cluster formation. From a theoretical perspective, several aggregation mechanisms have been proposed that include spatially heterogeneous protein surface coverage, with areas of high protein density and low protein density.[11,22–27] However, such mechanisms are often omitted from models due to their complexity, and the lack of direct experimental support. In this work, dynamic protein-protein interactions were directly observed using intermolecular resonance energy transfer (RET) and SM-TIRFM.

RET studies have typically been designed to observe *specific* interactions, involving either intramolecular structure (e.g. DNA secondary structure, protein folding)[28,29] or intermolecular binding (e.g. protein-ligand complexes).[30,31] Because protein-protein interactions at interfaces are often non-specific and may not have well-defined geometric requirements, the structurally-specific labeling approaches used to study specific binding are not well-suited for studying this phenomenon. In the current work, proteins are labeled at multiple random sites in order to capture non-specific protein-protein interactions. Stochastically-labeled proteins display fluorophores that are, on average, well-distributed across a protein's surface, insuring that when two proteins interact, at least one RET pair is in close enough proximity for energy transfer to occur. Multiple labels are also useful because many proteins are of comparable size or larger than typical distances over which RET occurs (i.e. the Förster radius). While singly-labeled interacting proteins could orient such that their fluorophores are too far apart for measurable RET to occur, this situation is much less likely with multiple labels. While the presence of multiple labels complicates the quantitative interpretation of specific types of associated objects (e.g. the relative distance between proteins or the number of proteins involved in an associated

object), it does qualitatively capture association events and permit discrimination between broad classes of associated protein objects (e.g. dimers vs. larger clusters).

Using intermolecular RET and SM-TIRFM, this work makes direct observations of the frequency of protein-protein associations, types of associations, and time intervals prior to dissociation (contact times) for BSA on a polyethylene glycol (PEG)-modified surface. Protein-protein interactions were found to be frequent and reversible, and the characteristic time scale for dissociation (i.e. the contact time) correlated with the type of association. Furthermore, the interfacial aggregation dynamics were found to depend in a predictable way upon BSA concentration in solution.

4.2 Materials and Methods

4.2.1 Surface and Protein Solution Preparation

Fused silica wafers were functionalized with a hydrophilic methyl-terminated polyethylene glycol silane (mPEG MW 5000, Nanocs) as described previously.[15] Briefly, cleaned fused silica wafers (e.g. immersed in warm piranha solution and UV-ozone treated) were immersed in a toluene solution of 0.15 mg/ml mPEG for two hours at 60°C then rinsed thoroughly with toluene and isopropanol. The contact angle was measured to be 33 ± 2°, consistent with previous contact angle values measured for PEG-modified surfaces.[15,32,33] This contact angle was previously reported to corresponded to a surface thickness of 2. ± 0.3 nm (measured by variable angle ellipsometry) and a grafting density of 0.28 ± 0.04 chains/nm^2 or 31 ± 4 monomer units/nm^2.[15] This grafting density, which has been shown to confer improved protein resistance to the surface,[34,35] indicated a polymer brush in which the grafting sites were separated by less than two times the radius of gyration such that there were no bare patches of fused silica. Therefore PEG self-assembled monolayers were approximated as homogenous surfaces. Further analysis of the spatial distribution of association locations showed that the number of unique locations for protein-protein interactions increased systematically with

increasing bulk protein concentration, suggesting that cluster formation did not occur preferentially at surface defect sites. A further discussion of this analysis is presented in the Supporting Information.

4.2.2 Single-Molecule Total Internal Reflection Fluorescence Microscopy and Image Processing

Fluorescence from individual proteins was visualized with a custom-built prism-based TIRFM system, flow cell, and Nikon TE-2000 microscope with 60x objective as described previously.[15,36] Illumination was provided by a diode-pumped solid-state laser (Cobalt Samba, 532nm) to excite donor fluorophores. Phosphate buffered saline (Gibco, pH 7.4) solution containing both $1x10^{-6}$ - $1x10^{-7}$ mg/ml donor-labeled BSA (BSA_D, on average 5 Alexa Fluor 555 fluorophores per molecule, Invitrogen) and $2.5x10^{-4}$ – $2.5x10^{-6}$ mg/ml acceptor-labeled BSA (BSA_A, on average 5 Alexa Fluor 647 fluorophores per molecule, Invitrogen) was introduced to the surface via the flow cell. In the mixture of BSA_D and BSA_A, the concentration of BSA_D was selected such that the point spread functions of individual molecules did not overlap. The concentration of BSA_A was one to two orders of magnitude greater than that of BSA_D to yield sufficiently frequent BSA_D-BSA_A associations. BSA_A-BSA_A associations were therefore even more probable, but not observed directly due to the lack of direct excitation of acceptor fluorophores. Flow was stopped after introduction of BSA solution (static or starvation conditions) and the temperature was maintained at 25ºC ± 1ºC. In each experiment, a movie, or sequence of 1000 frames, was recorded with an acquisition time of 200 ms, giving satisfactory signal-to-noise while also providing the ability to capture sufficiently fast protein dynamics. Fifteen or more movies were recorded for each concentration over a 2 h time period. Dynamic protein behavior was not observed to change significantly over this time period.

Dual-channel imaging was accomplished with an Optosplit II (Cairn) containing a dichroic mirror with a nominal separation wavelength of 610 nm (Chroma), a 565 ± 20 nm bandpass filter (Semrock) for the donor channel, and a 685 ± 40 nm bandpass filter (Semrock)

for the acceptor channel. Channels were aligned within 1-2 pixels before experiments using an alignment grid. Fine sub-pixel alignment corrections were made during object identification and tracking analysis by convolving the two channels as a function of an offset and identifying the offset that maximized the intensity-intensity product of the two channels. Essentially, this strategy aligns the channels using objects that appear in both channels as “alignment marks”.

Single molecules trajectories were constructed by identifying objects in each image frame and then linking nearest object positions from frame-to-frame. Objects, appearing as diffraction limited spots, were identified by convolving the image with a disk matrix prior to thresholding, as described previously.[17] Object positions for a given image frame were calculated as the centroid of intensity with a localization precision of ~50 nm. Duplicate objects, which appeared in the same position simultaneously in both donor and acceptor channels, were identified and combined. The center of intensity position used for this combined object was determined by the channel with the better ratio of fluorescence signal to local background. The center of intensity positions were linked together to form a trajectory for each molecule by identifying the nearest object in sequential frames that were also less than 4 pixels (908 nm) apart. A molecule’s intensity for each frame in each channel (donor intensity, F_D, and complementary acceptor intensity, F_A) was calculated as the sum of all pixels assigned to the objectby the thresholding algorithm, minus a local median background contribution for each pixel.

4.2.3 Analysis of Protein-Protein Associations

A BSA molecule (66.5 kDa) can be approximated as an equilateral triangular prism with sides of ~8.0 nm and width of ~3.0 nm respectively.[37] The Förster radius, the radius at which energy transfer is 50% efficient, for the RET pair used in these studies was calculated to be 5.1 nm.[38] Given the number of fluorescent labels per molecule BSA (~5) and BSA’s dimensions, assuming stochastic labeling of protein lysine residues, it is highly likely that any collision

between a BSA_D and a BSA_A molecule resulted in at least one proximal RET-pair. Similarly, it is also likely that donor fluorophores farther from this proximal RET-pair underwent less efficient RET, resulting in non-zero donor fluorescence.

Intermolecular RET was used as a direct indicator of protein-protein associations. Due to the presence of multiple labels on each molecule, any significant emission in the acceptor channel was presumed to indicate an interaction (contact) between one BSA_D molecule and one or more BSA_A molecules. We defined 'significant emission' in the acceptor channel as any observation for which we could state with 84% confidence that $F_A > 0$. In order to do this, we calculated the error (σ) in F_A, considering uncertainty due both to assignment of the per-pixel background subtraction and to an expected Poisson distribution in the number of emitted and collected acceptor photons. Assuming that observations of F_A were distributed normally about their true value, a one-tailed *z*-test allowed us to conclude that $F_A > 0$ (i.e. 'significant emission') with 84% confidence (i.e. $z = 1$) if $F_A > z\sigma$. Thus, any observation of acceptor intensity greater than its uncertainty was deemed 'associated'. We also note that although classification of data into discrete associated and unassociated states requires an arbitrary choice of confidence interval, we found that numerical values to describe associations varied only weakly with confidence interval (e.g. higher confidence intervals slightly decreased the frequency and duration of apparent association events). More importantly, the qualitative trends described in the Results were unaffected by choice of confidence interval.

The extent of RET observed (measured via F_A and F_D) is function of the physical distance between all donor and acceptor fluorophores present in a BSA_D-BSA_A interaction. Tan apparent relative donor-acceptor distance, $d_{app} = (F_D / F_A)^{1/6}$ was examined in order to better understand the potential geometries of protein-protein associations.[38–41] Here, the apparent relative distance provides a convenient quantitative way to display the RET signal, but should not be interpreted as a quantitative distance between multiple RET pairs with stochastically distributed donor-acceptor distances. Nevertheless, d_{app} was found to be a useful index for

qualitatively distinguishing between broad classes of protein-protein interactions without quantifying individual donor-acceptor separations. Three broad categories of RET efficiencies, and association geometries, were identified. Partial-RET associations, where both donor and acceptor emission were observed ($0.5 < d_{app} < 1.7$ in Figure 4.2), were defined as observations in which both F_A and F_D were greater than zero at 84% confidence. Complete-RET associations, representing situations where every donor fluorophore on the BSA_D molecule was close to one or more acceptor fluorophores, were defined as observations where only $F_A > 0$ (shown as $d_{app} < 0.5$ in Figure 4.2). This situation likely occurred only when multiple BSA_A molecules were present (Figure 4.1c). Finally unassociated, zero-RET, events (Figure 4.1a) were defined as trajectory steps where only $F_D > 0$ (shown as $d_{app} > 1.7$, Figure 4.2). An individual molecule may experience any of these states – partial-RET, complete-RET, and zero-RET – for various intervals during its surface residence time.

The amount of time two or more proteins remained associated, or the contact time, was calculated as the number of sequential frames - multiplied by the acquisition time – in which the acceptor intensity was significantly above local background noise. Objects that initially adsorbed in the associated state, and remained associated for their entire surface residence times were excluded from contact time distributions, since it was impossible to quantify the time spent between association and dissociation for these objects. Only associated objects, where association was observed in addition to either dissociation or desorption (with desorption from an associated state also presumed to represent the end of the association), were included in the contact time distribution. Donor fluorophore photobleaching could also erroneously cause apparent desorption as well as apparent dissociation of an associated protein. However, donor fluorophote photobleaching occurred on a time scale that was an order of magnitude slower than observed contact times (see Supporting Information in Appendix C).

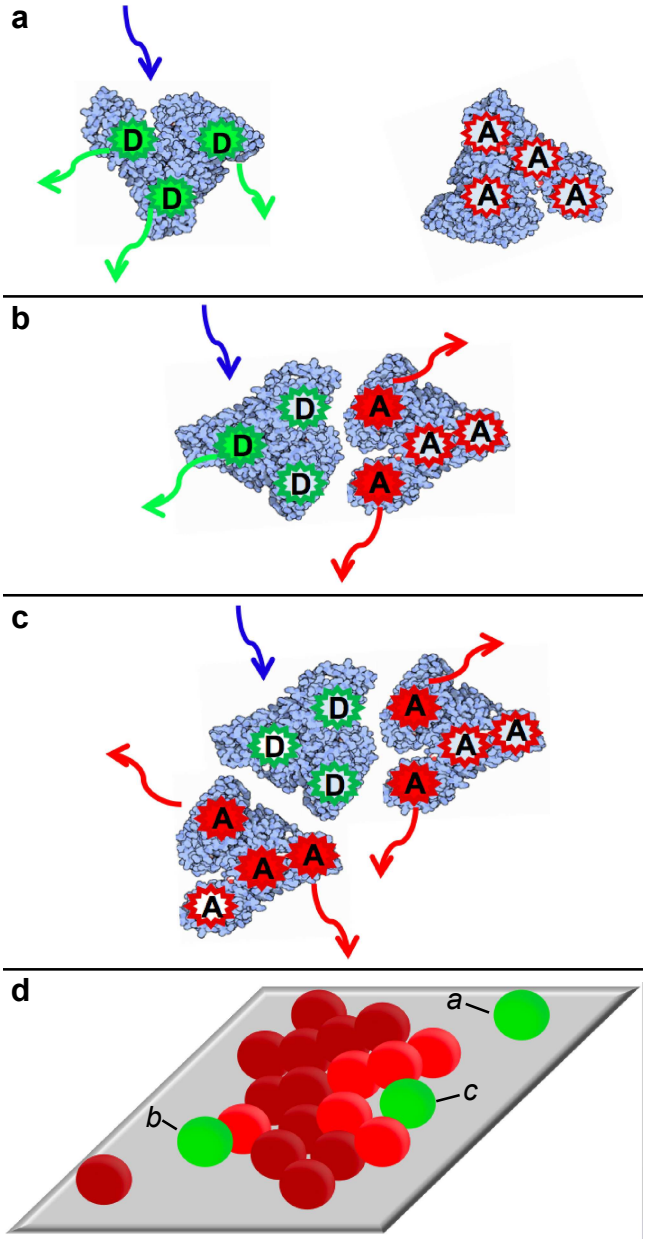

Figure 4.1: Multiply-labeled BSA RET (a) zero-RET, donor fluorescence only; (b) partial-RET, both donor and acceptor fluorescence; (c) complete-RET, acceptor fluorescence only; (d) physical interpretation of RET states a-c.

The cumulative probability, *P,* of observing a given contact time, *t*, or greater was then constructed by determining the number of associations, *n*, with a contact time greater than *t* and normalizing by the total number of associations observed:

$$(1) \qquad P(t) = \sum_{t'>t} n(t') \,/\, \sum_{t'} n(t')$$

For part of the analysis, associations were classified as either partial-RET or complete-RET. Association intervals that contained both partial-RET and complete-RET observations were assigned as either a complete-RET or partial-RET association based on which state represented a larger fraction of the interval. Association intervals with an equal number of partial-RET and complete-RET observations were classified as complete-RET associations.

Like desorption, to a first approximation, dissociation is expected to be a first-order process with respect to the labeled observable species. However, protein-protein interactions were inherently heterogeneity (e.g. orientation, number of proteins). This heterogeneity can lead to varied association and dissociation dynamics and a range of characteristic corresponding kinetic rates. In the case where there are multiple first-order dissociation rates, the cumulative contact time distribution can be modeled by Equation 2.

$$(2) \qquad P(t) = A^{-1} \sum_{i=1}^{M} f_i e^{-\frac{t}{\tau_i}}$$

where f_j is the relative fraction of all contact time associations represented by population *j* and a characteristic contact time of τ_i for *M* populations. The normalization constant, *A*, is not a free parameter, but is given by $A = \sum_{i=1}^{N} f_i e^{-t_{min}/\tau_i}$ such that $f(t)=1$ at $t=t_{min}$, where t_{min} is the minimum observable contact time. A value of A^{-1} corrects for the fact that finite time resolution inherently neglects short-lived associations.[42] The given formula for *A* performs this correction self-consistently by calculating the number of objects that would be neglected based on the model fit to the measurable contact time distribution. Fractions and characteristic contact times were extracted by fitting eq 2 to an experimental cumulative distribution, *P(t)*, described in eq 1. We reported the standard error of the fit for each parameter.

An object's surface residence time (i.e. the time between adsorption and desorption) was calculated by the number of frames in which the object was identified multiplied by the acquisition time of 200 ms. The deactivation of donor fluorophores through photobleaching would also appear as a desorption event. The characteristic time scale of donor fluorophore

photobleaching was quantified by immobilizing BSA_D molecules at the interface and measuring the rate of apparent desorption (see Supporting Information for details). The characteristic photobleaching time of 57 ± 2 s was an order of magnitude longer than the mean characteristic residence time of associating proteins, indicating that photobleaching did not significantly contribute to desorption events. Objects with residence times of two image frames or less were not used in subsequent analysis in order to eliminate false protein identifications that were actually due to stochastic noise. Cumulative residence time distributions from multiple movies for each bulk protein concentration were averaged by weighting each movie by the number of objects observed in that movie. The number of objects with a given residence time follows Poisson statistics with the error shown for each data point representing 68% confidence intervals for a Poisson distribution as described previously.[42] Additionally, previously described corrections were made for the fact that objects with longer surface residence times had a lower a priori probability of being observed in movies of finite length.

4.3 Results

4.3.1 Direct Observation of Protein-Protein Interactions

We observed dynamic protein associations and dissociations under conditions of intermediate protein surface coverage, which was substantially higher than the situation where all proteins are isolated, but also substantially lower than complete monolayer coverage. In these experiments, PEG-modified surfaces were exposed to protein solutions comprised of 10^{-6}-10^{-7} mg/ml of BSA_D and 1-2 orders of magnitude greater concentration ($2.5x10^{-4}$-$2.5x10^{-6}$ mg/ml) of BSA_A. As an upper limit, the volume to surface area ratio in our flow cell ($1.3x10^{-4}$ m), at $2.5x10^{-4}$ mg/ml concentration, would yield 0.033 mg/m^2 if all protein adsorbed. The surface coverage of BSA on our PEG-modified surfaces at $2.5x10^{-4}$ mg/ml was estimated to be 0.0011 ± 0.0004 mg/m^2, consistent with previous observations of low BSA surface coverage, relative to other surface chemistries, on PEG-modified surfaces. Thus the bulk concentrations used were

greater than two orders of magnitude below the theoretical amount of protein required to cover the surface in a monolayer (typically 1-5 mg/m^2).[43] These concentrations allowed us to assess dynamic protein behavior at low overall protein surface coverage, representative of early stages of layer formation sometimes known as the induction phase.[18,43–46] In previous SM-TIRFM experiments of protein adsorption we used extremely low bulk protein solution concentrations (equivalent to a maximum coverage of 1.3x10^{-5} mg/m^2 assuming all protein adsorbed) to ensure isolated protein molecules at the interface.[15–17] The concentrations used here were 10^2-10^4 fold higher, leading to a measurable frequency of protein-protein interactions, which was evident by the observation of dynamic RET signals. Therefore even at the highest BSA_D and BSA_A solution concentration of 1 x 10^{-6} mg/mL and 2.5 x 10^{-4} mg/mL, respectively, we were able to resolve single molecule diffraction limited spots due to the low BSA_D surface coverage (0.098 molecules per μm^2 or 0.0051 molecules per pixel) and to measure protein-protein associations due to relatively high BSA surface coverage (estimated at 25 molecules per μm^2).

After exposing a PEG-modified surface to a BSA solutions described above solutions, no further protein solution was added to the system and movies were taken over a 2-hour period. The surface coverage and distribution of associations did not change significantly over the entire 2 hours. We therefore concluded that, under the conditions studied here, an equilibrium between surface and solution protein populations was quickly established and does not evolve with time (e.g. no observable irreversible cluster growth at these concentrations). Therefore we believe we observed the dynamic exchange of protein monomers and clusters to and from the surface as well as well as association and dissociation of interfacial protein oligomers and clusters under a steady-state, dynamic equilibrium process.

Figure 4.2 shows the distribution of average relative donor to acceptor distances, d_{app}, for each observation in a representative experiment (i.e. F_D and F_A for all steps associated with a given molecule and for all trajectories). Given the criteria for 'significant emission' described above, the d_{app}-value ranges for three RET states – zero-RET, partial-RET, and complete-RET

– can be directly distinguished in the distribution. Due to the complexity of our system (e.g., multiply labeled BSA molecules, diversity of protein-protein orientations, and averaging of different orientations over each observation window) d_{app}-value should not be interpreted as quantitative distances but as a convenient way to qualitatively distinguish structural states. Partial-RET ($F_A > 0$ and $F_D > 0$) and complete-RET (only $F_A > 0$) protein-protein associations ($d_{app} < 1.7$) were clearly differentiated from isolated BSA_D molecules ($d_{app} > 1.7$) exhibiting zero-RET ($F_D > 0$ and $F_A = 0$). In Figure 4.2, step-functions were used to describe extreme d_{app} -values of zero-RET and complete-RET observations as these d_{app}-values could not be calculated.

The distribution of partial-RET d_{app}-values exhibited two peaks. The presence of two apparent peaks (rather than one peak) was an artifact due to the relatively lower probability of identifying objects where $F_D \cong F_A$ (i.e. objects that appear dim in both channels). Indeed the two peaks converged towards one peak when the threshold for identifying objects was decreased (see Supporting Information). While decreasing the threshold allowed us to capture more objects where $F_D \cong F_A$, the erroneous identification of objects increased. Therefore we set thresholds conservatively to minimize artifacts due to misidentifying noise as fluorescent proteins.

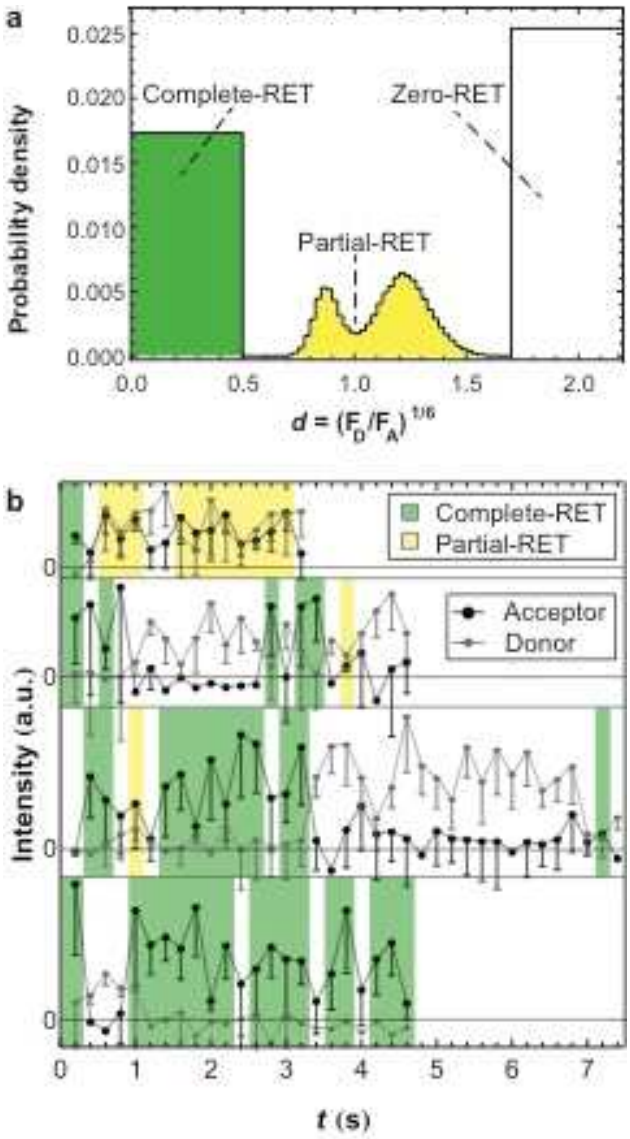

Figure 4.2: (a) Probability distribution of average relative distance, d_{app}, for BSA on PEG at an [BSA_A] = 2.5x10^{-4} mg/ml. The 'box-like' ends of the distribution represent object times where either F_D or F_A was not significantly greater than 0, and the d_{app}-value could not be accurately calculated. A step-function was used to describe these extreme d_{app}-values. The area under each 'box' is proportional to the number of observation where F_D was not significant for $0.0 < d_{app} < 0.5$ and the number of observations where F_A was not significant for $1.7 < d_{app} < 2.2$. (b) Object fluorescence intensities in the acceptor channel and donor channel are shown for several trajectories at [BSA_A] = 2.5x10^{-4} mg/ml. Acceptor channel intensities significantly above 0 represent protein-protein associations and are highlighted as either complete-RET or partial-RET. Zero-RET states are shown in white. Protein-protein association contact times are extracted from many individual object trajectories.

Dynamic protein-protein association and dissociation events were inferred from transitions between the three RET states. The times spent associated, or contact times, were

calculated as the time between association and dissociation or desorption for 10,000-100,000 molecular trajectories. Several representative trajectories of donor and acceptor channel intensity are shown in Figure 4.2b. These trajectories contain examples of both complete-RET and partial-RET associations and zero-RET unassociated intervals. As is common with single-molecule data, the trajectory intensities were sometimes noisy. Because of this noise, any strict criterion used to define 'significant emission' will necessarily make a non-zero number of erroneous state assignments. However, by choosing a reasonable criterion that can be applied in a rigorous algorithm, we were able to process large numbers of trajectories without potentially introducing human bias. The consequences of occasional misidentification are two-fold. First, by erroneously identifying partial-RET or complete-RET one-frame association events (e.g. due to short signal fluctuations) we may overestimate the number of short-lived associations. We might choose to ignore associations that last for only one image except that we may then also be ignoring true short-lived associations. Second, mistaken identification of zero-RET states in the middle of complete-RET or partial-RET would break up long associations into many shorter ones, resulting in an inflated total number of associations and shorter contact times. This concern is greatly mitigated by the fact that our main findings do not rely on a strictly quantitative analysis, instead examining the *relative* frequencies of each state. Keeping these caveats in mind, the characteristic contact times can reasonably be used as order of magnitude estimates.

4.3.2 Protein-Protein Associations were Heterogeneous and Reversible

Interestingly, most proteins remained associated for very short times, with greater than 90% of associated proteins dissociating in less than 2 s. Cumulative contact time distributions, representing the probability that two (or more) proteins remained associated for a time t or greater, are depicted in Figure 4.3. Under the low coverage conditions of these experiments, one might naively expect dissociation to be a first order process (i.e. one associated protein

oligomer/cluster splitting into two or more protein molecules). On this log-linear plot in Figure 4.3, a single first-order (decaying exponential) process would appear as a straight line. Clearly the behavior appears nonlinear on these axes, suggesting that multiple classes of association processes occurred, each with a characteristic contact time or dissociation rate. For example, three populations were sufficient to describe the contact time cumulative distribution in Figure 4.3.

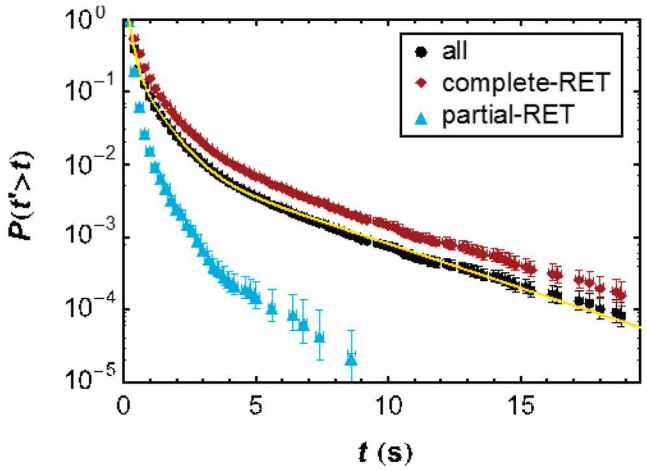

Figure 4.3: Cumulative contact time distributions of BSA (2.5 x 10^{-4} mg/ml) on PEG for all associations, only complete-RET associations, and only partial-RET associations. Error bars represent the Poisson distribution confidence interval of 68%. The yellow line is a fit to the data for all associations using equation 2 with M = 3.

The majority of dissociation events belonged to the population with the shortest characteristic contact time, and successively longer contact times represented smaller and smaller fractions of events (see Table 4.1). At a BSA_A concentration of 2.5x10^{-4} mg/ml (shown in Figure 4.3) 88.3 ± 0.2% of the association events exhibited a characteristic contact time of 0.127 ± 0.002s, 10.3 ± 0.2% of the events dissociated with a characteristic time of 0.75 ± 0.02s, and the remaining 1.4 ± 0.1% had a characteristic time of 4.4 ± 0.1s. Notably, as the bulk concentration decreased, the fraction of short-lived associations increased, as shown in Table 4.1. The contact time distribution shown in Figure 4.3 represented 65,588 dynamic associations, allowing relatively rare, long-lived associations to be characterized with statistical significance.

Table 4.1 Association population fractions and characteristic contact times for each bulk BSA_A concentration.

	$[BSA_A]$					
	$2.5x10^{-4}$ mg/ml		**$2.5x10^{-5}$ mg/ml**		**$2.5x10^{-6}$ mg/ml**	
population	f_i	τ_i (s)	f_i	τ_i (s)	f_i	τ_i (s)
1	0.883(2)	0.127(2)	0.948(2)	0.113(2)	0.971(2)	0.103(1)
2	0.103(2)	0.75(2)	0.045(2)	0.52(2)	0.026(2)	0.44(2)
3	0.014(1)	4.4(1)	0.0075(3)	2.68(6)	0.0022(2)	2.26(9)

It is interesting to note that the majority of associations exhibit a characteristic contact time that was less than the frame rate of 200ms. Indeed, this suggests that many short-lived associations were presumably not detected. However, this time resolution was sufficient to allow us to identify associations with contact times on the order of 200ms or greater that belonged to this short-lived population. Thus it was possible to determine the characteristic contact time for the entire short-lived population (according to eq 2) based on the tail of this population.

We found that the association state (i.e. complete-RET or partial-RET) greatly influenced the contact time. In particular, complete-RET associations accounted for all contact times longer than 10 s in Figure 4.3. Importantly, while complete-RET contact times were longer, partial-RET associations accounted for the majority of associations. For example, at $[BSA_A] = 2.5x10^{-4}$ mg/ml, partial-RET associations accounted for 65 ± 9% of all dynamic associations and this fraction rose with decreasing $[BSA_A]$.

4.3.3 Protein-Protein Associations Led to Longer Surface Residence Times

Proteins that associated at some point during their surface residence time, on average, resided on the surface longer than proteins that remained unassociated for their entire surface residence time. Previous work in our group had shown that dimers and larger oligomers resided on the surface for significantly longer time intervals than monomeric protein.[15] In the current work, we found that protein oligomerization was dynamic, allowing us to directly compare the

surface behavior of objects that dynamically associated (olibomer formation) to those that remained unassociated (monomers). Molecular trajectories that underwent at least one association event resided on the surface for 3-4 times longer on average and accounted for all surface residence times longer than 10 s (Figure 4.4). Because interacting and associated proteins remained on the surface much longer, they contribute disproportionally to the total surface coverage. These findings support the notion that protein-protein interactions are crucial in explaining protein interfacial phenomena at high surface coverage (i.e., protein layer formation).

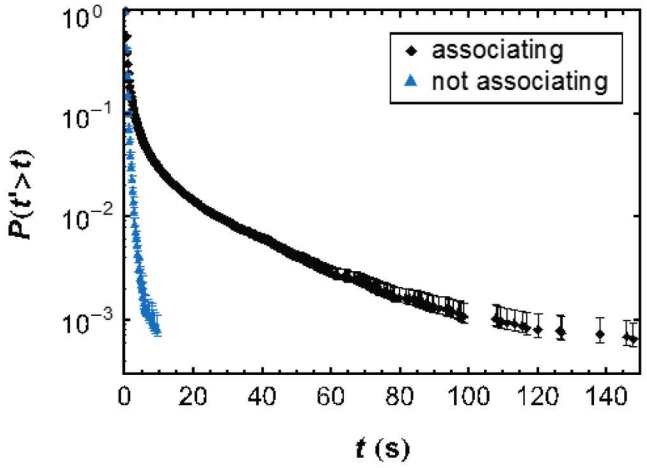

Figure 4.4: Cumulative surface residence time distribution of objects associated at some time during their trajectory and those that remained unassociated for their entire surface residence times for a [BSA_A] = $2.5x10^{-5}$ mg/ml.

4.3.4 Fraction of Clusters and Free Monomers Changed Systematically with Protein Concentrations

To examine the effects of surface coverage on protein-protein interactions, bulk protein solution concentrations were varied by 2 orders of magnitude. The average fraction of time a molecule spent in the complete-RET state ($t_{complete}$), partial-RET state ($t_{partial}$), or zero-RET ($t_{unassociated}$) state was quantified for each concentration in Figure 4.5. These fractions were calculated by counting the number of observations of all steps of all trajectories in each state, including molecular trajectories that were either unassociated (monomers) or associated

(oligomers/clusters) for their entire trajectories, and normalizing by the total number of observations. Two clear trends emerged: (1) the fraction of time molecules spent unassociated decreased with increasing concentration; and (2) the fraction of time molecules spent completely associated increased with increasing concentration. The latter trend could indicate either that protein-cluster interactions were more frequent or longer-lasting at higher surface densities. However, as we discuss below, Figure 4.6a shows that the complete-RET contact times were similar across all concentrations. Thus, protein-cluster interactions became more frequent at higher surface density, and this was likely due to an increasing number density of clusters with increasing surface coverage. Further analysis of cluster locations did indeed increase with increasing bulk protein concentrations (Supporting Information in Appendix D).

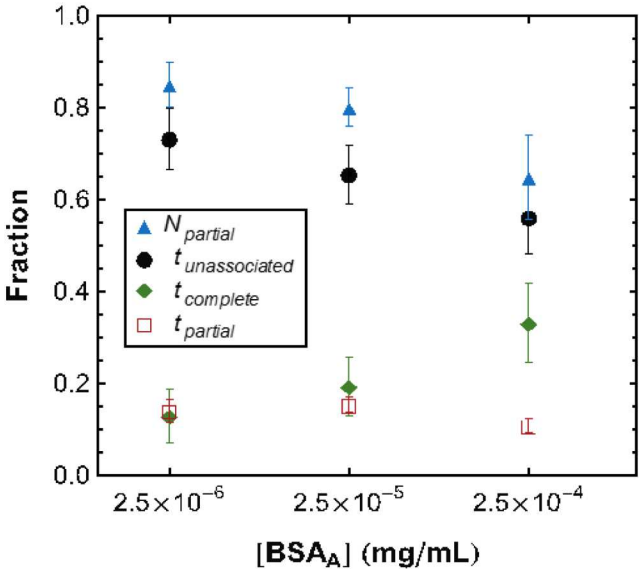

Figure 4.5: Effects of total BSA concentration. Average fraction of time spent in complete-RET associated ($t_{complete}$), partial-RET associated ($t_{partial}$), and zero-RET unassociated ($t_{unassociated}$) states as a function of bulk BSA_A concentration. The average number fraction of all associations that were partial-RET associations ($N_{partial}$) is also shown. Error bars represent the standard deviation between movies for experiments at a given concentration.

Unlike the case for complete-RET associations, the fraction of time spent partially associated remained relatively low, at 10-15%, and did not exhibit a clear trend as bulk concentration varied. Although higher surface coverage implies that more proteins are available

to interact, the partial-RET state must compete with the longer-lasting complete-RET state. Indeed, Figure 4.5 shows that the relative number of partial-RET associations ($N_{partial}$) decreases with increasing concentration. Our data suggest that proteins added to a cluster-laden surface preferentially associate with clusters in much the same way that surfactant monomers form micelles above a critical concentration. Ultimately we would expect partial-RET states to be absent at complete monolayer coverage, since cluster formation, unlike micellization, is not necessarily self-limiting.

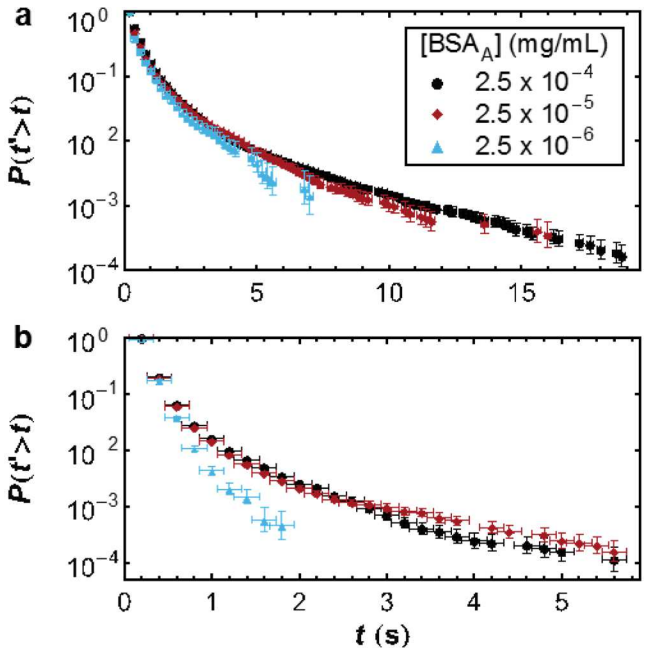

Figure 4.6: Contact time cumulative distribution for (a) complete-RET associations and (b) partial-RET associations for each bulk BSA_A concentration.

Figure 4.6b shows the cumulative contact time distribution for partial-RET associations at different bulk concentrations of BSA_A. At the lowest concentration, contact times followed nearly a mono-exponential decay, but heavier tails of the contact time distribution indicated the presence of some longer-lived partial-RET associations at higher BSA_A concentrations. Thus, we hypothesize that partial-RET interactions are mostly monomer-monomer at the lowest BSA_A concentration but that some BSA_D monomers interact with the borders of larger clusters at

higher BSA_A concentrations. In these proposed partial-RET border interactions, even though a BSA_D molecule only interacts closely with approximately one BSA_A at a time, it may interact sequentially with different BSA_A molecules in the cluster, thereby increasing the total amount of time it spends associated with the cluster.

4.4 Discussion

The surface coverage in these experiments was two to 4 orders of magnitude below that required for full monolayer coverage yet high enough to observe protein-protein associations. Because the surface was only partially covered with protein, we envision a surface with distinct local environments: areas with high local surface density (i.e. protein clusters) and areas with low surface density (where isolated monomers interact directly with the surface). This picture is consistent with previous observations of BSA clustering at the oil-water interface and other proteins at the solid-liquid interface.[12,18,21,22,26,27]

We propose that the observation of a partial-RET event versus a complete-RET event was related to the number of proteins involved in the association (as shown schematically Figure 4.1). Because proteins are labeled with multiple fluorescent dyes, complete-RET is extremely unlikely for an individual BSA_D-BSA_A interaction because some donor fluorophores will always be far (relative to the Förster radius) from the nearest acceptor. A similar situation would result when a BSA_D molecule associates with the protrusion of a larger cluster of BSA_A molecules. If, however, a BSA_D molecule interacts simultaneously with multiple BSA_A molecules, it is possible for each donor fluorophore to abut an acceptor fluorophore, leading to a high-RET situation where little or no donor radiation is emitted. In this scenario, partial-RET events are proposed to represent dynamic dimers or a BSA_D molecule interacting with the edge of a BSA_A cluster. Complete-RET events are proposed to represent a BSA_D molecule interacting with multiple BSA_A monomers, oligomers, or larger clusters.

This interpretation of partial-RET and complete-RET is also consistent with contact time observations (Figure 4.3). One might expect two interacting proteins to remain associated for less time than multiple proteins or protein clusters. Indeed, partial-RET contact times are significantly shorter-lived than complete-RET contact times. While some longer-lived partial-RET associations are observed at high concentrations (see Figure 4.6b), it is clear from Figure 4.3 that the partial-RET state is dominated by the short-lived association.

Heterogeneous surface coverage models generally predict that the ratio of surface area occupied by protein clusters to the area occupied by monomers will change with protein surface coverage. Intuitively, we expect to see more high density, cluster regions at higher concentrations, and this matches observations made in this work. The average fraction of time spent in complete-RET states (high density/clusters), as well as the number of unique cluster locations (see Supporting Information), did indeed increase with increasing bulk concentration while the time spent in the zero-RET state decreased (Figure 4.5).

Interestingly, contact times of complete-RET associations were essentially independent of concentration (Figure 4.6a). Similarly, partial-RET contact times were similar for the two higher concentrations tested in this work (Figure 4.6b). Therefore, we propose that BSA_D-BSA_A interactions within a cluster depend primarily on the local environment and are independent of the global surface coverage. Thus, the number or size of clusters might change with concentration but the dynamics in these local environments remain relatively constant.

Ultimately these findings support a nucleation and growth model of BSA at protein surface coverage below that of a close-packed monolayer. A nucleation and growth model of surface coverage has been proposed and developed for many different interfacial phenomena including epitaxial growth and self-assembled monolayer growth.[47–49] Similar models have been applied to protein crystallization in solution as well.[50,51] Surface clustering has been proposed previously for protein surface layer formation, and data from optical waveguide lightmode spectroscopy and atomic force microscopy experiments have indicated the presence of surface

clusters.[11,12,21,22,24,46,52,53] Due to poor spatial or temporal resolution of these techniques, it has been difficult, until now, to make dynamic *in situ* measurements of cluster formation. This capability, demonstrated in the present work, helps to address the underlying mechanisms of surface clustering in protein layers.

Three cluster formation mechanisms have previously been proposed: (1) oligomer adsorption from solution, (2) cooperative adsorption of protein molecules onto existing clusters, and (3) protein adsorption and surface diffusion to clusters.[7,12,24] Kastantin et al showed that oligomers formed in solution adsorbed to the interface, demonstrating that mechanism 1 is feasible and that mechanism 2 is also possible, although it was not directly tested.[15]

Protein surface mobility has generally been ignored in adsorption models, mainly because protein surface mobility has not been extensively studied. The implicit assumption of surface immobility has usually led to a preference for mechanism 2 over mechanism 3.[26,27] However, lateral protein diffusion has recently become more widely acknowledged. An upper limit of protein mobility has been measured with fluorescence recovery after photobleaching (FRAP) techniques on the order of 10^{-9} – 10^{-10} $cm^2\ s^{-1}$.[54–57] Our lab has observed protein surface diffusion and quantified surface diffusion distributions for fibrinogen and BSA on several surfaces, where monomers exhibit diffusion coefficients on the order of 10^{-9} – 10^{-10} $cm^2\ s^{-1}$, consistent with FRAP measurements.[15,16]

In the present work, molecules moved on the surface with an averaged diffusion coefficient of 4.5 ± 0.1 x 10^{-10} $cm^2\ s^{-1}$ (see Supporting Information). This diffusion coefficient implies that a single BSA_D molecule collides with at least one BSA_A molecule every 1 s given a surface coverage 25 molecules/μm^2 at a [BSA_A] = 2.5 x 10^{-5} mg/mL. Consistent with this estimations, a high frequency of dynamic association and dissociation events were observed (~60% of all object trajectories experienced at least one association or dissociation event). Observation of protein diffusion and dynamic protein association at the surface clearly show that mechanism 3 is important to include in any mechanistic picture of surface clustering under these

solution and surface conditions. Certainly the molecular mobility might be expected to change as the surface becomes increasingly covered by an incipient protein layer, and in principle this might be probed by following fluorescently labeled proteins in the presence of very high concentrations of unlabeled protein. In fact, we have performed such experiments, and have observed continued mobility even at high surface coverage. However, these observations are difficult to interpret due to the inability to explicitly distinguish between molecules adsorbed directly to the surface and proteins adsorbed to the protein layer itself. The later process is insignificant at the low surface coverage utilized for the RET experiments reported here, but becomes increasingly important at high surface coverage.

Based on this experimental evidence, we propose a mechanism whereby individual proteins can adsorb to a surface, diffuse to, associate with, and/or dissociate from a cluster, and desorb from the surface. This is consistent with the mechanism proposed by Kim et al.[12] who hypothesized that clusters formed when lysozyme molecules diffused slowly on a mica surface and collided with other adsorbed lysozyme molecules. A similar, more detailed mechanism was proposed for BSA at the liquid-liquid interface that included adsorption, nucleation, growth, and desorption (dissociation was ignored).[18] Our observations indicate that this mechanism applies to solid-liquid interfaces as well. However, clusters may form and grow more slowly at the solid-liquid interface due to slower diffusion and the ability of clusters to dissociate.

4.5 Conclusions

Intermolecular RET and SM-TIRFM was used to identify three distinct RET states for donor-labeled BSA diffusion on a PEG monolayer: partial-RET associated, complete-RET associated, and zero-RET unassociated. The frequency of protein-protein associations and time intervals of associations (contact time) were quantified by observing transitions between these three states. Protein-protein associations were shown to be both heterogeneous (partial-RET and complete-RET associations exhibited different contact times) and reversible (90% remained

associated for 2 s or shorter) and proteins that underwent associations exhibited increased surface residence times. Therefore, not only are protein-protein interactions on the surface dynamic, these interactions can also result in increased time for direct protein-surface interactions that have been proposed to drive protein unfolding over relatively slow time scales.[53,58]

At the partial surface coverage conditions used here, the surface distribution of proteins was heterogeneous, consisting of local environments of high protein density (clusters) and low protein density (free monomers) and the relative fractions of clusters and free monomers were surface coverage dependent. However, the dynamics within a local environment (e.g. within a cluster) were independent of surface coverage. In particular, the complete-RET contact time distribution did not change significantly with concentration. These observations suggest a model of heterogeneous surface coverage of clusters and free monomers where the local surface environment dynamics (near clusters or in free space) are independent of surface coverage in the coverage regime studied in this work.

The direct observation of dynamic non-specific protein-protein associations at the solid-liquid interface provides important insights into the complex mechanism by which protein layer formation occurs. Many previous kinetic models of protein adsorption, such as random sequential adsorption (RSA), assume immobile, non-associating proteins.[8,59] Protein cluster formation, especially dynamic protein cluster formation, are not anticipated for proteins in such models. These experiments provide direct evidence that surface diffusion and dynamic surface protein-protein association and dissociation must be incorporated in such kinetic models. Further application of this experimental approach will examine the effects of surface chemistry, environmental conditions, and choice of protein on clustering behavior.

Acknowledgements

BBL acknowledges support from the National Science Foundation Industry/University Cooperative Research Center for Membrane Science, Engineering and Technology (IIP1034720). Support for RW and the development of high-throughput dual-channel tracking methods was provided by the U.S. Department of Energy Basic Energy Sciences, Chemical Sciences, Geosciences, and Biosciences Division (under award DE-SC0001854). Support for MK was provided by the National Institute of Biomedical Imaging and Bioengineering of the National Institutes of Health (under award #5R21EB015532-02).

4.6 References

(1) Nakanishi, K.; Sakiyama, T.; Imamura, K. On the adsorption of proteins on solid surfaces, a common but very complicated phenomenon. *J. Biosci. Bioeng.* **2001**, *91*, 233–244.

(2) Vogler, E. A. Protein adsorption in three dimensions. *Biomaterials* **2012**, *33*, 1201–1237.

(3) Ratner, B. D.; Bryant, S. J. Biomaterials: Where we have been and where we are going. *Annu. Rev. Biomed. Eng.* **2004**, *6*, 41–75.

(4) Mansouri, J.; Harrisson, S.; Chen, V. Strategies for controlling biofouling in membrane filtration systems: Challenges and opportunities. *J. Mater. Chem.* **2010**, *20*, 4567–4586.

(5) Bee, J. S.; Randolph, T. W.; Carpenter, J. F.; Bishop, S. M.; Dimitrova, M. N. Effects of surfaces and leachables on the stability of biopharmaceuticals. *J. Pharm. Sci.* **2011**, *100*, 4158–4170.

(6) Norde, W. My voyage of discovery to proteins in flatland ...and beyond. *Colloids Surf., B* **2008**, *61*, 1–9.

(7) Rabe, M.; Verdes, D.; Seeger, S. Understanding protein adsorption phenomena at solid surfaces. *Adv. Colloid Interface Sci.* **2011**, *162*, 87–106.

(8) Talbot, J.; Tarjus, G.; Van Tassel, P. R.; Viot, P. From car parking to protein adsorption: An overview of sequential adsorption processes. *Colloids Surf., A* **2000**, *165*, 287–324.

(9) Wang, X.; Wang, Y.; Xu, H.; Shan, H.; Lu, J. R. Dynamic adsorption of monoclonal antibody layers on hydrophilic silica surface: A combined study by spectroscopic ellipsometry and AFM. *J. Colloid Interface Sci.* **2008**, *323*, 18–25.

(10) McMaster, T. J.; Miles, M. J.; Shewry, P. R.; Tatham, A. S. In situ surface adsorption of the protein C Hordein using atomic force microscopy. *Langmuir* **2000**, *16*, 1463–1468.

(11) Mulheran, P.; Pellenc, D.; Bennett, R. A.; Green, R. J.; Sperrin, M. Mechanisms and dynamics of protein clustering on a solid surface. *Phys. Rev. Lett.* **2008**, *100*, 068102.

(12) Kim, D. T.; Blanch, H. W.; Radke, C. J. Direct imaging of lysozyme adsorption onto mica by atomic force microscopy. *Langmuir* **2002**, *18*, 5841–5850.

(13) Cullen, D. C.; Lowe, C. R. AFM studies of protein adsorption. *J. Colloid Interface Sci.* **1994**, *166*, 102–108.

(14) Daly, S. M.; Przybycien, T. M.; Tilton, R. D. Aggregation of lysozyme and of poly(ethylene glycol)-modified lysozyme after adsorption to silica. *Colloids Surf., B* **2007**, *57*, 81–8.

(15) Kastantin, M.; Langdon, B. B.; Chang, E. L.; Schwartz, D. K. Single-molecule resolution of interfacial fibrinogen behavior: Effects of oligomer populations and surface chemistry. *J. Am. Chem. Soc.* **2011**, *133*, 4975–4983.

(16) Langdon, B. B.; Kastantin, M.; Schwartz, D. K. Apparent activation energies associated with protein dynamics on hydrophobic and hydrophilic surfaces. *Biophys. J.* **2012**, *102*, 2625–2633.

(17) Walder, R.; Schwartz, D. K. Single molecule observations of multiple protein populations at the oil-water interface. *Langmuir* **2010**, *26*, 13364–13367.

(18) Walder, R.; Schwartz, D. K. Dynamics of protein aggregation at the oil–water interface characterized by single molecule TIRF microscopy. *Soft Matter* **2011**, *7*, 7616–7622.

(19) Kastantin, M.; Keller, T. F.; Jandt, K. D.; Schwartz, D. K. Single-molecule tracking of fibrinogen dynamics on nanostructured poly(ethylene) films. *Adv. Funct. Mater.* **2012**, *22*, 2617–2623.

(20) Keller, T. F.; Schönfelder, J.; Reichert, J.; Tuccitto, N.; Licciardello, A.; Messina, G. M. L.; Marletta, G.; Jandt, K. D. How the surface nanostructure of polyethylene affects protein assembly and orientation. *ACS Nano* **2011**, *5*, 3120–3131.

(21) Ramsden, J. J.; Bachmanova, G. I.; Archakov, A. I. Kinetic evidence for protein clustering at a surface. *Phys. Rev. E: Stat., Nonlinear, Soft Matter Phys.* **1994**, *50*, 5072–5076.

(22) Pellenc, D.; Bennett, R. A.; Green, R. J.; Sperrin, M.; Mulheran, P. A. New insights on growth mechanisms of protein clusters at surfaces: An AFM and simulation study. *Langmuir* **2008**, *24*, 9648–9655.

(23) Minton, A. P. Effects of excluded surface area and adsorbate clustering on surface adsorption of proteins. I. Equilibrium models. *Biophys. Chem.* **2000**, *86*, 239–247.

(24) Minton, A. P. Effects of excluded surface area and adsorbate clustering on surface adsorption of proteins. II. Kinetic models. *Biophys. J.* **2001**, *80*, 1641–1648.

(25) Rabe, M.; Verdes, D.; Seeger, S. Surface-induced spreading phenomenon of protein clusters. *Soft Matter* **2009**, *5*, 1039–1047.

(26) Rabe, M.; Verdes, D.; Seeger, S. Understanding cooperative protein adsorption events at the microscopic scale: A comparison between experimental data and Monte Carlo simulations. *J. Phys. Chem. B* **2010**, *114*, 5862–5869.

(27) Rabe, M.; Verdes, D.; Zimmermann, J.; Seeger, S. Surface organization and cooperativity during nonspecific protein adsorption events. *J. Phys. Chem. B* **2008**, *112*, 13971–13980.

(28) Kastantin, M.; Schwartz, D. K. DNA hairpin stabilization on a hydrophobic surface. *Small* **2013**, *9*, 933–941.

(29) Kastantin, M.; Schwartz, D. K. Connecting rare DNA conformations and surface dynamics using single-molecule resonance energy transfer. *ACS Nano* **2011**, *5*, 9861–9869.

(30) Alvarez-Curto, E.; Pediani, J. D.; Milligan, G. Applications of fluorescence and bioluminescence resonance energy transfer to drug discovery at G protein coupled receptors. *Anal. Bioanal. Chem.* **2010**, *398*, 167–80.

(31) Truong, K.; Ikura, M. The use of FRET imaging microscopy to detect protein–protein interactions and protein conformational changes in vivo. *Curr. Opin. Struct. Biol.* **2001**, *11*, 573–578.

(32) Papra, A.; Gadegaard, N.; Larsen, N. B. Characterization of ultrathin poly (ethylene glycol) monolayers on silicon substrates. *Langmuir* **2001**, *17*, 1457–1460.

(33) Janssen, D.; De Palma, R.; Verlaak, S.; Heremans, P.; Dehaen, W. Static solvent contact angle measurements, surface free energy and wettability determination of various self-assembled monolayers on silicon dioxide. *Thin Solid Films* **2006**, *515*, 1433–1438.

(34) Unsworth, L. D.; Sheardown, H.; Brash, J. L. Protein-resistant poly(ethylene oxide)-grafted surfaces: Chain density-dependent multiple mechanisms of action. *Langmuir* **2008**, *24*, 1924–1929.

(35) Pasche, S.; De Paul, S. M.; Vörös, J.; Spencer, N. D.; Textor, M. Poly(L-lysine)-graft-poly(ethylene glycol) assembled monolayers on niobium oxide surfaces: A quantitative study of the influence of polymer interfacial architecture on resistance to protein adsorption by ToF-SIMS and in situ OWLS. *Langmuir* **2003**, *19*, 9216–9225.

(36) Honciuc, A.; Harant, A. W.; Schwartz, D. K. Single-molecule observations of surfactant diffusion at the solution-solid interface. *Langmuir* **2008**, *24*, 6562–6566.

(37) Carter, D. C.; Ho, J. X. Structure of serum albumin. *Adv. Protein Chem.* **1994**, *45*, 153–203.

(38) Lakowicz, J. R. Energy Transfer. In *Principles of Fluorescence Spectroscopy*; Lakowicz, J. R., Ed.; Springer New York, 2006; pp. 443–475.

(39) Jares-Erijman, E. A.; Jovin, T. M. FRET imaging. *Nat. Biotechnol.* **2003**, *21*, 1387–1395.

(40) Roda, A.; Guardigli, M.; Michelini, E.; Mirasoli, M. Nanobioanalytical luminescence: Förster-type energy transfer methods. *Anal. Bioanal. Chem.* **2009**, *393*, 109–123.

(41) Wu, P.; Brand, L. Resonance energy transfer: Methods and applications. *Anal. Biochem.* **1994**, *218*, 1–13.

(42) Kastantin, M.; Schwartz, D. K. Identifying multiple populations from single-molecule lifetime distributions. *ChemPhysChem* **2013**, *14*, 374–380.

(43) Norde, W.; Favier, J. P. Structure of adsorbed and desorbed proteins. *Colloids Surf.* **1992**, *64*, 87–93.

(44) Kwok, K. C.; Yeung, K. M.; Cheung, N. H. Adsorption kinetics of bovine serum albumin on fused silica: Population heterogeneities revealed by single-molecule fluorescence microscopy. *Langmuir* **2007**, *23*, 1948–52.

(45) Tanaka, M.; Mochizuki, A.; Shiroya, T.; Motomura, T.; Shimura, K.; Onishi, M.; Okahata, Y. Study on kinetics of early stage protein adsorption on poly(2-methoxyethylacrylate) (PMEA) surface. *Colloids Surf., A* **2002**, *203*, 195–204.

(46) Calonder, C.; Tie, Y.; Van Tassel, P. R. History dependence of protein adsorption kinetics. *Proc. Natl. Acad. Sci. U. S. A.* **2001**, *98*, 10664–10669.

(47) Amar, J. G.; Family, F.; Lam, P. Dynamic scaling of the island-size distribution and percolation in a model of submonolayer molecular-beam epitaxy. *Phys. Rev. B: Condens. Matter Mater. Phys.* **1994**, *50*, 8781–8797.

(48) Doudevski, I.; Schwartz, D. K. Concentration dependence of self-assembled monolayer island nucleation and growth. *J. Am. Chem. Soc.* **2001**, *123*, 6867–6872.

(49) Doudevski, I.; Schwartz, D. K. Self-assembled monolayers in the context of epitaxial film growth. *Appl. Surf. Sci.* **2001**, *175-176*, 17–26.

(50) Durbin, S. D.; Feher, G. Protein crystallization. *Annu. Rev. Phys. Chem.* **1996**, *47*, 171–204.

(51) Durbin, S. D.; Carlson, W. E. Lysozyme crystal growth studied by atomic force microscopy. *J. Cryst. Growth* **1992**, *122*, 71–79.

(52) Nygren, H.; Alaeddin, S.; Lundström, I.; Magnusson, K.-E. Effect of surface wettability on protein adsorption and lateral diffusion. Analysis of data and a statistical model. *Biophys. Chem.* **1994**, *49*, 263–272.

(53) Tie, Y.; Calonder, C.; Van Tassel, P. R. Protein adsorption: Kinetics and history dependence. *J. Colloid Interface Sci.* **2003**, *268*, 1–11.

(54) Yang, Z.; Galloway, J. A.; Yu, H. Protein interactions with poly(ethylene glycol) self-assembled monolayers on glass substrates: Diffusion and adsorption. *Langmuir* **1999**, *15*, 8405–8411.

(55) Yuan, Y.; Velev, O. D.; Lenhoff, A. M. Mobility of adsorbed proteins studied by fluorescence recovery after photobleaching. *Langmuir* **2003**, *19*, 3705–3711.

(56) Tilton, R.; Gast, A.; Robertson, C. Surface diffusion of interacting proteins. Effect of concentration on the lateral mobility of adsorbed bovine serum albumin. *Biophys. J.* **1990**, *58*, 1321–1326.

(57) Tilton, R.; Robertson, C.; Gast, A. Lateral diffusion of bovine serum albumin adsorbed at the solid-liquid interface. *J. Colloid Interface Sci.* **1990**, *137*, 192–203.

(58) Wertz, C. F.; Santore, M. M. Effect of surface hydrophobicity on adsorption and relaxation kinetics of albumin and fibrinogen: Single-species and competitive behavior. *Langmuir* **2001**, *17*, 3006–3016.

(59) Andrade, J. D.; Hlady, V. Protein adsorption and materials biocompatibility: A tutorial review and suggested hypotheses. *Adv. Polym. Sci.* **1986**, *79*, 1–63.

Chapter 5: Single-Molecule Resolution of Protein Dynamics on Polymeric Membrane Surfaces: The Role of Spatial and Population Heterogeneity

Blake B. Langdon[a], Roya B. Mirhossaini[a], Joshua N. Mabry[a], Indira Sriram[a], Ajay Lajmi[b], Yanxia Zhang[c], Orlando J. Rojas[c,d], Daniel K. Schwartz[a,*]

[a] Department of Chemical and Biological Engineering, University of Colorado Boulder

[b] Pall Life Sciences, Pensacola, FL

[c] Departments of Forest Biomaterials and Chemical and Biomolecular Engineering, North Carolina State University [d] School of Chemical Technology, Aalto University, Finland

(Published February 2015, *ACS Applied Materials and Interfaces*, 10.1021/am507730k)

Abstract

While polymeric membranes are widely used in the purification of protein pharmaceuticals, interactions between biomolecules and membrane surfaces can lead to reduced membrane performance and damage to the product. In this study, single-molecule fluorescence microscopy provided direct observation of bovine serum albumin (BSA) and human monoclonal antibody (IgG) dynamics at the interface between aqueous buffer and polymeric membrane materials including regenerated cellulose and unmodified polyethersulfone (PES) blended with either polyvinylpyrrolidone (PVP), polyvinyl acetate-co-polyvinylpyrrolidone (PVAc-PVP), or polyethylene glycol methacrylate (PEGM) before casting. These polymer surfaces were compared with model surfaces comprised of hydrophilic bare fused silica and hydrophobic trimethylsilane-coated fused silica.

At extremely dilute protein concentrations (10^{-3} – 10^{-7} mg/mL), protein surface exchange was highly dynamic with protein monomers desorbing from the surface within ~1 s after adsorption. Protein oligomers (e.g. non-specific dimers, trimers, or larger aggregates), while less common, remained on the surface for five times longer than monomers. Using newly developed super-resolution methods, we could localize adsorption sites with ~50 nm resolution

and quantify the spatial heterogeneity of the various surfaces. On a small anomalous subset of the adsorption sites, proteins adsorbed preferentially and tended to reside for significantly longer times (i.e. on “strong” sites). Proteins resided for shorter times overall on surfaces that were more homogeneous and exhibited fewer strong sites (e.g. PVAc-PVP/PES). We propose that strong surface sites may nucleate protein aggregation, initiated preferentially by protein oligomers, and accelerate ultrafiltration membrane fouling.

At high protein concentrations (0.3 – 1.0 mg/mL), fewer strong adsorption sites were observed, and surface residence times were reduced. This suggests that at high concentrations adsorbed proteins block strong sites from further protein adsorption. Importantly, this demonstrates that strong binding sites can be modified by changing solution conditions. Membrane surfaces are intrinsically heterogeneous; by employing single-molecule techniques, we have provided a new framework for understanding protein interactions with such surfaces.

5.1 Introduction

Membrane processes are increasingly used in the commercial purification and sterilization of protein biopharmaceuticals.[1–4] However, membrane fouling – due to pore narrowing, pore plugging, and cake formation – is a fundamental challenge to be addressed when implementing and optimizing membrane separation.[5] Membrane fouling ultimately reduces separation efficiency and may contribute to protein aggregates or other impurities in downstream products.[6,7]

While protein fouling of membranes has been widely studied, the molecular-level mechanisms – including protein adsorption, aggregation, and unfolding –remain poorly understood. For example, online process measurements often provide macroscopic information (e.g. flux and transmembrane pressure drop), measuring the effects of protein adsorption only indirectly.[8] By varying the feed concentration and other process parameters, models of fouling mechanisms have been proposed and evaluated.[9,10] For example, Kelly et al. showed that microfiltration membrane flux declined more rapidly when BSA protein oligomers (e.g. dimers, trimers) and aggregates were present (unfiltered solutions) in the feed solution than when only BSA monomers were present (300 kDa filtered solutions). Further, they observed that membrane flux continued to decline in sequential filtrations of unfiltered and filtered BSA solutions. Based on these finding, they propose a two-step process in which BSA aggregates deposited quickly on pore walls, narrowing or blocking the flow, and subsequently served as nucleation sites for BSA aggregation, further reducing membrane flux.[11,12] More detailed information about protein membrane fouling has been obtained by other surface sensitive techniques such as quartz crystal microbalance (amount of protein),[13,14] atomic force microscopy (protein layer topography)[15], and ATR/FTIR (protein conformation)[16]. However, these techniques measure ensemble-averaged or net behavior, and are generally insensitive to the various forms of heterogeneity and complexity that characterize these processes.

Single-molecule total internal reflection fluorescence microscopy (sm-TIRFM) is uniquely suited to separate competing kinetic protein processes (e.g. adsorption, desorption, and interfacial diffusion) as well as to capture the entire distribution of protein dynamics.[17,18] In previous work at oil-water and solid-water interfaces, protein surface species (e.g. monomers, dimers, trimers, larger oligomers, and larger aggregates) were found to exhibit distinct behaviors.[19,20] For example, protein oligomers were found to reside on solid surfaces longer and execute smaller and fewer diffusive steps than protein monomers.[19] Surface spatial heterogeneity (e.g. hydrophobic and hydrophilic regions, surface defects) has also been identified by examining the spatial variation of interfacial molecular dynamic.[21,22] In the work reported here, we used single-molecule tracking capabilities to characterize heterogeneity involving protein populations and surface chemistry and topographic variation on polymer thin films relevant to ultrafiltration.

Many factors can determine the mechanism and rate of membrane fouling, including flow hydrodynamics and protein and membrane physicochemical properties. In this work, we have focused on the latter by comparing the interactions of two different proteins, bovine serum albumin (BSA) and a monoclonal antibody (IgG), on several polymer films under no-flow conditions. The distinct differences in the molecular shape, size, and isoelectric point of BSA and IgG – both commonly used protein classes in the separations literature – allowed us to begin to assess the relative universality of protein interactions with these surfaces. For example, BSA and IgG have opposite net charges at a pH of 7.4, the molecular weight of IgG is twice as large as that of BSA, and the secondary structure of BSA is dominated by alpha helices while IgG is mainly composed of beta sheets (see Materials and Methods).[23] Therefore BSA and IgG might be expected to be attracted to surfaces of opposite charges as well as bind, diffuse, or unfold differently on various surfaces.

Regenerated cellulose (RC) and unmodified polyethersulfone (PES) were used in our experiments because they are commonly used membrane materials.[16,24] Because PES is

hydrophobic, polymeric "wetting agents" are often either blended with PES prior to casting or post-treated after casting to produce more hydrophilic membrane materials.[25] In our experiments, we blended PES with either polyvinyl pyrrolidone (PVP), polyvinylacetate-co-polyvinylpyrrolidone (PVAc-PVP), or polyethyleneglycolmethacrylate (PEGM) prior to casting. All prepared polymer surfaces (RC and PES blends) showed similar hydrophobicity, thickness, and roughness (see Materials and Methods and Supporting Information) and were expected to be negatively charged at neutral pH in 158 mM phosphate buffered saline.[26,27] These surfaces were also compared to model hydrophilic, negatively charged bare fused silica (FS) and hydrophobic trimethylsilane-modified (TMS) surfaces. All of the surfaces differed in their composition, hydrogen-bonding capacity, and – as we explore below – their spatial heterogeneity.

We investigated interfacial protein dynamics at (1) extremely dilute (~10^{-7} mg/mL) and (2) higher (0.3-1 mg/mL) protein concentration conditions, which are relevant to early and intermediate processes, respectively, in membrane fouling. While these protein concentrations were lower than may be used in industrial ultrafiltration (e.g. 100-200 mg/mL IgG), they were useful in contrasting protein-surface interaction in the absence and presence of protein-protein interactions.[1] For the higher concentration experiments, the same protein concentration was used across all surfaces studied, as is typical in macroscopic membrane fouling studies.[15,16] This also allowed us to separate and examine the impact of protein-membrane and protein-protein interactions on interfacial dynamics. While less common, both protein oligomers and anomalously strong adsorption sites accounted disproportionately for longer-lived surface species that may nucleate further protein surface accumulation. We found that these effects were modulated by surface chemistry and protein concentration.

5.2 Materials and Methods

5.2.1 Thin Polymer Film Preparation and Characterization

Cleaning and Preparation of Surfaces - All surfaces were prepared on fused silica (FS) and silicon wafers (Mark Optics). Wafers were cleaned by immersion in a warm piranha solution (concentrated sulfuric acid (Fisher Scientific) and 30% aqueous hydrogen peroxide (Fisher Scientific), 3:1 v/v) for 1 h then treated with UV-ozone for 1 h, as described previously.[19] Trimethyl-silane (TMS) coatings were prepared by exposing wafers to hexamethyldisilazane (Fisher Scientific) vapor for 18 h at room temperature. FS and TMS served as model surfaces, representing very hydrophilic and very hydrophobic surfaces, respectively. A methyl-polyethylene glycol silane (mPEG-silane; Gelest) self-assembled monolayer was formed via solution deposition as previously reported[19] and used as an anchoring layer for PEGM/PES polymer thin films. TMS was used as an anchoring layer for all other polymer thin films.

Polymer films were prepared by spin-coating a polymer solution in organic solvent (i.e. toluene, dichloromethane, or N,N-dimethyl formamide) onto a wafer. A regenerated cellulose precursor trimethylsilyl cellulose (TMSC) was prepared as previously reported.[28] PES (molecular weight (MW) 48,000 Da), PVP (MW 1,300,000 Da), and PVAc-PVP (MW 47,000 Da) were used for PVP/PES and PVAc-PVP/PES films. PEG monomethacrylate (MW 400 Da) and PEG dimethacrylate (MW 400 Da) were polymerized with PES (MW 48,000 Da) to form PEGM/PES films. Molecular structures of the polymeric materials used are shown in Figure E1 in Appendix E and additional polymer film preparation details are provided in the Supporting Information.

Contact-Angle Measurements - A custom-built contact-angle goniometer was used to measure the static water contact angle (WCA) on the surface of the materials considered in these studies. WCA were measured by depositing a 1 μL drop of deionized water, purified to 18.2 MΩ cm (Millipore Mill-Q UV+), on the surface. A minimum of five drops on each of at least

two independent samples were averaged and reported in Table 5.1. Interestingly, all membrane polymer films had similar WCA and therefore similar hydrophobicities and macroscopic surface energy. Nearly complete wetting was observed on bare FS, consistent with previous work. The WCA measured on TMS was 95 ± 3°, also consistent with previously-measured values.[19] Prior to hydrolysis, the TMSC film WCA was 94 ± 3°. This was similar to previously-reported values for thin films prepared via Langmuir-Blodgett deposition (85° and 100° for static and advancing WCA). [29,30] After hydrolysis, RC had a static WCA of 51 ± 11°, consistent with previous cellulose films prepared using this approach. [29–31]

Table 5.1: Polymer thin film characteristics. The standard deviation between at least three measurements is reported (see contact angle measurements, ellipsometry, and atomic force microscopy sections for details).

Polymer film	Static WCA (°)	Thickness (nm)	RMS Roughness (nm^2)
PVP/PES	60 ± 3	26 ± 7	0.47 ± 0.07
PVAc-PVP/PES	54 ± 1	24 ± 1	0.98 ± 0.04
PEGM/PES	50 ± 1	30.6 ± 0.4	0.18 ± 0.09
RC	51 ± 11	23.5 ± 0.9	1.2 ± 0.1

Ellipsometry and FTIR Spectroscopy – Both ellipsometry and FTIR spectroscopy were performed on silicon substrates (WRS Materials). Polymer film thicknesses were measured in air with a variable angle spectroscopic ellipsometer (V-VASE, J.A. Woollam). For each surface, a minimum of three separately prepared surfaces were measured and account for the error in each thickness value. Changes in amplitude, Ψ, and phase, Δ, were measured at 5° intervals for 60° - 80° and over the spectroscopic range of 400 - 900 nm. An isotropic, three-interface optical model (comprised of air, polymer film, silicon dioxide, and silicon) was used to determine the polymer film layer thickness. TMSC surfaces had a thickness of 60.5 ± 0.2 nm, which was reduced to 23.5 ± 0.9 nm when hydrolyzed to RC. Hydrolysis was confirmed with Fourier Transform Infrared Spectroscopy (FTIR) using a Thermo Scientific Nicolet 6700 FT-IR in a specular reflection geometry. The TMSC IR spectrum showed typical wave number v(Si-C)

signals near 1243, 878, 839, and 752 cm^{-1} and no hydroxyl signal.[32] When hydrolyzed, the RC IR spectrum had no measureable v(Si-C) signals and had a strong, broad v(O-H) signal between 3450-3400 cm^{-1}, suggesting that the hydrolysis of trimethyl silane groups was essentially complete (see Figure E2 in the Supporting Information in Appendix E).

Atomic Force Microscopy (AFM) - A Nanoscope III instrument (Digital Instruments, now Bruker) using tapping mode in air was used to image the polymer films. Reported roughness values were averaged from 1 μm x 1 μm areas on at least three samples. Representative AFM images of all polymer films are shown in Figure E3 in Appendix E.

5.2.2 Protein Labeling and Solution Preparation

Alexa Fluor 555 labeled BSA (MW 67,000 Da, isoelectric point (pI) 4.7)[33] was purchased from Invitrogen (5 fluorophores per protein molecule on average). A purified humanized IgG1 monoclonal antibody (MW ~146,000 Da, calculated pI ~8.9), here denoted as "IgG", was used in these studies. IgG was fluorescently labeled with Alexa Fluor 555 dye using a commercially available protein labeling kit (Invitrogen); the primary amine dye conjugation chemistry was performed in phosphate buffered saline at pH ~8.3. The fluorescently labeled proteins were separated from unreacted free dyes using a Bio-Scale mini Bio-Gel P-6 desalting cartridge (Bio-Rad) on a BioLogic DuoFlow medium-pressure chromatography system with UV-visible detection (Bio-Rad), which showed visual separation between low molecular weight unreacted dye and high molecular weight fluorescently-labeled IgG. IgG was labeled on average with 8 dyes per protein molecule determined with a UV-visible spectrophotometer (Thermo Scientific).

All experiments were performed in phosphate buffered saline (Gibco, pH 7.4). Extremely dilute protein concentration experiments were performed with labeled protein concentrations of 10^{-5}-10^{-6} and 10^{-3}-10^{-7} mg/mL for IgG and BSA, respectively, such that single molecules could be resolved as distinct diffraction limited spots and protein surface coverage were similar (see Supporting Information Table S3). For high concentration experiments,

solutions contained unlabeled proteins at 0.3 or 1.0 mg/mL concentrations of IgG or BSA, respectively, and labeled protein in the same concentrations that were used for dilute concentration experiments on the given functionalized surface.

5.2.3 Image Acquisition and Single-Molecule Tracking

Fluorescently-labeled proteins were imaged with a custom-built prism-based TIRFM system and flow cell as previously described,[19] and were illuminated by a 532 nm DPSS LASER (Cobalt Samba) at a power density of 6 ± 1 μW/μm^2. For each experiment, multiple movies (i.e. sequences of 1000 images) were captured with an acquisition time of 200 ms. This acquisition time provided a satisfactory signal-to-noise ratio while also allowing us to capture protein surface dynamics. The flow cell was maintained at 25 ± 1 °C, and flow was stopped prior to movie capture in order to increase the stability of our optical setup. Additionally, no significant differences in adsorption rates were observed over the course of a 2 hr experiment. For each type of surface (FS, TMS, or polymer film), protein dynamics were captured on at least three independent surface areas.

Single molecule trajectories were constructed by identifying objects in each frame and then linking objects from frame-to-frame, as described previously.[17,19] Briefly, diffraction-limited objects in each frame were identified by convoluting the image with a disk matrix, subtracting local background, and thresholding the image (i.e. groups of pixels above this threshold were identified as objects). An object's intensity in each frame was the total intensity of all contiguous pixels after subtraction of the local background intensity. Object positions were calculated as the centroid of intensity with a localization precision of ~50 nm.[22] Molecular trajectories were constructed by linking an object's center of intensity to the nearest center of intensity within a distance (i.e. tracking radius) of 4 pixels (1.08 μm) in subsequent frames. Protein kinetics were found to be insensitive to the tracking radius selected (see Fig. E12 in the Supporting

Information Appendix E). Surface residence times were calculated as the number of consecutive frames for which an object was identified multiplied by the acquisition time.

5.2.4 Data Analysis

Single-Molecule Trajectory Analysis - Accumulated surface residence times were used to calculate the complementary cumulative residence time distribution (CRTD), which represents the fraction of molecules that remain on the surface for time *t* or longer after the initial adsorption event. CRTD's have the advantage of being especially sensitive to rare populations compared to raw distributions.[34] Assuming that the surface residence time of a given protein population follows first-order desorption kinetics, the CRTD for the sum of all populations can be described using an exponential mixture model,

$$p(t) = \sum_i f_i e^{-t/\tau_i} \qquad (1)$$

where *p(t)* is the probability that a given object will have residence time of *t* or greater. Each population is denoted with a subscript *i* and is described by the fraction of molecules, f_i, belonging to the population and a characteristic residence time, τ_i (i.e. the inverse of the first-order desorption rate constant). The mean surface residence time, τ, can be calculated as $\tau = \sum_i^P f_i \tau_i$ where *P* is the total number of populations. Further details of constructing CRTDs and additional calculations have been described previously.[19,34] Trajectories spanning two or more images were used to construct experimental CRTDs due to the sensitivity of single image object identification to noise. For each experiment, a CRTD was constructed for each movie and fit using Equation 1. These fit values were averaged by weighting each movie by the number of objects observed in that movie; the error reported corresponds to the standard error of these weighted fit values.

In previous work, using fibrinogen proteins, we identified a correlation between residence times and fluorescence intensity, where molecules with a higher mean fluorescence intensity, (determined to represent pre-formed oligomers), resided on the surface for longer time

intervals.[19] In this work, we used fluorescence intensity to separate protein monomers from oligomers. A representative histogram of the mean of the fluorescence intensities of all frames comprising each observed trajectory is shown in Figure 5.1b. An object's fluorescence intensity for each frame was calculated as above – the total intensity of all contiguous pixels after subtracting a local background intensity. Since monomers were the dominant species in solution, we expected the lowest and dominant intensity peak to describe the monomeric species. This peak was successfully approximated as a normal distribution. Only the left-hand side of the lowest intensity peak was fit to a Gaussian distribution, since the right-hand side overlapped significantly with higher intensity peaks. Molecular trajectories with mean intensities within the lower 95% and the upper 68% confidence intervals were considered monomers while molecular trajectories above the monomer normal distribution mean by 3 standard deviations (2-3 times the monomer peak mean for all protein-surface combinations) were considered oligomers (consisting of dimers, trimers, and potentially larger oligomers). Such consistent and conservative intervals were selected in order to ensure that only monomer and oligomer dynamics were examined for each protein-surface combination. We could then characterize interfacial dynamics (e.g. surface residence time) of monomers and oligomers separately by selecting molecular trajectories by their mean fluorescence intensity.

Super-Resolution Imaging and Adsorption Site Analysis - A variation of the localization technique known as "motion blur" point accumulation for imaging in nanoscale topography (mbPAINT)[35] was used to construct super-resolution maps of protein adsorption events and adsorption sites. This technique takes advantage of increased localization precision from taking the centroid of the point spread function (~50 nm, compared to a camera pixel of 227 nm). By creating these maps, we were able to accurately measure adsorption and desorption kinetics for molecular-scale surface sites and, importantly, identify distinct populations of sites. The specific mapping methods were described previously by Mabry et al.[22] The initial position of each molecular trajectory was placed on a pseudo-image with 22.7 nm pixels (10x smaller than

camera pixels) and blurred such that an adsorption center was represented by Gaussian peak with a standard deviation σ_{loc} and an amplitude of 1 adsorption event. Super-resolution adsorption event maps were constructed by summing all blurred pseudo-image adsorption events. On these adsorption event maps, adsorption sites were identified as any group of connected pixels with an amplitude of ≥ 1 adsorption event.

The adsorption event count, *n*, of a given site was defined by the maximum pixel value of all pixels assigned to that site. A probability histogram of adsorption events on a surface's adsorption sites was constructed and could be described by a Poisson mixture model, $f_{ads}(n)$, normalized for $n \geq 1$:

$$f_{ads}(n) = \sum_{j=1} p_j \frac{{\lambda_j}^n e^{-\lambda_j}}{n!(1-e^{-\lambda_j})} \qquad (2)$$

where the j^{th} population of sites had a characteristic (i.e. mean) number of adsorption events, λ_j, and represented a fraction p_j of total sites, with $\sum p_j = 1$. The average site had $\lambda = \sum p_j \lambda_j$ adsorption events. With *N* total adsorption events, the number of predicted adsorption sites was given by N/λ. Therefore, the predicted adsorption site density takes into account the variation of adsorption sites strengths. By fitting the tail of the adsorption site distribution (i.e. for sites with n ≥ 1), we were able to measure populations with less than one adsorption event on average. Simple counting of observed adsorption sites cannot accurately account for such populations of sites. For this reason, the number of predicted adsorption sites was a better indicator of the true surface site distribution than would be determined by simple site-counting.

On a perfectly homogeneous surface, proteins would adsorb to any surface site with equal probability. In order to evaluate the relative "heterogeneity" of a surface (i.e. the deviation from a perfectly adsorbing surface), we calculated a normalized heterogeneity parameter,

$$h = \frac{maximum\ \ theoretical\ number\ of\ adsorption\ \ sites}{fitted\ number\ of\ adsorption\ sites} = \frac{A/a}{N/\lambda}$$

where the imaged surface area was *A* and the molecule's footprint was *a*. As protein oligomers were rare, *a* values were specified as 5.6 nm^2 and 15.2 nm^2 for the area of BSA (ellipsoid) and IgG (y-shaped) monomers lying "side-on" with dimensions 4.0 x 4.0 x 14.0 nm^3 and 15.2 x 10.0 x 3.8 nm^3, respectively.[36,37] The relative heterogeneity measured for a surface also depended on the protein (e.g. BSA or IgG) used to probe the surface, since protein-surface interactions could depend on a protein's size, structure, or composition. For more heterogeneous surfaces, where the site adsorption events probability distribution was heavy-tailed, *h* was larger than for homogenous surfaces. The error in *h* was calculated as the standard error between three or more experimental surface regions. The existence of discrete adsorption sites was independently confirmed by examining positional correlation between adsorption sites and is further discussed in the Supporting Information.

5.3 Results and Discussion

It is frequently observed that membranes with nominally similar pore sizes and structures, but comprising different materials, exhibit different flux declines that are attributed to protein-material interactions.[15,16] Similarly, the polymeric membrane surfaces considered here all showed similar static WCA (reflecting a surface's surface energy and hydrophobicity) and film thicknesses (see Table 5.1). In order to directly probe isolated protein-material (or in our case protein-surface) interactions, single-molecule interfacial dynamics were observed using sm-TIRFM at extremely dilute protein solution concentrations such that the average density of molecules on the surface was <0.1 molecule μm^{-2}. In addition, with the addition of higher concentrations of unlabeled protein (0.3-1.0 mg/mL), we were able to contrast interfacial protein behavior in the absence and presence of protein-protein interactions. Such conditions are relevant to the very initial and intermediate stages of protein adsorption to membrane interfaces, which may ultimately determine the structure of the adsorbed protein layer and the speed and extent of protein membrane fouling. Below we present (I) the role of protein population

heterogeneity, (II) the role a surface spatial heterogeneity, and (III) the effects of increased protein concentrations on observed protein adsorption and desorption dynamics.

5.3.1 Protein Oligomers Remain on the Surface Longer than Protein Monomers

Each molecule in our experiments was characterized by its mean intensity, surface residence time, and molecular trajectory. Figure 5.1a shows a representative cumulative residence time distribution (CRTD) of IgG on RC. CRTDs were shown to be insensitive to photobleaching and photoblinking, see Supporting Information Appendix E Fig E10. A single first-order desorption process would appear as a straight-line on the CRTD log-linear plot shown in Figure 5.1a. Instead, this curved CRTD can be modeled by a mixture of multiple first-order desorption processes (Equation 1). As was the case for all surface and protein combinations examined, more than one characteristic residence time, or desorption rate, was required to fit these distributions indicating heterogeneous protein dynamics. There are several potential sources for such heterogeneity including multiple oligomeric states at the surface: monomers, reversible (or irreversible) dimers, or even larger aggregates species (with different configurations and exposed hydrophobic and hydrophilic amino acid side groups). In addition, multiple protein conformations or orientations at the interface[38], or surface regions or sites with different protein binding energies[39] may also contribute to heterogeneous protein behavior. Initially, we considered the influence of oligomers (non-specific dimers or larger oligomers formed in solution) on overall protein dynamics.

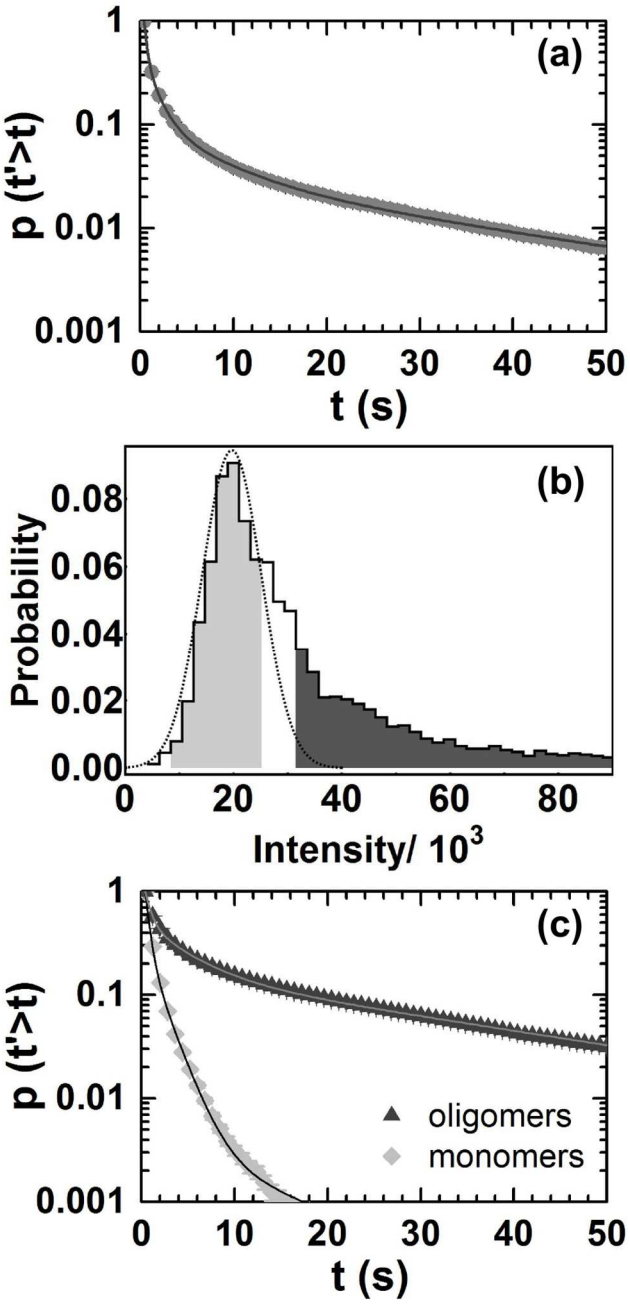

Figure 5.1: (a) the CRTD of IgG on RC at extremely dilute protein concentration. (b) The probability distribution of the mean fluorescence intensities of IgG molecule trajectories on RC. The fluorescence intensities of objects identified as monomers and oligomers are highlighted in light and dark gray, respectively. (c) CRTDs for IgG monomers and oligomers on RC as identified by their mean fluorescence intensities. Equation 1 population fit parameters are tabulated in Table E1 in the Supporting Information Appendix E.

Kastantin *et al.* previously showed that protein monomers and oligomers (preformed in solution), were responsible for the heterogeneity observed in characteristic residence times for fibrinogen on various surfaces, including FS and TMS.[19] Since an object's mean fluorescence intensity indicates its oligomerization state (i.e. monomer, dimer, trimer, or larger oligomer), the

authors used these fluorescence intensities to directly connect oligomerization state to populations identified by surface residence times (e.g. low intensity monomers accounted for the shortest-live characteristic residence time while oligomers accounted for longer characteristic residence times).

In order to evaluate the role of population heterogeneity (e.g. protein monomers, nonspecific dimers, trimers, and larger oligomers), we examined the mean fluorescence intensity distribution of all observed molecular trajectories. For each protein-surface combination, the distribution of fluorescence intensities was broad with a major peak at low intensity, as shown for IgG on RC in Figure 5.1b. At dilute protein concentrations, pH 7.4, and 25 °C, protein monomers represented the vast majority of molecules in solution. IgG and BSA solutions contained 96 ± 3% and 78 ± 3% monomers, respectively, as measured by size exclusion chromatography (see Fig. E4 in the Supporting Information). Therefore, on the surface, we expect monomers to be represented by the major peak in the intensity distribution.[40] Indeed if we selected only molecules within this intensity peak and compared their behavior to molecules selected from the high-intensity tail of the distribution, we found that the low intensity molecules were much shorter-lived, consistent with previous findings.[19] High-intensity objects (oligomers) were found to remain on the surface up to ten-times longer than low intensity objects (monomers), as shown in Figure 5.1c for IgG on RC. The mean characteristic residence times of monomers for all surface-protein combinations were 0.33-0.84 s while mean characteristic residence times of oligomers ranged from 0.99 ± 0.02 to 4.4 ± 0.9 s for IgG on PVAc-PVP/PES and FS, respectively, and from 1.7 ± 0.2 to 7 ± 1 s for BSA on the same respective surfaces (see Table E3 in the Supporting Information).

At the protein surface coverage observed at such dilute protein concentrations (see Table E3 in Supporting Information), and considering that protein monomers remained on the surface for short times, we suspect that observed oligomers were most likely preformed in

solution. If oligomers formed on the surface under these conditions, we might expect a molecule's fluorescence to increase, indicating oligomerizaiton. This does not appear to be the case; the probability distribution of all molecules' fluorescence intensities just after adsorption and just before desorption were similar (see Fig. E11 in the Supporting Information).

While less common, at any given time point oligomers disproportionally accounted for more adsorbed species since they remained on the surface for much longer than monomers. We speculate that these oligomers would therefore be more likely to interact with other proteins on the surface and could nucleate further oligomerization and aggregation and ultimately protein layer formation. The consequence of aggregate surface adsorption was demonstrated by Kelly and Zydney where microfiltration membrane fouling and flux decline occurred much faster when large BSA aggregates were present in solution compared to aggregate-free solutions obtained after pre-filtration.[10] They proposed a two-step process explaining this flux decline: (1) BSA aggregates deposit in early stages and (2) "native" (monomeric) BSA attach to deposited aggregates (nucleation sites) in later stages. Other researchers have reported similar phenomena for different membranes and proteins.[41,42] In a related study, Kelly et al. observed that raising just the ratio of BSA dimers to monomers led to a faster flux reduction in membrane filtration.[12] It is clear that population heterogeneity, and its kinetic consequences observed here, can contribute to macroscopically observed flux declines.

The residence time distributions were heavy-tailed, requiring two or three populations to fit monomer and oligomer residence time distributions (as per Equation 1). This suggests there was significant heterogeneity in monomer-surface and oligomer-surface interactions. In the following section, we show that spatial variations are another important source of heterogeneity in interfacial dynamics.

5.3.2 Spatial Heterogeneity Increases Protein Residence Times

The unique capabilities of sm-TIRFM allowed us to spatially map heterogeneous protein dynamics on thin polymer films with high resolution (~50 nm). In general, spatial kinetic heterogeneity may be due to a combination of morphology/topography and surface chemistry. Kisley et al. used super-resolution imaging to identify and characterize protein adsorption to discrete charged sites on an agarose support involved in ion-exchange chromatography.[39,43] Similarly, Mabry et al. characterized strong adsorption sites on TMS functionalized silica and emphasized the importance of chemical surface heterogeneity.[22]

While we expect commercial membranes to have morphological heterogeneity across many length scales, the thin polymer films studied here approximate some of the potential consequences of small-scale membrane surface spatial heterogeneity due to topographic (see AFM images in the Supporting Information) and possibly chemical heterogeneity. Based on the thickness and roughness of the polymer films (see Table 5.1 and Figure E3 in the Supporting Information in Appendix E), we are confident that the spin-coated polymer layers completely covered the underlying surface. We suggest that surface spatial heterogeneity observed on polymer films was most likely due to a combination of topography and surface chemistry. For example, cellulose can exist in several oxidation states and RC surfaces may have sites with several different oxidation states.[44] Our model hydrophilic and hydrophobic surfaces were also expected to exhibit spatial heterogeneity. On FS, we expect that silanol groups with hydrogen-bonding potential, may lead to favorable protein-surface interactions and strong binding sites. On TMS, we expect that some remaining un-capped silanol groups also will be present.[22]

Super-resolution maps of IgG and BSA adsorption events visually captured this spatial heterogeneity, as shown for IgG on PEGM/PES in Figure 5.2a. Discrete sites where many protein adsorption events occurred could be clearly contrasted with sites where a single adsorption event occurred, over the course of the observation window. On a homogenous surface, the probability of observing more than one adsorption event within a 50 nm site would

be exceedingly low due to the finite number of adsorption events and so to observe such sites indicates anomalously-strong binding. The super-resolution maps clearly revealed that all of the surfaces were heterogeneous and had anomalously strong sites (see Figure E6 in Appendix E). However, there was a wide distribution of protein-surface interaction strengths. Below we explore the consequences of this spatial heterogeneity.

a. Proteins Preferentially Adsorb to and Remain Longer on Anomalous "Strong" Surface Sites

We characterized the identities and dynamics of molecules adsorbing to anomalously-strong and more prevalent weak binding sites. As mentioned above, an adsorption site where more than one adsorption event occurred was a highly unlikely occurrence because the number of potential surface adsorption sites was much greater than the number of molecules observed in our single-molecule experiments. For example, for the super-resolution map shown in Figure 5.2a we observed 20,000 IgG adsorption events on a RC surface image area of 0.011 mm^2. Given that an IgG monomer occupies an area of $1.2x10^{-10}$ mm^2, the observed molecules covered less than 0.02% of the total surface area imaged. Therefore, we nominally classified anomalous "strong" sites as sites with more than one adsorption event ($n > 1$, where n is the number of adsorption events) and "weak" sites as sites where only one adsorption event occurred ($n = 1$). Similar strong sites (or adsorption hot spots) have been observed on TMS previously.[22]

For all protein-surface combinations, monomers were much more likely to be observed on the strong sites than on weak sites, despite the presumed prevalence of weak sites. This can be seen in Figure 5.2b, where the monomer intensity peak dominates the strong adsorption site intensity distribution for IgG on RC. In contrast, IgG objects observed on weak sites were equally likely to be monomers, dimers, and larger oligomers. It is tempting to interpret this observation as suggesting that monomers preferentially adsorb to strong sites. However, due to

the finite frame time (0.2 s) used in our experiments, it is more likely that monomers also adsorbed on weak sites but resided on these sites for very short durations of time such that they were not observed. This appeared to be the case when we examined monomer residence times on weak and strong sites. The mean characteristic residence times of IgG monomers on weak sites were between 0.2 and 0.4 s while the characteristic residence times of IgG monomers on strong sites were nearly twice as long (0.5 – 0.8 s) on the polymer films (see Supporting Information Table E2). Despite only observing the relatively "long-lived" tail of monomers on weak sites, by fitting the entire residence time distribution we could infer the behavior of the "short-lived" monomers as well.[34,45] The mean characteristic residence times indicated that we observed fewer monomers adsorbing on weak sites compared with strong sites.

In fact, both monomers and oligomers were found to reside on strong sites longer than on weak sites as shown in Figure 5.2c for IgG on RC (see the Supporting Information for mean characteristic times for all protein-surface combinations). From this finding, and the observation of more adsorption events on strong sites, we can infer that protein-surface interactions on strong sites were associated with greater adsorption free energies than on weaker sites. This also suggests, that, while less common, strong sites disproportionally adsorb proteins. We propose that proteins remaining longer on these strong sites have more opportunities to re-orient, undergo conformation changes, and interact with other proteins. Therefore, surfaces with more anomalous sites and/or sites with stronger protein-surface binding could develop a protein layer faster.

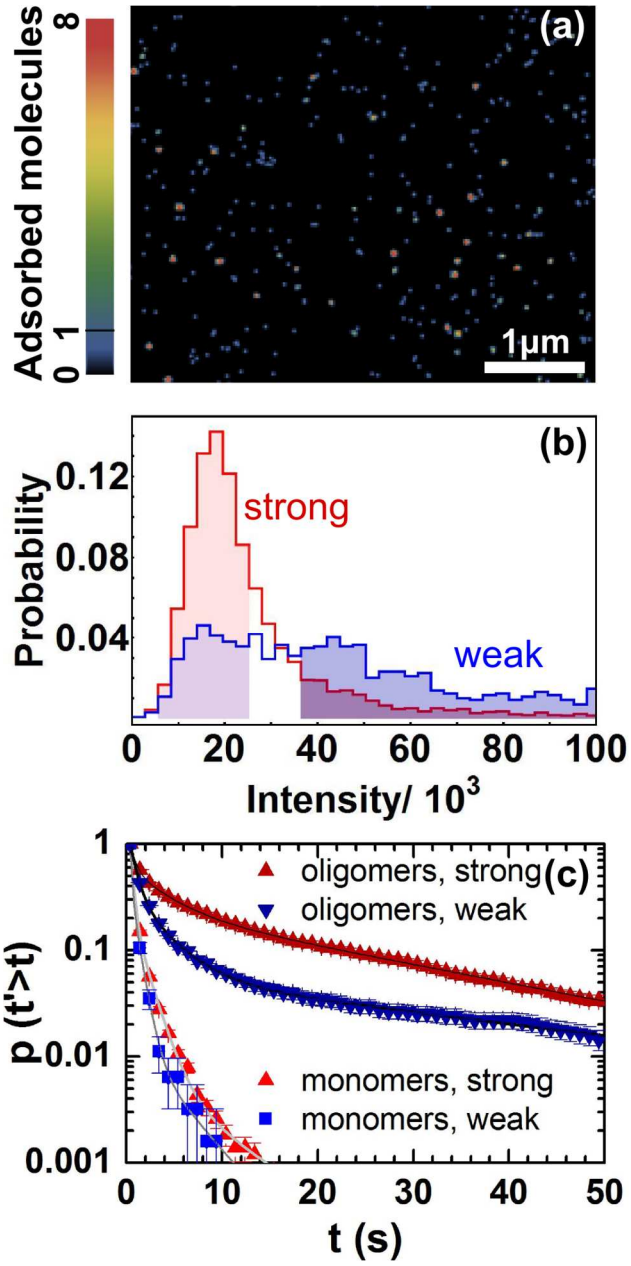

Figure 5.2: (a) Representative super-resolution map of 20,000 IgG adsorption events on RC. (b) Mean molecule fluorescence intensity probability distributions for IgG on RC at a dilute protein concentration. Molecules were separated by their initial location on either a strong (n > 1, red) or a weak site (n = 1, blue). (c) CRTDs for IgG on RC of monomers and oligomers initially adsorbed on either strong or weak sites. Multiple exponential fits to Equation 1 are indicated by gray lines for each CRTD. The mean characteristic residence times of monomers and oligomers on strong or weak sites for all protein-surface combinations are tabulated in Table E2 in the Supporting Information.

b. Surfaces Exhibit a Distribution of Surface Sites

In order to quantify a given surface's relative spatial heterogeneity, we examined the distribution of adsorption event counts per surface site. Figure 5.3 shows three representative probability histograms of site adsorption event counts for IgG on PVP/PES, PEGM/PES, and PVAc-PVP/PES (the adsorption event probability distribution on RC was similar to those of PEGM/PES and PVP/PES). The adsorption event count histograms shown in Figure 5.3 were

created from 5,000 adsorption events on surface areas of 0.01 mm^2. If surfaces were homogeneous – where every surface site had the same adsorption probability– we would expect these distributions to follow a single Poisson distribution. It is clear, however, that these distributions are heavy-tailed, with some sites adsorbing proteins much more frequently than others. This suggests that these surfaces were not homogeneous, since a single Poisson distribution did not adequately explain the data. Instead, we assumed that adsorption resulted from multiple types of sites exhibiting first-order kinetics and fit each histogram with a multi-component Poisson distribution (Equation 2). This assumption is consistent with previous studies that have shown individual sites exhibit first-order kinetics.[39]

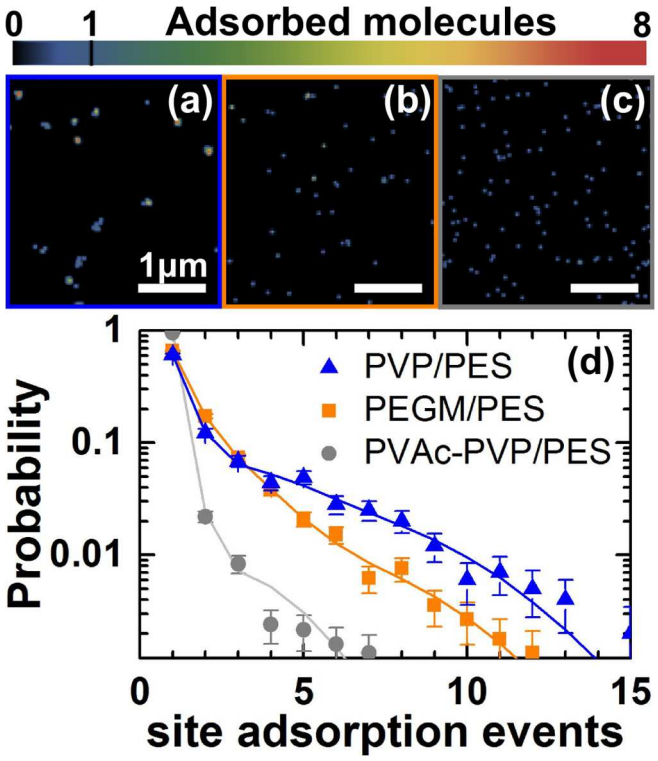

Figure 5.3: Representative super-resolution maps of 5,000 IgG adsorption events on (a) PVP/PES, (b) PEGM/PES, and (c) PVAc-PVP/PES. (d) Probability distribution of IgG site adsorption event counts for sites identified on PVP/PES, PEGM/PES, and PVAc-PVP/PES for 5,000 IgG adsorption events on each surface.

With a finite number of trajectories, we observed adsorption on only a fraction of the potential sites. However, for a given site, the number of adsorption events followed a Poisson distribution, and we could fit the tail of this distribution (i.e. when $n \geq 1$) to estimate the density of adsorption sites, which was related to the surface heterogeneity, *h*. We note that our 200 ms time resolution limited our ability to observe molecules on weak sites with characteristic residence times shorter than our acquisition time, and so our estimated site density would be expected to have a dependence on acquisition time. However, when we compared the site adsorption event count distributions of 1000 BSA trajectories on FS at an acquisition times of either 100 or 200 ms, we saw no significant changes over at least this factor of two difference (see Fig. E13 in the Supporting Information). Ultimately, we imaged all of our surfaces under similar conditions (i.e. acquisition time of 200 ms) such that we could consistently compare the heterogeneity of the different surfaces.

With these considerations in mind, we compared adsorption event histograms across surfaces in both qualitative and semi-quantitative terms. As shown in Figure 5.3, the site adsorption event histograms varied widely between surfaces. For example, PVP/PES and PEGM/PES site adsorption event distributions were more completely explained by three types of sites (i.e. three Poisson distributions) while for PVAc-PVP/PES two types of sites sufficed to describe the narrower distribution, suggesting that PVAc-PVP/PES surfaces were more homogeneous. Further, based on the multi-component Poisson distribution fitting, the majority of sites (97, 67, and 66%) were weak sites , with characteristic adsorption event counts of 0.036 ± 0.008, 0.30 ± 0.04, and 0.26 ± 0.05 for PVAc-PVP/PES, PEGM/PES, and PVP/PES respectively. All three surfaces had a second population of stronger sites with characteristic adsorption event counts of 3.0 ± 0.6, 2.2 ± 0.3, and 3.3 ± 0.6, representing 3, 28, and 23% of sites for PVAc-PVP/PES, PEGM/PES, and PVP/PES respectively. PEGM/PES and PVP/PES had an additional rare population of strong-binding sites representing 5 and 11% of sites with characteristic adsorption event counts of 6.6 ± 0.7 and 7 ± 1, respectively. A PVAc-PVP/PES

surface not only had fewer types of adsorption sites but was also comprised mainly of sites with weaker adsorption than was observed on PVP/PES and PEGM/PES. Based upon this analysis, we could conclude that PVAc-PVP/PES surfaces were more homogeneous than PVP/PES and PEGM/PES.

c. More Homogeneous Surfaces are Correlated with Shorter-Lived Adsorbed Proteins

As discussed above, site adsorption event histograms reflected a surface's spatial heterogeneity. In order to compare the relative spatial heterogeneity between different surface chemistries we calculated a dimensionless "heterogeneity" parameter, *h*, for each surface as defined in the Materials and Methods section. Surfaces with low *h* values were more homogenous than surfaces with high *h* values. Figure 5.4 shows the intriguing relationship between the mean characteristic residence times of monomers and oligomers and the surface heterogeneity, *h*. Monomer mean residence times were short-lived (~ 0.7 s) and similar for both proteins on all surfaces, suggesting that any actual variation in residence time was likely well below our time resolution. For oligomers, the mean characteristic residence times increased systematically with increasing *h*. This suggests that increasing surface homogeneity (by reducing the density and strength of strong adsorption sites) led to shorter residence times and that this surface heterogeneity metric may be a good predictor of oligomer residence times and ultimately membrane surface fouling.

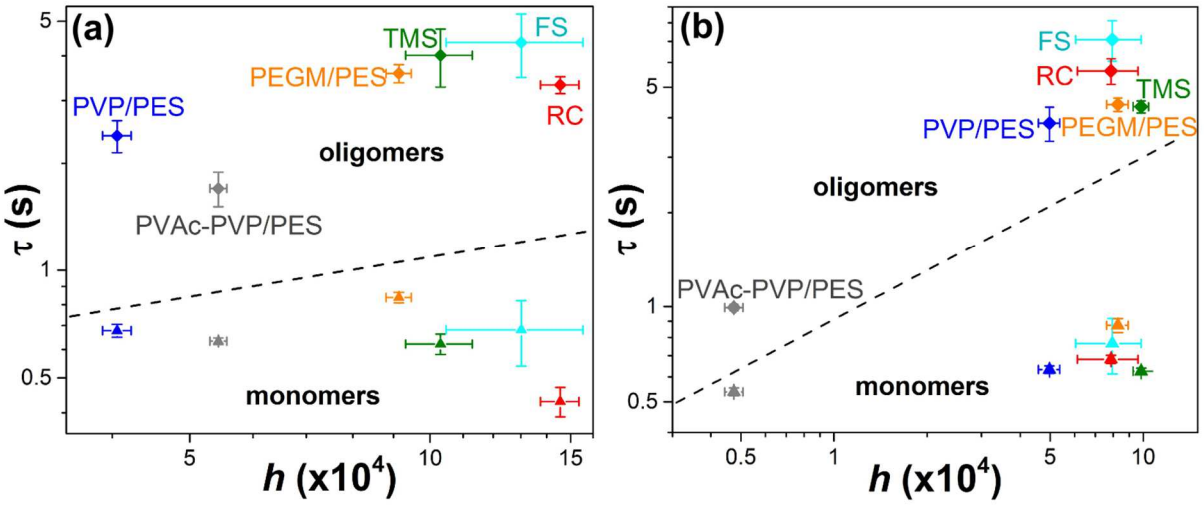

Figure 5.4: The relationship between heterogeneity, *h*, and protein monomer and oligomer mean characteristic residence times on: FS (cyan), RC (red), TMS (green), PEGM/PES (orange), PVP/PES (blue), and PVAc-PVP/PES (gray) for (a) BSA and (b) IgG. *N* was set at 1,000 trajectories for all protein-surface combinations. Error bars represent the standard error between experimental trials. Mean characteristic residence times for monomers and oligomers for all surface-protein combinations are tabulated in Table E3 of the Supporting Information.

This relationship was most pronounced for PVAc-PVP/PES and FS surfaces that represented extremely homogeneous and extremely heterogeneous behavior respectively. The oligomer surface residence times of BSA and IgG on PVAc-PVP/PES were, on average, two and four times shorter, respectively, than on all other surfaces (see Supporting Information, Table E3). Because protein-surface interactions were most homogenous and weakest on PVAc-PVP/PES compared with other wetting agents added to PES, this suggests that PVAc-PVP may also reduce protein membrane fouling better than the other wetting agents considered here.

IgG oligomer residence times varied more than BSA residence times on surfaces with similar homogeneity. For example, IgG oligomers resided longer on hydrophilic FS surfaces than on more hydrophobic TMS and PEGM/PES. This suggests that IgG interfacial dynamics were more sensitive to surface chemistry than were BSA interfacial dynamics. Such differences are not particularly surprising since BSA and IgG differ in several characteristics including the

structure and the reversibility and intermolecular forces involved in oligomerization and aggregation (see Materials and Methods for details). For example, BSA oligomers have been shown to be stabilized by intermolecular disulfide bonds.[46]

Despite hydrophobicity differences between hydrophilic FS and hydrophobic TMS, we observed similar residence times for both oligomers and monomers on both surfaces at dilute protein concentrations. This was consistent with previous single-molecule findings where both fibrinogen and BSA residence times were similar on FS and TMS surfaces.[19,47] Therefore, desorption kinetics depend on molecular phenomena that appear to be uncorrelated with macroscopic hydrophobicity.

5.3.3 Increased Protein Concentration Leads to Reduced Protein Surface Residence Times and Increased Surface Homogeneity

We have shown that at extremely dilute protein concentrations anomalous strong adsorption sites disproportionally account for proteins adsorbed to the surface and that proteins reside on these sites for significantly longer times, which may contribute to surface fouling. However, real membrane separations typically occur at high protein concentrations where protein-protein interactions could become more significant than protein-surface interactions. In previous work, we demonstrated that dynamic protein-protein interfacial associations occurred at solution concentrations as low as 10^{-5} mg/mL for BSA on a PEG monolayer (at a surface coverage of 2.5 molecules per μm^2).[45]

In the experiments described in this section, protein solution concentrations were increased to 0.3 mg/mL for IgG and 1.0 mg/mL for BSA by mixing unlabeled protein and low concentrations of fluorescently labeled protein (10^{-5} - 10^{-6} mg/mL). Labeled proteins served as reporter molecules of interfacial dynamics at these high protein concentrations. Experiments at dilute (labeled protein only) and high (labeled and unlabeled protein) concentrations were performed sequentially on the same surface sample and therefore any resulting differences in dynamics were due primarily to increased surface coverage. The same solution concentration

for each protein was used for all surfaces to account for the fact that protein surface coverage may vary on different surface chemistries. The surface coverage at high concentrations, for all protein-surface combinations, was at minimum four orders of magnitude greater than in the extremely dilute case described earlier. Calculated values for the fractional surface coverage are reported in the Supporting Information (Table E3). In brief, the surface coverage varied from less than one percent of monolayer coverage (BSA on PVAc-PVP/PES and PVP/PES) to full monolayer coverage (IgG on TMS and PVP/PES). In comparing the surfaces we found that surface heterogeneity was positively correlated with higher protein surface coverage (Table E3). This finding was consistent with our hypothesis that more heterogeneous surfaces accelerate protein layer formation.

At high protein concentrations, anomalous strong sites – that had been apparent at dilute concentrations – possibly were occupied by adsorbed proteins, preventing further adsorption to these sites. We term this phenomenon “site blocking”. As shown in Figure 5.5a and b for IgG on PVP/PES, the relatively strong sites that were identified at high protein concentrations had fewer adsorption events than on the same surface in contact with very dilute protein concentrations. The surface map at a very dilute concentration in Figure 5.5a has many strong sites and few weak sites while the surface map at high protein concentration in Figure 5.5b has more weak sites and relatively few strong sites. These qualitative observations were quantified in the site adsorption events probability distribution for 10,000 IgG adsorption events on PVP/PES (Figure 5.5c) for both protein concentration conditions. The fraction of strong sites was reduced (6 ± 1%) at a high protein concentration compared to that measured at dilute protein concentration conditions (32 ± 3%).

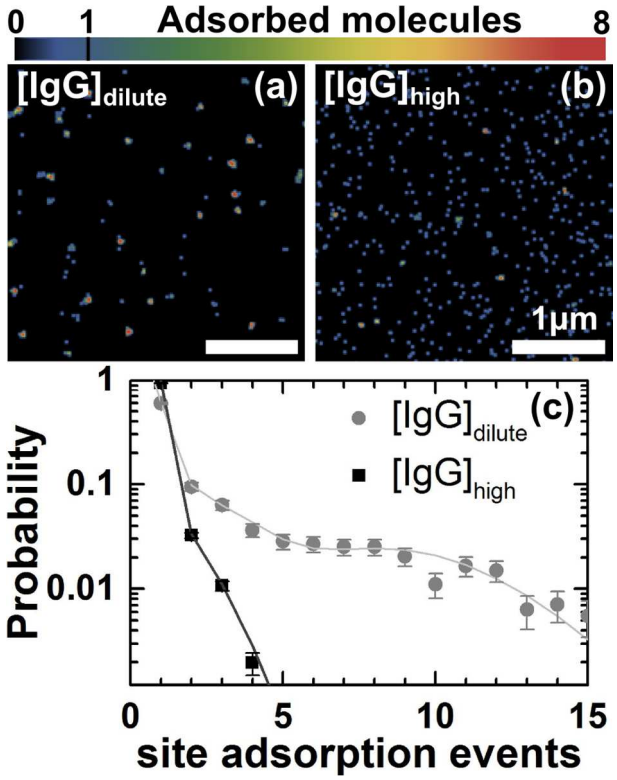

Figure 5.5: Super-resolution maps of 10,000 IgG adsorption events on PVP/PES (a) at an extremely dilute (10^{-6} mg/mL) and (b) high (0.3 mg/mL) IgG concentration of both monomer and oligomer adsorption events. (c) Site adsorption event probability distributions for 10,000 IgG adsorption events on PVP/PES at 10^{-6} mg/mL (gray) and 0.3 mg/mL (black) IgG concentrations.

In addition, IgG surface residence times at high protein concentrations were shorter than at extremely dilute concentrations on PVP/PES surfaces as shown in Figure 5.6, potentially as a result of adsorbed protein blocking further adsorption on strong sites, as suggested above. If the surfaces were perfectly homogeneous, we would expect the opposite trend, since protein-protein associations would result in more oligomers at the interface, which have longer residence times. For example, in previous work, transient protein-protein associations were observed to increase the surface residence time for BSA on a PEG monolayer at protein concentrations as low as 2.5×10^{-6} mg/mL.[45] While molecular fluorescence intensity serves as only a lower estimate of oligomerization state when unlabeled proteins are present, we saw both fluorescently-labeled monomers and oligomers at high protein concentrations on the surface (see Supporting Information). For both monomers and oligomers, we observed shorter residence times at high protein concentrations. This suggests that surface heterogeneity had a

greater impact on residence times than lateral protein-protein associations at high protein concentrations.

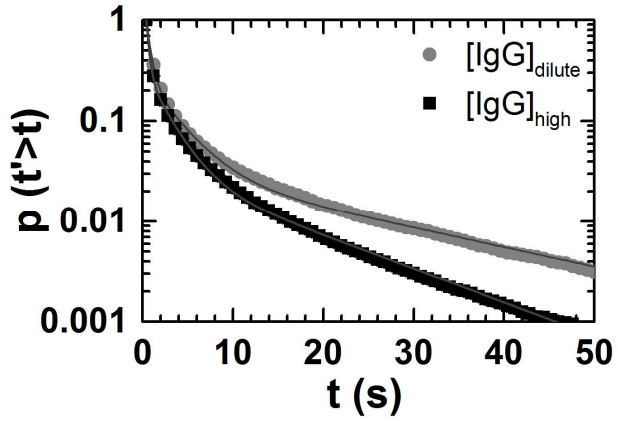

Figure 5.6: CRTDs for all IgG molecules (monomers and oligomers) on PVP/PES for an extremely dilute protein concentration (10^{-6} mg/mL, gray circles) and a high protein concentration (0.3 mg/mL, black squares). The multiple exponential population fit parameters to Equation 1 are tabulated in Table E4 in the Supporting Information.

This phenomenon of increased homogeneity and decreased residence times at high protein concentration was observed for all but the most homogenous surfaces (Table E3 in Appendix E). Of the 12 protein-surface combinations, at high protein concentrations, 9 showed an increase in homogeneity by an average factor of 2 (with the exception of BSA on PVP/PES and IgG on PVAc-PVP/PES and FS), and10 showed decreased residence time by an average factor of 2 (with the exception of IgG on PVAc-PVP/PES and RC). On none of the surfaces did we see a significant increase in residence times as protein concentration was increased (Table E3 in Appendix E).

By comparing dilute and high protein concentrations we were able to demonstrate interesting contrasts between surface chemistries. In particular, protein surface dynamics on PVAc-PVP/PES and PEGM/PES were markedly different. Both are promising protein-resistant surfaces when strong sites are greatly reduced (in the case of PVAc-PVP/PES) or blocked (in the case of PEGM/PES). PVAc-PVP/PES was the most homogenous surface, with fewer and weaker anomalous sites and short residence times at both dilute and high protein concentrations, as discussed above. In contrast, PEGM/PES was much more heterogeneous, and the residence time decrease from dilute to high protein concentrations was the most

dramatic decrease of all surfaces. On PEGM/PES the average characteristic residence times of all molecules at dilute and high IgG concentrations were 1.8 ± 0.1 and 0.33 ± 0.02 s respectively, almost an order of magnitude different (Table E3 in the Supporting Information in Appendix E). This suggests that the effect of blocking strong sites can be quite pronounced for more heterogeneous surfaces.

Another possible explanation for the reduced surface residence times at high protein concentrations is that protein-protein interactions may lead to reduced protein affinity for the surface. Unfavorable protein-protein interactions (e.g. due to electrostatics, confinement, etc.) in the adsorbed state have been previously proposed in the literature.[48,49] However, our previous work with BSA showed that protein-protein associations led to increased surface affinity and we hypothesize that BSA and IgG self-association was likely to increase surface affinity here as well.[45] Thus, we conclude that site blocking, and not protein-protein interactions, more likely played a more dominant role in the apparent decrease of protein surface affinity at high concentrations.

Surface exchange (i.e. the displacement of adsorbed proteins from the surface by proteins in solution) may also play a role in reducing surface residence times at high protein concentrations, where orders of magnitude more proteins were in solution.[50] However, we would not predict the striking change in the distribution of strong and weak surface sites nor the correlation between residence time and surface heterogeneity if surface exchange were the sole mechanism at play at high concentration. Instead, while surface exchange may play a role in reducing residence times, site blocking appeared to be the dominant cause of both reduced residence times and heterogeneity.

5.4 Conclusions

By observing individual BSA and IgG surface dynamics on polymer films with sm-TIRFM, population and spatial heterogeneity were both shown to influence protein desorption. At extremely dilute protein concentrations, protein oligomers, though less common, remained up to ten times longer on surfaces than protein monomers. Proteins – both monomers and oligomers – also remained longer on more heterogeneous surfaces that contained anomalously-strong surface sites. More proteins adsorbed and resided up to two times longer on strong sites than on more prevalent weak surface sites. We propose two potential mechanistic consequences of population and spatial heterogeneity relevant to membrane fouling: (1) longer-lived protein oligomers have more opportunities to interact with other surface species and therefore can nucleate further oligomerization and aggregation, accelerating protein layer formation; and (2) anomalously-strong sites effectively collect more protein monomers and oligomers and thus facilitate protein-protein associations, potentially leading to oligomerization and accelerated protein layer formation.

At high protein concentrations, we observed a decrease in both spatial heterogeneity and residence times for the majority of protein-surface combinations. We propose that at higher concentrations adsorbed proteins block further protein adsorption on strong sites. This suggests that at higher surface coverage heterogeneity can be mitigated by adsorbed proteins in the near surface environment.

From these findings, we recommend reducing population heterogeneity (e.g. by pre-filtering protein solutions if possible) and spatial heterogeneity (e.g. reducing the presence of anomalous sites by creating more topographically and chemically homogenous membranes or by adding blocking agents to solutions) in order to reduce protein membrane fouling. We have demonstrated a comprehensive method of characterizing and quantifying these anomalous

sites. The PVAc-PVP/PES polymer blend films appeared to reduce protein residence times, and to be the most homogenous surfaces at both dilute and high protein concentrations.

The differences observed between BSA and IgG interfacial behavior also highlight the importance of protein properties when studying membrane fouling. Often protein membrane fouling on novel membrane materials is characterized with only one type of protein feed solution, frequently BSA. As demonstrated here, BSA fouling behavior may not be representative of all protein fouling.

Finally, we note that protein oligomers and strong sites are rare phenomena, not necessarily captured with ensemble-averaged measurements. Thus, single-molecule methods are uniquely suited for studying such phenomena.

Acknowledgements

The authors (B.B.L., R.B.M., and I.S.) acknowledge primary support from Pall Corp. for many aspects of the research reported here, including salary and stipend support and polymer materials. Support for the development of high-throughput dual-channel tracking methods and instrumentation was provided by the U.S. Department of Energy Basic Energy Sciences, Chemical Sciences, Geosciences, and Biosciences Division (No. DE-SC0001854). J.N.M. was partially supported by a U.S. Department of Education Graduate Assistance in Areas of National Need Fellowship (No. P200A120125). O.J.R. is grateful for funding support by the Academy of Finland through its Center of Excellence Program (2014-2019) “Molecular Engineering of Biosynthetic Hybrid Materials Research” (HYBER). WE also thank Professor Ted Randolph and Lea Sorret at the University of Colorado Boulder for access to and assistance with their high performance liquid chromatography system.

5.5 References

(1) van Reis, R.; Zydney, A. Bioprocess Membrane Technology. *J. Membr. Sci.* **2007**, *297*, 16–50.

(2) Zydney, A. L. Membrane Technology for Purification of Therapeutic Proteins. *Biotechnol. Bioeng.* **2009**, *103*, 227–230.

(3) Saxena, A.; Tripathi, B. P.; Kumar, M.; Shahi, V. K. Membrane-Based Techniques for the Separation and Purification of Proteins: An Overview. *Adv. Colloid Interface Sci.* **2009**, *145*, 1–22.

(4) Charcosset, C. Membrane Processes in Biotechnology: An Overview. *Biotechnol. Adv.* **2006**, *24*, 482–492.

(5) Nabe, A.; Staude, E.; Belfort, G. Surface Modification of Polysulfone Ultrafiltration Membranes and Fouling by BSA Solutions. *J. Membr. Sci.* **1997**, *133*, 57–72.

(6) Chan, R.; Chen, V. Characterization of Protein Fouling on Membranes: Opportunities and Challenges. *J. Membr. Sci.* **2004**, *242*, 169–188.

(7) Zydney, A. L. Nonspecific Protein-Membrane Interactions: Adsorption and Fouling. In *Biofunctional Membranes*; Butterfield, D. A., Ed.; Plenum Press: New York, 1996; pp. 279–288.

(8) Kastantin, M.; Langdon, B. B.; Schwartz, D. K. A Bottom-up Approach to Understanding Protein Layer Formation at Solid-Liquid Interfaces. *Adv. Colloid Interface Sci.* **2014**, *207*, 240–252.

(9) Bowen, W. R.; Calvo, J. I.; Hernández, A. Steps of Membrane Blocking in Flux Decline during Protein Microfiltration. *J. Membr. Sci.* **1995**, *101*, 153–165.

(10) Reihanian, H.; Robertson, C. R.; Michaels, A. S. Mechanisms of Polarization and Fouling of Ultrafiltration Membranes by Proteins. *J. Membr. Sci.* **1983**, *16*, 237–258.

(11) Kelly, S. T.; Zydney, A. L. Mechanisms for BSA Fouling during Microfiltration. *J. Membr. Sci.* **1995**, *107*, 115–127.

(12) Kelly, S. T.; Opong, W. S.; Zydney, A. L. The Influence of Protein Aggregates on the Fouling of Microfiltration Membranes during Stirred Cell Filtration. *J. Membr. Sci.* **1993**, *80*, 175–187.

(13) Oom, A.; Poggi, M.; Wikström, J.; Sukumar, M. Surface Interactions of Monoclonal Antibodies Characterized by Quartz Crystal Microbalance with Dissipation: Impact of Hydrophobicity and Protein Self-interactions. *J. Pharm. Sci.* **2011**, *101*, 519–529.

(14) Liu, S. X.; Kim, J. T. Application of Kevin–Voigt Model in Quantifying Whey Protein Adsorption on Polyethersulfone Using QCM-D. *JALA* **2009**, *14*, 213–220.

(15) Huisman, I. H.; Prádanos, P.; Hernández, A. The Effect of Protein–Protein and Protein–Membrane Interactions on Membrane Fouling in Ultrafiltration. *J. Membr. Sci.* **2000**, *179*, 79–90.

(16) Pieracci, J.; Crivello, J. V.; Belfort, G. Photochemical Modification of 10 kDa Polyethersulfone Ultrafiltration Membranes for Reduction of Biofouling. *J. Membr. Sci.* **1999**, *156*, 223–240.

(17) Kastantin, M.; Walder, R.; Schwartz, D. K. Identifying Mechanisms of Interfacial Dynamics Using Single-Molecule Tracking. *Langmuir* **2012**, *28*, 12443–12456.

(18) Walder, R.; Kastantin, M.; Schwartz, D. K. High Throughput Single Molecule Tracking for Analysis of Rare Populations and Events. *Analyst* **2012**, *137*, 2987–2996.

(19) Kastantin, M.; Langdon, B. B.; Chang, E. L.; Schwartz, D. K. Single-Molecule Resolution of Interfacial Fibrinogen Behavior: Effects of Oligomer Populations and Surface Chemistry. *J. Am. Chem. Soc.* **2011**, *133*, 4975–4983.

(20) Walder, R.; Schwartz, D. K. Single Molecule Observations of Multiple Protein Populations at the Oil-Water Interface. *Langmuir* **2010**, *26*, 13364–13367.

(21) Walder, R.; Nelson, N.; Schwartz, D. K. Super-Resolution Surface Mapping Using the Trajectories of Molecular Probes. *Nat. Commun.* **2011**, *2*, 515.

(22) Mabry, J. N.; Skaug, M. J.; Schwartz, D. K. Single-Molecule Insights into Retention at a Reversed-Phase Chromatographic Interface. *Anal. Chem.* **2014**, *86*, 9451–9458.

(23) Sethuraman, A.; Han, M.; Kane, R. S.; Belfort, G. Effect of Surface Wettability on the Adhesion of Proteins. *Langmuir* **2004**, *20*, 7779–7788.

(24) Mahendran, R.; Malaisamy, R.; Mohan, D. R. Cellulose Acetate and Polyethersulfone Blend Ultrafiltration Membranes. Part I: Preparation and Characterizations. *Polym. Adv. Technol.* **2004**, *15*, 149–157.

(25) Zhao, C.; Xue, J.; Ran, F.; Sun, S. Modification of Polyethersulfone Membranes – A Review of Methods. *Prog. Mater. Sci.* **2013**, *58*, 76–150.

(26) Susanto, H.; Ulbricht, M. Characteristics, Performance and Stability of Polyethersulfone Ultrafiltration Membranes Prepared by Phase Separation Method Using Different Macromolecular Additives. *J. Membr. Sci.* **2009**, *327*, 125–135.

(27) Weis, A.; Bird, M. R.; Nyström, M.; Wright, C. The Influence of Morphology, Hydrophobicity and Charge upon the Long-Term Performance of Ultrafiltration Membranes Fouled with Spent Sulphite Liquor. *Desalination* **2005**, *175*, 73–85.

(28) Kontturi, E.; Thüne, P. C.; Niemantsverdriet, J. W. Cellulose Model Surfaces - Simplified Preparation by Spin Coating and Characterization by X-Ray Photoelectron Spectroscopy, Infrared Spectroscopy, and Atomic Force Microscopy. *Langmuir* **2003**, *19*, 5735–5741.

(29) Schaub, M.; Wenz, G.; Wegner, G.; Stein, A.; Klemm, D. Ultrathin Films of Cellulose on Silicon Wafers. *Adv. Mater.* **1993**, *5*, 919–922.

(30) Holmberg, M.; Berg, J.; Stemme, S.; Ödberg, L.; Rasmusson, J.; Claesson, P. Surface Force Studies of Langmuir-Blodgett Cellulose Films. *J. Colloid Interface Sci.* **1997**, *186*, 369–381.

(31) Kontturi, E.; Suchy, M.; Penttilä, P.; Jean, B.; Pirkkalainen, K.; Torkkeli, M.; Serimaa, R. Amorphous Characteristics of an Ultrathin Cellulose Film. *Biomacromolecules* **2011**, *12*, 770–777.

(32) Köhler, S.; Liebert, T.; Heinze, T. Interactions of Ionic Liquids with Polysaccharides. VI. Pure Cellulose Nanoparticles from Trimethylsilyl Cellulose Synthesized in Ionic Liquids. *J. Polym. Sci., Part A: Polym. Chem.* **2008**, *46*, 4070–4080.

(33) Norde, W.; Favier, J. P. Structure of Adsorbed and Desorbed Proteins. *Colloids Surf.* **1992**, *64*, 87–93.

(34) Kastantin, M.; Schwartz, D. K. Identifying Multiple Populations from Single-Molecule Lifetime Distributions. *ChemPhysChem* **2013**, *14*, 374–380.

(35) Chen, J. X.; Bremauntz, A.; Kisley, L.; Shuang, B.; Landes, C. F. Super-Resolution mbPAINT for Optical Localization of Single-Stranded DNA. *ACS Appl. Mater. Interfaces* **2013**, *5*, 9338–9343.

(36) Buijs, J.; Lichtenbelt, J. W. T.; Norde, W.; Lyklema, J. Adsorption of Monoclonal IgGs and Their F (ab′) 2 Fragments onto Polymeric Surfaces. *Colloids Surf., B* **1995**, *5*, 11–23.

(37) Wertz, C. F.; Santore, M. M. Adsorption and Relaxation Kinetics of Albumin and Fibrinogen on Hydrophobic Surfaces: Single-Species and Competitive Behavior. *Langmuir* **1999**, *15*, 8884–8894.

(38) McLoughlin, S. Y.; Kastantin, M.; Schwartz, D. K.; Kaar, J. L. Single-Molecule Resolution of Protein Structure and Interfacial Dynamics on Biomaterial Surfaces. *Proc. Natl. Acad. Sci.* **2013**, *110*, 19396–19401.

(39) Kisley, L.; Chen, J.; Mansur, A. P.; Shuang, B.; Kourentzi, K.; Poongavanam, M. V.; Chen, W. H.; Dhamane, S.; Willson, R. C.; Landes, C. F. Unified Superresolution Experiments and Stochastic Theory Provide Mechanistic Insight into Protein Ion-Exchange Adsorptive Separations. *Proc. Natl. Acad. Sci. U. S. A.* **2014**, *111*, 2075–2080.

(40) Babcock, J. J.; Brancaleon, L. Bovine Serum Albumin Oligomers in the E- and B-Forms at Low Protein Concentration and Ionic Strength. *Int. J. Biol. Macromol.* **2013**, *53*, 42–53.

(41) Kanani, D. M.; Sun, X.; Ghosh, R. Reversible and Irreversible Membrane Fouling during in-Line Microfiltration of Concentrated Protein Solutions. *J. Membr. Sci.* **2008**, *315*, 1–10.

(42) Cutler, H. E.; Husson, S. M.; Wickramasinghe, S. R. Prefiltration to Suppress Protein Fouling of Microfiltration Membranes. *Sep. Purif. Technol.* **2012**, *89*, 329–336.

(43) Kisley, L.; Chen, J.; Mansur, A. P.; Dominguez-Medina, S.; Kulla, E.; Kang, M. K.; Shuang, B.; Kourentzi, K.; Poongavanam, M. V.; Dhamane, S.; Willson, R.C.; Landes, C.F. High Ionic Strength Narrows the Population of Sites Participating in Protein Ion-Exchange Adsorption: A Single-Molecule Study. *J. Chromatogr. A* **2014**, *1343*, 135–142.

(44) Rutherford, H. A.; Minor, F. W.; Martin, A. R.; Harris, M. Oxidation of Cellulose: The Reaction of Cellulose with Periodic Acid. *J. Res. Natl. Bur. Stand.* **1942**, *29*, 131–141.

(45) Langdon, B. B.; Kastantin, M.; Walder, R.; Schwartz, D. K. Interfacial Protein-Protein Associations. *Biomacromolecules* **2014**, *15*, 66–74.

(46) Maruyama, T.; Katoh, S.; Nakajima, M.; Nabetani, H. Mechanism of Bovine Serum Albumin Aggregation during Ultrafiltration. *Biotechnol. Bioeng.* **2001**, *75*, 233–238.

(47) Langdon, B. B.; Kastantin, M.; Schwartz, D. K. Apparent Activation Energies Associated with Protein Dynamics on Hydrophobic and Hydrophilic Surfaces. *Biophys. J.* **2012**, *102*, 2625–2633.

(48) Sethuraman, A.; Belfort, G. Protein Structural Perturbation and Aggregation on Homogeneous Surfaces. *Biophys. J.* **2005**, *88*, 1322–1333.

(49) Rabe, M.; Verdes, D.; Rankl, M.; Artus, G. R. J.; Seeger, S. A Comprehensive Study of Concepts and Phenomena of the Nonspecific Adsorption of Beta-Lactoglobulin. *ChemPhysChem* **2007**, *8*, 862–872.

(50) Vogler, E. A. Protein Adsorption in Three Dimensions. *Biomaterials* **2012**, *33*, 1201–1237.

Chapter 6: Surface Chemistry Influences the Dynamics of Fibrinogen Self-Associations

Blake B. Langdon, Mark Kastantin, and Daniel K. Schawrtz (In preparation)

Abstract

Surface chemistry modifications have been exploited in many applications in order to tune protein adsorption, layer formation, and aggregation. However, the mechanisms by which surface chemistry influences protein layer formation remains elusive. By combining intermolecular resonance energy transfer (RET) with high-throughput single-molecule tracking, we compared the dynamics of fibrinogen (Fg) interfacial protein-protein associations on solid surfaces modified with hydrophobic trimethyl silane (TMS) or hydrophilic oligoethylene glycol (OEG). We directly observed dynamic and reversible Fg-Fg associations from Low-RET (unassociated) to High-RET (associated) states. While the interactions between isolated Fg molecules and TMS surfaces were actually weaker than isolated Fg-OEG interactions, desorption from TMS showed a greater dependence on protein concentration than from OEG, such that at higher concentrations, Fg surface residence times became longer on TMS than on OEG. Unassociated molecules showed greater mobility and a greater propensity to associate on TMS than on OEG, suggesting that the TMS surface promoted protein-protein associations. Moreover, the time intervals corresponding to protein-protein associations (i.e. characteristic contact times) also showed a greater dependence on protein concentration on TMS than on OEG, such that contact times were longer on TMS than on OEG at higher concentrations but shorter at low concentration. This suggests that protein conformations and/or orientations on hydrophobic TMS increasingly stabilized protein-protein interactions at higher protein surface coverage, in contrast to the situation on OEG surfaces. These findings strongly suggest that surface chemistry not only influences protein-surface interactions but can also promote interfacial aggregation on one surface (hydrophobic TMS) relative to another (hydrophilic OEG), and that the latter may well be the more important factor in some situations. Therefore, when

designing materials and interfaces that interact with proteins, the effects of surface chemistry on protein-protein interactions should also be considered.

6.1 Introduction

Non-specific protein adsorption at the solid-liquid interface is a phenomenon common to many applications including biomaterials, biopharmaceuticals, and biosensing.[1–4] For implantable biomaterials in particular, the creation of surfaces that resist protein adsorption, or render a material “inert”, has been a major goal. Non-specific adsorption to implanted materials of many different types of serum proteins can trigger the foreign body reaction and greatly reduce the efficacy of the implanted material.[5] In particular, fibrinogen (Fg) adsorption on such surfaces is a preliminary step in a pathological response that can result in inflammation and thormobosis.[6,7]

The physical and chemical surface properties of a biomaterial determine the type, amount, orientation, and extent of denaturation and aggregation of proteins at these interfaces.[8–10] For example, both the nanostructure and hydrophobicity of ultrahigh molecular weight polyethylene (UHMWPE) surfaces were shown to change the interfacial dynamics and aggregation behavior of Fg.[9,10] At high protein concentrations, both the nanostructure and a hydrophobic surface were required to observe Fg assembly into a side-on oriented, ordered Fg layer on UHMWPE. Many other studies have suggested that proteins have a greater affinity for hydrophobic surfaces through the observation of stronger protein-surface adhesion forces as well as greater accumulated protein on hydrophobic surface than on hydrophilic surfaces.[11–16] By understanding how surface properties influence interfacial protein behavior, we can better control protein interactions and, ultimately, *in vivo* cell interactions with such surfaces.

Polyethylene glycol (PEG) modified surfaces and materials are commonly used to reduce protein accumulation and resist cell adhesion.[14,17] In the case of grafted brushes, a dense PEG brush can greatly reduce net protein adsorbed compared with similar hydrophilic

and more hydrophobic surfaces.[18,19] Several research groups have variously proposed that PEG's ability to reduce protein adsorption may be due to steric repulsion, favorable hydration of PEG polymers, an inability to form strong hydrogen bonds, and weak PEG-protein adhesion forces.[20–23] However, the consequences of dense PEG brush-modified surfaces for dynamic interfacial protein behavior have not been explored extensively.

Previous work in our group used high-throughput single-molecule techniques to observe the dynamics of *isolated* Fg molecules on a PEG-grafted polymer surface as well as model hydrophobic and hydrophilic surfaces.[24,25] At very dilute protein concentrations, Fg adsorption was reversible, where Fg monomers were weakly bound (apparent desorption energy of approximately 4 kJ/mol) and desorbed within seconds from all surfaces. Fg oligomers (e.g. dimers, trimers, and larger aggregates) pre-formed in solution remained on the surface for up to ten-times longer than monomers and each additional molecule in an oligomeric species increased the apparent activation energy of desorption by approximately 4 kJ/mol.[25] Surprisingly, isolated Fg monomers and oligomers desorbed more slowly from the supposedly "protein-resistant" PEG-modified surface than from the model hydrophobic surface. Moreover, Fg diffusion on the PEG-modified surface was much slower than on the hydrophobic surface.[24] From these findings we hypothesized that, rather than promote protein desorption (i.e. reduce the surface affinity for isolated protein), PEG may influence dynamic Fg behavior after adsorption (e.g. slowing diffusion and reducing protein-protein interactions). Similarly, we hypothesize that faster diffusion may lead to greater protein-protein interactions on hydrophobic surfaces, such that the effects of surface chemistry on protein-protein interactions explain macroscopic observations at higher protein concentrations of reduced protein adsorption on PEG-modified surfaces, compared with on hydrophobic surfaces.[23,26,27] Indeed, dynamic interfacial BSA self-associations on a PEG-modified surface were found to increase protein surface residence times at BSA solution concentrations as low as 2.5×10^{-5} mg/mL.[28] Here, we

explored how surface chemistry influences the frequency, duration, and interfacial dynamic consequences of protein-protein associations.

In the present study, we investigated the effects of surface chemistry on the interfacial protein-protein associations of human Fg on a hydrophilic oligoethyleneglycol-modified (OEG) surface and a hydrophobic trimethylsilane-modified (TMS) surface. As demonstrated previously for bovine serum albumin (BSA), by employing intermolecular resonance energy transfer (RET) and single-molecule total internal reflection fluorescence microscopy (TIRFM), we were able to directly observe Fg-Fg associations at low-to-intermediate protein concentrations (10^{-5}-10^{-4} mg/mL).[28] We investigated Fg surface mobility, the frequency and duration of protein-protein associations, and the effects of increasing surface coverage on the average desorption behavior of Fg. Our findings suggest that protein-protein interactions can slow desorption significantly, especially on hydrophobic surfaces, and such interactions contribute to macroscopically observed protein layer formation kinetic trends with hydrophobicity.

6.2 Materials and Methods

6.2.1 Sample Preparation

Human Fg, labeled with either Alexa Fluor 546 (Fg_D, 6-9 dyes per molecule) or Alexa Fluor 647 (Fg_A, 8-9 dyes per molecule) was purchased from Invitrogen. Protein solutions were prepared in phosphate buffered saline (Gibco, pH 7.4) and diluted to a concentration of 1.6×10^{-8} mg/mL Fg_D and a concentration of Fg_A of approximately 500, 5000, or 10,000 times greater. A higher concentration of Fg_A was used in order to yield sufficiently frequent Fg_D-Fg_A associations, as previously described.[28]

We have described the surface cleaning and self-assembled monolayer functionalization in previous work.[29,30] Briefly, fused silica wafers were cleaned with a 2% (v/v) Micro90 (Electron Microscopy Science) and rinsed with MilliQ water (18 MΩ cm). Wafers were then immersed for one hour in a piranha solution (70% concentrated sulfuric acid, 30% hydrogen peroxide v/v),

dried, and UV-ozone treated for an additional hour. TMS monolayers were formed by exposing cleaned fused silica wafers to hexamethyldisilazane (Fisher Scientific) for ~18 h at room temperature. OEG silane monolayers were formed by immersing fused silica wafers in a solution composed of toluene (Fisher Scientific), methyoxy(triethyleneoxy)-propoyltrimethoxy silane (MW 326 Da, Gelest), and n-butylamine (Fisher Scientific), in a ratio of 17:2:1, respectively, for 2 hours, and then rinsed thoroughly with toluene and dried under nitrogen. Static contact angle measurements were performed with a custom-built goniometer and deionized water, described previously.[24] Contact angles of TMS and OEG monolayer modified surfaces were 90° ± 3° and 30° ± 3° respectively, consistent with previously characterized TMS and OEG modified surfaces characterized in our group.[29,30]

6.2.2 Single-Molecule Tracking

Single-molecule dynamics of fluorescently labeled Fg molecules were observed using a custom built prism-based total internal refection fluorescence microscope, at 60x magnification (0.227 μm per pixel), and a custom built flow cell, described previously.[25,31] The sample was illuminated with a fiber coupled diode-pumped solid state laser (Cobalt Samba 532 nm), used to directly excite Fg_D. After a solution containing Fg_D and Fg_A was introduced into the flow cell, flow was stopped and experiments were performed over 1 hr at room temperature. Over this time scale there was no perceivable change in protein dynamics (e.g. slowing diffusion), suggesting a steady-state process in dynamic equilibrium. In each experiment, we recorded multiple movies, or sequences of 3000 frames, with an acquisition time of 100 ms.

In order to record the fluorescence of both donor and acceptor fluorophores (and quantify RET events), an Optosplit III (Cairn Research) was used for dual-channel imaging, separating the collected photons by wavelength. The Optosplit III was composed of a dichroic mirror with a nominal separation wavelength of 610 nm (Chroma), a 585 ± 20 nm bandpass filter (Semrock) for the donor channel, and a 685 ± 20 nm bandpass filter (Semrock) for the acceptor

channel. Direct excitation of the acceptor fluorophore and donor fluorescence bleed-through into the acceptor channel were not significant due to the spectral differences in the RET pair and the optical system used as demonstrated previously[28]; control experiments, where Fg_D was only present, showed no significant signal in the acceptor channel for single molecules identified in the donor channel (not shown here). The channels were aligned within 1-2 pixels prior to capturing movies and further aligned in post-processing steps before object identification and tracking, as described previously.[28,32]

A custom-developed single-molecule tracking algorithm was used to identify objects (diffraction limited spots) in each frame, by image convolution with a disk-matrix followed by thresholding, and then linking objects from frame-to-frame (within a maximum radius of 4 pixels). Duplicate objects identified in both channels were combined. A molecule's position, donor channel intensity (F_D), acceptor channel intensity (F_A), and radius were recorded for every frame of a molecule's trajectory, as described previously.[28] The apparent relative distance, d_{app}, between the donor fluorophores attached to Fg_D molecule and the acceptor fluorophores attached to Fg_A molecule was defined as $d_{app} = (F_D/F_A)^{1/6}$. Because both Fg_D and Fg_A molecules were labeled with multiple fluorophores, d_{app} could not be interpreted as a quantitative distance but provided a useful metric for separating protein-protein association states. Based on the fairly rigid, rod-like geometry of human Fg (47.5 nm x 9 nm x 6 nm), an observation of $d_{app} < \sim 1$ (High-RET) most likely represented a side-on association between a Fg_D molecule and one or more Fg_A molecules while $d_{app} \geq \sim 1$ (Low-RET) likely represented unassociated Fg_D molecules. The probability histogram of d_{app} values showed two distinct peaks below and above d_{app} ~1 corresponding to these two states (Figure 6.1). The threshold for defining High-RET and Low-RET states was set at the d_{app} value corresponding to minimum between these two peaks (~1 for most cases) for each experimental condition (Figure F1 in the Supporting Information in Appendix F). Each frame in a trajectory was assigned to one of two RET states: Low-RET (unassociated) or High-RET (associated). While the classification of frames into these 2 RET

states may not capture all possible association orientations, it provided a useful distinction for comparing Fg association dynamics on TMS and OEG.

6.2.3 Analysis of Dynamic Molecular Behavior

A molecule's surface residence time was calculated as the number of frames in a molecule's trajectory (between adsorption and desorption) multiplied by the acquisition time. As defined above, a molecule was either in a High-RET (associated) or Low-RET (unassociated) state for each frame in its trajectory. The time interval spent in a High-RET state, or contact time $\tau_{contact}$, was calculated similarly for sequential frames of d_{app} < 1 specifically for High-RET state periods which were preceded and followed by Low-RET states (i.e. both association and dissociation was observed at the interface). Cumulative probability distributions were used to describe the residence and contact times for all accumulated Fg_D trajectories. A mean characteristic time, τ, was calculated by fitting these distributions to a weighted sum of first-order processes as in equation 1

(1) $$p(t) = \sum_i f_i e^{-t/\tau_i}$$

where *p(t)* is the probability of a molecule residing on the surface for a time, *t*, or longer, and each first-order process, *i*, used to fit the cumulative distributions could be described by a fraction of molecules, f_i, and a characteristic time, τ_i, as described previously.[28]

Interfacial diffusive motion of Fg molecules – either while in a High-RET or Low-RET state – was described using a cumulative squared displacement distribution (CSDD),[24] $C\,(r^2, t)$, for all steps taken within either RET state, for each experimental condition. This function represents the probability that a molecule moves a distance equal to or greater than a radius, r, over a time interval, t (in this case t = 100ms, the acquisition time).[24] CSDDs were conveniently fit using a Gaussian mixture model for multiple modes of diffusion

(2) $$C\,(r^2, t) = \sum_j f_j e^{-r^2/4D_j t}$$

where f_j represents the fraction of observed displacements in mode j, characterized by the diffusion coefficient, D_j. Importantly, a molecule may experience multiple diffusive modes over its trajectory and within a given RET state. Some molecules experienced periods of immobility, or confinement. Due to the positional uncertainty of our measurements (~55 nm in the donor channel and ~70 nm in the acceptor channel) these periods of confinement correspond to an apparent diffusion coefficient, $D_{confined}$ (~0.016 and 0.025 μm^2/s for donor and acceptor channel, respectively), and were described by one of the modes. Because $D_{confined}$ depends predominately on positional uncertainty at our current resolution limit, this value was held constant when fitting. Previous work in our group suggested that interfacial mobility does not follow normal random walk and Gaussian statistics.[33] Therefore, the Gaussian modes of diffusion used to fit the data were intended only to determine an apparent diffusion coefficient of mobile steps between experimental conditions. In the case where three modes were used to fit, a weighted average of the two modes with the largest D_i values were used to calculate the D_{mobile} value. Values reported in the tables below in parenthesis represent the fitting error and correspond to the error in the final digit.

6.3 Results and Discussion

6.3.1 Direct Observations of Protein-Protein Associations with RET

While sometimes neglected in simple models of protein adsorption,[34] researchers have hypothesized that protein-protein interactions are important in protein adsorption phenomena observed with macroscopic techniques.[35–40] For example, Minton proposed a model for interfacial cluster formation and demonstrated that this cluster formation model could account for the positive cooperativity observed in some protein equilibrium isotherms.[38,39] Here we postulate that surface chemistry influences the frequency and extent of protein-protein interactions, and ultimately protein cluster formation. By directly observing protein-protein

associations using intermolecular RET and single-molecule TIRFM, we explored the impact of surface chemistry on Fg-Fg association dynamics.

Dynamic protein-protein associations were observed at low-to-intermediate surface coverage. In these experiments, we exposed OEG or TMS surfaces to a phosphate buffered saline solution containing $1.6x10^{-8}$ mg/mL of donor-labeled Fg (Fg_D) and either 10^{-5}, 10^{-4}, or $2x10^{-4}$ mg/mL acceptor-labeled Fg (Fg_A) under stagnant conditions. The concentrations of Fg_A used were 2-4 orders of magnitude larger than the dilute concentrations used in previous work, where isolated protein-surface interactions were observed.[24] These concentrations were also well below the protein concentration needed to form a complete protein monolayer (on the order of 1-10 mg/m^2).[41] For example, the surface coverage of Fg at the lowest Fg_A concentration was 150 ± 30 and 32 ± 6 ng/m^2 on TMS and OEG, respectively. The surface coverage was calculated from the time-averaged number of observed Fg_D molecules per area, multiplied by the ratio of [Fg_A]:[Fg_D] (see the Supporting Information Table F1 for details). These protein concentrations allowed us to resolve individual diffraction limited spots (single Fg_D proteins) as well as access protein-protein dynamics that occur at a low to intermediate surface coverage.

Figure 6.1a shows the distribution of apparent relative distances, d_{app}, between donor-labeled and acceptor-labeled molecules for all observations of Fg on TMS at a Fg_A concentration of $2x10^{-4}$ mg/mL (i.e. d_{app} for all frames of all molecular trajectories). Importantly, the apparent relative distances values should not be interpreted as physical distances due to the complexity of our system (e.g. multiply labeled Fg, diversity of protein-protein orientations averaged over each observation window). However d_{app} does provide a convenient RET index to qualitatively distinguish associated and unassociated states. The distribution was dominated by two central peaks, either below or above a d_{app} value of ~1, which represents the minimum between the two peaks. Here, we designated observations where d_{app} < ~1 as High-RET (i.e. associated, at least one Fg_A and Fg_D molecule undergoing RET) and observations where d_{app} ≥ ~1 as Low-RET (i.e. unassociated, a Fg_D molecule not closely interacting with a Fg_A molecule).

We hypothesized that the lower d_{app} peak (High-RET), shown in Figure 6.1a, corresponded to a side-on (rather than end-on) Fg_D-Fg_A interaction where multiple fluorophores along the length of the Fg molecules were likely undergoing RET. We also observed that the relative height and area under the two central peaks changed with Fg_A concentration on TMS (i.e. the High-RET peak height increased while the Low-RET peak decreased with increasing [Fg_A], see Figure F1 in the Supporting Information). These qualitative observations suggested that these peaks were physically significant.

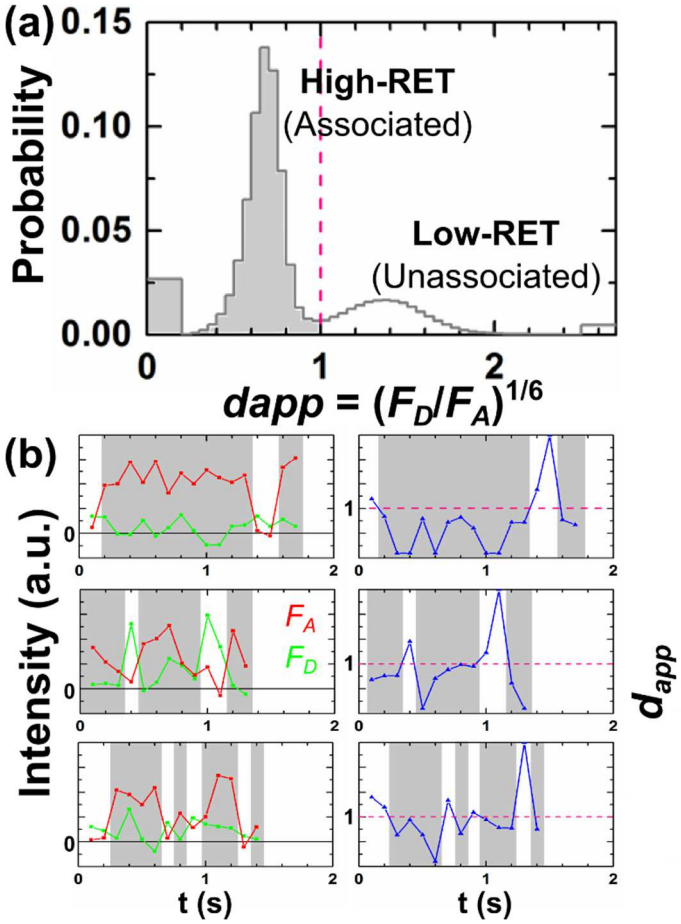

Figure 6.1: (a) Probability distribution of apparent relative distance, d_{app}, for Fg on TMS at [Fg_A] = 2x10^{-4} mg/mL. An object was identified as High-RET (gray fill) if d_{app} < 1 while an object with d_{app} ≥ 1 was identified as Low-RET. The step functions, or "boxes", at either end of the distribution represent the scenario where either F_D or F_A was less than the local background, such that d_{app} could not be calculated accurately. The area under each "box" is proportional to the number of association states where either F_D (0.0 < d_{app} < 0.02) or F_A (2.5 < d_{app} < 2.7) was insignificant such that the total area under the "boxes" and curve integrates to unity. (b) Fluorescent intensities in the acceptor and donor channels and d_{app} values are shown for three representative Fg_D trajectories on TMS at a [Fg_A] = 2x10^{-4} mg/mL. The High-RET states of each trajectory, where d_{app} < 1, are highlighted in gray while Low-RET states, where d_{app} ≥ 1, are highlighted in white.

During a molecule's surface residence time, a molecule could be either in High-RET or Low-RET states and could transition dynamically between these states (i.e. associate or dissociate). Figure 6.1b shows the fluorescent intensities in the donor and acceptor channels, and calculated d_{app}-value, for each frame of three representative dynamically-associating

molecular trajectories. Importantly, these trajectories demonstrate that Fg-Fg associations could be reversible. In Figure 6.1b, the time intervals that Fg_D molecules resided in a High-RET state (contact times) and a Low-RET state (search times) are highlighted in gray and white, respectively. Both contact times and search times provide kinetic information about dissociation and association rates, respectively. By defining High-RET (associated) and Low-RET (unassociated) states, we examined the interfacial dynamics (e.g. diffusion) of each RET state and compared Fg's interfacial behavior between surface chemistries.

6.3.2 Surface Residence Times Are More Sensitive to Solution Concentration on TMS Than on OEG

In previous work examining BSA-BSA associations on PEG, molecules that dynamically associated (e.g. a BSA_D protein associated and/or dissociated with at least one BSA_A protein) at the interface remained on the surface longer than molecules that remained unassociated.[28] Similarly, in the current work Fg_D proteins that dynamically associated with other Fg_A proteins (i.e. associating molecules) remained on the surface for longer than Fg_D proteins that were unassociated for their entire surface residence time on both TMS and OEG (see Figure F2). This was consistent with other single molecule observations of Fg and BSA where pre-formed dimers, trimers, and larger oligomers had up to ten times longer surface residence times than monomers.[24,25] Therefore, more frequent and longer-lasting protein-protein associations often resulted in longer surface residences times, especially as a surface became more crowded with proteins.

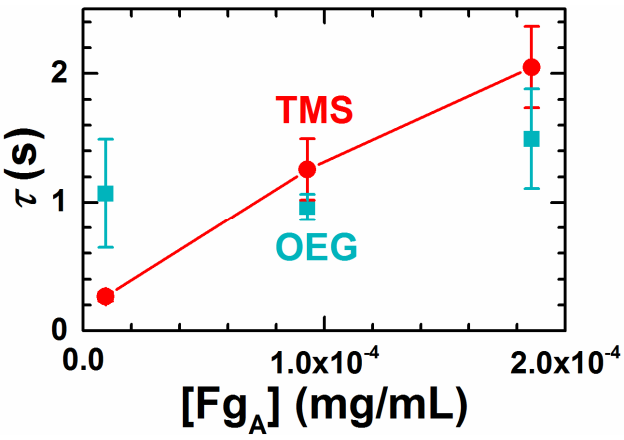

Figure 6.2: Mean characteristic surface residence times, τ, of associating Fg_D proteins (i.e. Fg_D proteins that undergo an association or dissociation while at the interface) on OEG and TMS. Error bars represent the standard deviation between movies. CRTDs of associating Fg_D molecules for all conditions are shown in Figure F3 in Appendix F. Figure F5 shows a similar trend for all molecules' surface residence times (i.e. both associating and unassociated Fg_D proteins).

The mean characteristic residence times of associating molecules, calculated from the cumulative surface residence time distribution (CRTD, see Figure F3 in the Supporting Information), increased by an order of magnitude on TMS from 0.27 ± 0.03 s at a 10^{-5} mg/mL to 2.0 ± 0.3 s at $2x10^{-4}$ mg/mL, as shown in Figure 6.2. In contrast, the mean characteristic surface residence times of associating molecules on OEG was relatively insensitive to changes in $[Fg_A]$. Importantly, we propose that these observations explain the discrepancy between macroscopic observations of reduced protein adsorption to PEG surfaces at high protein concentrations[19,42] and single-molecule observations at very dilute protein concentrations, where isolated Fg molecules were longer-lived on PEG than on TMS.[24] At a Fg_A concentration of 10^{-5} mg/mL, residence times on TMS were shorter than on OEG, similar to the situation for completely isolated proteins. However, at Fg_A concentrations of 10^{-4} mg/mL and higher, associating Fg_D molecules resided on TMS for longer than on OEG. Thus, there was a crossover concentration at which dynamic protein-protein associations become significant and residence times on TMS become longer than on OEG (see Supporting Information Figure F3 for the mean characteristic residence times of all molecules, unassociated and associating). Because Fg residence time on

TMS increased more dramatically than on OEG, we propose that surface chemistry influenced the extent and frequency of protein-protein interactions in different ways.

We hypothesize that the crossover of mean characteristic residence times at higher Fg_A concentrations reflected differences in the frequency and extent of protein-protein interactions on TMS and OEG. The observation of concentration-dependent residence times on TMS was consistent with a previously proposed mechanism whereby individual proteins adsorb to a surface, diffuse to, associate with, and/or dissociate from other proteins, and desorb from the surface.[28,43,44] In this proposed mechanism, the relative rates of each process (e.g. adsorption, diffusion, association, dissociation, and desorption) determine the frequency and extent (e.g. orientation and number of proteins interacting) of protein-protein associations at the interface. Such rates are inherently sensitive to surface chemistry. For example, by simulating and modifying Fg adsorption, interfacial diffusion, and protein-protein interaction strengths, Siegismund et al. found that the number, size, and conformation of the associated protein clusters or aggregates varied, where more adhesive surfaces resulted in larger networks of Fg clusters.[45] Below, we explore experimentally the ways in which surface chemistry influences the dynamics (e.g. diffusion, frequency of protein-protein associations, and contact times) of Fg on TMS and on OEG.

6.3.4 Fg is More Mobile on TMS Than on OEG

Greater interfacial mobility is expected to increase the frequency of protein-protein collisions. Previous studies have shown that surface chemistry can greatly influence a molecule's interfacial mobility.[24,46,47] Here, we examined the effect of surface chemistry on Low-RET state (unassociated) Fg diffusion. Figure 6.3a and 6.3b show representative surface displacement trajectories on OEG and TMS, respectively, of Fg_D molecules that adsorbed unassociated and then associated with at least one Fg_A molecule. In order to examine the interfacial diffusive motion of Fg more quantitatively, we examined the CSDD for all molecule

steps taken while in a unassociated state. Figure 6.3c shows CSDDs of Fg displacements made in Low-RET states (i.e. unassociated, monomeric Fg) on OEG and TMS, at a Fg_A concentration of 10^{-5} mg/mL, and indicates that on TMS unassociated Fg had a greater probability of executing longer steps than on OEG. The representative surface trajectories in Figures 6.3a and 6.3b show that unassociated Fg_D molecules executed both short and long steps. In addition, in the representative trajectories, Fg_D molecules were clearly more likely to take more long steps on TMS than on OEG, consistent with previous findings that isolated Fg molecules diffused more quickly on TMS than on PEG.[24]

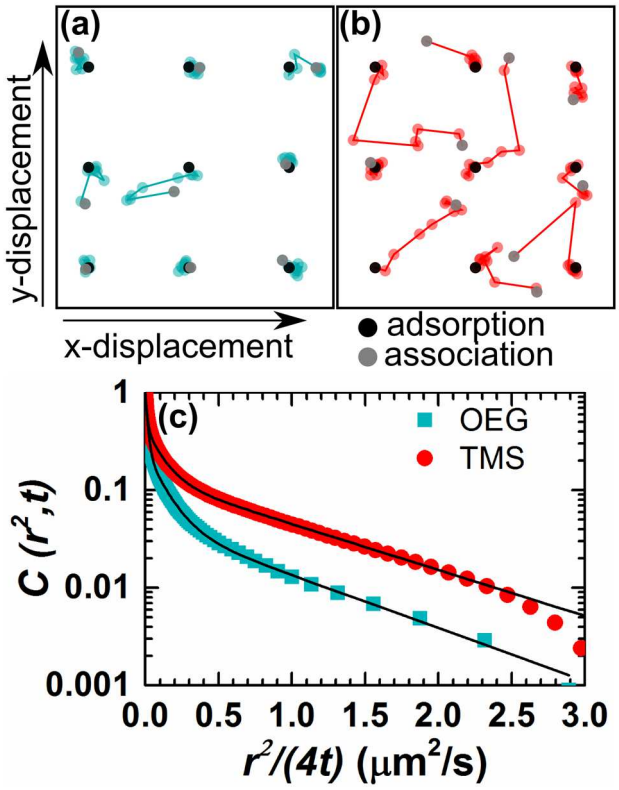

Figure 6.3: Representative displacement trajectories of molecules that adsorbed and then associated on (a) OEG (cyan), or (b) TMS (red) at $[Fg_A] = 10^{-5}$ mg/mL. Each point represents a molecule's localized position in a given frame and the lines connecting the points represent surface displacements executed between frames. A molecule's initial (adsorption) and final (association) positions are indicated by the black and gray points, respectively. (c) CSDDs for Fg diffusive steps made while in a Low-RET (unassociated) state on OEG and TMS at $[Fg_A] = 10^{-5}$ mg/mL.

Previous work in our group, and others, has indicated that many different types of molecules (including proteins) undergo intermittent random walks at the solid-liquid interface.[31,33,48] For example, Skaug et al. showed that molecules became temporarily "confined" for a distribution of waiting times and then executed larger surface displacements, or "mobile" steps.[33] The confined and mobile diffusion coefficients, and the relative fraction of displacements in each, are quantified in Table 6.1. Low-RET, unassociated Fg molecules were mobile for approximately 60% more steps and took longer steps (by approximately 50% in squared displacement) on TMS than on OEG. This trend can qualitatively be seen in the representative surface trajectories shown in Figures 6.3a and 6.3b where more and longer mobile steps (represented by the colored segments of the trajectories) were seen on TMS. Importantly, a single Fg_D molecule could take both "confined" and "mobile" steps.

Table 6.1: Mobile and confined diffusion mode parameters for Low-RET Fg_D steps on OEG and TMS at $[Fg_A] = 10^{-5}$ mg/mL.

	OEG		**TMS**	
mode	*f*	*D* (μm²/s)	*f*	*D* (μm²/s)
confined	0.747(6)	0.016	0.597(6)	0.016
mobile	0.253(6)	0.25(2)	0.403(6)	0.38(2)

The length and frequency of these "mobile" steps can be influenced by a molecule's affinity for the surface, or its re-adsorption and desorption potentials. For, example, the absence of specific short-range interactions of the TMS surface is hypothesized to create fewer barriers for surface diffusion on TMS such that molecules are more likely to take execute longer surface displacements.[25,30] On the other hand, the observation of fewer and shorter diffusive steps on OEG has been proposed to result from greater short-range interactions between the molecule, surface, and the aqueous environment (e.g. the greater affinity of bound water molecules at the OEG interface, interacting with grafted polymer chain)[49], reducing the potential of both protein desorption and re-adsorption.[30]

Because Fg molecules in Low-RET states moved more frequently and faster on TMS than on OEG, they were also more likely to associate with and dissociate from other molecules on the surface. Below we demonstrate some of the consequences of greater mobility for interfacial protein-protein associations.

6.3.5 Fg-Fg Associations Occur More Frequently on TMS Than on OEG

Fg-Fg associations occurred more readily on TMS than on OEG. Interestingly, the mean characteristic search time (i.e., the time between adsorbing in a Low-RET state to either association or desorption) of ~0.8 s was the same on OEG and TMS. However, the fraction of successful searches that ended in association, rather than desorption, was greater on TMS than on OEG with 54 ± 2% and 43 ± 2% of all searches ending in an association on TMS and OEG, respectively, for a Fg_A concentration of 10^{-5} mg/mL. This suggested that greater mobility and higher Fg surface coverage on TMS enabled more successful protein-protein associations.

The greater frequency of protein-protein associations was also apparent when we compared the number density of associating molecular trajectories per second, $n_{associating}$ (i.e. all trajectories that experienced both RET states normalized by time and area), on both surfaces as shown in Figure 6.4. At all Fg_A concentrations considered, we observed significantly more associating Fg_D proteins on TMS than on OEG for the same bulk Fg_D concentrations. Strikingly, at the lowest [Fg_A] (10^{-5} mg/mL), there were 20 times more dynamically associating trajectories on TMS (14,000 ± 4,000 molecules s^{-1} mm^{-2}) than on OEG (700 ± 200 molecules s^{-1} mm^{-2}) while the relative Fg surface coverage on TMS was less than 5 times that on OEG at this concentration (see Table F1 in the Supporting Information).

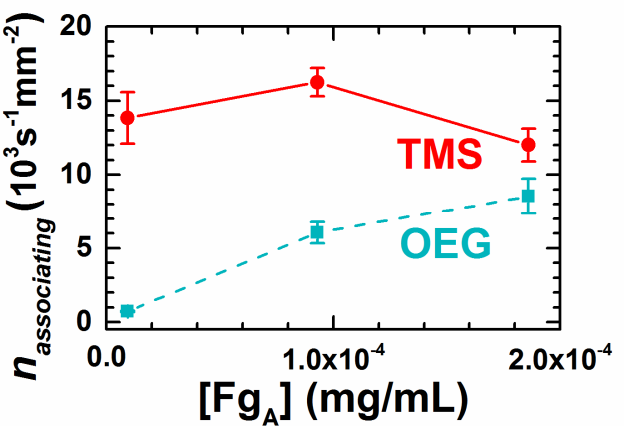

Figure 6.4: The number density of associating molecules (i.e. exhibited both High-RET and Low-RET states over their surface residence time) per second and mm^2, $n_{associating}$, as a function of [Fg$_A$].

On OEG, the number density of associating molecules increased with increasing Fg$_A$ concentration, consistent with an increasing Fg surface coverage (see Table F1 in Appendix F). Thus, on OEG the fraction of associating molecules remained fairly constant at all [Fg$_A$] (~14% of all molecules associated or dissociated while at the interface). On TMS, the number density of associating Fg$_D$ proteins remained high and fairly constant with increasing [Fg$_A$], despite Fg surface coverage changes (see Table F1). We suspect that this may be due to the increased surface coverage of Fg$_A$ molecules where Fg$_D$ molecules could directly adsorb on top of Fg$_A$ molecules at the interface at higher Fg$_A$ concentrations, such that the number density of associating trajectories at higher concentrations was underestimated, because we could not observe interfacial association and dissociations. Indeed, we observed a higher fraction of molecules that adsorbed directly into the associated state at higher Fg$_A$ concentrations on TMS: at a Fg$_A$ concentration of 10^{-5} mg/mL, 59% of molecules adsorbed in a High-RET state while at a Fg$_A$ concentration of 2×10^{-4} mg/mL, 86% of molecules adsorbed in a High-RET state. In all cases, there were more dynamic protein-protein interactions occurring on TMS than on OEG. Below, we show that these associations also were increasingly longer-lived at higher concentrations on TMS.

6.3.6 Fg-Fg Associations Are More Sensitive to Solution Concentration on TMS than on OEG

Contact times for Fg-Fg associations were more sensitive to bulk Fg_A concentration on TMS than on OEG, becoming longer-lived on TMS with increasing [Fg_A] (see Figure F4 in the Supporting Information). Figure 6.5 shows the mean characteristic contact times for Fg-Fg associations at all Fg_A concentrations on TMS and OEG. Similar to the surface residence times, on TMS the mean characteristic contact time at $2x10^{-4}$ mg/mL (1.2 ± 0.2 s) was 6 times longer than at 10^{-5} mg/mL (0.19 ± 0.05 s), while on OEG the contact times were apparently independent of [Fg_A].

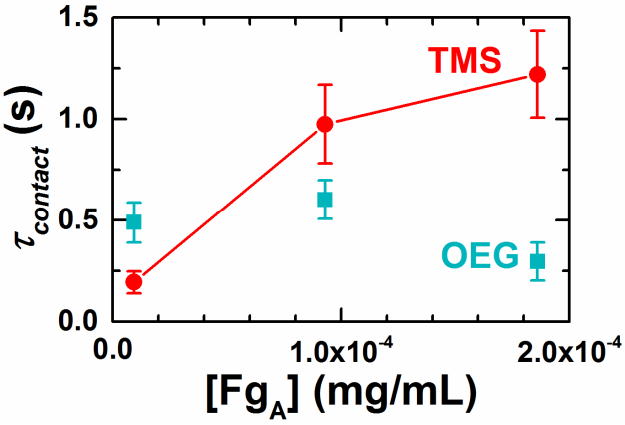

Figure 6.5: Mean characteristic contact times, $\tau_{contact}$, of Fg_D-Fg_A associations on OEG and TMS. Cumulative contact time distributions used to fit and calculate $\tau_{contact}$ are shown in Figure F4 of the Supporting Information. Error bars represent the standard deviation between movies.

In a previous single-molecule intermolecular RET study of BSA-BSA associations, we observed two distinct types of associations, Partial-RET and Complete-RET, which we attributed to a BSA_D molecule associating with one BSA_A molecule or multiple BSA_A molecules, respectively.[28] Similar to the Fg-Fg associations on OEG observed here, both Complete-RET and Partial-RET contact times were independent of bulk BSA concentration. We attributed BSA's dissociation behavior to heterogeneous distributions of proteins on the surface, with areas of high protein density (clusters) and low protein density (isolated monomers).

Heterogeneously distributed lysozyme surface coverage on mica was also previously observed with atomic force microscopy.[44] Therefore BSA dissociation dynamics were influenced only by the local environment rather than the global surface coverage. We propose that this is also the case for Fg on OEG at the surface coverage studied here.

On the other hand, we speculate that the orientation, conformation, and/or number of Fg molecules involved in an association on TMS changes with Fg_A concentration/surface coverage, resulting in longer associations at higher coverage. For example, Song et al. also observed greater Fg packing order with increasing Fg surface coverage on polystyrene-*block*-poly(methyl methacrylate) surfaces.[8] In the present work, High-RET (associated) states on TMS spent a greater fraction of time confined at higher [Fg_A] (see Table 6.2), consistent with the previous observation of larger Fg aggregates (e.g. trimers and tetramers) taking relatively fewer large steps than Fg monomers or dimers.[24] In addition, as residence times increased with Fg_A concentration on TMS, Fg may also have more opportunities to undergo conformation or orientation changes at the interface and may instead be forming more strongly bound aggregates. For example, at increasing Fg concentrations, a combination of both conformation and aggregate size was proposed to stabilize Fg self-associations in solution, potentially due to specific Fg-Fg associations through Fg's αC-domains.[50] Perhaps, specific interactions that promote Fg-Fg association do not occur on OEG due to a preferred Fg orientation on OEG, resulting in a stabilized monomeric state.

Table 6.2: Mobile and confined diffusion mode parameters for High-RET (associated) state steps on TMS at various [Fg_A].

	10^{-5} mg/mL		10^{-4} mg/mL		$2x10^{-4}$ mg/mL	
mode	*f*	*D* ($\mu m^2/s$)	*f*	*D* ($\mu m^2/s$)	*f*	*D* ($\mu m^2/s$)
confined	0.260(8)	0.025	0.741(6)	0.025	0.786(6)	0.025
mobile	0.740(8)	0.40(1)	0.259(7)	0.34(3)	0.214(7)	0.35(4)

6.4 Conclusion

Single-molecule observations of Fg-Fg associations at low-to-intermediate protein surface coverage suggested that hydrophobic TMS surfaces promoted protein-protein associations relative to hydrophilic OEG surfaces. Intermolecular RET allowed us distinguish between High-RET (associated) or Low-RET (unassociated) states and examine protein dynamics within (e.g. diffusion) and between (e.g. contact times) these states. Interestingly, Fg residence times on TMS, initially shorter at low protein concentrations than on OEG, were longer at higher protein concentrations on TMS than on OEG. Unassociated Fg molecules were more likely to execute large surface displacements and to associate with other Fg molecules on TMS surfaces than on OEG surfaces. This behavior was also correlated with a greater fraction of molecules dynamically associated on TMS than on OEG. Finally, the amount of time proteins remained associated (i.e. contact time) showed a greater dependence on protein concentration on TMS (e.g. increasing with increasing [Fg_A]) than on OEG. Based on these findings, we suggest that greater mobility and more frequent and longer-lived protein-protein interactions on TMS led to slower desorption from TMS as the protein concentration increased. In contrast, desorption from OEG was relatively insensitive to concentration. Therefore, in addition to influencing protein-surface interactions directly, protein surface chemistry also appears to plays an important indirect role by tuning protein-protein associations at the interface. For the rational design of blood-contacting biomaterials, these results suggest that lateral protein mobility, which may be tuned by surface hydrophobicity but also by other parameters like surface topography,[51] can be used to control the propensity of the surface to gather protein aggregates.

Acknowledgements

B.B.L. and M.K. acknowledge support from the National Institute of Biomedical Imaging and Bioengineering of the National Institutes of Health (under award #5R21EB015532-02). Support for the development of high-throughput dual-channel tracking methods was provided by the U.S. Department of Energy Basic Energy Sciences, Chemical Sciences, Geosciences, and Biosciences Division (under award DE-SC00018654).

6.5 References

(1) Bee, J. S.; Randolph, T. W.; Carpenter, J. F.; Bishop, S. M.; Dimitrova, M. N. Effects of Surfaces and Leachables on the Stability of Biopharmaceuticals. *J. Pharm. Sci.* **2011**, *100*, 4158–4170.

(2) Kim, K. J.; Chen, V.; Fane, A. G. Some Factors Determining Protein Aggregation during Ultrafiltration. *Biotechnol. Bioeng.* **1993**, *42*, 260–265.

(3) Ratner, B. D.; Bryant, S. J. Biomaterials: Where We Have Been and Where We Are Going. *Annu. Rev. Biomed. Eng.* **2004**, *6*, 41–75.

(4) Nath, N.; Hyun, J.; Ma, H.; Chilkoti, A. Surface Engineering Strategies for Control of Protein and Cell Interactions. *Surf. Sci.* **2004**, *570*, 98–110.

(5) Anderson, J. M.; Rodriguez, A.; Chang, D. T. Foreign Body Reaction to Biomaterials. *Semin. Immunol.* **2008**, *20*, 86–100.

(6) Hu, W. J.; Eaton, J. W.; Ugarova, T. P.; Tang, L. Molecular Basis of Biomaterial-Mediated Foreign Body Reactions. *Blood* **2001**, *98*, 1231–1238.

(7) Gorbet, M. B.; Sefton, M. V. Biomaterial-Associated Thrombosis: Roles of Coagulation Factors, Complement, Platelets and Leukocytes. *Biomaterials* **2004**, *25*, 5681–5703.

(8) Song, S.; Ravensbergen, K.; Alabanza, A.; Soldin, D.; Hahm, J. Distinct Adsorption Configurations and Self-Assembly Characteristics of Fibrinogen on Chemically Uniform and Alternating Surfaces Including Block Copolymer Nanodomains. *ACS Nano* **2014**, *8*, 5257–5269.

(9) Kastantin, M.; Keller, T. F.; Jandt, K. D.; Schwartz, D. K. Single-Molecule Tracking of Fibrinogen Dynamics on Nanostructured Poly(ethylene) Films. *Adv. Funct. Mater.* **2012**, *22*, 2617–2623.

(10) Keller, T. F.; Schönfelder, J.; Reichert, J.; Tuccitto, N.; Licciardello, A.; Messina, G. M. L. M.; Marletta, G.; Jandt, K. D. How the Surface Nanostructure of Polyethylene Affects Protein Assembly and Orientation. *ACS Nano* **2011**, *5*, 3120–3131.

(11) Rabe, M.; Verdes, D.; Seeger, S. Understanding Protein Adsorption Phenomena at Solid Surfaces. *Adv. Colloid Interface Sci.* **2011**, *162*, 87–106.

(12) Hlady, V.; Buijs, J. Protein Adsorption on Solid Surfaces. *Curr. Opin. Biotechnol.* **1996**, *7*, 72–77.

(13) Norde, W.; Horbett, T. A.; Brash, J. L. Proteins at Interfaces III: Introductory Overview. In *Proteins at Interfaces III State of the Art*; 2012; pp. 1–34.

(14) Ostuni, E.; Chapman, R. G.; Holmlin, R. E.; Takayama, S.; Whitesides, G. M. A Survey of Structure-Property Relationships of Surfaces That Resist the Adsorption of Protein. *Langmuir* **2001**, *17*, 5605–5620.

(15) Xu, L.-C.; Siedlecki, C. A. Effects of Surface Wettability and Contact Time on Protein Adhesion to Biomaterial Surfaces. *Biomaterials* **2007**, *28*, 3273–3283.

(16) Xu, L.-C.; Siedlecki, C. a. Atomic Force Microscopy Studies of the Initial Interactions between Fibrinogen and Surfaces. *Langmuir* **2009**, *25*, 3675–3681.

(17) Castner, D. G.; Ratner, B. D. Biomedical Surface Science: Foundations to Frontiers. *Surf. Sci.* **2002**, *500*, 28–60.

(18) Hu, Y.; Jin, J.; Han, Y.; Yin, J.; Jiang, W.; Liang, H. Study of Fibrinogen Adsorption on Poly(ethylene Glycol)-Modified Surfaces Using a Quartz Crystal Microbalance with Dissipation and a Dual Polarization Interferometry. *RSC Adv.* **2014**, *4*, 7716.

(19) Sofia, S.; Premnath, V.; Merrill, E. Poly(ethylene Oxide) Grafted to Silicon Surfaces: Grafting Density and Protein Adsorption. *Macromolecules* **1998**, *31*, 5059–5070.

(20) Jeon, S. I.; Lee, J. H.; Andrade, J. D.; De Gennes, P. G. Protein—surface Interactions in the Presence of Polyethylene Oxide: I. Simplified Theory. *J. Colloid Interface Sci.* **1991**, *142*, 149–158.

(21) Unsworth, L. D.; Sheardown, H.; Brash, J. L. Protein-Resistant Poly(ethylene Oxide)-Grafted Surfaces: Chain Density-Dependent Multiple Mechanisms of Action. *Langmuir* **2008**, *24*, 1924–1929.

(22) Currie, E. P. K.; Norde, W.; Cohen Stuart, M. a. *Tethered Polymer Chains: Surface Chemistry and Their Impact on Colloidal and Surface Properties.*; 2003; Vol. 100-102, pp. 205–265.

(23) Prime, K. L.; Whitesides, G. M. Adsorption of Proteins onto Surfaces Containing End-Attached Oligo (ethylene Oxide): A Model System Using Self-Assembled Monolayers. *J. Am. Chem. Soc.* **1993**, 10714–10721.

(24) Kastantin, M.; Langdon, B. B.; Chang, E. L.; Schwartz, D. K. Single-Molecule Resolution of Interfacial Fibrinogen Behavior: Effects of Oligomer Populations and Surface Chemistry. *J. Am. Chem. Soc.* **2011**, *133*, 4975–4983.

(25) Langdon, B. B.; Kastantin, M.; Schwartz, D. K. Apparent Activation Energies Associated with Protein Dynamics on Hydrophobic and Hydrophilic Surfaces. *Biophys. J.* **2012**, *102*, 2625–2633.

(26) Nygren, H.; Alaeddin, S.; Lundström, I.; Magnusson, K.-E. Effect of Surface Wettability on Protein Adsorption and Lateral Diffusion. Analysis of Data and a Statistical Model. *Biophys. Chem.* **1994**, *49*, 263–272.

(27) Prime, K. L.; Whitesides, G. M. Self-Assembled Organic Monolayers: Model Systems for Studying Adsorption of Proteins at Surfaces. *Science (80-.).* **1991**, *252*, 1164–1167.

(28) Langdon, B. B.; Kastantin, M.; Walder, R.; Schwartz, D. K. Interfacial Protein-Protein Associations. *Biomacromolecules* **2014**, *15*, 66–74.

(29) Kastantin, M.; Schwartz, D. K. DNA Hairpin Stabilization on a Hydrophobic Surface. *Small* **2013**, *9*, 933–941.

(30) Monserud, J. H.; Schwartz, D. K. Effects of Molecular Size and Surface Hydrophobicity on Oligonucleotide Interfacial Dynamics. *Biomacromolecules* **2012**, *13*, 4002–4011.

(31) Honciuc, A.; Harant, A. W.; Schwartz, D. K. Single-Molecule Observations of Surfactant Diffusion at the Solution-Solid Interface. *Langmuir* **2008**, *24*, 6562–6566.

(32) Kastantin, M.; Schwartz, D. K. Connecting Rare DNA Conformations and Surface Dynamics Using Single-Molecule Resonance Energy Transfer. *ACS Nano* **2011**, *5*, 9861–9869.

(33) Skaug, M. J.; Mabry, J.; Schwartz, D. K. Intermittent Molecular Hopping at the Solid-Liquid Interface. *Phys. Rev. Lett.* **2013**, *110*, 256101.

(34) Kastantin, M.; Langdon, B. B.; Schwartz, D. K. A Bottom-up Approach to Understanding Protein Layer Formation at Solid-Liquid Interfaces. *Adv. Colloid Interface Sci.* **2014**, *207*, 240–252.

(35) Marucco, A.; Turci, F.; O'Neill, L.; Byrne, H. J.; Fubini, B.; Fenoglio, I. Hydroxyl Density Affects the Interaction of Fibrinogen with Silica Nanoparticles at Physiological Concentration. *J. Colloid Interface Sci.* **2014**, *419*, 86–94.

(36) Rabe, M.; Verdes, D.; Seeger, S. Understanding Cooperative Protein Adsorption Events at the Microscopic Scale: A Comparison between Experimental Data and Monte Carlo Simulations. *J. Phys. Chem. B* **2010**, *114*, 5862–5869.

(37) Rabe, M.; Verdes, D.; Zimmermann, J.; Seeger, S. Surface Organization and Cooperativity during Nonspecific Protein Adsorption Events. *J. Phys. Chem. B* **2008**, *112*, 13971–13980.

(38) Minton, A. A. P. Effects of Excluded Surface Area and Adsorbate Clustering on Surface Adsorption of Proteins. II. Kinetic Models. *Biophys. J.* **2001**, *80*, 1641–1648.

(39) Minton, A. P. Effects of Excluded Surface Area and Adsorbate Clustering on Surface Adsorption of Proteins I. Equilibrium Models. *Biophys. Chem.* **2000**, *86*, 239–247.

(40) Joshi, O.; Lee, H. J.; McGuire, J.; Finneran, P.; Bird, K. E. Protein Concentration and Adsorption Time Effects on Fibrinogen Adsorption at Heparinized Silica Interfaces. *Colloids Surfaces B Biointerfaces* **2006**, *50*, 26–35.

(41) Wertz, C. F.; Santore, M. M. Effect of Surface Hydrophobicity on Adsorption and Relaxation Kinetics of Albumin and Fibrinogen: Single-Species and Competitive Behavior. *Langmuir* **2001**, *17*, 3006–3016.

(42) Sigal, G. B.; Mrksich, M.; Whitesides, G. M. Effect of Surface Wettability on the Adsorption of Proteins and Detergents. *J. Am. Chem. Soc.* **1998**, *120*, 3464–3473.

(43) Walder, R.; Schwartz, D. K. Dynamics of Protein Aggregation at the Oil–water Interface Characterized by Single Molecule TIRF Microscopy. *Soft Matter* **2011**, *7*, 7616–7622.

(44) Kim, D. T.; Blanch, H. W.; Radke, C. J. Direct Imaging of Lysozyme Adsorption onto Mica by Atomic Force Microscopy. *Langmuir* **2002**, *18*, 5841–5850.

(45) Siegismund, D.; Keller, T. F.; Jandt, K. D.; Rettenmayr, M. Fibrinogen Adsorption on Biomaterials--a Numerical Study. *Macromol. Biosci.* **2010**, *10*, 1216–1223.

(46) Skaug, M. J.; Schwartz, D. K. Using the Dynamics of Fluorescent Cations to Probe and Map Charged Surfaces. *Soft Matter* **2012**, *8*, 12017.

(47) Tilton, R.; Robertson, C.; Gast, A. Lateral Diffusion of Bovine Serum Albumin Adsorbed at the Solid-Liquid Interface. *J. Colloid Interface Sci.* **1990**, *137*, 192–203.

(48) Yu, C.; Guan, J.; Chen, K.; Bae, S. C.; Granick, S. Single-Molecule Observation of Long Jumps in Polymer Adsorption. *ACS Nano* **2013**, *7*, 9735–9742.

(49) Wang, R. L. C.; Kreuzer, H. J.; Grunze, M. Molecular Conformation and Solvation of Oligo (ethylene Glycol)-Terminated Self-Assembled Monolayers and Their Resistance to Protein Adsorption. *J. Phys. Chem. B* **1997**, *101*, 9767–9773.

(50) Tsurupa, G.; Hantgan, R. R.; Burton, R. a.; Pechik, I.; Tjandra, N.; Medved, L. Structure, Stability, and Interaction of the Fibrin(ogen) alphaC-Domains. *Biochemistry* **2009**, *48*, 12191–12201.

(51) Wang, D.; He, C.; Stoykovich, M. P.; Schwartz, D. K. Nanoscale Topography Influences Polymer Surface Diffusion. *ACS Nano* **2015**, DOI: 10.1021/nn506376n.

Bibliography

(1) Nakanishi, K.; Sakiyama, T.; Imamura, K. On the Adsorption of Proteins on Solid Surfaces, a Common but Very Complicated Phenomenon. *J. Biosci. Bioeng.* **2001**, *91*, 233–244.

(2) Vogler, E. A. Protein Adsorption in Three Dimensions. *Biomaterials* **2012**, *33*, 1201–1237.

(3) Ratner, B. D.; Bryant, S. J. Biomaterials: Where We Have Been and Where We Are Going. *Annu. Rev. Biomed. Eng.* **2004**, *6*, 41–75.

(4) Mansouri, J.; Harrisson, S.; Chen, V. Strategies for Controlling Biofouling in Membrane Filtration Systems: Challenges and Opportunities. *J. Mater. Chem.* **2010**, *20*, 4567–4586.

(5) Bee, J. S.; Chiu, D.; Sawicki, S.; Stevenson, J. L.; Chatterjee, K.; Freund, E.; Carpenter, J. F.; Randolph, T. W. Monoclonal Antibody Interactions with Micro-and Nanoparticles: Adsorption, Aggregation, and Accelerated Stress Studies. *J. Pharm. Sci.* **2009**, *98*, 3218–3238.

(6) Norde, W. My Voyage of Discovery to Proteins in Flatland ...and beyond. *Colloids Surf. B. Biointerfaces* **2008**, *61*, 1–9.

(7) Rabe, M.; Verdes, D.; Seeger, S. Understanding Protein Adsorption Phenomena at Solid Surfaces. *Adv. Colloid Interface Sci.* **2011**, *162*, 87–106.

(8) Gray, J. J. The Interaction of Proteins with Solid Surfaces. *Curr. Opin. Struct. Biol.* **2004**, *14*, 110–115.

(9) McCue, J. T.; Engel, P.; Ng, A.; Macniven, R.; Thömmes, J. Modeling of Protein Monomer/aggregate Purification and Separation Using Hydrophobic Interaction Chromatography. *Bioprocess Biosyst. Eng.* **2008**, *31*, 261–275.

(10) Choi, S.; Goryll, M.; Sin, L. Y. M.; Wong, P. K.; Chae, J. Microfluidic-Based Biosensors toward Point-of-Care Detection of Nucleic Acids and Proteins. *Microfluid. Nanofluidics* **2010**, *10*, 231–247.

(11) Bee, J. S.; Randolph, T. W.; Carpenter, J. F.; Bishop, S. M.; Dimitrova, M. N. Effects of Surfaces and Leachables on the Stability of Biopharmaceuticals. *J. Pharm. Sci.* **2011**, *100*, 4158–4170.

(12) Diener, A.; Nebe, B.; Lüthen, F.; Becker, P.; Beck, U.; Neumann, H. G.; Rychly, J. Control of Focal Adhesion Dynamics by Material Surface Characteristics. *Biomaterials* **2005**, *26*, 383–392.

(13) Keselowsky, B. G.; Collard, D. M.; García, A. J. Surface Chemistry Modulates Focal Adhesion Composition and Signaling through Changes in Integrin Binding. *Biomaterials* **2004**, *25*, 5947–5954.

(14) Rabe, M.; Verdes, D.; Seeger, S. Understanding Cooperative Protein Adsorption Events at the Microscopic Scale: A Comparison between Experimental Data and Monte Carlo Simulations. *J. Phys. Chem. B* **2010**, *114*, 5862–5869.

(15) Andrade, J. D.; Hlady, V.; Wei, A. P. Adsorption of Complex Proteins at Interfaces. *Pure Appl. Chem.* **1992**, *64*, 1777–1781.

(16) Norde, W.; Lyklema, J. Why Proteins Prefer Interfaces. *J. Biomater. Sci. Polym. Ed.* **1991**, *2*, 183–202.

(17) Prime, K. L.; Whitesides, G. M. Self-Assembled Organic Monolayers: Model Systems for Studying Adsorption of Proteins at Surfaces. *Science (80-.).* **1991**, *252*, 1164–1167.

(18) Prime, K. L.; Whitesides, G. M. Adsorption of Proteins onto Surfaces Containing End-Attached Oligo (ethylene Oxide): A Model System Using Self-Assembled Monolayers. *J. Am. Chem. Soc.* **1993**, 10714–10721.

(19) Andrade, J. D.; Hlady, V. Protein Adsorption and Materials Biocompatibility: A Tutorial Review and Suggested Hypotheses. *Adv. Polym. Sci.* **1986**, *79*, 1–63.

(20) Ostuni, E.; Chapman, R. G.; Holmlin, R. E.; Takayama, S.; Whitesides, G. M. A Survey of Structure-Property Relationships of Surfaces That Resist the Adsorption of Protein. *Langmuir* **2001**, *17*, 5605–5620.

(21) Kastantin, M.; Keller, T. F.; Jandt, K. D.; Schwartz, D. K. Single-Molecule Tracking of Fibrinogen Dynamics on Nanostructured Poly(ethylene) Films. *Adv. Funct. Mater.* **2012**, *22*, 2617–2623.

(22) Skaug, M. J.; Lacasta, A. M.; Ramirez-Piscina, L.; Sancho, J. M.; Lindenberg, K.; Schwartz, D. K. Single-Molecule Diffusion in a Periodic Potential at a Solid-Liquid Interface. *Soft Matter* **2014**, *10*, 753–759.

(23) Sethuraman, A.; Han, M.; Kane, R. S.; Belfort, G. Effect of Surface Wettability on the Adhesion of Proteins. *Langmuir* **2004**, *20*, 7779–7788.

(24) Wertz, C. F.; Santore, M. M. Fibrinogen Adsorption on Hydrophilic and Hydrophobic Surfaces: Geometrical and Energetic Aspects of Interfacial Relaxations. *Langmuir* **2002**, *18*, 706–715.

(25) Wertz, C. F.; Santore, M. M. Effect of Surface Hydrophobicity on Adsorption and Relaxation Kinetics of Albumin and Fibrinogen: Single-Species and Competitive Behavior. *Langmuir* **2001**, *17*, 3006–3016.

(26) Wertz, C. F.; Santore, M. M. Adsorption and Relaxation Kinetics of Albumin and Fibrinogen on Hydrophobic Surfaces: Single-Species and Competitive Behavior. *Langmuir* **1999**, *15*, 8884–8894.

(27) Arai, T.; Norde, W. The Behavior of Some Model Proteins at Solid-Liquid Interfaces 1. Adsorption from Single Protein Solutions. *Colloids and Surfaces* **1990**, *51*, 1–15.

(28) Treuheit, M. J.; Kosky, A. a; Brems, D. N. Inverse Relationship of Protein Concentration and Aggregation. *Pharm. Res.* **2002**, *19*, 511–516.

(29) Sivaraman, B.; Fears, K. P.; Latour, R. A. Investigation of the Effects of Surface Chemistry and Solution Concentration on the Conformation of Adsorbed Proteins Using an Improved Circular Dichroism Method. *Langmuir* **2009**, *25*, 3050–3056.

(30) Kao, P.; Parhi, P.; Krishnan, A.; Noh, H.; Haider, W.; Tadigadapa, S.; Allara, D. L.; Vogler, E. A. Volumetric Interpretation of Protein Adsorption: Interfacial Packing of Protein Adsorbed to Hydrophobic Surfaces from Surface-Saturating Solution Concentrations. *Biomaterials* **2011**, *32*, 969–978.

(31) Chapman, R.; Ostuni, E.; Takayama, S.; Holmlin, R. E.; Yan, L.; Whitesides, G. M. Surveying for Surfaces That Resist the Adsorption of Proteins. *J. Am. Chem. Soc.* **2000**, *122*, 8303–8304.

(32) Currie, E. P. K.; Norde, W.; Cohen Stuart, M. a. *Tethered Polymer Chains: Surface Chemistry and Their Impact on Colloidal and Surface Properties.*; 2003; Vol. 100-102, pp. 205–265.

(33) Sofia, S.; Premnath, V.; Merrill, E. Poly(ethylene Oxide) Grafted to Silicon Surfaces: Grafting Density and Protein Adsorption. *Macromolecules* **1998**, *31*, 5059–5070.

(34) Mathes, J.; Friess, W. Influence of pH and Ionic Strength on IgG Adsorption to Vials. *Eur. J. Pharm. Biopharm.* **2011**, *78*, 239–247.

(35) Su, T. J.; Lu, J. R.; Thomas, R. K.; Cui, Z. F. Effect of pH on the Adsorption of Bovine Serum Albumin at the Silica/Water Interface Studied by Neutron Reflection. *J. Phys. Chem. B* **1999**, *103*, 3727–3736.

(36) Kisley, L.; Chen, J.; Mansur, A. P.; Dominguez-Medina, S.; Kulla, E.; Kang, M. K.; Shuang, B.; Kourentzi, K.; Poongavanam, M.-V.; Dhamane, S.; et al. High Ionic Strength Narrows the Population of Sites Participating in Protein Ion-Exchange Adsorption: A Single-Molecule Study. *J. Chromatogr. A* **2014**, *1343*, 135–142.

(37) Karpovich, D. S.; Blanchard, G. J. Direct Measurement of the Adsorption Kinetics of Alkanethiolate Self-Assembled Monolayers on a Microcrystalline Gold Surface. *Langmuir* **1994**, *10*, 3315–3322.

(38) Sarkar, D.; Chattoraj, D. Kinetics of Desorption of Proteins from the Surface of Protein-Coated Alumina by Various Desorbing Reagents. *J. Colloid Interface Sci.* **1996**, *178*, 606–613.

(39) Asanov, A. N.; Delucas, L. J.; Oldham, P. B.; Wilson, W. W. Heteroenergetics of Bovine Serum Albumin Adsorption from Good Solvents Related to Crystallization Conditions. *J. Colloid Interface Sci.* **1997**, *191*, 222–235.

(40) Van der Veen, M.; Stuart, M. C.; Norde, W. Spreading of Proteins and Its Effect on Adsorption and Desorption Kinetics. *Colloids Surf. B. Biointerfaces* **2007**, *54*, 136–142.

(41) Vasina, E. N.; Déjardin, P. Kinetics of Adsorption, Desorption, and Exchange of A-Chymotrypsin and Lysozyme on Poly (ethyleneterephthalate) Tracked Film and Track-Etched Membrane. *Biomacromolecules* **2003**, *4*, 304–313.

(42) Adamczyk, Z. Particle Adsorption and Deposition: Role of Electrostatic Interactions. *Adv. Colloid Interface Sci.* **2003**, *100-102*, 267–347.

(43) Schaaf, P.; Voegel, J. C.; Senger, B. From Random Sequential Adsorption to Ballistic Deposition: A General View of Irreversible Deposition Processes. *J. Phys. Chem. B* **2000**, *104*, 2204–2214.

(44) Schaaf, P.; Talbot, J. Surface Exclusion Effects in Adsorption Processes. *J. Chem. Phys.* **1989**, *91*, 4401.

(45) Cadilhe, A.; Araújo, N. A. M.; Privman, V. Random Sequential Adsorption: From Continuum to Lattice and Pre-Patterned Substrates. *J. Phys. Condens. Matter* **2007**, *19*, 065124.

(46) Norde, W. Adsorption of Proteins at Solid-Liquid Interfaces. *Cells Mater.* **1995**, *5*, 97–112.

(47) Kastantin, M.; Langdon, B. B.; Chang, E. L.; Schwartz, D. K. Single-Molecule Resolution of Interfacial Fibrinogen Behavior: Effects of Oligomer Populations and Surface Chemistry. *J. Am. Chem. Soc.* **2011**, *133*, 4975–4983.

(48) Zhou, H.-X.; Rivas, G.; Minton, A. P. Macromolecular Crowding and Confinement: Biochemical, Biophysical, and Potential Physiological Consequences. *Annu. Rev. Biophys.* **2008**, *37*, 375–397.

(49) Sips, R. On the Structure of a Catalyst Surface. II. *J. Chem. Phys.* **1950**, *18*, 1024.

(50) Sips, R. On the Structure of a Catalyst Surface. *J. Chem. Phys.* **1948**, *16*, 490.

(51) Low, M. J. D. Kinetics of Chemisorption of Gases on Solids. *Chem. Rev.* **1960**, *60*, 267–312.

(52) Johnson, R. D.; Arnold, F. H. The Temkin Isotherm Describes Heterogeneous Protein Adsorption. *Biochim. Biophys. Acta* **1995**, *1247*, 293–297.

(53) Tóth, J. Uniform Interpretation of Gas/solid Adsorption. *Adv. Colloid Interface Sci.* **1995**, *55*, 1–239.

(54) Rabe, M.; Verdes, D.; Rankl, M.; Artus, G. R. J.; Seeger, S. A Comprehensive Study of Concepts and Phenomena of the Nonspecific Adsorption of Beta-Lactoglobulin. *ChemPhysChem* **2007**, *8*, 862–872.

(55) Green, R. J.; Davies, J.; Davies, M. C.; Roberts, C. J.; Tendler, S. J. B. Surface Plasmon Resonance for Real Time in Situ Analysis of Protein Adsorption to Polymer Surfaces. *Biomaterials* **1997**, *18*, 405–413.

(56) Snopok, B. a; Kostyukevich, E. V. Kinetic Studies of Protein-Surface Interactions: A Two-Stage Model of Surface-Induced Protein Transitions in Adsorbed Biofilms. *Anal. Biochem.* **2006**, *348*, 222–231.

(57) Calonder, C.; Tie, Y.; Van Tassel, P. R. History Dependence of Protein Adsorption Kinetics. *Proc. Natl. Acad. Sci. U. S. A.* **2001**, *98*, 10664–10669.

(58) Höök, F.; Rodahl, M.; Kasemo, B.; Brzezinski, P. Structural Changes in Hemoglobin during Adsorption to Solid Surfaces: Effects of pH, Ionic Strength, and Ligand Binding. *Proc. Natl. Acad. Sci.* **1998**, *95*, 12271–12276.

(59) Höök, F.; Vörös, J.; Rodahl, M.; Kurrat, R.; Böni, P.; Ramsden, J. J.; Textor, M.; Spencer, N. D.; Tengvall, P.; Gold, J.; et al. A Comparative Study of Protein Adsorption on Titanium Oxide Surfaces Using in Situ Ellipsometry, Optical Waveguide Lightmode Spectroscopy, and Quartz Crystal Microbalance/dissipation. *Colloids Surfaces B Biointerfaces* **2002**, *24*, 155–170.

(60) Jin, J.; Jiang, W.; Yin, J.; Ji, X.; Stagnaro, P. Plasma Proteins Adsorption Mechanism on Polyethylene-Grafted Poly(ethylene Glycol) Surface by Quartz Crystal Microbalance with Dissipation. *Langmuir* **2013**, *29*, 6624–6633.

(61) Berglin, M.; Pinori, E.; Sellborn, A.; Andersson, M.; Hulander, M.; Elwing, H. Fibrinogen Adsorption and Conformational Change on Model Polymers: Novel Aspects of Mutual Molecular Rearrangement. *Langmuir* **2009**, *25*, 5602–5608.

(62) Jönsson, U.; Malmqvist, M.; Ronnberg, I. Adsorption of Immunoglobulin G, Protein A, and Fibronectin in the Submonolayer Region Evaluated by a Combined Study of Ellipsometry and Radiotracer Techniques. *J. colloid interface …* **1985**, *103*, 360–372.

(63) Myers, G. A.; Gacek, D. A.; Peterson, E. M.; Fox, C. B.; Harris, J. M. Microscopic Rates of Peptide-Phospholipid Bilayer Interactions from Single-Molecule Residence Times. *J. Am. Chem. Soc.* **2012**, *134*, 19652–19660.

(64) Langdon, B. B.; Kastantin, M.; Schwartz, D. K. Apparent Activation Energies Associated with Protein Dynamics on Hydrophobic and Hydrophilic Surfaces. *Biophys. J.* **2012**, *102*, 2625–2633.

(65) Kwok, K. C.; Yeung, K. M.; Cheung, N. H. Adsorption Kinetics of Bovine Serum Albumin on Fused Silica: Population Heterogeneities Revealed by Single-Molecule Fluorescence Microscopy. *Langmuir* **2007**, *23*, 1948–1952.

(66) Yeung, K. M.; Lu, Z. J.; Cheung, N. H. Adsorption of Bovine Serum Albumin on Fused Silica: Elucidation of Protein-Protein Interactions by Single-Molecule Fluorescence Microscopy. *Colloids Surf. B. Biointerfaces* **2009**, *69*, 246–250.

(67) Pandey, L. M.; Pattanayek, S. K.; Delabouglise, D. Properties of Adsorbed Bovine Serum Albumin and Fibrinogen on Self-Assembled Monolayers. *J. Phys. Chem. C* **2013**, *117*, 6151–6160.

(68) Monserud, J. H.; Schwartz, D. K. Effects of Molecular Size and Surface Hydrophobicity on Oligonucleotide Interfacial Dynamics. *Biomacromolecules* **2012**, *13*, 4002–4011.

(69) Nelson, N.; Walder, R.; Schwartz, D. K. Single Molecule Dynamics on Hydrophobic Self-Assembled Monolayers. *Langmuir* **2012**, *28*, 12108–12113.

(70) Walder, R.; Schwartz, D. K. Single Molecule Observations of Multiple Protein Populations at the Oil-Water Interface. *Langmuir* **2010**, *26*, 13364–13367.

(71) Sriram, I.; Walder, R.; Schwartz, D. K. Stokes–Einstein and Desorption-Mediated Diffusion of Protein Molecules at the Oil–water Interface. *Soft Matter* **2012**, *8*, 6000.

(72) Dobbs, K. D.; Doren, D. J. Dynamics of Molecular Surface Diffusion: Origins and Consequences of Long Jumps. *J. Chem. Phys.* **1992**, *97*, 3722.

(73) Axelrod, D. Total Internal Reflection Fluorescence Microscopy in Cell Biology. *Methods Enzymol.* **2003**, *361*, 1–33.

(74) Axelrod, D.; Koppel, D. E.; Schlessinger, J.; Elson, E.; Webb, W. W. Mobility Measurement by Analysis of Fluorescence Photobleaching Recovery Kinetics. *Biophys. J.* **1976**, *16*, 1055–1069.

(75) Krägel, J.; Wüstneck, R.; Husband, F.; Wilde, P. J.; Makievski, A. V; Grigoriev, D. O.; Li, J. B. Properties of Mixed Protein/surfactant Adsorption Layers. *Colloids surfaces B …* **1999**, *12*, 399–407.

(76) Gambin, Y.; Lopez-Esparza, R.; Reffay, M.; Sierecki, E.; Gov, N. S.; Genest, M.; Hodges, R. S.; Urbach, W. Lateral Mobility of Proteins in Liquid Membranes Revisited. *Proc. Natl. Acad. Sci. U. S. A.* **2006**, *103*, 2098–2102.

(77) Vieira, E. P.; Rocha, S.; Carmo Pereira, M.; Möhwald, H.; Coelho, M. A. N. Adsorption and Diffusion of Plasma Proteins on Hydrophilic and Hydrophobic Surfaces: Effect of Trifluoroethanol on Protein Structure. *Langmuir* **2009**, *25*, 9879–9886.

(78) Mrksich, M.; Sigal, G. B.; Whitesides, G. M. Surface Plasmon Resonance Permits in Situ Measurement of Protein Adsorption on Self-Assembled Monolayers of Alkanethiolates on Gold. *Langmuir* **1995**, *11*, 4383–4385.

(79) Kim, D. T.; Blanch, H. W.; Radke, C. J. Direct Imaging of Lysozyme Adsorption onto Mica by Atomic Force Microscopy. *Langmuir* **2002**, *18*, 5841–5850.

(80) Fainerman, V. B.; Miller, R.; Ferri, J. K.; Watzke, H.; Leser, M. E.; Michel, M. Reversibility and Irreversibility of Adsorption of Surfactants and Proteins at Liquid Interfaces. *Adv. Colloid Interface Sci.* **2006**, *123-126*, 163–171.

(81) Dijt, J. C.; Stuart, M. A. C.; Fleer, G. J. Kinetics of Polymer Adsorption and Desorption in Capillary Flow. *Macromolecules* **1992**, *25*, 5416–5423.

(82) Bee, J. S.; Schwartz, D. K.; Trabelsi, S.; Freund, E.; Stevenson, J. L.; Carpenter, J. F.; Randolph, T. W. Production of Particles of Therapeutic Proteins at the Air–water Interface during Compression/dilation Cycles. *Soft Matter* **2012**, *8*, 10329.

(83) Tunc, S.; Maitz, M. F.; Steiner, G.; Vázquez, L.; Pham, M. T.; Salzer, R. In Situ Conformational Analysis of Fibrinogen Adsorbed on Si Surfaces. *Colloids Surf. B. Biointerfaces* **2005**, *42*, 219–225.

(84) Baldwin, R. L. Temperature Dependence of the Hydrophobic Interaction in Protein Folding. *Proc. Natl. Acad. Sci.* **1986**, *83*, 8069–8072.

(85) Dill, K. A. Dominant Forces in Protein Folding. *Biochemistry* **1990**, *29*, 7133–7155.

(86) Baugh, L.; Vogel, V. Structural Changes of Fibronectin Adsorbed to Model Surfaces Probed by Fluorescence Resonance Energy Transfer. *J. Biomed. Mater. Res. A* **2004**, *69*, 525–534.

(87) Brynda, E.; Hlady, V.; Andrade, J. D. Protein Packing in Adsorbed Layers Studied by Excitation Energy Transfer. *J. Colloid Interface Sci.* **1990**, *139*, 374–380.

(88) Daly, S.; Przybycien, T.; Tilton, R. Coverage-Dependent Orientation of Lysozyme Adsorbed on Silica. *Langmuir* **2003**, 3848–3857.

(89) Nygren, H. Attractive Adsorbate Interaction in Biological Surface Reactions. *Biophys. Chem.* **1996**, *61*, 73–84.

(90) Nygren, H.; Stenberg, M. Surface-Induced Aggregation of Ferritin. Concentration Dependence of Adsorption onto a Hydrophobic Surface. *Biophys. Chem.* **1990**, *38*, 77–85.

(91) Mulheran, P.; Pellenc, D.; Bennett, R. A.; Green, R. J.; Sperrin, M. Mechanisms and Dynamics of Protein Clustering on a Solid Surface. *Phys. Rev. Lett.* **2008**, *100*, 068102.

(92) Pellenc, D.; Bennett, R. A.; Green, R. J.; Sperrin, M.; Mulheran, P. A. New Insights on Growth Mechanisms of Protein Clusters at Surfaces: An AFM and Simulation Study. *Langmuir* **2008**, *24*, 9648–9655.

(93) Rabe, M.; Verdes, D.; Zimmermann, J.; Seeger, S. Surface Organization and Cooperativity during Nonspecific Protein Adsorption Events. *J. Phys. Chem. B* **2008**, *112*, 13971–13980.

(94) Siegismund, D.; Keller, T. F.; Jandt, K. D.; Rettenmayr, M. Fibrinogen Adsorption on Biomaterials--a Numerical Study. *Macromol. Biosci.* **2010**, *10*, 1216–1223.

(95) Minton, A. P. Adsorption of Globular Proteins on Locally Planar Surfaces. II. Models for the Effect of Multiple Adsorbate Conformations on Adsorption Equilibria and Kinetics. *Biophys. J.* **1999**, *76*, 176–187.

(96) Lopez, A. E.; Moreno-Flores, S.; Pum, D.; Sleytr, U. B.; Toca-Herrera, J. L. Surface Dependence of Protein Nanocrystal Formation. *Small* **2010**, *6*, 396–403.

(97) Keller, T. F.; Schönfelder, J.; Reichert, J.; Tuccitto, N.; Licciardello, A.; Messina, G. M. L. M.; Marletta, G.; Jandt, K. D. How the Surface Nanostructure of Polyethylene Affects Protein Assembly and Orientation. *ACS Nano* **2011**, *5*, 3120–3131.

(98) Sethuraman, A.; Vedantham, G.; Imoto, T.; Przybycien, T.; Belfort, G. Protein Unfolding at Interfaces: Slow Dynamics of Alpha-Helix to Beta-Sheet Transition. *Proteins* **2004**, *56*, 669–678.

(99) Sethuraman, A.; Belfort, G. Protein Structural Perturbation and Aggregation on Homogeneous Surfaces. *Biophys. J.* **2005**, *88*, 1322–1333.

(100) Robertson, B. C.; Zydney, A. L. Protein Adsorption in Asymmetric Ultrafiltration Membranes with Highly Constricted Pores. *J. Colloid Interface Sci.* **1990**, *134*, 563–575.

(101) Gerhardt, A.; Mcgraw, N. R.; Schwartz, D. K.; Bee, J. S.; Carpenter, J. F.; Randolph, T. W. Protein Aggregation and Particle Formation in Prefilled Glass Syringes. *J. Pharm. Sci.* **2014**, *103*, 1601–1612.

(102) Silin, V.; Weetall, H.; Vanderah, D. SPR Studies of the Nonspecific Adsorption Kinetics of Human IgG and BSA on Gold Surfaces Modified by Self-Assembled Monolayers (SAMs). *J. Colloid Interface Sci.* **1997**, *185*, 94–103.

(103) Noh, H.; Vogler, E. A. Volumetric Interpretation of Protein Adsorption: Partition Coefficients, Interphase Volumes, and Free Energies of Adsorption to Hydrophobic Surfaces. *Biomaterials* **2006**, *27*, 5780–5793.

(104) Servoli, E.; Maniglio, D.; Aguilar, M. R.; Motta, A.; San Roman, J.; Belfiore, L. a; Migliaresi, C. Quantitative Analysis of Protein Adsorption via Atomic Force Microscopy and Surface Plasmon Resonance. *Macromol. Biosci.* **2008**, *8*, 1126–1134.

(105) Pegueroles, M.; Tonda-Turo, C.; Planell, J. a; Gil, F.-J.; Aparicio, C. Adsorption of Fibronectin, Fibrinogen, and Albumin on TiO2: Time-Resolved Kinetics, Structural Changes, and Competition Study. *Biointerphases* **2012**, *7*, 48.

(106) Jiang, J.; Zhu, L.; Zhu, L.; Zhang, H.; Zhu, B.; Xu, Y. Antifouling and Antimicrobial Polymer Membranes Based on Bioinspired Polydopamine and Strong Hydrogen-Bonded poly(N-Vinyl Pyrrolidone). *ACS Appl. Mater. Interfaces* **2013**, *5*, 12895–12904.

(107) Andrade, J. D.; Hlady, V. L.; Van Wagenen, R. A. Effects of Plasma Protein Adsorption on Protein Conformation and Activity. *Pure Appl. Chem.* **1984**, *56*, 1345–1350.

(108) Maste, M. C. L.; Norde, W.; Visser, A. J. W. G. Adsorption-Induced Conformational Changes in the Serine Proteinase Savinase: A Tryptophan Fluorescence and Circular Dichroism Study. *J. Colloid Interface Sci.* **1997**, *196*, 224–230.

(109) Schwinté, P.; Ball, V.; Szalontai, B.; Haikel, Y.; Voegel, J.-C.; Schaaf, P. Secondary Structure of Proteins Adsorbed onto or Embedded in Polyelectrolyte Multilayers. *Biomacromolecules* **2002**, *3*, 1135–1143.

(110) Xu, L.-C.; Siedlecki, C. a. Atomic Force Microscopy Studies of the Initial Interactions between Fibrinogen and Surfaces. *Langmuir* **2009**, *25*, 3675–3681.

(111) Agnihotri, A.; Siedlecki, C. a. Time-Dependent Conformational Changes in Fibrinogen Measured by Atomic Force Microscopy. *Langmuir* **2004**, *20*, 8846–8852.

(112) Holzmeister, P.; Acuna, G. P.; Grohmann, D.; Tinnefeld, P. Breaking the Concentration Limit of Optical Single-Molecule Detection. *Chem. Soc. Rev.* **2014**, *43*, 1014–1028.

(113) Deniz, A. a; Mukhopadhyay, S.; Lemke, E. a. Single-Molecule Biophysics: At the Interface of Biology, Physics and Chemistry. *J. R. Soc. Interface* **2008**, *5*, 15–45.

(114) Moerner, W. E. Illuminating Single Molecules in Condensed Matter. *Science (80-.).* **1999**, *283*, 1670–1676.

(115) Betzig, E.; Chichester, R. J. Single Molecules Observed by near-Field Scanning Optical Microscopy. *Science (80-.).* **1993**, *262*, 1422–1425.

(116) Betzig, E.; Patterson, G. H.; Sougrat, R.; Lindwasser, O. W.; Olenych, S.; Bonifacino, J. S.; Davidson, M. W.; Lippincott-Schwartz, J.; Hess, H. F. Imaging Intracellular Fluorescent Proteins at Nanometer Resolution. *Science (80-.).* **2006**, *313*, 1642–1645.

(117) Hell, S. W. Far-Field Optical Nanoscopy. *Science (80-.).* **2007**, *316*, 1153–1158.

(118) Hell, S. W.; Wichmann, J. Breaking the Diffraction Resolution Limit by Stimulated Emission: Stimulated-Emission-Depletion Fluorescence Microscopy. *Opt. Lett.* **1994**, *19*, 780–782.

(119) Leake, M. The Physics of Life: One Molecule at a Time. *Philos. Trans. R. Soc. B* **2012**, *368*.

(120) Pirchi, M.; Ziv, G.; Riven, I.; Cohen, S. S.; Zohar, N.; Barak, Y.; Haran, G. Single-Molecule Fluorescence Spectroscopy Maps the Folding Landscape of a Large Protein. *Nat. Commun.* **2011**, *2*, 493.

(121) Stigler, J.; Ziegler, F.; Gieseke, A.; Gebhardt, J. C. M.; Rief, M. The Complex Folding Network of Single Calmodulin Molecules. *Science (80-.).* **2011**, *334*, 512–516.

(122) Zarrabi, N.; Ernst, S.; Verhalen, B.; Wilkens, S.; Börsch, M. Analyzing Conformational Dynamics of Single P-Glycoprotein Transporters by Förster Resonance Energy Transfer Using Hidden Markov Models. *Methods* **2014**, *66*, 168–179.

(123) Chang, C.; Althaus, J. C.; Carruthers, C. J. L.; Sutton, M. A.; Steel, D. G.; Gafni, A. Synergistic Interactions between Alzheimer's Aβ40 and Aβ42 on the Surface of Primary Neurons Revealed by Single Molecule Microscopy. *PLoS One* **2013**, *8*, 1–8.

(124) Bowen, M. E.; Weninger, K.; Ernst, J.; Chu, S.; Brunger, A. T. Single-Molecule Studies of Synaptotagmin and Complexin Binding to the SNARE Complex. *Biophys. J.* **2005**, *89*, 690–702.

(125) Levy-Sakin, M.; Grunwald, A.; Kim, S.; Gassman, N. R.; Gottfried, A.; Antelman, J.; Kim, Y.; Ho, S. O.; Samuel, R.; Michalet, X.; et al. Toward Single-Molecule Optical Mapping of the Epigenome. *ACS Nano* **2014**, *8*, 14–26.

(126) Wang, B.; Kuo, J.; Bae, S. C.; Granick, S. When Brownian Diffusion Is Not Gaussian. *Nat. Mater.* **2012**, *11*, 481–485.

(127) Yu, C.; Guan, J.; Chen, K.; Bae, S. C.; Granick, S. Single-Molecule Observation of Long Jumps in Polymer Adsorption. *ACS Nano* **2013**, *7*, 9735–9742.

(128) Skaug, M. J.; Mabry, J.; Schwartz, D. K. Intermittent Molecular Hopping at the Solid-Liquid Interface. *Phys. Rev. Lett.* **2013**, *110*, 256101.

(129) Walder, R.; Honciuc, A.; Schwartz, D. K. Phospholipid Diffusion at the Oil-Water Interface. *J. Phys. Chem. B* **2010**, *114*, 11484–11488.

(130) Elliott, L. C. C.; Barhoum, M.; Harris, J. M.; Bohn, P. W. Trajectory Analysis of Single Molecules Exhibiting Non-Brownian Motion. *Phys. Chem. Chem. Phys.* **2011**, *13*, 4326–4334.

(131) McCain, K. S.; Hanley, D. C.; Harris, J. M. Single-Molecule Fluorescence Trajectories for Investigating Molecular Transport in Thin Silica Sol-Gel Films. *Anal. Chem.* **2003**, *75*, 4351–4359.

(132) Schmidt, T.; Schütz, G. J.; Baumgartner, W.; Gruber, H. J.; Schindler, H. Characterization of Photophysics and Mobility of Single Molecules in a Fluid Lipid Membrane. *J. Phys. Chem.* **1995**, *99*, 17662–17668.

(133) Wirth, M. J.; Legg, M. A. Single-Molecule Probing of Adsorption and Diffusion on Silica Surfaces. *Annu. Rev. Phys. Chem.* **2007**, *58*, 489–510.

(134) Peterson, E. M.; Harris, J. M. Single-Molecule Fluorescence Imaging of DNA at a Potential-Controlled Interface. *Langmuir* **2013**, *29*, 8292–8301.

(135) Zareh, S. K.; Wang, Y. M. Single-Molecule Imaging of Protein Adsorption Mechanisms to Surfaces. *Microsc. Res. Tech.* **2011**, *74*, 682–687.

(136) Weiss, S. Fluorescence Spectroscopy of Single Biomolecules. *Science (80-.).* **1999**, *283*, 1676–1683.

(137) Mabry, J. N.; Skaug, M. J.; Schwartz, D. K. Single-Molecule Insights into Retention at a Reversed-Phase Chromatographic Interface. *Anal. Chem.* **2014**, *86*, 9451–9458.

(138) Wazawa, T.; Ueda, M. Total Internal Reflection Fluorescence Microscopy in Single Molecule Nanobioscience. *Adv. Biochem. Eng. Biotechnol.* **2005**, *95*, 77–106.

(139) Lok, B. K.; Cheng, Y.-L.; Robertson, C. R. Total Internal Reflection Fluorescence: A Technique for Examining Interactions of Macromolecules with Solid Surfaces. *J. Colloid Interface Sci.* **1983**, *91*, 87–103.

(140) Lakowicz, J. R. Introduction to Fluorescence. In *Principles of fluorescence spectroscopy*; Lakowicz, J. R., Ed.; Springer New York, 2006; pp. 1–26.

(141) Schuster, J.; Brabandt, J.; von Borczyskowski, C. Discrimination of Photoblinking and Photobleaching on the Single Molecule Level. *J. Lumin.* **2007**, *127*, 224–229.

(142) Shuang, B.; Byers, C. P.; Kisley, L.; Wang, L.-Y.; Zhao, J.; Morimura, H.; Link, S.; Landes, C. F. Improved Analysis for Determining Diffusion Coefficients from Short, Single-Molecule Trajectories with Photoblinking. *Langmuir* **2013**, *29*, 228–234.

(143) Jung, S.; Dickson, R. M. Hidden Markov Analysis of Short Single Molecule Intensity Trajectories. *J. Phys. Chem. B* **2009**, *113*, 13886–13890.

(144) Eggeling, C.; Widengren, J.; Rigler, R.; Seidel, C. A. M. Photobleaching of Fluorescent Dyes under Conditions Used for Single-Molecule Detection: Evidence of Two-Step Photolysis. *Anal. Chem.* **1998**, *70*, 2651–2659.

(145) Widengren, J.; Chmyrov, A.; Eggeling, C.; Löfdahl, P.-A.; Seidel, C. A. M. Strategies to Improve Photostabilities in Ultrasensitive Fluorescence Spectroscopy. *J. Phys. Chem. A* **2007**, *111*, 429–440.

(146) Rasnik, I.; McKinney, S. a; Ha, T. Nonblinking and Long-Lasting Single-Molecule Fluorescence Imaging. *Nat. Methods* **2006**, *3*, 891–893.

(147) Lakowicz, J. R. Energy Transfer. In *Principles of Fluorescence Spectroscopy*; Lakowicz, J. R., Ed.; Springer New York, 2006; pp. 443–475.

(148) Rabe, M.; Verdes, D.; Seeger, S. Surface-Induced Spreading Phenomenon of Protein Clusters. *Soft Matter* **2009**, *5*, 1039–1047.

(149) McLoughlin, S. Y.; Kastantin, M.; Schwartz, D. K.; Kaar, J. L. Single-Molecule Resolution of Protein Structure and Interfacial Dynamics on Biomaterial Surfaces. *Proc. Natl. Acad. Sci.* **2013**, *110*, 19396–19401.

(150) Fox, C. B.; Wayment, J. R.; Myers, G. A.; Endicott, S. K.; Harris, J. M. Single-Molecule Fluorescence Imaging of Peptide Binding to Supported Lipid Bilayers. *Anal. Chem.* **2009**, *81*, 5130–5138.

(151) Truong, K.; Ikura, M. The Use of FRET Imaging Microscopy to Detect Protein–protein Interactions and Protein Conformational Changes in Vivo. *Curr. Opin. Struct. Biol.* **2001**, *11*, 573–578.

(152) Shrestha, D.; Bagosi, A.; Szöllősi, J.; Jenei, A. Comparative Study of the Three Different Fluorophore Antibody Conjugation Strategies. *Anal. Bioanal. Chem.* **2012**, *404*, 1449–1463.

(153) McDonagh, P.; Williams, S. The Preparation and Use of Fluorescent-Protein Conjugates for Microvascular Research. *Microvasc. Res.* **1984**, *27*, 14–27.

(154) Gajraj, A.; Ofoli, R. Effect of Extrinsic Fluorescent Labels on Diffusion and Adsorption Kinetics of Proteins at the Liquid-Liquid Interface. *Langmuir* **2000**, *16*, 8085–8094.

(155) Walder, R.; Kastantin, M.; Schwartz, D. K. High Throughput Single Molecule Tracking for Analysis of Rare Populations and Events. *Analyst* **2012**, *137*, 2987–2996.

(156) Walder, R.; Schwartz, D. K. Dynamics of Protein Aggregation at the Oil–water Interface Characterized by Single Molecule TIRF Microscopy. *Soft Matter* **2011**, *7*, 7616–7622.

(157) Savin, T.; Doyle, P. S. Static and Dynamic Errors in Particle Tracking Microrheology. *Biophys. J.* **2005**, *88*, 623–638.

(158) Kastantin, M.; Schwartz, D. K. Distinguishing Positional Uncertainty from True Mobility in Single-Molecule Trajectories That Exhibit Multiple Diffusive Modes. *Microsc. Microanal.* **2012**, *18*, 793–797.

(159) Kastantin, M.; Schwartz, D. K. DNA Hairpin Stabilization on a Hydrophobic Surface. *Small* **2013**, *9*, 933–941.

(160) Kastantin, M.; Schwartz, D. K. Connecting Rare DNA Conformations and Surface Dynamics Using Single-Molecule Resonance Energy Transfer. *ACS Nano* **2011**, *5*, 9861–9869.

(161) Doolittle, R. Fibrinogen and Fibrin. *Annu. Rev. Biochem.* **1984**, *53*, 195–229.

(162) Mosesson, M. W. Fibrinogen and Fibrin Structure and Functions. *J. Thromb. Haemost.* **2005**, *3*, 1894–1904.

(163) Hu, W. J.; Eaton, J. W.; Ugarova, T. P.; Tang, L. Molecular Basis of Biomaterial-Mediated Foreign Body Reactions. *Blood* **2001**, *98*, 1231–1238.

(164) Sivaraman, B.; Latour, R. A. The Relationship between Platelet Adhesion on Surfaces and the Structure versus the Amount of Adsorbed Fibrinogen. *Biomaterials* **2010**, *31*, 832–839.

(165) Chan, B. M. .; Brash, J. L. Adsorption of Fibrinogen on Glass: Reversibility Aspects. *J. Colloid Interface Sci.* **1981**, *82*, 217–225.

(166) Retzinger, G.; Cook, B.; DeAnglis, A. The Binding of Fibrinogen to Surfaces and the Identification of Two Distinct Surface-Bound Species of the Protein. *J. Colloid Interface Sci.* **1994**, *168*, 514–521.

(167) Schmitt, A.; Varoqui, R.; Uniyal, S. Interaction of Fibrinogen with Solid Surfaces of Varying Charge and Hydrophobic—hydrophilic Balance: I. Adsorption Isotherms. *J. Colloid Interface Sci.* **1983**, *92*.

(168) Watt, K. W. K.; Cottrell, B. A.; Strong, D. D.; Doolittle, R. F. Amino Acid Sequence Studies on the Alpha Chain of Human Fibrinogen. Overlapping Sequences Providing the Complete Sequence. *Biochemistry* **1979**, *18*, 5410–5416.

(169) Kim, S. H.; Haimovich-Caspi, L.; Omer, L.; Yu, C.-M.; Talmon, Y.; Wang, N.-H. L.; Franses, E. I. Stability and State of Aggregation of Aqueous Fibrinogen and Dipalmitoylphosphatidylcholine Lipid Vesicles. *Langmuir* **2007**, *23*, 5657–5664.

(170) Gref, R.; Lück, M.; Quellec, P.; Marchand, M.; Dellacherie, E.; Harnisch, S.; Blunk, T.; Müller, R. H. “Stealth”corona-Core Nanoparticles Surface Modified by Polyethylene Glycol (PEG): Influences of the Corona (PEG Chain Length and Surface Density) and of the Core Composition on Phagocytic Uptake and Plasma Protein Adsorption. *Colloids Surfaces B Biointerfaces* **2000**, *18*, 301–313.

(171) Woodle, M. C. Sterically Stabilized Liposome Therapeutics. *Adv. Drug Deliv. Rev.* **1995**, *16*, 249–265.

(172) Wang, R. L. C.; Kreuzer, H. J.; Grunze, M. Molecular Conformation and Solvation of Oligo (ethylene Glycol)-Terminated Self-Assembled Monolayers and Their Resistance to Protein Adsorption. *J. Phys. Chem. B* **1997**, *101*, 9767–9773.

(173) Peanasky, J.; Schneider, H. M.; Granick, S.; Kessel, C. R. Self-Assembled Monolayers on Mica for Experiments Utilizing the Surface Forces Apparatus. *Langmuir* **1995**, *11*, 953–962.

(174) Abou-Saleh, R. H.; Connell, S. D.; Harrand, R.; Ajjan, R. a; Mosesson, M. W.; Smith, D. A. M.; Grant, P. J.; Ariëns, R. a S. Nanoscale Probing Reveals That Reduced Stiffness of Clots from Fibrinogen Lacking 42 N-Terminal Bbeta-Chain Residues Is due to the Formation of Abnormal Oligomers. *Biophys. J.* **2009**, *96*, 2415–2427.

(175) Cacciafesta, P.; Humphris, A. D. L.; Jandt, K. D.; Miles, M. J. Human Plasma Fibrinogen Adsorption on Ultraflat Titanium Oxide Surfaces Studied with Atomic Force Microscopy. *Langmuir* **2000**, *16*, 8167–8175.

(176) Jamadagni, S. Hydrophobicity of Proteins and Interfaces: Insights from Density Fluctuations. *Annu. Rev. Chem. Biomol. Eng.* **2011**, *2*, 147–171.

(177) Ostuni, E.; Grzybowski, B.; Mrksich, M. Adsorption of Proteins to Hydrophobic Sites on Mixed Self-Assembled Monolayers. *Langmuir* **2003**, *19*, 1861–1872.

(178) Siegel, R. R.; Harder, P.; Dahint, R.; Grunze, M.; Josse, F.; Mrksich, M.; Whitesides, G. M. On-Line Detection of Nonspecific Protein Adsorption at Artificial Surfaces. *Anal. Chem.* **1997**, *69*, 3321–3328.

(179) Noh, H.; Yohe, S. T.; Vogler, E. A. Volumetric Interpretation of Protein Adsorption: Ion-Exchange Adsorbent Capacity, Protein pI, and Interaction Energetics. *Biomaterials* **2008**, *29*, 2033–2048.

(180) Jackler, G.; Steitz, R.; Czeslik, C. Effect of Temperature on the Adsorption of Lysozyme at the Silica/Water Interface Studied by Optical and Neutron Reflectometry. *Langmuir* **2002**, *18*, 6565–6570.

(181) Honciuc, A.; Baptiste, D. J.; Campbell, I. P.; Schwartz, D. K. Solvent Dependence of the Activation Energy of Attachment Determined by Single Molecule Observations of Surfactant Adsorption. *Langmuir* **2009**, *25*, 7389–7392.

(182) Honciuc, A.; Schwartz, D. K. Probing Hydrophobic Interactions Using Trajectories of Amphiphilic Molecules at a Hydrophobic/water Interface. *J. Am. Chem. Soc.* **2009**, *131*, 5973–5979.

(183) Honciuc, A.; Howard, A. L.; Schwartz, D. K. Single Molecule Observations of Fatty Acid Adsorption at the Silica/Water Interface: Activation Energy of Attachment †. *J. Phys. Chem. C* **2009**, *113*, 2078–2081.

(184) Walder, R.; Nelson, N.; Schwartz, D. K. Single Molecule Observations of Desorption-Mediated Diffusion at the Solid-Liquid Interface. *Phys. Rev. Lett.* **2011**, *107*, 156102.

(185) Noh, H.; Vogler, E. A. Volumetric Interpretation of Protein Adsorption: Mass and Energy Balance for Albumin Adsorption to Particulate Adsorbents with Incrementally Increasing Hydrophilicity. *Biomaterials* **2006**, *27*, 5801–5812.

(186) Steinbach, P. J.; Ionescu, R.; Matthews, C. R. Analysis of Kinetics Using a Hydbrid Maximum-Entropy/ Nonlinear-Least-Squares Method: Application to Protein Folding. *Biophys. J.* **2002**, *82*, 2244–2255.

(187) Tilton, R. D.; Gast, A. P.; Robertson, C. R. Surface Diffusion of Interacting Proteins. Effect of Concentration on the Lateral Mobility of Adsorbed Bovine Serum Albumin. *Biophys. J.* **1990**, *58*, 1321–1326.

(188) Tilton, R.; Robertson, C.; Gast, A. Lateral Diffusion of Bovine Serum Albumin Adsorbed at the Solid-Liquid Interface. *J. Colloid Interface Sci.* **1990**, *137*, 192–203.

(189) Nygren, H.; Alaeddin, S.; Lundström, I.; Magnusson, K.-E. Effect of Surface Wettability on Protein Adsorption and Lateral Diffusion. Analysis of Data and a Statistical Model. *Biophys. Chem.* **1994**, *49*, 263–272.

(190) Jamadagni, S. N.; Godawat, R.; Garde, S. How Surface Wettability Affects the Binding, Folding, and Dynamics of Hydrophobic Polymers at Interfaces. *Langmuir* **2009**, *25*, 13092–13099.

(191) Feyereisen, M. W.; Feller, D.; Dixon, D. a. Hydrogen Bond Energy of the Water Dimer. *J. Phys. Chem.* **1996**, *100*, 2993–2997.

(192) Latour, R. A. Thermodynamic Perspectives on the Molecular Mechanisms Providing Protein Adsorption Resistance That Include Protein- surface Interactions. *J. Biomed. Mater. Res. Part A* **2006**, *78A*, 843–854.

(193) Wisniewski, N.; Reichert, M. Methods for Reducing Biosensor Membrane Biofouling. *Colloids Surfaces B Biointerfaces* **2000**, *18*, 197–219.

(194) Roach, P.; Farrar, D.; Perry, C. C. Interaction of Protein Adsorption: Surface-Induced Conformational Changes. *J. Am. Chem. Soc.* **2005**, *127*, 8168–8173.

(195) Sigal, G. B.; Mrksich, M.; Whitesides, G. M. Effect of Surface Wettability on the Adsorption of Proteins and Detergents. *J. Am. Chem. Soc.* **1998**, *120*, 3464–3473.

(196) Ostuni, E.; Yan, L.; Whitesides, G. M. The Interaction of Proteins and Cells with Self-Assembled Monolayers of Alkanethiolates on Gold and Silver. *Colloids Surfaces B Biointerfaces* **1999**, *15*, 3–30.

(197) Curtiss, L. a.; Frurip, D. J.; Blander, M. Studies of Molecular Association in H2O and D2O Vapors by Measurement of Thermal Conductivity. *J. Chem. Phys.* **1979**, *71*, 2703.

(198) Wei, Y.; Latour, R. A. Correlation between Desorption Force Measured by Atomic Force Microscopy and Adsorption Free Energy Measured by Surface Plasmon Resonance Spectroscopy for Peptide-Surface Interactions. *Langmuir* **2010**, *26*, 18852–18861.

(199) Talbot, J.; Tarjus, G.; Van Tassel, P. R.; Viot, P. From Car Parking to Protein Adsorption: An Overview of Sequential Adsorption Processes. *Colloids Surf. A. Physicochem. Eng. Asp.* **2000**, *165*, 287–324.

(200) Wang, X.; Wang, Y.; Xu, H.; Shan, H.; Lu, J. R. Dynamic Adsorption of Monoclonal Antibody Layers on Hydrophilic Silica Surface: A Combined Study by Spectroscopic Ellipsometry and AFM. *J. Colloid Interface Sci.* **2008**, *323*, 18–25.

(201) McMaster, T. J.; Miles, M. J.; Shewry, P. R.; Tatham, A. S. In Situ Surface Adsorption of the Protein C Hordein Using Atomic Force Microscopy. *Langmuir* **2000**, *16*, 1463–1468.

(202) Cullen, D. C.; Lowe, C. R. AFM Studies of Protein Adsorption. *J. Colloid Interface Sci.* **1994**, *166*, 102–108.

(203) Daly, S. M.; Przybycien, T. M.; Tilton, R. D. Aggregation of Lysozyme and of Poly(ethylene Glycol)-Modified Lysozyme after Adsorption to Silica. *Colloids Surf. B. Biointerfaces* **2007**, *57*, 81–88.

(204) Ramsden, J. J.; Bachmanova, G. I.; Archakov, A. I. Kinetic Evidence for Protein Clustering at a Surface. *Phys. Rev. E* **1994**, *50*, 5072–5076.

(205) Alvarez-Curto, E.; Pediani, J. D.; Milligan, G. Applications of Fluorescence and Bioluminescence Resonance Energy Transfer to Drug Discovery at G Protein Coupled Receptors. *Anal. Bioanal. Chem.* **2010**, *398*, 167–180.

(206) Papra, A.; Gadegaard, N.; Larsen, N. B. Characterization of Ultrathin Poly (ethylene Glycol) Monolayers on Silicon Substrates. *Langmuir* **2001**, *17*, 1457–1460.

(207) Janssen, D.; De Palma, R.; Verlaak, S.; Heremans, P.; Dehaen, W. Static Solvent Contact Angle Measurements, Surface Free Energy and Wettability Determination of Various Self-Assembled Monolayers on Silicon Dioxide. *Thin Solid Films* **2006**, *515*, 1433–1438.

(208) Pasche, S.; De Paul, S. M.; Vörös, J.; Spencer, N. D.; Textor, M. Poly(L-Lysine)-Graft-Poly(ethylene Glycol) Assembled Monolayers on Niobium Oxide Surfaces: A Quantitative Study of the Influence of Polymer Interfacial Architecture on Resistance to Protein Adsorption by ToF-SIMS and in Situ OWLS. *Langmuir* **2003**, *19*, 9216–9225.

(209) Carter, D. C.; Ho, J. X. Structure of Serum Albumin. *Adv. Protein Chem.* **1994**, *45*, 153–203.

(210) Jares-Erijman, E. A.; Jovin, T. M. FRET Imaging. *Nat. Biotechnol.* **2003**, *21*, 1387–1395.

(211) Roda, A.; Guardigli, M.; Michelini, E.; Mirasoli, M. Nanobioanalytical Luminescence: Förster-Type Energy Transfer Methods. *Anal. Bioanal. Chem.* **2009**, *393*, 109–123.

(212) Wu, P. P.; Brand, L. Resonance Energy Transfer: Methods and Applications. *Anal. Biochem.* **1994**, *218*, 1–13.

(213) Kastantin, M.; Schwartz, D. K. Identifying Multiple Populations from Single-Molecule Lifetime Distributions. *ChemPhysChem* **2013**, *14*, 374–380.

(214) Norde, W.; Favier, J. P. Structure of Adsorbed and Desorbed Proteins. *Colloids and Surfaces* **1992**, *64*, 87–93.

(215) Tanaka, M.; Mochizuki, A.; Shiroya, T.; Motomura, T.; Shimura, K.; Onishi, M.; Okahata, Y. Study on Kinetics of Early Stage Protein Adsorption on poly(2-Methoxyethylacrylate) (PMEA) Surface. *Colloids Surfaces, A. Physicochem. Eng. Asp.* **2002**, *203*, 195–204.

(216) Amar, J. G.; Family, F.; Lam, P. P. Dynamic Scaling of the Island-Size Distribution and Percolation in a Model of Submonolayer Molecular-Beam Epitaxy. *Phys. Rev. B* **1994**, *50*, 8781–8797.

(217) Doudevski, I.; Schwartz, D. K. Concentration Dependence of Self-Assembled Monolayer Island Nucleation and Growth. *J. Am. Chem. Soc.* **2001**, *123*, 6867–6872.

(218) Doudevski, I.; Schwartz, D. K. Self-Assembled Monolayers in the Context of Epitaxial Film Growth. *Appl. Surf. Sci.* **2001**, *175-176*, 17–26.

(219) Durbin, S. D.; Feher, G. Protein Crystallization. *Annu. Rev. Phys. Chem.* **1996**, *47*, 171–204.

(220) Durbin, S. D.; Carlson, W. E. Lysozyme Crystal Growth Studied by Atomic Force Microscopy. *J. Cryst. Growth* **1992**, *122*, 71–79.

(221) Tie, Y.; Calonder, C.; Van Tassel, P. R. Protein Adsorption: Kinetics and History Dependence. *J. Colloid Interface Sci.* **2003**, *268*, 1–11.

(222) Yuan, Y.; Velev, O. D.; Lenhoff, A. M. Mobility of Adsorbed Proteins Studied by Fluorescence Recovery after Photobleaching. *Langmuir* **2003**, *19*, 3705–3711.

(223) Van Reis, R.; Zydney, A. Bioprocess Membrane Technology. *J. Memb. Sci.* **2007**, *297*, 16–50.

(224) Zydney, A. L. Membrane Technology for Purification of Therapeutic Proteins. *Biotechnol. Bioeng.* **2009**, *103*, 227–230.

(225) Saxena, A.; Tripathi, B. P.; Kumar, M.; Shahi, V. K. Membrane-Based Techniques for the Separation and Purification of Proteins: An Overview. *Adv. Colloid Interface Sci.* **2009**, *145*, 1–22.

(226) Charcosset, C. Membrane Processes in Biotechnology: An Overview. *Biotechnol. Adv.* **2006**, *24*, 482–492.

(227) Nabe, A.; Staude, E.; Belfort, G. Surface Modification of Polysulfone Ultrafiltration Membranes and Fouling by BSA Solutions. *J. Memb. Sci.* **1997**, *133*, 57–72.

(228) Chan, R.; Chen, V. Characterization of Protein Fouling on Membranes: Opportunities and Challenges. *J. Memb. Sci.* **2004**, *242*, 169–188.

(229) Zydney, A. L. Nonspecific Protein-Membrane Interactions: Adsorption and Fouling. In *Biofunctional membranes*; Butterfield, D. A., Ed.; Plenum Press, 1996; pp. 279–288.

(230) Kastantin, M.; Langdon, B. B.; Schwartz, D. K. A Bottom-up Approach to Understanding Protein Layer Formation at Solid-Liquid Interfaces. *Adv. Colloid Interface Sci.* **2014**, *207*, 240–252.

(231) Bowen, W. R.; Calvo, J. I.; Hermindez, A. Steps of Membrane Blocking in Flux Decline during Protein Microfiltration. *J. Memb. Sci.* **1995**, *101*, 153–165.

(232) Reihanian, H.; Robertson, C. R.; Michaels, A. S. Mechanisms of Polarization and Fouling of Ultrafiltration Membranes by Proteins. *J. Memb. Sci.* **1983**, *16*, 237–258.

(233) Kelly, S. T.; Zydney, A. L. Mechanisms for BSA Fouling during Microfiltration. *J. Memb. Sci.* **1995**, *107*, 115–127.

(234) Kelly, S. T.; Opong, W. S.; Zydney, A. L. The Influence of Protein Aggregates on the Fouling of Microfiltration Membranes during Stirred Cell Filtration. *J. Memb. Sci.* **1993**, *80*, 175–187.

(235) Oom, A.; Poggi, M. Surface Interactions of Monoclonal Antibodies Characterized by Quartz Crystal Microbalance with Dissipation: Impact of Hydrophobicity and Protein Self-interactions. *J. Pharm. Sci.* **2011**, *101*, 519–529.

(236) Liu, S. X.; Kim, J.-T. Application of Kevin–Voigt Model in Quantifying Whey Protein Adsorption on Polyethersulfone Using QCM-D. *J. Assoc. Lab. Autom.* **2009**, *14*, 213–220.

(237) Huisman, I. H.; Prádanos, P.; Hernández, A. The Effect of Protein–protein and Protein–membrane Interactions on Membrane Fouling in Ultrafiltration. *J. Memb. Sci.* **2000**, *179*, 79–90.

(238) Pieracci, J.; Crivello, J. V; Belfort, G. Photochemical Modification of 10 kDa Polyethersulfone Ultrafiltration Membranes for Reduction of Biofouling. *J. Memb. Sci.* **1999**, *156*, 223–240.

(239) Kastantin, M.; Walder, R.; Schwartz, D. K. Identifying Mechanisms of Interfacial Dynamics Using Single-Molecule Tracking. *Langmuir* **2012**, *28*, 12443–12456.

(240) Walder, R.; Nelson, N.; Schwartz, D. K. Super-Resolution Surface Mapping Using the Trajectories of Molecular Probes. *Nat. Commun.* **2011**, *2*, 515.

(241) Mahendran, R.; Malaisamy, R.; Mohan, D. R. Cellulose Acetate and Polyethersulfone Blend Ultrafiltration Membranes. Part I: Preparation and Characterizations. *Polym. Adv. Technol.* **2004**, *15*, 149–157.

(242) Zhao, C.; Xue, J.; Ran, F.; Sun, S. Modification of Polyethersulfone Membranes – A Review of Methods. *Prog. Mater. Sci.* **2013**, *58*, 76–150.

(243) Kontturi, E.; Thüne, P. C.; Niemantsverdriet, J. W. Cellulose Model Surfaces - Simplified Preparation by Spin Coating and Characterization by X-Ray Photoelectron Spectroscopy, Infrared Spectroscopy, and Atomic Force Microscopy. *Langmuir* **2003**, *19*, 5735–5741.

(244) Schaub, M.; Wenz, G.; Wegner, G.; Stein, A.; Klemm, D. Ultrathin Films of Cellulose on Silicon Wafers. *Adv. Mater.* **1993**, *5*, 919–922.

(245) Holmberg, M.; Berg, J.; Stemme, S.; Ödberg, L.; Rasmusson, J.; Claesson, P. Surface Force Studies of Langmuir-Blodgett Cellulose Films. *J. Colloid Interface Sci.* **1997**, *186*, 369–381.

(246) Kontturi, E.; Suchy, M.; Penttilä, P.; Jean, B.; Pirkkalainen, K.; Torkkeli, M.; Serimaa, R. Amorphous Characteristics of an Ultrathin Cellulose Film. *Biomacromolecules* **2011**, *12*, 770–777.

(247) Köhler, S.; Liebert, T.; Heinze, T. Interactions of Ionic Liquids with Polysaccharides. VI. Pure Cellulose Nanoparticles from Trimethylsilyl Cellulose Synthesized in Ionic Liquids. *J. Polym. Sci. Part A Polym. Chem.* **2008**, *46*, 4070–4080.

(248) Chen, J.; Bremauntz, A.; Kisley, L.; Shuang, B.; Landes, C. F. Super-Resolution mbPAINT for Optical Localization of Single-Stranded DNA. *ACS Appl. Mater. Interfaces* **2013**, *5*, 9338–9343.

(249) Buijs, J.; Lichtenbelt, J. W. T.; Norde, W.; Lyklema, J. Adsorption of Monoclonal IgGs and Their F (ab′) 2 Fragments onto Polymeric Surfaces. *Colloids Surfaces B Biointerfaces* **1995**, *5*, 11–23.

(250) Kisley, L.; Chen, J.; Mansur, A. P.; Shuang, B.; Kourentzi, K.; Poongavanam, M.-V.; Chen, W.-H.; Dhamane, S.; Willson, R. C.; Landes, C. F. Unified Superresolution Experiments and Stochastic Theory Provide Mechanistic Insight into Protein Ion-Exchange Adsorptive Separations. *Proc. Natl. Acad. Sci. U. S. A.* **2014**, *111*, 2075–2080.

(251) Babcock, J. J.; Brancaleon, L. Bovine Serum Albumin Oligomers in the E-and B-Forms at Low Protein Concentration and Ionic Strength. *Int. J. Biol. Macromol.* **2013**, *53*, 42–53.

(252) Kanani, D. M.; Sun, X.; Ghosh, R. Reversible and Irreversible Membrane Fouling during in-Line Microfiltration of Concentrated Protein Solutions. *J. Memb. Sci.* **2008**, *315*, 1–10.

(253) Cutler, H. E.; Husson, S. M.; Wickramasinghe, S. R. Prefiltration to Suppress Protein Fouling of Microfiltration Membranes. *Sep. Purif. Technol.* **2012**, *89*, 329–336.

(254) Rutherford, H. A.; Minor, F. W.; Martin, A. R.; Harris, M. Oxidation of Cellulose: The Reaction of Cellulose with Periodic Acid. *J. Res. Natl. Bur. Stand. (1934).* **1942**, *29*, 131–141.

(255) Langdon, B. B.; Kastantin, M.; Walder, R.; Schwartz, D. K. Interfacial Protein-Protein Associations. *Biomacromolecules* **2014**, *15*, 66–74.

(256) Kim, K. J.; Chen, V.; Fane, A. G. Some Factors Determining Protein Aggregation during Ultrafiltration. *Biotechnol. Bioeng.* **1993**, *42*, 260–265.

(257) Nath, N.; Hyun, J.; Ma, H.; Chilkoti, A. Surface Engineering Strategies for Control of Protein and Cell Interactions. *Surf. Sci.* **2004**, *570*, 98–110.

(258) Anderson, J. M.; Rodriguez, A.; Chang, D. T. Foreign Body Reaction to Biomaterials. *Semin. Immunol.* **2008**, *20*, 86–100.

(259) Gorbet, M. B.; Sefton, M. V. Biomaterial-Associated Thrombosis: Roles of Coagulation Factors, Complement, Platelets and Leukocytes. *Biomaterials* **2004**, *25*, 5681–5703.

(260) Hlady, V.; Buijs, J. Protein Adsorption on Solid Surfaces. *Curr. Opin. Biotechnol.* **1996**, *7*, 72–77.

(261) Norde, W.; Horbett, T. A.; Brash, J. L. Proteins at Interfaces III: Introductory Overview. In *Proteins at Interfaces III State of the Art*; 2012; pp. 1–34.

(262) Xu, L.-C.; Siedlecki, C. A. Effects of Surface Wettability and Contact Time on Protein Adhesion to Biomaterial Surfaces. *Biomaterials* **2007**, *28*, 3273–3283.

(263) Castner, D. G.; Ratner, B. D. Biomedical Surface Science: Foundations to Frontiers. *Surf. Sci.* **2002**, *500*, 28–60.

(264) Hu, Y.; Jin, J.; Han, Y.; Yin, J.; Jiang, W.; Liang, H. Study of Fibrinogen Adsorption on Poly(ethylene Glycol)-Modified Surfaces Using a Quartz Crystal Microbalance with Dissipation and a Dual Polarization Interferometry. *RSC Adv.* **2014**, *4*, 7716.

(265) Jeon, S.; Lee, J.; Andrade, J.; De Gennes, P. Protein—surface Interactions in the Presence of Polyethylene Oxide: I. Simplified Theory. *J. Colloid Interface Sci.* **1991**, *142*, 149–158.

(266) Unsworth, L. D.; Sheardown, H.; Brash, J. L. Protein-Resistant Poly(ethylene Oxide)-Grafted Surfaces: Chain Density-Dependent Multiple Mechanisms of Action. *Langmuir* **2008**, *24*, 1924–1929.

(267) Honciuc, A.; Harant, A. W.; Schwartz, D. K. Single-Molecule Observations of Surfactant Diffusion at the Solution-Solid Interface. *Langmuir* **2008**, *24*, 6562–6566.

(268) Marucco, A.; Turci, F.; O'Neill, L.; Byrne, H. J.; Fubini, B.; Fenoglio, I. Hydroxyl Density Affects the Interaction of Fibrinogen with Silica Nanoparticles at Physiological Concentration. *J. Colloid Interface Sci.* **2014**, *419*, 86–94.

(269) Minton, A. A. P. Effects of Excluded Surface Area and Adsorbate Clustering on Surface Adsorption of Proteins. II. Kinetic Models. *Biophys. J.* **2001**, *80*, 1641–1648.

(270) Minton, A. P. Effects of Excluded Surface Area and Adsorbate Clustering on Surface Adsorption of Proteins I. Equilibrium Models. *Biophys. Chem.* **2000**, *86*, 239–247.

(271) Hall, C. E.; Slayter, H. S. The Fibrinogen Molecule: Its Size, Shape, and Mode of Polymerization. *J. Biophys. Biochem. Cytol.* **1959**, *5*, 11–16.

(272) Berney, C.; Danuser, G. FRET or No FRET: A Quantitative Comparison. *Biophys. J.* **2003**, *84*, 3992–4010.

(273) Veatch, S. L.; Machta, B. B.; Shelby, S. A.; Chiang, E. N.; Holowka, D. A.; Baird, B. A. Correlation Functions Quantify Super-Resolution Images and Estimate Apparent Clustering due to Over-Counting. *PLoS One* **2012**, *7*, e31457.

Appendix A: The Effects of Electrostatics on the Dynamics of BSA on Fused Silica

Abstract

In this study we have used single-molecule total internal reflection fluorescent microscopy to observe the effects of electrostatics on the interfacial dynamics (e.g. adsorption, desorption, and diffusion) of bovine serum albumin (BSA) on a negatively charged fused silica surface by varying the solution pH and ionic strength. At low ionic strength, repulsive electrostatic interactions reduced adsorption at high pH, when BSA was negatively charged. The addition of 500 mM of sodium chloride increased the BSA adsorption rate at high pH, suggesting that this repulsive electrostatic interaction was screened by the presence of the salt. In contrast, BSA desorption and diffusion were relatively insensitive to pH or ionic strength, suggesting that once BSA is at the interface, other forces (e.g. hydrogen bonding, van der Waals interactions) drive these dynamics.

A.1 Introduction

The importance of protein interfacial phenomena in many different applications (e.g. bioseparations, biomaterials, biosensors) cannot be overstated. In particular, the effects of electrostatics and pH have been widely studied in order to better control protein interactions with materials such as ion-exchange chromatographic adsorbents and ultrafiltration membranes.[1–4] However, mechanistic understandings of protein interfacial dynamics – adsorption, interfacial diffusion, conformational changes, aggregation, and desorption – are still elusive and controversial.[5,6] This is partially due to the lack of experimental techniques that can both separate different dynamics (e.g. examine adsorption and desorption individually vs. *net* adsorption) and different protein populations (e.g. protein conformation, orientation, or aggregation) at the interface. Here we employ single-molecule techniques to directly separate adsorption, interfacial diffusion, and desorption dynamics on a molecule-by-molecule basis.

Ensemble-averaged techniques, coupled with single-molecule techniques, such as single-molecule total internal reflection fluorescence microscopy (SM-TIRFM) used here, can provide valuable insights into the mechanisms of non-specific protein adsorption.

Because proteins are composed of both positively-charged (e.g. lysine, arginine) and negatively-charged (e.g. aspartic acid or glutamic acid) amino acids, the net charge of protein depends on the number of these amino acids as well as the pH of the solution. A given protein's isoelectric point (pI, the pH at which its net charge is zero) is determined by the balance of positively- and negatively-charged amino acids. In the simplest case, at low ionic strength, charged surfaces are thought to either increase or decrease protein adsorption depending on whether the protein-surface interactions are attractive or repulsive. Similarly, higher ionic strength solutions can shield protein-surface interactions (either attractive or repulsive) and protein-protein interactions (repulsive at pH values well above and below the protein's pI).[7] Such observation have previously been made with ensemble-averaged measurements.[2,8–10]

However, as many researchers in this field have acknowledged, electrostatics is only one of many forces determining protein stability, structure, and dynamics at the interface. In addition, electrostatics may affect distinct dynamics (e.g. adsorption, desorption, and diffusion) differently. In this study we directly observed adsorption, desorption, and diffusion of fluorescently labeled bovine serum albumin (BSA, 66.5 kDa) at the bare fused silica (FS) and aqueous interface. In order to probe the effects of electrostatics on adsorption and desorption, the pH and ionic strength were varied from pH 1.5-7.5 and 30–500 mM. We found that at low ionic strength adsorption to the interface was sensitive to protein-surface electrostatic interactions such that adsorption was enhanced at low pH while adsorption was reduced at high pH. Higher ionic strengths mitigated these effects. In contrast to adsorption, desorption and diffusion did not significantly change with pH or ionic strength.

A.2 Material and Methods

BSA was labeled on average with 5 Alexa Fluor 488 fluorophores. The photostability of Alexa Fluor 488 is essentially insensitive to pH. Alexa Fluor 488 contains groups that may be charged at different pHs: a carboxylic acid, a primary imine, and two sulfonate groups. Previous studies have shown that fluorescent dyes may change a protein's pI.[11] We expect that this was the case in these studies.

Protein solutions were composed of Milli-Q water (18.2 MΩ*cm) and sodium chloride (0-500 mM). The pH was adjusted by adding 0.1 M sodium hydroxide or 0.1 M hydrochloric acid to desired pH. Fluorescently-labeled BSA concentration of 10^{-7}-10^{-9} mg/ml were used. Surface modification and SM-TIRFM tracking techniques were performed as described previously.[12,13] The mean characteristic residence times and diffusion coefficients were calculated from the weighted average of fitting parameters to cumulative residence time distributions and cumulative squared-displacement distributions as discussed in Chapter 2 through 6.

A.3 Results and Discussion

In this work we have examined the effects of electrostatics on protein interfacial dynamics by systematically varying pH and ionic strength. At least three single-molecule movies (frame time: 200ms, length 1000 frames) were taken under two different ionic strength, *I*, conditions of 0.03 M and 0.50 M, over a pH range of 1.5-7.2, and in phosphate buffered saline (I = 0.18M) for BSA on FS. A minimum of 2,500 objects were tracked for each pH and ionic strength condition. At some conditions up to 24,000 molecules were tracked.

FS is known to have a negative surface charge at pH > 2.[1] In the case where electrostatics are important to interfacial dynamics, we expected that the kinetic rates of these dynamics would reflect an attractive protein-surface electrostatic force at pH<pI and a repulsive force at pH>pI. For example, at low ionic strength we expected BSA adsorption to decrease and desorption to increase at pH > pI due to an electrostatic repulsion between protein and

surface. Similarly, we hypothesized that by increasing ionic strength, electrostatic forces would diminish due to electrostatic shielding. In contrast, if hydrophobic effects or other forces (e.g. hydrogen bonding, van der Waals interactions) are more important for certain dynamics, we expected that these dynamics would not change with solution pH or ionic strength.

BSA adsorption on FS was observed to be sensitive to electrostatic effects. The mean adsorption rate, shown in Figure A1a, shows that adsorption decreased by 80% at high pH from low pH adsorption rates at low ionic strength, abruptly changing at pH ~3.8. This general trend was expected considering that FS was negatively-charged at all pH and BSA has an isoelectric point (pI) of 4.6-5.2. However the adsorption rate change occurred at a lower pH (pH 3.8) than expected based on BSA's pI. We attribute this shift covalently attaching fluorescent labels to BSA. BSA was labeled with 5 Alexa Fluor 488 dyes on average. Alexa Fluor 488 that has a net negative charge at neutral pH (see Materials and Methods). Previous studies have shown that labeling can result in a pI shift away from the pI of the native protein.[11]

The low adsorption rates observed at higher pH most likely resulted from electrostatic repulsion. DLVO theory suggests that at I = 0.03 M the effective length (i.e. Debye length) of the repulsion between BSA and FS is greater than the distances at which attractive forces (e.g. van der Walls interactions, hydrophobic effect) start to become important in protein adsorption. Indeed, at high ionic strength where the Debye length is greatly reduced, ions shielded the electrostatic repulsion between protein and surface, allowing greater protein adsorption due to other attractive forces.

Previous protein adsorption studies measuring the total amount of protein adsorbed have shown that a maximum occurs around the protein pI, regardless of surface chemistry. This effect is thought to result from protein-protein electrostatic interactions which are minimized at a protein's pI.[7] For the studies described here a very dilute protein concentration was used such that protein-protein interactions were negligible. Therefore, the fact that we did not observe a maximum and instead observed a single inflection point change from attract to

repulsive interactions suggests that this pI maximum seen at higher protein concentrations most likely is due to protein-protein interactions. By incorporating a higher concentration of unlabeled BSA molecules, similar future studies could specifically test this hypothesis.

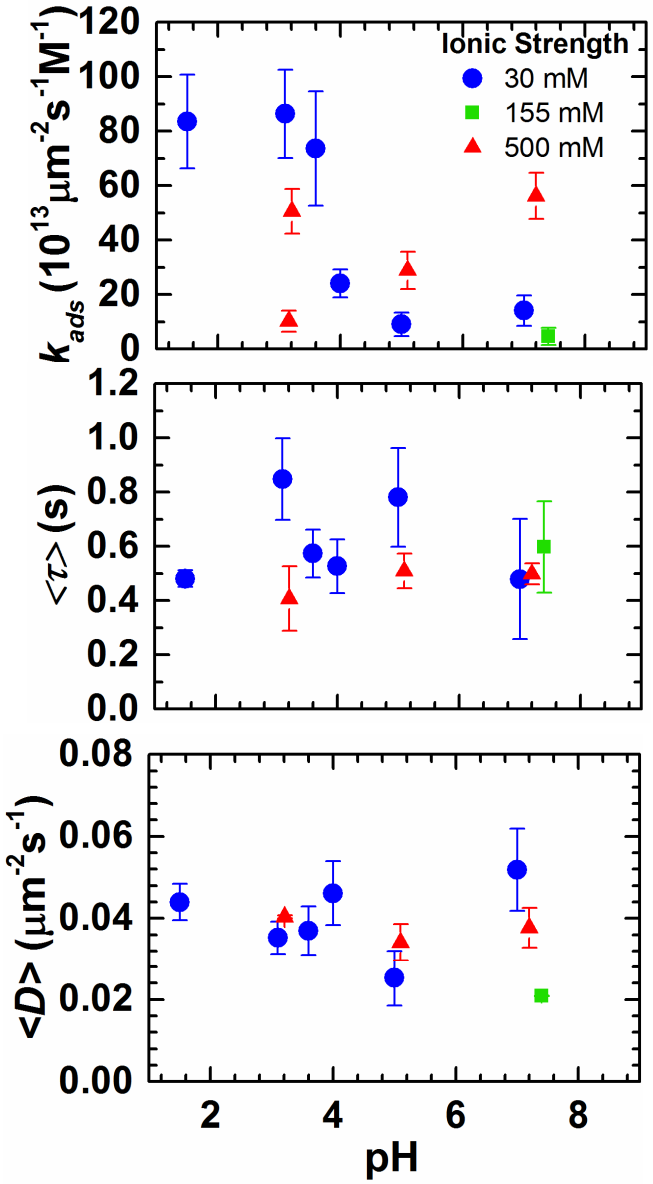

Figure A1: (a) Mean adsorption rate, k_{ads}, (b) mean characteristic residence times, <τ>, and (c) mean diffusion coiefficient, <*D*> as a function of pH and ionic strength (blue = low, green = physiological, red = high) for BSA on FS.

We also examined the effect of pH and ionic strength on BSA surface residence time (rate of desorption) on FS. The observed residence times were plotted on a cumulative probability plot and a multiple exponential fit was performed, as described in Chapter 2. From the relative fractions and mean residence times of these fractions, a mean residence time was

calculated for each condition. Figure A1b shows the mean characteristic residence times as a function of pH. Unlike adsorption, no systematic trend was observed for the surface residence time as a function of pH. In fact, the mean residence times for all pH values at the same protein concentration were statistically similar. The mean diffusion coefficients, shown in Figure A1c, also did not show any trend with pH or ionic strength. This suggests that protein-surface non-electrostatic interactions dominate protein-surface interactions once a protein adsorbs (e.g. hydrogen bonding, van der Waals interactions). The difference between the adsorption and residence time trends highlights the power of this technique to identify the detailed mechanisms involved in protein dynamics at the interface.

A.4 Conclusions

BSA adsorption to a bare fused silica was sensitive to both pH and ionic strength changes indicating the electrostatics dominate these interactions. In contrast, protein desorption and diffusion showed no dependence on pH or ionic strength. Together these findings suggest that at long BSA-FS distances, electrostatic repulsion can play a role in protein adsorption. However, in the near surface region, where BSA can interact directly with the surface, non-electrostatic interactions dominate protein-surface interactions (e.g. hydrogen bonding, van der Waals interactions, and hydrophobic effects). These experiments demonstrate how single-molecule techniques can be used to separate the effects of different forces on distinct interfacial processes.

A.5 References

(1) Mathes, J.; Friess, W. Influence of pH and Ionic Strength on IgG Adsorption to Vials. *Eur. J. Pharm. Biopharm.* **2011**, *78*, 239–247.

(2) Dąbkowska, M.; Adamczyk, Z. Ionic Strength Effect in HSA Adsorption on Mica Determined by Streaming Potential Measurements. *J. Colloid Interface Sci.* **2012**, *366*, 105–113.

(3) Tsapikouni, T. S.; Missirlis, Y. F. pH and Ionic Strength Effect on Single Fibrinogen Molecule Adsorption on Mica Studied with AFM. *Colloids Surf. B. Biointerfaces* **2007**, *57*, 89–96.

(4) Mo, H.; Tay, K. G.; Ng, H. Y. Fouling of Reverse Osmosis Membrane by Protein (BSA): Effects of pH, Calcium, Magnesium, Ionic Strength and Temperature. *J. Memb. Sci.* **2008**, *315*, 28–35.

(5) Vogler, E. A. Protein Adsorption in Three Dimensions. *Biomaterials* **2012**, *33*, 1201–1237.

(6) Norde, W.; Horbett, T. A.; Brash, J. L. Proteins at Interfaces III: Introductory Overview. In *Proteins at Interfaces III State of the Art*; 2012; pp. 1–34.

(7) Haynes, C. a.; Norde, W. Globular Proteins at Solid/liquid Interfaces. *Colloids Surfaces B Biointerfaces* **1994**, *2*, 517–566.

(8) Jones, K. L.; O'Melia, C. R. Protein and Humic Acid Adsorption onto Hydrophilic Membrane Surfaces: Effects of pH and Ionic Strength. *J. Memb. Sci.* **2000**, *165*, 31–46.

(9) Kopac, T.; Bozgeyik, K.; Yener, J. Effect of pH and Temperature on the Adsorption of Bovine Serum Albumin onto Titanium Dioxide. *Colloids Surf. A. Physicochem. Eng. Asp.* **2008**, *322*, 19–28.

(10) Xu, X.-H. N.; Yeung, E. S. Long-Range Electrostatic Trapping of Single-Protein Molecules at a Liquid-Solid Interface. *Science (80-.).* **1998**, *281*, 1650–1653.

(11) Bingaman, S.; Huxley, V. H.; Rumbaut, R. E. Fluorescent Dyes Modify Properties of Proteins Used in Microvascular Research. *Microcirculation* **2003**, *10*, 221–231.

(12) Langdon, B. B.; Kastantin, M.; Schwartz, D. K. Apparent Activation Energies Associated with Protein Dynamics on Hydrophobic and Hydrophilic Surfaces. *Biophys. J.* **2012**, *102*, 2625–2633.

(13) Kastantin, M.; Langdon, B. B.; Chang, E. L.; Schwartz, D. K. Single-Molecule Resolution of Interfacial Fibrinogen Behavior: Effects of Oligomer Populations and Surface Chemistry. *J. Am. Chem. Soc.* **2011**, *133*, 4975–4983.

Appendix B: Chapter 2 Supporting Information

B.1 Analytical Ultracentrifugation

Materials and Methods. A Beckman XL-A analytical ultracentrifuge equipped with UV adsorption optics was used to make measurements at a wavelength of 230 nm approximately every 4 minutes. A 1 cm long cell was placed 6.3 cm from the center of rotation. A rotor speed of 30,000 rpm was used at 25°C. Alexa Fluor ® 488 labeled human fibrinogen samples with a concentration of 1.0 μM in PBS were dialyzed overnight at 4°C against PBS to remove residual salts from the labeling and lyophilization process. Velocity sedimentation was carried out overnight in PBS at two initial fibrinogen concentrations of 40 and 74 nM. The fibrinogen concentration distribution was measured as a function of time and the distance from the center of rotation. After background subtraction, this concentration distribution was numerically fit to the Lamm equation describing the evolution of the concentration distribution of a species with a given diffusion coefficient and sedimentation coefficient (s) using the Sedfit program.[1] From this fit the sedimentation coefficient distribution, $c(s)$ was determined. The frictional coefficient was fit to the data using the Sedfit program and an initial guess calculated using the Svedberg equation.[2,3]

Results. Analytical ultracentrifugation was used to determine the relative fractions of fibrinogen monomer and oligomer in solution. The sedimentation coefficient distribution can be seen in Figure B1. The peak at lower sedimentation coefficient for 40 and 74 nM injection concentrations corresponds to fibrinogen monomer populations with average sedimentation coefficients of 8.8 ± 0.6 S and 8.6 ± 0.4 S, respectively. The peak at higher sedimentation coefficient corresponds to objects with average sedimentation coefficients of 14 ± 1.5 S and 13 ± 1.1 S for the 40 and 74 nM injection concentrations, respectively. By integrating the area under each peak in Figure B1, the fraction of the monomer in solution was found to be 0.94 ±

0.02 where the error represents the standard deviation between measurements taken at the two concentrations.

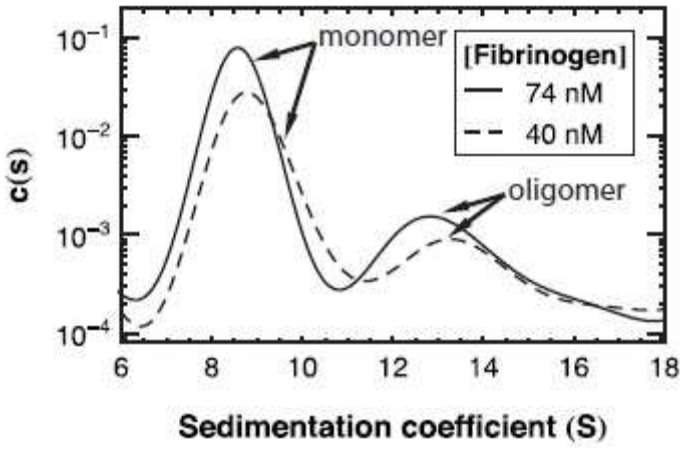

Figure B1: The sedimentation coefficient distribution of fluorescently labeled human fibrinogen at 40 and 74 nM loading concentrations calculated from analytical ultracentrifugation experiments.

B.2 Size-Exclusion Chromatography

Materials and methods. Size-Exclusion Chromatography (SEC) was also used to investigate fibrinogen monomer and aggregate populations in solution. Analysis was performed with a Beckman Coulter Systems Gold HPLC system, associated UV 166 detector (set at 230 nm) and a Wyatt Dawn EOS multiangle detector positioned at a scattering angle of 90°. A TSK-Gel G3000SW column (Tosoh Biosciences) at room temperature was used in fibrinogen studies with a mobile phase of PBS. Studies were carried out at a flow rate of 1.0 mL/min for 30 minutes with a 100 µL injection volume for a 0.5 µM solution of Alexa Fluor ® 488 labeled human fibrinogen, kept at 4°C for 8 h prior to injection. ASTRA software was used for peak integration of UV absorption data.

Results. SEC was used as an orthogonal technique to AUC in order to determine the relative fractions of fibrinogen monomer and oligomer in solution. In Figure B2, light-scattering data indicates two distinct fibrinogen populations. The first peak corresponds to the shoulder in

the major peak of UV absorbance and is indicative of fibrinogen aggregates. The major peak in the absorbance trace of Figure B2 represents the fibrinogen monomer population and accounts for a weight fraction of 0.95 ± 0.01 where the error represents the standard deviation of multiple trials. Monomer fractions were determined by integration of the UV absorbance signal over the time interval corresponding to the peak in the scattering signal. These values are consistent with those calculated in AUC experiments.

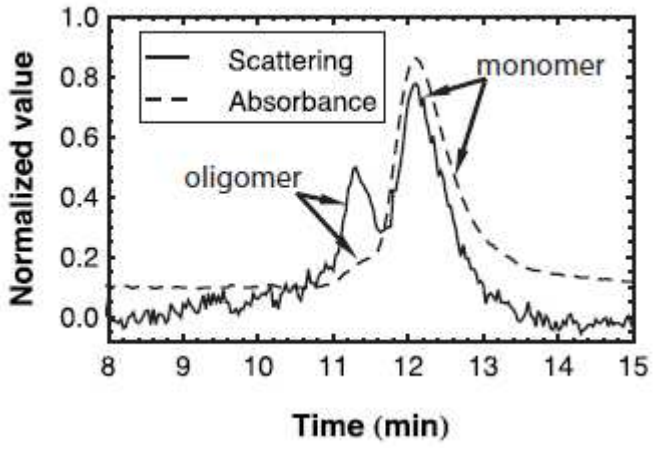

Figure B2: SEC results showing absorbance and light-scattering traces of fluorescently labeled human fibrinogen at room temperature in PBS.

B.3 Additional Tables and Figures

Diffusion coefficients for populations A-D. The numerical values for diffusion data presented in Figures 2.3 and 2.5 are given in Tables B1–B3, along with uncertainties representing 95% confidence in the last significant figure given.

Table B1: Parameters used to fit equation (2) to the experimental cumulative squared-displacement distributions on the FS surface.

Population	Intensity units	Residence time (s)	x_1 D_1 (μm²/s)	x_2 D_2 (μm²/s)	$\bar{D}$(μm2/s)
A	0.51-0.77	4	1 0.0197(2)		0.0197(2)
B	1.9-2.2	4-6	0.13(2) 0.028(3)	0.87(2) 0.0084(2)	0.0109(7)
C	2.8-3.0	10-14	0.36(1) 0.0118(2)	0.64(1) 0.00340(5)	0.0064(1)
D	3.6-4.1	50-120	0.168(5) 0.0100(2)	0.832(5) 0.00238(2)	0.0037(1)

Table B2: Parameters used to fit equation 2 to the experimental cumulative squared-displacement distributions on the TMS surface.

Population	Intensity units	Residence time (s)	x_1 D_1 (μm²/s)	x_2 D^2 (μm²/s)	x_3 D_3 (μm²/s)	$\bar{D}$ (μm²/s)
A	0.49-0.74	4	1 0.0284(2)			0.0284(2)
B	1.9-2.1	4-6	0.85(2) 0.0198(2)	0.15(2) 0.0044(6)		0.0175(4)
C	2.8-3.1	10-14	0.55(1) 0.0166(2)	0.45(1) 0.0029(1)		0.0104(2)
C'	2.8-3.1	40-120	0.12(5) 0.020(3)	0.62(3) 0.006(1)	0.26(5) 0.0016(2)	0.007(1)
D	3.6-4.0	40-120	0.07(1) 0.019(2)	0.84(1) 0.0032(6)	0.09(1) 0.00015(4)	0.0042(2)
D'	3.6-4.0	10-14	0.41(2) 0.0155(6)	0.59(1) 0.0025(1)		0.0078(4)

Table B3: Parameters used to fit equation (2) to the experimental cumulative squared-displacement distributions on the PEG(5000) surface.

Population	Intensity units	Residence time (s)	x_1 D_1 ($\mu m^2/s$)	x_2 D_2 ($\mu m^2/s$)	x_3 D_3 ($\mu m^2/s$)	$\bar{D}$ ($\mu m^2/s$)
A	0.50-0.75	4	1 0.0138(1)			0.0138(1)
B	1.9-2.1	8-12	0.32(1) 0.0132(2)	0.68(1) 0.00419(4)		0.0071(2)
C	2.7-3.0	20-26	0.01(1) 0.03(2)	0.33(5) 0.006(1)	0.66(6) 0.0027(1)	0.0041(6)
D	3.8-4.0	70-200	0.017(4) 0.0261(4)	0.246(2) 0.00456(3)	0.737(3) 0.00163(1)	0.0028(1)

Cumulative distributions for first, middle, last, and all steps in a trajectory. The cumulative squared-displacement distributions used to generate Figure 2.6 are shown in Figure B3 for fibrinogen on fused silica. The tail of the distribution for "middle" and "all" steps decays more quickly than that for "first" and "last" steps in a trajectory, indicating that fast diffusion is more likely to follow adsorption and precede desorption.

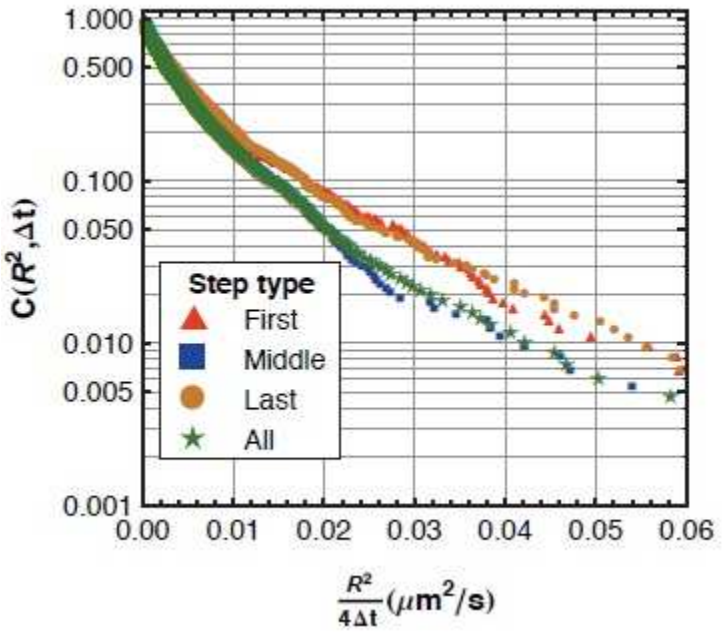

Figure B3: The cumulative squared-displacement distributions are shown for different positions in trajectories observed on a fused silica surface. These distributions were used to produce the values given in Figure 2.6.

Atypical protein populations. Table B2 shows two populations that have not been previously mentioned, C' and D' on TMS surfaces. These populations have the intensity selection criteria of populations C and D but the residence time selection criteria from neighboring populations. This method of transposing residence time selection criteria with different populations was done for all populations on all surfaces and typically did not change the observed diffusive behavior since molecules of the same intensity have the same aggregation number regardless of characteristic residence time. In the cases of C' and D', however, diffusive behavior was observed that was drastically different than populations C and D. That is to say that the x_j and D_j for population C' are closer to those of population D than C. Similarly, values for population D' are closer to those of population C than D. This suggests that while the primed populations have the same aggregation state as their unprimed counterparts (based on intensity data), they have different three-dimensional arrangements of fibrinogen monomers that cause surface interactions atypical of their aggregation number.

Interestingly, these atypical populations were observed only on the hydrophobic TMS surface. This suggests that fibrinogen-TMS interactions may exist at specific local contact points where the protein or aggregate has exposed hydrophobic regions. Consequently, the precise geometric arrangement of fibrinogen monomers within the aggregate can give rise to surface interactions of varying strength while maintaining the same aggregation number. Put another way, one arrangement of monomers may expose more hydrophobic patches to the exterior of the aggregate than another and the type of surface may or may not have any influence over the preferred arrangement. In contrast, the FS and PEG(5000) surfaces may interact very weakly with fibrinogen, but over the entire contact area of the protein. The combined effect of all these weak interactions is therefore insensitive to subtle differences in the arrangement of monomers in an aggregate. The above-mentioned difference between hydrophobic and hydrophilic surfaces is reminiscent of the multiple observed energy barriers for fibrinogen desorption from hydrophobic colloidal probes by Xu and Siedlecki whereas only a single barrier was observed

using hydrophilic probes.[4] However, neither the present work nor that of Xu and Siedlecki provides concrete evidence of the mechanism leading to this difference and further efforts directed at understanding this phenomenon should be undertaken.

Representative images and surface uniformity. Figure B4 shows representative images from TMS surfaces at several different times. Diffraction-limited spots are randomly distributed throughout the images and no other surface features are visible indicating uniformity of the underlying surface. Surface uniformity was quantified by mapping the mean residence time as a function of position. A movie was captured on a representative TMS-coated surface with a 0.2 ms frame exposure time for 10 minutes in order to observe more molecules in a given area and increase the spatial resolution of the map. The resulting map is shown in Figure B5 with bins that are 1.45 μm on a side. Mean residence times are mostly under 2 s while some mean values approach 5 s. Some heterogeneity is to be expected for random adsorption of a heterogeneous population onto a uniform surface. More importantly, the areas with higher mean residence times are not different than the mean residence time over the entire surface (1.6 s) with any reasonable statistical significance. This provides evidence that the surface is devoid of micron-scale defects that might support anomalously strong fibrinogen adsorption. Similar results are observed on representative PEG and FS surfaces.

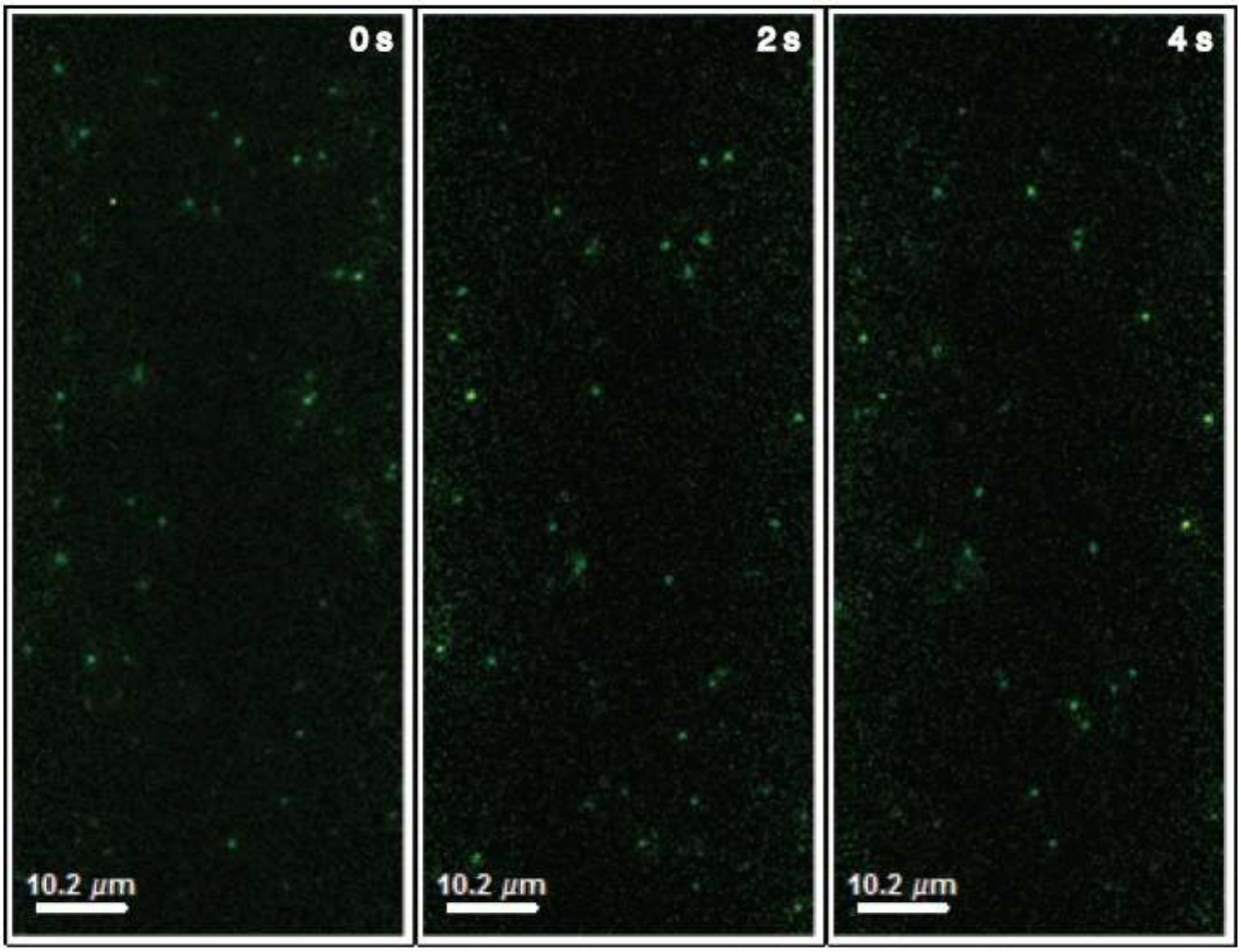

Figure B4: A sample sequence of images from fibrinogen on a TMS-coated substrate is shown. Bright diffraction-limited spots are the main features in each image with background noise appearing as faint, smaller spots. Image convolution with a disk matrix increases recognition of diffraction-limited spots over background noise.

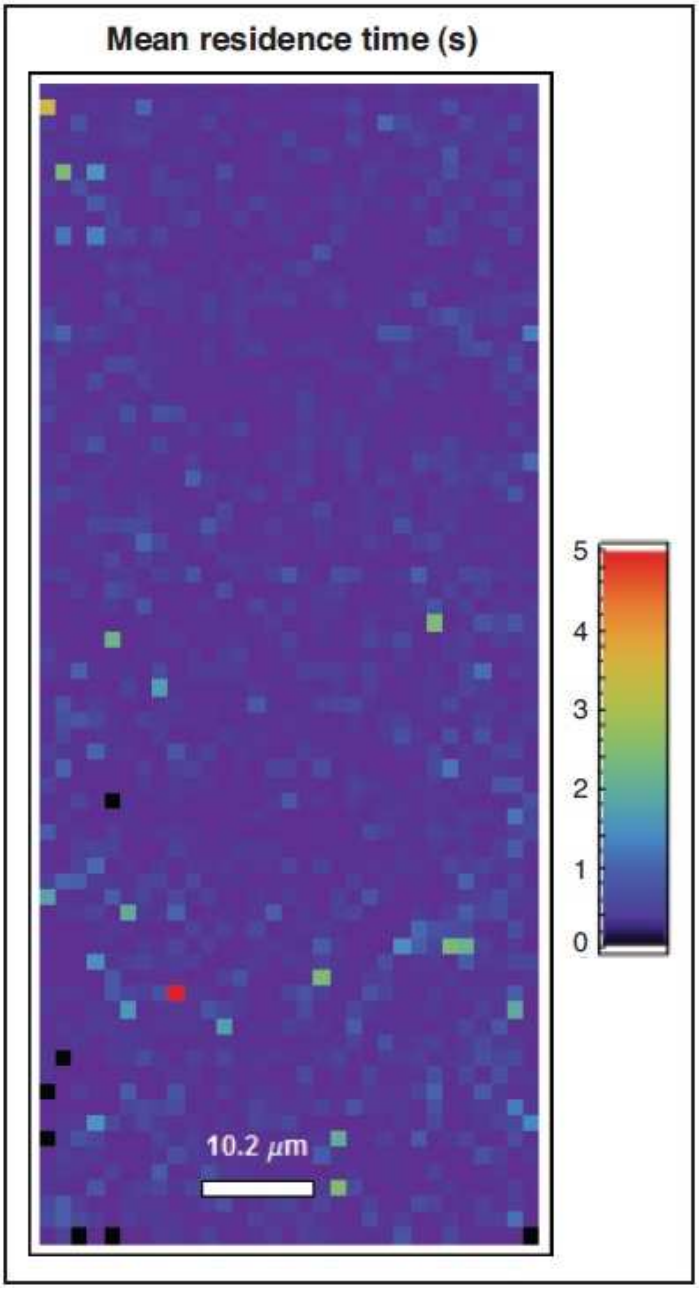

Figure B5: The mean residence time of all objects that adsorbed in a given area is shown as a function of position on a TMS-coated surface. Each bin is 1.45 μm on a side. This surface mapping demonstrates that micron-scale surface heterogeneities that could lead to anomalous protein-surface attraction are not present. Most mean values are less than 2 seconds but all mean values are not statistically different than the surface-averaged mean residence time of 1.6 seconds. Black represents areas in which no objects were observed to adsorb.

B.4 References

(1) Schuck, P., *Biophysical Journal* **2000,** *78* (3), 1606-1619.

(2) Johnson, P.; Mihalyi, E., *Biochimica Et Biophysica Acta* **1965,** *102* (2), 476-486.

(3) Robert, C. H., *Biophysical Journal* **1995,** *69* (3), 840-848.

(4) Xu, L. C.; Siedlecki, C. A., *Langmuir* **2009,** *25* (6), 3675-3681.

Appendix C: Chapter 3 Supporting Information

C.1 Materials and Methods

Protein Sample Preparation. Human fibrinogen (Fg) labeled with AlexaFluor 488 and bovine serum albumin (BSA) labeled with AlexaFluor 555 were purchased from Molecular Probes, Inc. (Eugene, OR). Fg was labeled on average with 15 fluorophores per protein molecule while BSA was labeled on average with 5 fluorophores per molecule, as specified by the manufacturer. Phosphate-buffered saline (PBS) at pH 7.2 was purchased from Gibco (Carlsbad, CA). To achieve low surface densities required for single-molecule experiments, protein solutions at concentrations of 10^{-14} and 10^{-12} M were prepared for use in experiments involving TMS and FS surfaces, respectively.

Surface Preparation and Characterization. Fused silica (FS) wafers, purchased from Mark Optics, Inc (Santa Ana, CA), were cleaned with cationic detergent (Micro 90, International Product Corp., Burlington, NJ) and thoroughly rinsed with water purified to 18.2 MΩ•cm (Millipore Milli-Q UV+). Wafers were then immersed in warm piranha solution (70% sulfuric acid, 30% hydrogen peroxide) for 1h and UV-ozone treated (Jelight UVO cleaner, Irvine, CA) for 1h. These surfaces were either used without further treatment or were coated with monolayers of trimethyl-silane (TMS) by exposing clean wafers to hexamethyldixilazine (Sigma-Aldrich St. Louis, MO) vapors for 18h at room temperature.

Static contact angles of deionized water on functionalized surfaces were measured with a custom-built contact-angle goniometer. A 1 μL drop of water was deposited on the surface and contact angle measured after relaxing. At least six drops on three independent surfaces were averaged for reported values. No contact angle could be measured on bare fused silica indicating essentially complete wetting. A contact angle of 95° ± 3° was measured for the TMS functionalized surface, consistent with a hydrophobic surface and with previous reports of TMS contact angles (1).

Data Acquisition. The total internal reflection fluorescence microscope has been described previously (2) and consists of a custom-built prism-based illumination system, flow cell, Nikon TE-2000 microscope with 60x objective, and a 491 nm DPSS LASER. A temperature-controlled flow cell was used to maintain a specified temperature to within 0.2°C. Protein solution was slowly injected into the flow cell and the flow was stopped prior to imaging. Several movies were acquired of each sample using acquisition times for individual frames of 200 ms. Other single-molecule TIRFM considerations were described previously (3).

The evanescent field created by total internal reflection decays exponentially with distance from the interface with a decay length of less than 100 nm, exciting only objects near the solid-liquid interface. While fluorescent objects in solution within the penetration depth may be excited, they are typically not resolved as discrete objects. Since objects diffusing in solution exhibit diffusion coefficients that are 2-3 orders of magnitude higher than that of objects adsorbed to the interface, the residence time of objects in solution was negligible within a given camera pixel compared to that from a surface-adsorbed object. Therefore, while objects in solution contribute to background fluorescence levels they were not identified as actual objects by our tracking algorithm.

An object-recognition algorithm involving disk matrix convolution followed by thresholding was used to identify diffraction-limited objects (described previously (4)). The centroid of intensity was used to determine the position of an object. Object tracking between movie frames was accomplished by identifying the closest objects within a 4 pixel (908 nm) distance in sequential frames. Surface residence times were calculated by multiplying the number of frames in which an object was identified by the exposure time of each frame. For each frame, the intensity of an object was calculated by integrating all pixels assigned by disk convolution and thresholding while subtracting the local background intensity just beyond the perimeter of the object.

Data Analysis

Residence Times. Experimental residence time distributions were constructed by calculating the cumulative probability of objects remaining on the surface for a time *t* or greater. The corrected experimental cumulative residence time distribution was then given by

$$p(t) = \frac{\sum_{t'>t} n_{t'} c(t')}{\sum_{t'} n_{t'} c(t')}$$

where n_t is the number of objects observed to have a given residence time *t* and *c(t)* is a correction factor due to the finite movie length and thus fewer opportunities to observe both adsorption and desorption of objects with longer residence times. The correction factor *c(t)* is given by

$$c(t) = \left[H(T-t)\left(1-\frac{t}{T}\right)\right]^{-1}$$

where *T* is the length of the movie and *H* is the Heaviside step function.

Objects with a residence time of only a single frame were ignored in this analysis due to the sensitivity of object identification for a single frame to noise. The error shown for each data point represents 68% confidence intervals for a Poisson distribution, assuming that the number of objects with a given residence time follows Poisson statistics.

Our data analysis methods have been described previously in detail (3). Briefly, desorption kinetics were assumed to be first-order processes. The integrated or cumulative residence time distribution could be described by the sum over all populations

$$p(t) = \sum_{i=1} f_i e^{-t/\tau_i} \qquad \text{(C1)}$$

where *p(t)* is the probability that a given object has a residence time greater than or equal to time *t* and f_i is the relative fraction of all objects represented by population *i*. Each population had a characteristic surface residence time of τ_i, which is the inverse of that population's effective first-order desorption rate constant ($k_{des,i} = 1/\tau_i$).

Synergistic fitting using the distributed maximum entropy method (MEM) and discrete maximum likelihood (ML) algorithm was performed using MemExp (5) (described in citations within). This fitting method independently confirmed the number of exponentials used to fit cumulative residence time distributions.

Diffusion. Experimental cumulative squared-displacement distributions were calculated by sorting the displacement data in ascending order and ranking each data point such that $C(R_k^2,\Delta t)$ is given by:

$$C\left(R_k{}^2,\Delta t\right) = 1 - k/N$$

where k is the rank of the sorted object and N is the total number of sorted data points (2). The error for each data point represents 68% confidence intervals for a Poisson distribution with mean of ($N + 1 - k$).

By default, the interfacial diffusion of a particle was expected to follow a two-dimensional random walk with Gaussian statistics. Because diffusing molecules were capable of multiple modes of diffusion (1-3), in general the cumulative squared-displacement distribution was given by

$$C(R^2,\Delta t) = \sum_{j=1} x_j e^{-R^2/4D_j\Delta t}$$

where x_j is the fraction of observed steps in mode j and D_j is the characteristic diffusion coefficient of mode j.

Instrument noise caused uncertainty in the calculation of super-resolution spatial position and this effect has been noted to cause the apparent motion of stationary particles (6). In systems exhibiting multiple diffusive modes, the slowest observed diffusion coefficient is often interpreted as a stationary population, with analyses performed on other diffusion coefficients without correction. This strategy was insufficient for the current work because positional uncertainty also elevates the apparent diffusion of moving particles. A correction for this effect

was important when extracting quantitative values for slow, but non-stationary, modes of diffusion, as was here.

The correction is detailed in reference (6) but essentially each apparent value of D_j is elevated by a factor of $\sigma^2/\Delta t$ where σ is the positional uncertainty and Δt is the time window between observations. More specifically, σ is the standard deviation of an assumed Gaussian probability distribution for localizing an object at its true position.

These considerations led to the use of Eq. C2 in which positional uncertainty was explicitly accounted for and was determined experimentally through the use of methods discussed in reference (6).

$$C(R^2, \Delta t) = \sum_{j=1} x_j e^{-R^2/4(D_j \Delta t + \sigma^2)} \quad \text{(C2)}$$

Data Fitting. Eq. C1 and Eq. C2 were used to fit experimental cumulative distributions of residence time and squared-displacement data, respectively, by minimizing the variance weighted by the data point (e.g. residence time or squared-displacement) divided by the squared error for the data point. The distributions were fit to an increasing number of exponentials until an order of magnitude reduction of squared errors, based on the chi-squared value (χ^2), was no longer achieved. The reported diffusion coefficients (D_j) and characteristic residence time constants (τ_i) were averaged between multiple movies with a relative weight of the number of objects observed in each movie. The reported uncertainties correspond to the standard error in determining τ_i for each movie, propagated through the weighted average.

In order to determine the apparent activation energy (E_a), Arrhenius plots were constructed for each corresponding population or mode. Arrhenius plots were linearly fit and E_a was determined using the Arrhenius relationship:

$$\ln(k) = \frac{-E_a}{R}\frac{1}{T} + \ln(A)$$

where k is the desorption rate constant (k_{des}) or diffusion coefficient (k_{diff}) for a given population, R is the universal gas constant, and A is the (variable) pre-exponential factor. Errors in fitted activation energies correspond to the standard error associated with fitted coefficients.

C.2 Results and Discussion

Characteristic Desorption and Diffusion Fit Parameters for Each Protein/Surface Combination. Cumulative residence time distributions and cumulative squared-displacement distributions were fit as described in the Materials and Methods for each protein-surface combination and temperature. In the Results it was shown that fit parameters vary with temperature following Arrhenius trends. Table C1 shows representative fit parameters – characteristic residence times (τ), diffusion coefficients (D), and the relative fraction each represents – for each protein-surface combination. Representative fit parameters were taken from 25°C parameter fits. For example, for residence time cumulative distributions, the shortest-lived population (P1), with characteristic residence times in the range 0.4–0.7s, was the most common, representing ~70–80% of all objects. A longer-lived population (P2), with characteristic residence times in the range 1.5–2.6s, represented ~15–20% of all objects. Finally, relatively rare, but long-lived populations (P3 and P4), with characteristic residence times of 9–13s and 30-75s respectively, represented the remaining 2–9% of objects.

There is a greater difference in fit parameters between BSA and Fg on TMS than on FS (which have fit parameters that are very similar). For Fg on TMS the fraction of fast trajectories is 3-4 times larger than this fraction for any other protein-surface combination.

Table C1: Representative parameters determined from fits to cumulative residence time distribution (of multiple movie) with error representing error between movie fits.

	Desorption							
	P1		P2		P3		P4	
	f	τ (s)	f	τ (s)	f	τ (s)	F	τ (s)
BSA FS	0.807(6)	0.55(2)	0.15(2)	2.40(7)	0.039(8)	9(2)	0.007(2)	60(30)
BSA TMS	0.72(5)	0.61(3)	0.19(4)	3(1)	0.06(1)	12(6)	0.019(6)	59(10)
Fg FS	0.82(3)	0.54(3)	0.14(2)	2.2(5)	0.04(4)	9(4)	-	-
Fg TMS	0.82(3)	0.43(3)	0.16(3)	1.8(4)	0.02(1)	10(5)	-	-

Table C2: Representative parameters determined from fits to cumulative squared-displacement distribution (of multiple movie) with error representing error between movie fits.

	Diffusion					
	M1		M2		M3	
	f	D ($\mu m^2/s$)	f	D ($\mu m^2/s$)	f	D ($\mu m^2/s$)
BSA FS	0.050(7)	0.24(1)	0.44(4)	0.033(1)	0.51(4)	0.0092(5)
BSA TMS	0.10(1)	0.244(7)	0.21(2)	0.033(2)	0.69(2)	0.007(1)
Fg FS	0.07(2)	0.23(3)	0.4(1)	0.05(1)	0.5(1)	0.014(5)
Fg TMS	0.337(6)	0.322(6)	0.438(3)	0.033(6)	0.226(4)	0.007(2)

Data Fitting Using the Method of Maximum Entropy. The maximum entropy method (MEM) was previously described (5). This method was used to qualitatively confirm the number of populations used to fit cumulative residence time distribution (CRTD). Due to a finite frame rate of 200ms, only objects that remain on the surface for less than this amount of time are not included in experimental CRTDs (true CRTDs would include these objects). These experimental CRTDs were employed in MEM fitting. Because the experimental CRTDs do not account for objects residing on the surface for less than the frame rate, this CRTD, quantitative characteristic residence time do not match our calculated characteristic residence time values. However MEM fitting can give us qualitative information about the number of populations to include in our fitting. Four peaks were found for BSA on FS at 25°C in Figure C1a, which is consistent with the number of populations used to fit BSA CRTDs. Three peaks were found for Fg on FS at 30°C in Figure C1b consistent with three populations used to fit Fg CRTDs.

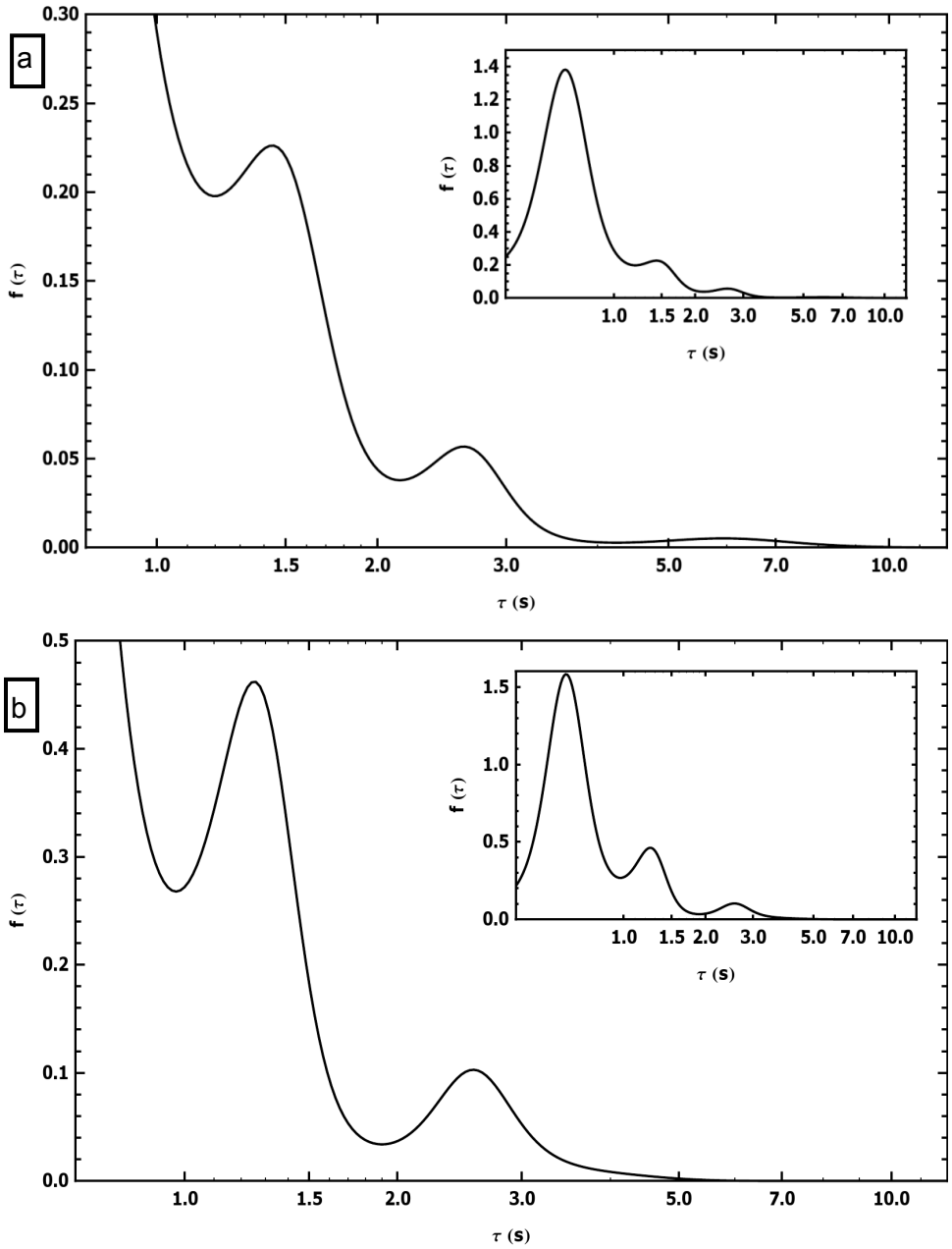

Figure C1: MemExp characteristic residence time distribution of the cumulative residence time distribution of (a) BSA on FS at 25°C and (b) Fg on FS at 30°C. Four peaks exist (indicating four distinct populations) for BSA on FS while three peaks exist (indicating three distinct populations) for Fg on FS.

Cumulative Distributions for Oligomer Intensity Binned Objects. Previous work in our lab has observed that objects with longer surface residence time systematically corresponded to objects with greater median intensities (3, 4). Further, Kastantin and coworkers went on to show

that discrete intensities, corresponding to different oligomeric states, can be identified by examining the probability distribution of fluorescence intensity as a function of minimum surface residence time (3, 4). In this work, intensity bins (for a given protein-surface temperature movie) were selected that captured characteristic objects of the identified oligomeric states. For each oligomeric state, residence time and squared-displacement cumulative distributions are shown in Figure C2 and Figure C3, respectively, where population A corresponds to mainly monomers and populations B, C, and D to increasing oligomeric states, e.g. dimers, trimers, and larger oligomers. For BSA (data and analysis not previously reported for the solid-liquid interface) again as intensity increases residence times also increases. As described in Results, for BSA on TMS the monomer population A has a single characteristic residence time (i.e. oligomeric states can be directly related to populations identified by residence time analysis) while exhibiting multiple diffusive modes (i.e. diffusive modes are not directly coupled with oligomeric state). For both surfaces, while multiple diffusive modes exist for each oligomeric state a larger fraction of objects diffusing faster is seen for smaller oligomeric states.

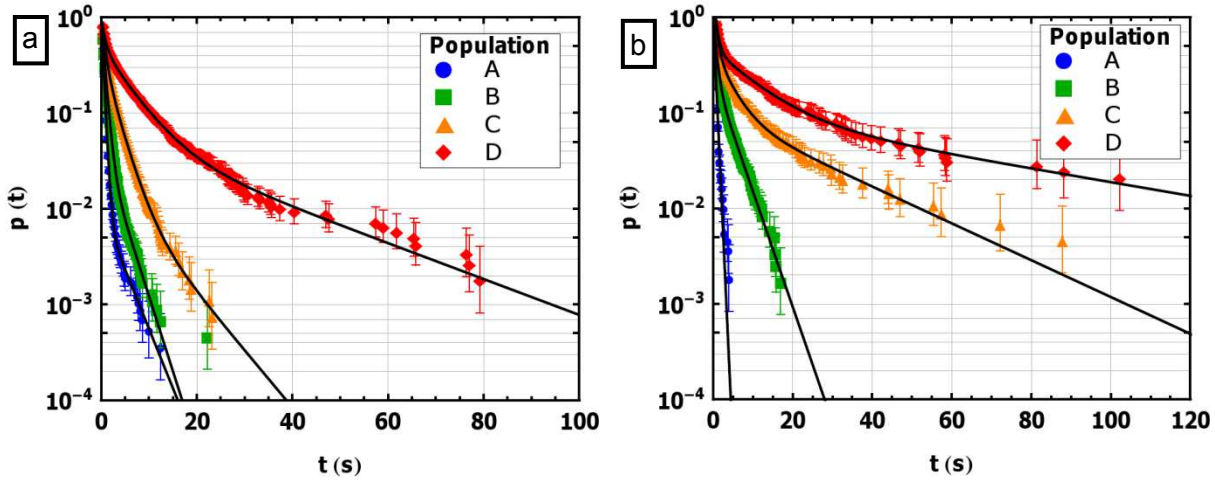

Figure C2: Cumulative residence time distribution at 25°C binned by intensities for (a) BSA on FS and (b) BSA on TMS. Intensity increases from A to D where a greater fraction of brighter objects remain on the surface longer.

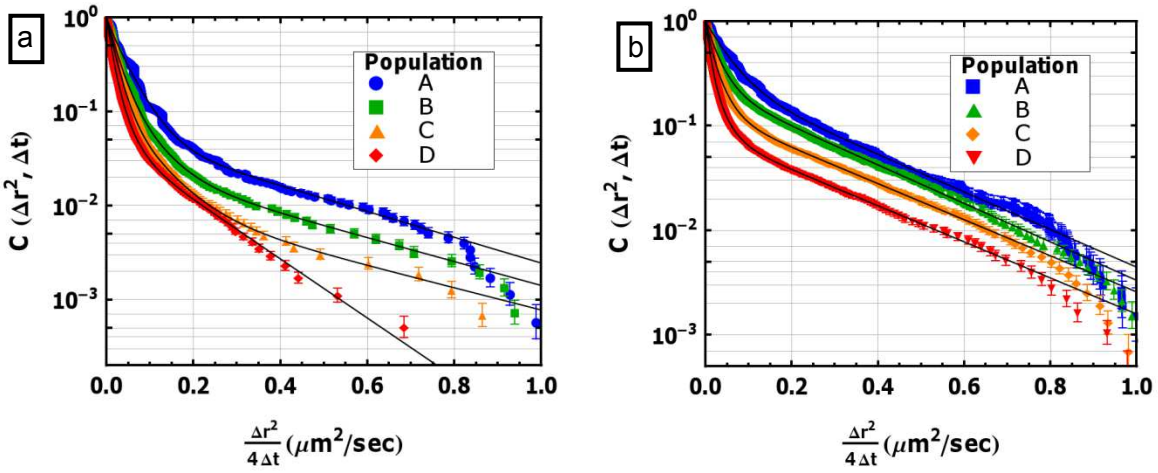

Figure C3: Cumulative squared-displacement distribution at 25°C of (a) BSA on FS and (b) BSA on TMS for trajectories that have been binned by intensity. Intensity increases from A to D where a greater fraction of brighter objects move slower.

C.3 References

1. Honciuc, A., and D. K. Schwartz. 2009. Probing hydrophobic interactions using trajectories of amphiphilic molecules at a hydrophobic/water interface. *J. Am. Chem. Soc.* 131:5973-5979.

2. Honciuc, A., A. W. Harant, and D. K. Schwartz. 2008. Single-molecule observations of surfactant diffusion at the solution-solid interface. *Langmuir* 24:6562-6566.

3. Kastantin, M., B. B. Langdon, E. L. Chang, and D. K. Schwartz. 2011. Single-molecule resolution of interfacial fibrinogen behavior: Effects of oligomer populations and surface chemistry. *J. Am. Chem. Soc.* 133:4975-4983.

4. Walder, R., and D. K. Schwartz. 2010. Single molecule observations of multiple protein populations at the oil-water interface. *Langmuir* 26:13364-13367.

5. Steinbach, P. J., R. Ionescu, and C. R. Matthews. 2002. Analysis of kinetics using a hybrid maximum-entropy/nonlinear-least-squares method: Application to protein folding. *Biophys. J.* 82:2244-2255.

6. Kastantin, M., and D. K. Schwartz. 2012. Distinguishing positional uncertainty from true mobility in single-molecule trajectories that exhibit multiple diffusive modes. *Microsc Microanal.* 18: 793-797.

Appendix D: Chapter 4 Supporting Information

D.1 Concentration-dependence of cluster formation provides insight into surface homogeneity

Mapping using accumulated probe trajectories (MAPT), a super-resolution technique developed in our lab, was used to visualize the spatial distribution of adsorbed molecules and associations at the interface.[1] In MAPT different dynamic properties of molecular trajectories (e.g. surface residence time, adsorption, desorption, or association) are grouped using their interfacial positions into two-dimensional bins. The average or cumulative dynamic properties of all trajectory steps within a two-dimensional bin are then calculated. Finally, the accumulated observations for each bin are used to create a 'map' of the surface based on the chosen dynamic property. In these experiments, one movie of 1000 images was acquired over 200 s for each surface site, resulting in 1,000-20,000 accumulated molecular trajectories to construct each MAPT image. Figure D1a-c shows sample MAPT images of BSA_A-BSA_D associations (red pixels) and unassociated BSA_D (gray pixels) for different [BSA_A] solution concentrations. By quantifying the size of each distinct protein association area (i.e. contiguous red pixels where associations occurred, ignoring unassociated proteins), a frequency distribution of apparent protein cluster sizes was constructed for 12 MAPT images at each concentration in Figure D1d.

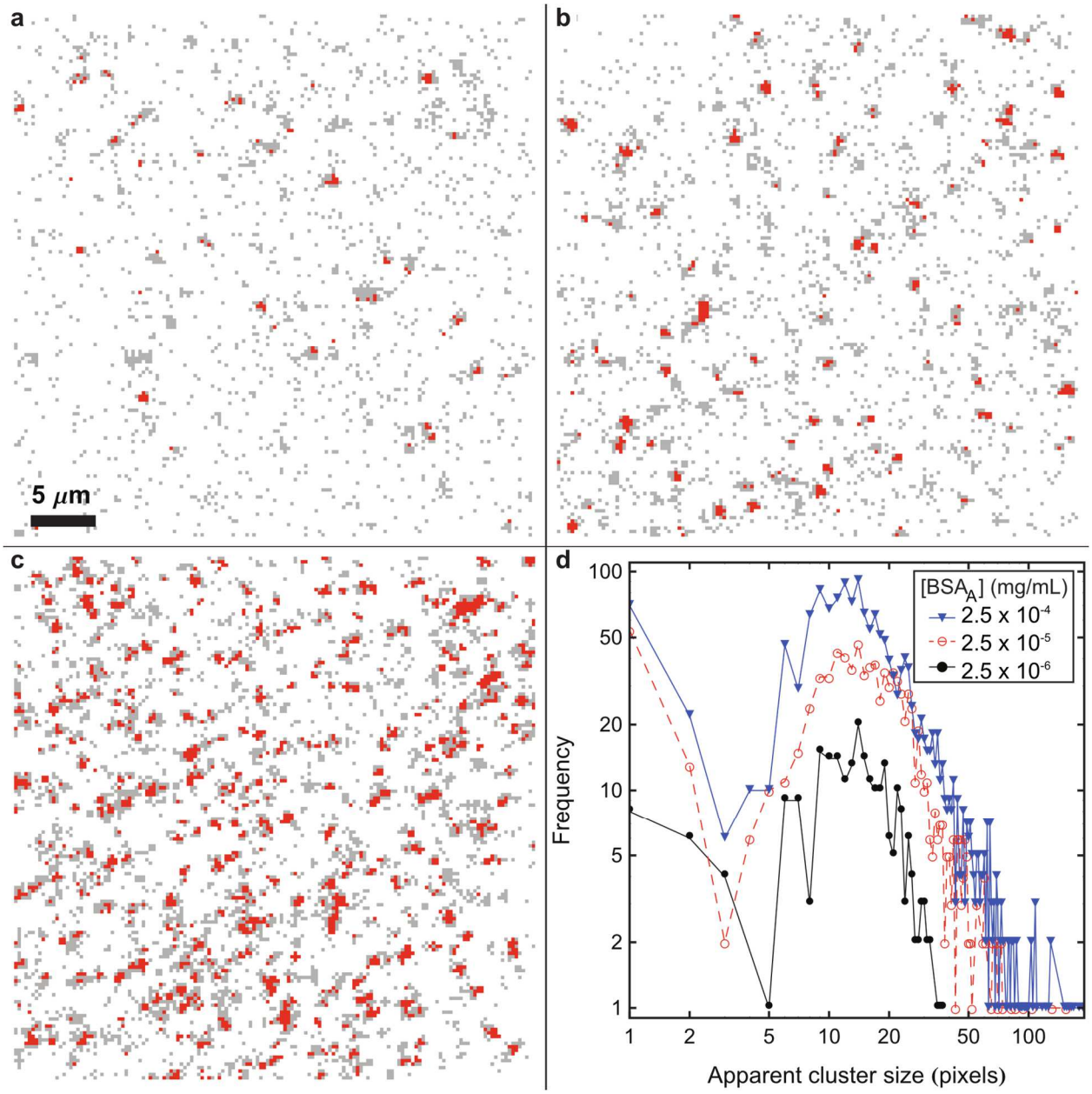

Figure D1. Mapping using accumulated probe trajectories (MAPT) images of BSA_A-BSA_D contacts (red pixels) and unassociated BSA_D (gray pixels) for BSA_A concentrations of (a) $2.5x10^{-4}$ mg/ml, (b) $2.5x10^{-5}$ mg/ml, and (c) $2.5x10^{-6}$ mg/ml. Each pixel in the MAPT images represents one pixel on the EMCCD camera and corresponds to a square area with sides of 227 nm in real space. Each MAPT image represents trajectories collected over a period of 200 s with 0.2 s time resolution. (d) Frequency distribution of apparent cluster sizes is shown for different BSA_A concentrations. Cluster size was quantified in 12 MAPT images, like those shown in (a-c), for each concentration.

Two important conclusions about surface heterogeneity can be drawn from Figure D1. First, while molecules explored some larger contiguous areas, molecules also explored many

smaller disconnected areas in Figures D1a-c. If PEG self-assembled monolayer formation were incomplete and contained 'defect sites' of bare fused silica, we would expect proteins to reside preferentially on these 'defect sites' due to favorable interactions with bare fused silica. However, molecules appeared to explore the surface indiscriminately under all conditions. Second, Figure D1d shows that as [BSA_A] increased, the frequency of observing a given apparent cluster size increased and larger apparent cluster sizes were increasingly observed. This indicates that increased [BSA_A] resulted in the formation of clusters at more locations around the surface. In contrast, if aggregation occurred preferentially at special 'defect sites' the frequency of apparent cluster sizes, or number of cluster locations, would be directly related to the surface density of defects, a value that is expected to be independent of [BSA_A]. Instead, apparent cluster frequency was concentration-dependent, indicating that the BSA association and dissociation behavior described here was representative of protein behavior on a PEG monolayer and not dominated by defect sites.

D.2 Observation bias in identifying partial-RET associations

In order to identify objects in each image, a disk matrix image convolution algorithm was performed followed by image thresholding in each channel.[2] Thresholds were selected conservatively such that only diffraction-limited spots above noise were identified as objects. Consequently, objects undergoing partial-RET with similar (and relatively low) F_A and F_D, resulting in average relative distances of ~1, were less likely to be identified in either channel. We hypothesized that the two peaks present in the d_{app} distribution resulted from the identification bias against these objects. In order to test this hypothesis we decreased the identification threshold (by the same fraction in both channels). A larger fraction of neglected objects were identified near d_{app}~1, confirming that the two peaks present in the d_{app} probability distribution were accentuated by the omission of objects with equally low F_A and F_D. While lower thresholds provided better sensitivity to the population at d_{app}~1, they also increased

contributions to the data from noise that was anomalously treated as a fluorescent protein; therefore, the lower threshold was not used for results presented elsewhere in this work. Finally, it is important to note that this analysis does not rule out the possibility of multiple RET states in the partial-RET population. However, due to the random labeling scheme used in this work, we could not connect different partial-RET states to different types of BSA-BSA interactions and consequently chose to bin them into a single partial-RET category.

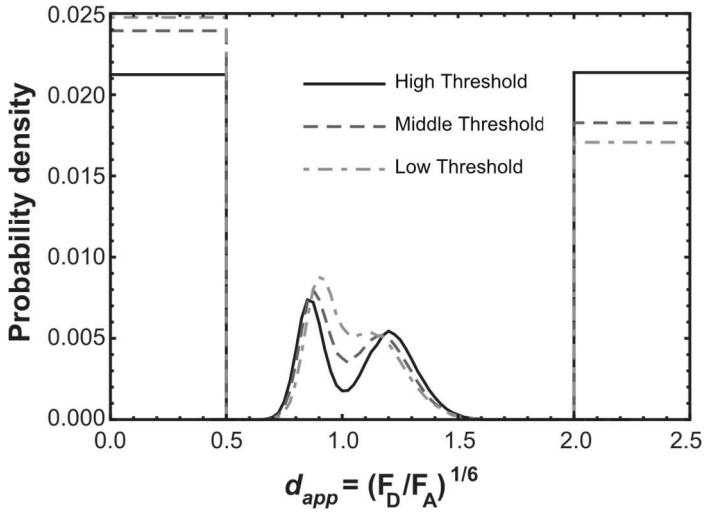

Figure D2. Probability distribution of apparent relative distance, d_{app}, for BSA on PEG at [BSA_A] = 2.5x10^{-4} mg/ml. A step function was used to describe the extreme d_{app}-values of the distribution where F_D or F_A was not significantly greater than 0 and d_{app}-value could not be accurately calculated. The object identification threshold for each channel was decreased by 85% (middle) and 66% (low) from the threshold used to identify objects for these experiments (high).

D.3 Donor fluorophore photobleaching

When using fluorescent labels, photobleaching on time scales relevant to dynamic observations can lead to erroneous interpretations. For example, photobleaching of donor fluorophores attached to a BSA_D molecule would be treated as a desorption event when in fact the molecule may remain at the interface. Similarly, for associating BSA_D-BSA_A molecules the deactivation of donor fluorophores would be treated as both an apparent desorption event and

an apparent dissociation event. Ultimately photobleaching has the potential to shorten the surface residence times and contact times measured in these experiments. Fluorophore photobleaching would only significantly affect our results if it occurred on a time scale comparable to or shorter than the physical time scales being measured. In order to assess the effect of photobleaching, the first-order time constant for donor fluorophore photobleaching was quantified by measuring the apparent surface residence time distribution of BSA_D molecules that were covalently attached to the surface. The apparent desorption of immobilized proteins results solely from donor photobleaching.

Fused silica wafers were cleaned by piranha exposure, drying, and UV-ozone treatment as described in materials and methods. A monolayer of 3-glycidoxypropyltrimethoxysilane (GPTMS) was then deposited on cleaned fused silica wafers by vapor deposition using a solution of toluene (85%), GPTMS (10%), and *n*-butylamine (5%) for 24 h at room temperature. BSA_D molecules were immobilized on the GPTMS monolayer through the reaction of the epoxide ring of GPTMS with primary amines on lysine residues, as described previously.[5] The GPTMS monolayer was exposed to a solution of BSA_D ($[BSA_D] = 10^{-7}$ mg/mL) at pH 9.0 with 150mM sodium chloride. After 20 h, any unreacted BSA_D molecules were removed with a series of vigorous solvent rinses including deionized water, toluene, isopropanol, and acetone. Finally, wafers were exposed to a deionized water bath at 50ºC.

The apparent surface residence times were then measured using SM-TIRFM tracking for the immobilized BSA_D molecules under the same buffer solution, laser power, and filter conditions used elsewhere in the work. Several time-lapse series of images, taken at 1 s intervals, were acquired while the laser remained on continuously. After image processing and object identification and tracking, the apparent surface residence times for all immobile molecules were used to create an apparent residence time cumulative distribution (Figure D3). This distribution exhibited a mono-exponential decay with a characteristic photobleaching time constant of 57 ± 2 s. The measured photobleaching time constant was at least an order of

magnitude longer than the mean characteristic surface residences time for associating molecules (1.11 ± 0.04 s for [BSA_A] = 2.5x10^{-5} mg/ml) and two orders of magnitude longer than the mean characteristic contact time (0.25 ± 0.03 s for [BSA_A] = 2.5x10^{-4} mg/ml), indicating that photobleaching had a negligible effect on the results presented in this work.

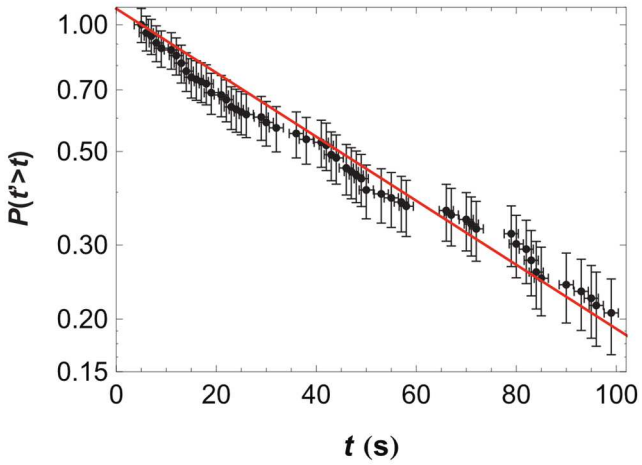

Figure D3: Apparent cumulative surface residence time distribution of immobilized BSA_D when illuminated by 532nm. Molecules were covalently attached to the surface such that apparent desorption was the result of photobleaching.

D.4 Interfacial diffusion promotes cluster formation

Single-molecule tracking enables the measurement of molecular diffusion by tracking a molecule's movement from frame-to-frame. By default, interfacial diffusion is expected to follow two-dimensional Gaussian random-walk statistics. As with previous studies of protein interfacial diffusion, an object may diffuse via multiple diffusion modes – each characterized by a diffusion coefficient, D_j – during its time on the surface.[2,6,7] The cumulative squared-displacement distribution can be modeled simply by the sum of the cumulative distributions for each mode weighted by the fraction of observed steps, f_j, corresponding to that mode:

$$C(R^2, \Delta t) = \sum_j f_j e^{-R^2/4D_j\Delta t}$$

where R^2 is the squared-displacement for the time interval Δt. The average diffusion coefficient, $\bar{D}$, can then be calculated as the fraction-weighted average of each mode:

$$\bar{D} = \sum_j f_j D_j$$

Figure D4a shows a cumulative squared-displacement distribution of all steps observed for all trajectories. On this log-linear graph, a single diffusive mode would appear linear. Instead several modes were present with 48 ± 2% of steps coming from a diffusive mode characterized by a diffusion coefficient of 0.0151 ± 0.0004 $\mu m^2/s$. This diffusion coefficient essentially represents the apparent movement of immobile objects due to imperfect spatial localization.[8] Two mobile diffusive modes were also observed, with 46 ± 2% and 6.8 ± 0.2% of steps belonging to modes characterized by diffusion coefficients of 0.047 ± 0.001 $\mu m^2/s$ and 0.243 ± 0.004 $\mu m^2/s$, respectively (Table D1). On average BSA_D molecules exhibited a diffusion coefficient of 0.045 ± 0.001 $\mu m^2/s$, indicating significant interfacial mobility. We estimated that a single BSA_D molecule collides with BSA_A molecules at a frequency of ~1 s^{-1} for a surface coverage of 25 BSA_A molecules per μm^2 at a $[BSA_A] = 2.5x10^{-4}$ mg/ml.

Another way to understand a molecule's interfacial mobility is to consider the total Euclidean distance between a molecule's initial adsorption position to its final desorption position. As shown in Figure D4b, many molecules move significantly from their initial adsorption position; e.g. ~10% of molecules moved more than 1 μm, which is more than 100 molecular lengths of BSA.

Table D1. Diffusion mode fractions and diffusion coefficients for $[BSA_A] = 2.5x10^{-5}$ mg/ml shown in Figure D4a.

mode	f_j	D_j ($\mu m^2/s$)
1	0.48(2)	0.0151(4)
2	0.46(2)	0.047(1)
3	0.068(2)	0.243(4)

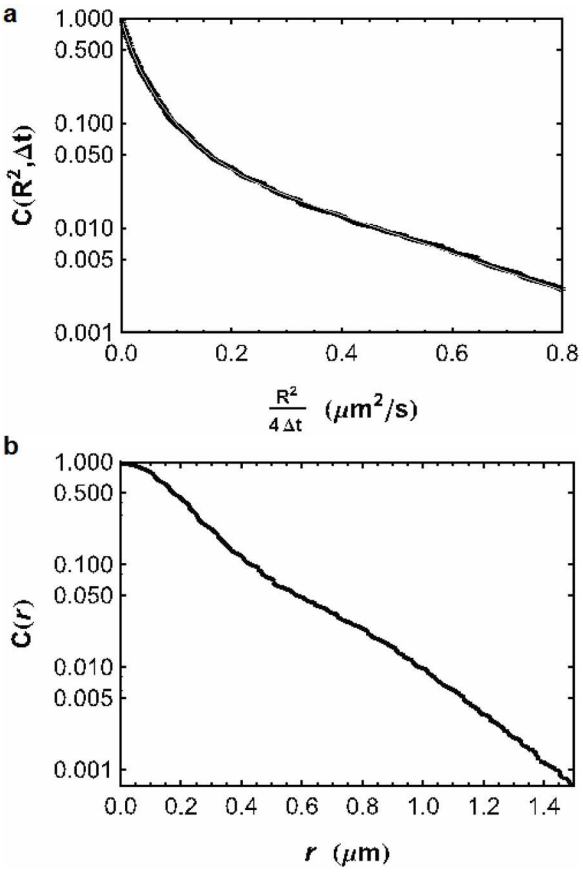

Figure D4: (a) Cumulative squared-displacement distribution of all trajectory steps at [BSA_A] = 2.5×10^{-5} mg/ml with multimodal diffusion. The mode fractions and diffusion coefficients corresponding to the fit shown in gray are presented in Table D1. (b) Cumulative distribution of surface displacements over the course of each trajectory's surface residence time (i.e. the Euclidean distance between adsorption and desorption positions) at [BSA_A] = 2.5×10^{-5} mg/ml.

D.5 References

(1) Walder, R.; Nelson, N.; Schwartz, D. K. *Nat. Commun.* **2011**, *2*.

(2) Walder, R.; Schwartz, D. K. *Langmuir* **2010**, *26*, 13364–13367.

(3) Berney, C.; Danuser, G. *Biophys. J.* **2003**, *84*, 3992–4010.

(4) Lakowicz, J. R. In *Principles of Fluorescence Spectroscopy*; Lakowicz, J. R., Ed.; Springer New York, 2006; pp. 443–475.

(5) McLoughlin, S. Y.; Kastantin, M.; Schwartz, D. K.; Kaar, J. L. *Proc. Natl. Acad. Sci.* **In Press**. DOI: 10.1073/pnas.1311761110

(6) Kastantin, M.; Langdon, B. B.; Chang, E. L.; Schwartz, D. K. *J. Am. Chem. Soc.* **2011**, *133*, 4975–4983.

(7) Langdon, B. B.; Kastantin, M.; Schwartz, D. K. *Biophys. J.* **2012**, *102*, 2625–2633.

(8) Kastantin, M.; Schwartz, D. K. *Microsc. Microanal.* **2012**, *18*, 793–7.

Appendix E: Chapter 5 Supporting Information

E.1 Polymer film preparation

Details of polymer film preparation are presented below. Figure E1 shows the structure of the polymers used to prepare the polymer thin films.

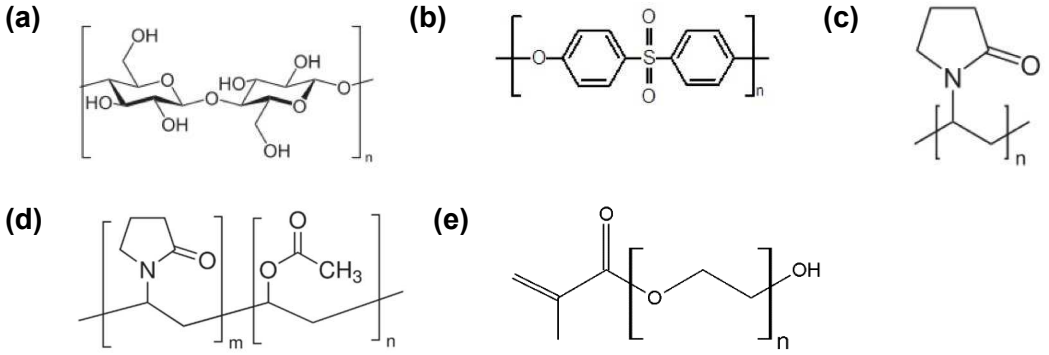

Figure E1: Monomer structures for (a) RC, (b) PES, (c) PVP, (d) PVAc-PVP, and (e) PEGMM precursor.

RC film preparation. Regenerated cellulose (RC) films were prepare from a trimethylsilyl cellulose (TMSC) precursor. TMSC was prepared as described previously.[1] A 10 mg/mL TMSC solution in toluene (Fisher Scientific) was spin-cast onto TMS monolayer modified wafers at 4,000 rpm for 45 s. TMSC films were acid hydrolyzed to RC by exposing films to hydrochloric acid (Sigma-Aldrich) vapors under vacuum for 30 min. Hydrolysis was confirmed with FTIR as specified in the Materials and Methods. Figure E2 shows the FTIR spectra before and after hydrolysis.

PVP/PES and PVAc-PVP/PES film preparation. Dry polyvinylpyrrolidone (PVP, MW 1,300,000 Da) or polyvinyl acetate-co-polyvinylpyrrolidone (PVAc-PVP, MW 47,000 Da) were added to dry polyethersulfone (PES, MW 48,000 Da) to final concentrations of 6% w/w or 12% w/w respectively, and the polymers were dissolved in dichloromethane (Sigma-Aldrich) with a total polymer concentration of 0.35 w/v%. PVP/PES and PVAc-PVP/PES solutions were sonicated for 30 min and filtered using 0.2 μm nylon syringe filters (Pall Corp.). These solutions

were then spin-cast onto TMS-coated wafers at 5,000 rpm for 45 s and cured at 70 °C for 60 min.

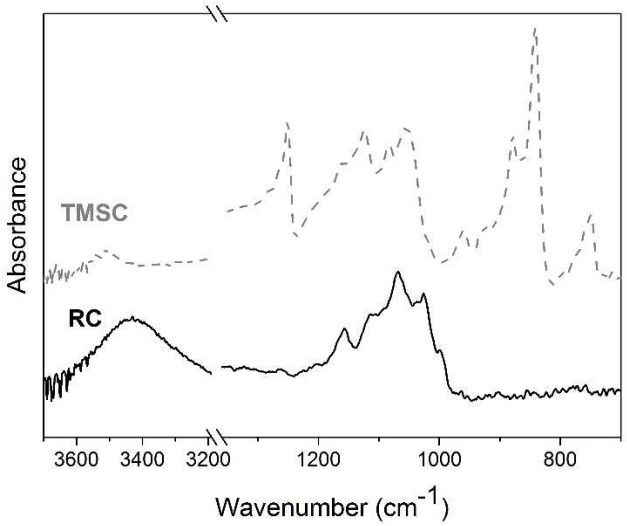

Figure E2: FTIR spectra of TMSC (before hydrolysis) and RC (after hydrolysis) thin films. Important peaks and stretches, indicating a successful hydrolysis, are described in the Materials and Methods.

PEGM/PES film preparation. Polyethylene glycol methacrylate (PEGM) refers to a polymerized product of PEG monomethacrylate (PEGMM, MW 400 Da) and PEG dimethacrylate (PEGDM, MW 400 Da) mixed in a 1:1 ratio. Dry PEGMM and PEGDM were added to PES, each at 6% w/w, and then dissolved in N,N-dimethyl-formamide (DMF) with a total polymer concentration of 1.9% w/v. This solution was sonicated for 30 min and filtered using 0.2 μm nylon syringe filters (Pall Corp.). Ammonium persulfate was used as a polymerization initiator. A solution of 1 mg/mL ammonium persulfate in DMF was sonicated and filtered as above. The ammonium persulfate solution was added in 1:10 ratio to the PEGM/PES solution in DMF and immediately spin-cast onto mPEG-silane-modified wafers at 5000 rpm for 45 s. The wafers were baked at 70 °C for 60 min.

E.2 Topographic surface characterization

Each surface's roughness was characterized using atomic force microscopy (AFM). Figure E3 shows representative AFM images of the four polymer thin films in air. The AFM images of PES blends (Figure E3a-c) and RC (Figure E3d) showed surface indentations with characteristic horizontal length scales that varied widely between 10 and 200nm. Line scans of transects indicated on the AFM images show that such indentations varied vertically over 1-10 nm. Such variations are less than the film thicknesses of 20-30 nm measured by ellipsometry (see Table 5.1) suggesting that the underlying surface was completely covered by the film.

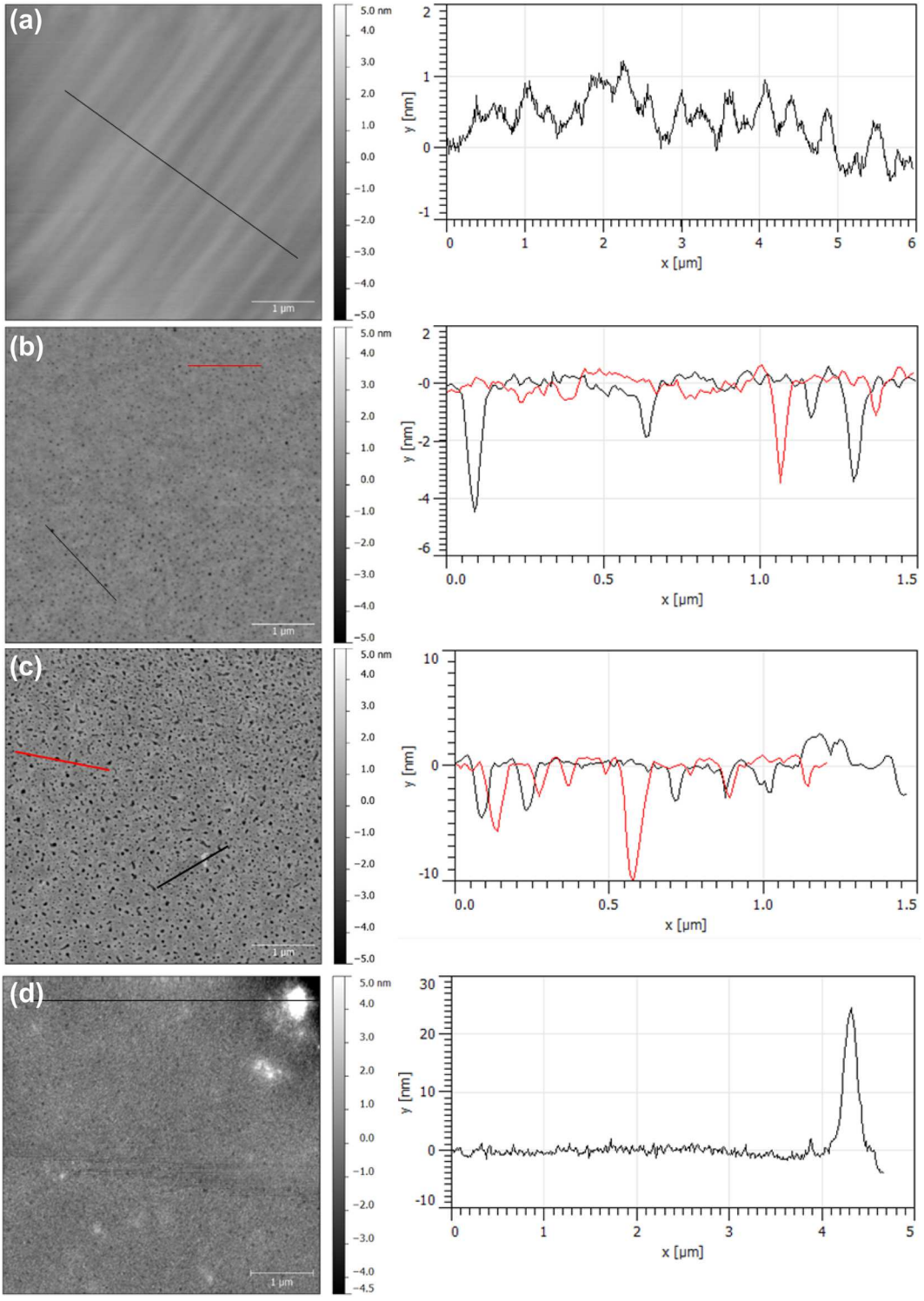

Figure E3: Representative AFM images and line scans (lines indicated on image) of (a) PEGM/PES, (b) PVP/PES, (c) PVAc-PVP/PES, and (d) RC in air. The root mean square (rms) roughness for each image were 0.360 nm, 0.399 nm, 1.02 nm, 1.17 nm, respectively.

E.3 Protein solution characterization

In order to characterize the relative fractions of monomers and oligomers in solution size exclusion chromatography (SEC) was performed. A Beckman Coulter Systems Gold HPLC system with UV 168 detector (set at 280 nm) with a TSK-Gel G3000SW column (Tosoh Biosciences) was used for analysis. Studies were carried out with a mobile phase of phosphate buffered saline (PBS, pH 7.4) and a 150 µL injection volume of 0.1 or 0.01 mg/mL. A flow rate of 1.0 or 0.6 mL/min for 30 minutes was used for Alexa Fluor 555 labeled BSA and IgG, respectively.

Figure E4 shows the SEC normalized absorption chromatogram results for 0.1 and 0.01 mg/mL of protein in PBS. The major peak at longer time represents the protein monomer population and accounts for 78 ± 3% and 95 ± 3% of species in solution for BSA and IgG respectively, as determined from peak integration, with error representing the standard deviation across replicates and concentrations. A smaller peak at short time, representing BSA dimers, and a shoulder at even shorter time, representing BSA trimers or larger aggregates, were clearly present in Figure E4a and accounted for 14.0 ± 0.4% and 8 ± 3% of solutions species, respectively. The inset in Figure E4b suggests that some IgG oligomers and larger aggregates were also present in solution, although IgG oligomers represented a smaller fraction (5 ± 2%) of solution species than did BSA oligomers. As observed at the interface (see Fig. 1b), protein solution characterization by SEC showed that protein aggregates represented a small fraction of species in solution.

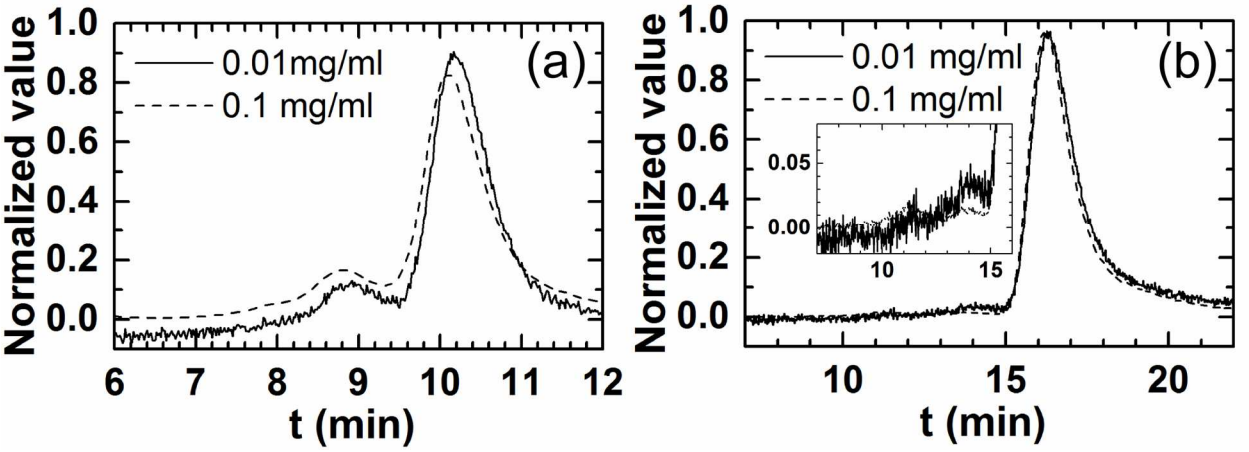

Figure E4: SEC results showing absorbance at 280 nm of fluorescently labeled (a) BSA and (b) IgG at room temperature in PBS. Flow rates through the column were 1.0 or 0.6 mL/min for BSA and IgG, respectively.

E.4 Population heterogeneity at dilute protein concentrations

As shown in Figure 5.1, cumulative residence time distributions (CRTDs) indicated heterogeneous desorption kinetics, suggesting multiple dynamic populations each exhibiting first-order desorption kinetics. The multiple populations may be due to different oligomerization states, surface heterogeneity, or protein binding orientation or conformation. In Table E1 we have tabulated the population parameters described by an exponential mixture model (Equation 1), used to fit the CRTDs depicted in Figures 5.1a and 5.1c. Similar fits were performed for all other protein-surface combinations.

Table E1: Fraction and characteristic residence time for each population, fit by Equation 1 to each CRTD shown in Figures 5.1a and 5.1c, for IgG on RC at extremely dilute protein concentrations. Standard error for each data point is reported in parenthesis and corresponds to the last digit shown.

	All		**Monomers**		**Oligomers**	
Population	f_i	τ_i(s)	f_i	τ_i(s)	f_i	τ_i(s)
1	0.79(4)	0.51(6)	0.89(4)	0.50(7)	0.82(6)	1.4(2)
2	0.17(3)	3.1(7)	0.11(4)	2.2(5)	0.18(6)	26(6)
3	0.04(2)	29(7)				
Mean		2.1(2)		0.68(2)		5.6(5)

E.5 Strong vs. weak site desorption kinetics

In the Chapter 5 Results Section we compared the desorption kinetics on adsorption sites that were visited more than once (n > 1, i.e. anomalously strong sites) to those visited a single time (n = 1, i.e. weak sites). In Figure 5.2c, IgG monomers and oligomers were shown to reside on stronger sites longer than on weak sites on an RC surface. Table E2 shows the mean characteristic residence times for monomers and oligomers on strong or weak sites for all protein-surface combinations. Protein monomer and oligomer mean characteristic residence times on strong sites were longer than on weak sites for all protein-surface combinations. Mean characteristic residence times for both monomers and oligomers tended to be shorter at higher protein concentrations than at dilute concentrations.

Table E2: Mean characteristic residence times (in seconds) of IgG and BSA monomers and oligomers at extremely dilute and high protein concentrations on strong sites (S) or weak sites (W). Protein monomers and oligomers were identified by a molecule's mean fluorescence intensity. The number in parenthesis represents the standard error and is associated with the final digit.

		FS	RC	PEGM/PES	PVAc-PVP/PES	PVP/PES	TMS
$[BSA]_{dilute}$	$\tau_{monomer,S}$	0.48(4)	0.52(3)	0.75(2)	0.52(1)	0.55(3)	0.51(5)
	$\tau_{monomer,W}$	0.27(3)	0.30(3)	0.35(4)	0.37(2)	0.31(4)	0.28(2)
	$\tau_{oligomer,S}$	4(1)	3.4(3)	4.1(4)	2.1(3)	2.38(8)	5.5(9)
	$\tau_{oligomer,W}$	0.9(2)	2.5(5)	3.6(3)	1.5(2)	2.2(5)	4(2)
$[BSA]_{high}$	$\tau_{monomer,S}$	0.43(4)	0.64(5)	0.55(5)	0.40(1)	0.28(1)	0.43(1)
	$\tau_{monomer,W}$	0.10(1)	0.5(2)	0.22(1)	0.30(2)	0.16(1)	0.25(2)
	$\tau_{oligomer,S}$	3(1)	4.1(4)	1.2(1)	1.27(5)	1.6(1)	1.70(9)
	$\tau_{oligomer,W}$	0.35(9)	0.68(7)	0.56(6)	1.02(4)	0.38(3)	0.9(1)
$[IgG]_{dilute}$	$\tau_{monomer,S}$	0.8(3)	0.48(9)	0.76(7)	0.5(1)	0.50(3)	0.51(3)
	$\tau_{monomer,W}$	0.7(2)	0.27(7)	0.4(2)	0.31(4)	0.20(4)	0.32(7)
	$\tau_{oligomer,S}$	6.4(5)	5(2)	5.0(5)	2.1(6)	4.1(2)	4.0(1)
	$\tau_{oligomer,W}$	0.87(5)	2.1(4)	4(2)	0.48(5)	2.3(4)	3.3(1)
$[IgG]_{high}$	$\tau_{monomer,S}$	0.54(8)	0.48(3)	0.57(6)	0.42(2)	0.52(5)	0.61(4)
	$\tau_{monomer,W}$	0.23(6)	0.10(3)	0.17(3)	0.21(4)	0.16(1)	0.35(3)
	$\tau_{oligomer,S}$	7(3)	3.1(5)	1.2(3)	3(1)	0.77(4)	3.5(1)
	$\tau_{oligomer,W}$	3(1)	0.8(1)	0.42(3)	0.48(6)	0.38(3)	1.74(9)

E.6 Surface heterogeneity and protein desorption kinetics

In Table E3 we report the estimated protein surface coverage, the surface heterogeneity indexes, and the mean characteristic residence times for monomers, oligomers, and all molecules for all protein-surface combinations. Figure 5.4 graphically shows the relationship between surface heterogeneity and mean characteristic residence times for protein monomers and oligomers, tabulated in Table E3. We observed a general shift to shorter residence times and greater surface homogeneity when the protein solution concentration was increased by several orders of magnitude, as shown in Figure E5. This shift was in agreement with an overall trend of proteins residing for shorter times on more homogeneous surfaces.

The relative magnitude of homogeneity and residence time difference at dilute and high concentrations varied greatly between surface chemistries. One possible reason for this variability may be the magnitude of protein surface coverage. We calculated the protein surface coverage – expressed as the fraction of monolayer coverage (θ/θ_{max}, where θ_{max} represents tight packing of side-on molecules with surface areas of 5.6 nm^2 and 15.2 nm^2 for BSA and IgG, respectively) – from the observed surface density of fluorescently-labeled objects (i.e. the number of fluorescently-labeled molecules observed in a single frame multiplied by the maximum area occupied by a protein monomer). The fraction of monolayer coverage most likely underestimated the true protein surface coverage due to our finite acquisition time and our assumption of monomer molecular area (we also observed oligomers). At higher protein concentrations, the fraction of monolayer coverage was extrapolated from the surface coverage of fluorescently-labeled molecules by multiplying the apparent coverage by the ratio of unlabeled molecules to fluorescently-labeled molecules. This estimate should be thought of as a lower boundary, in the case where this fraction is less than one monolayer, again due to our finite acquisition time and monomer molecular area assumption. We note that despite using a

lower unlabeled concentration of IgG (0.3 mg/mL) than BSA (1.0 mg/mL) the fraction of monolayer coverage was not systematically lower for IgG.

While the fraction of monolayer coverage at dilute concentrations was fairly consistent across surfaces (one molecule per ~50 μm^2, an area 10^5 times the size of a protein monomer) the fraction of monolayer coverage at higher protein concentrations varied greatly between surface chemistries. One might expect that on surfaces with a higher protein surface coverage most of the strong sites might be blocked by proteins, leading to a greater reduction in spatial heterogeneity and residence times than on surfaces with a lower protein surface coverage. However, we observed the opposite trend; on surfaces with more molecules (e.g. BSA on FS and TMS), proteins were actually longer-lived and surface heterogeneity was greater than on surfaces that were more sparsely covered (e.g. BSA on PVAc-PVP/PES and PVP/PES), suggesting that surface heterogeneity is more complex than a two-site model would suggest. The positive correlation between higher protein surface coverage, greater heterogeneity, and longer residence times supports the idea that greater strong site density and strength lead to greater protein accumulation on surfaces.

Representative super-resolution IgG adsorption event maps, used in calculating *h*, are shown in Figure E6 and E7. Visual inspection of these representative maps agrees with calculated *h* value trends (e.g. greater strong site density and strength at larger *h* value).

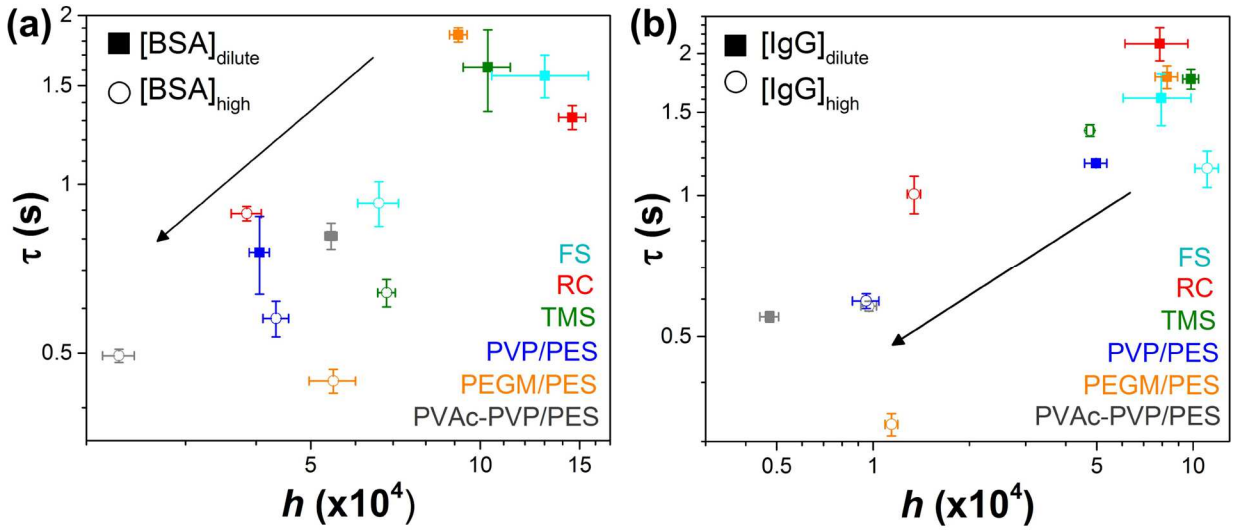

Figure E5: (a) BSA and (b) IgG mean characteristic residences time at dilute protein concentrations (filled) and higher concentrations (open) as a function of heterogeneity, *h*. Error bars represent the standard error between experimental samples. The arrow is a best fit line, vertically displaced, intended to guide the eye.

Table E3: Protein surface coverage (expressed as a fraction of monolayer coverage, θ/θ_{max}), apparent heterogeneity (h), and mean characteristic residence times (τ) for all proteins, protein monomers, and protein oligomers for each protein-surface combination at dilute and high protein concentrations. The apparent heterogeneity values were calculated from 1,000 protein adsorption events. Representative super-resolution adsorption maps used to calculate h are shown in Figures E6 and E7 for all IgG adsorption at dilute and high protein concentrations.

		FS	RC	PEGM/PES	PVAc-PVP/ PES	PVP/PES	TMS
[BSA]$_{dilute}$	θ/θ_{max} x10^{-7}	0.9(7)	3(1)	3(1)	4(1)	8(3)	0.52(9)
	h x10^4	13(3)	14.6(8)	9.1(3)	5.4(1)	4.1(2)	10(1)
	τ_{all} (s)	1.6(1)	1.32(6)	1.85(5)	0.81(4)	0.8(1)	1.6(3)
	$\tau_{monomer}$ (s)	0.7(1)	0.43(4)	0.84(3)	0.63(1)	0.68(3)	0.62(4)
	$\tau_{oligomer}$ (s)	4.4(9)	3.3(2)	3.6(2)	1.7(2)	2.4(3)	4.0(7)
[BSA]$_{high}$	θ/θ_{max}	0.3(2)	0.04(1)	0.02(2)	0.00040(7)	0.0037(4)	0.31(5)
	h x10^4	6.6(6)	3.9(2)	5.5(5)	2.3(1)	4.3(2)	6.8(2)
	τ_{all} (s)	0.93(8)	0.89(3)	0.45(2)	0.49(1)	0.58(4)	0.64(4)
	$\tau_{monomer}$ (s)	0.22(2)	0.38(5)	0.36(3)	0.28(2)	0.23(2)	0.40(3)
	$\tau_{oligomer}$ (s)	0.77(4)	1.27(6)	0.54(4)	0.91(5)	0.81(3)	1.33(8)
[IgG]$_{dilute}$	θ/θ_{max} x10^{-7}	3(1)	4(2)	2.2(7)	2.5(7)	2.5(6)	3.9(6)
	h x10^4	8(2)	8(2)	8.3(7)	0.47(3)	5.0(4)	9.8(6)
	τ_{all} (s)	1.6(2)	2.1(2)	1.8(1)	0.55(1)	1.17(1)	1.77(8)
	$\tau_{monomer}$ (s)	0.8(2)	0.68(2)	0.87(4)	0.54(2)	0.63(2)	0.62(2)
	$\tau_{oligomer}$ (s)	7(1)	5.6(5)	4.4(2)	0.99(2)	3.9(5)	4.3(2)
[IgG]$_{high}$	θ/θ_{max}	0.012(4)	0.039(8)	0.023(5)	0.019(4)	~1	~1
	h x10^4	11.1(9)	1.34(6)	1.14(5)	0.97(5)	0.95(9)	4.8(1)
	τ_{all} (s)	1.1(1)	1.01(9)	0.33(2)	0.58(1)	0.59(2)	1.37(4)
	$\tau_{monomer}$ (s)	0.33(2)	0.43(2)	0.26(2)	0.38(2)	0.48(4)	0.65(1)
	$\tau_{oligomer}$ (s)	3.72(4)	0.99(3)	0.35(2)	0.89(3)	0.72(2)	2.98(9)

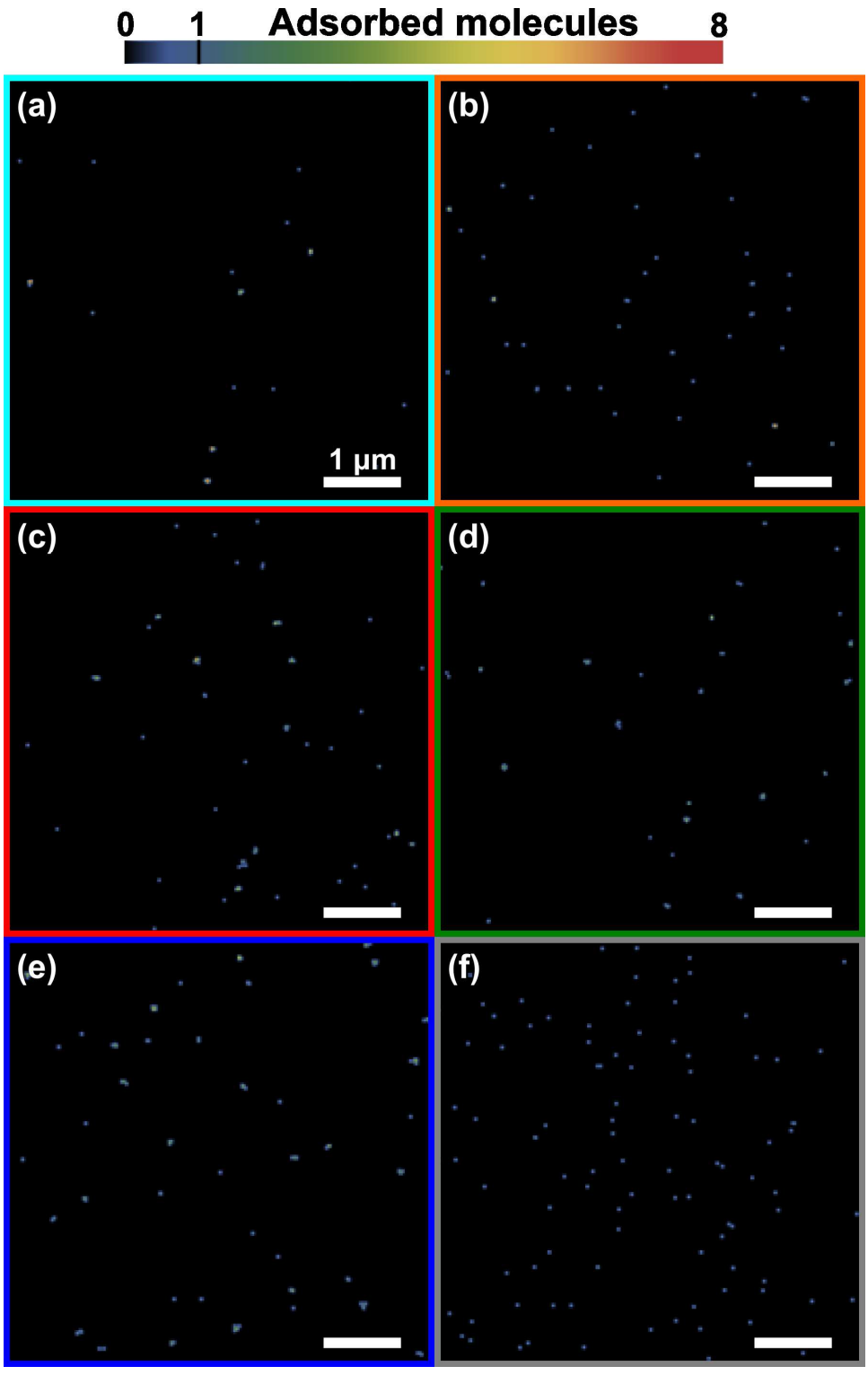

Figure E6: Super-resolution maps of adsorption events for 1000 IgG adsorption events at extremely dilute protein concentrations on (a) FS, (b) PEGM/PES, (c) RC, (d) TMS, (e) PVP/PES, and (f) PVAc-PVP/PES. All scale bars represent 1 µm.

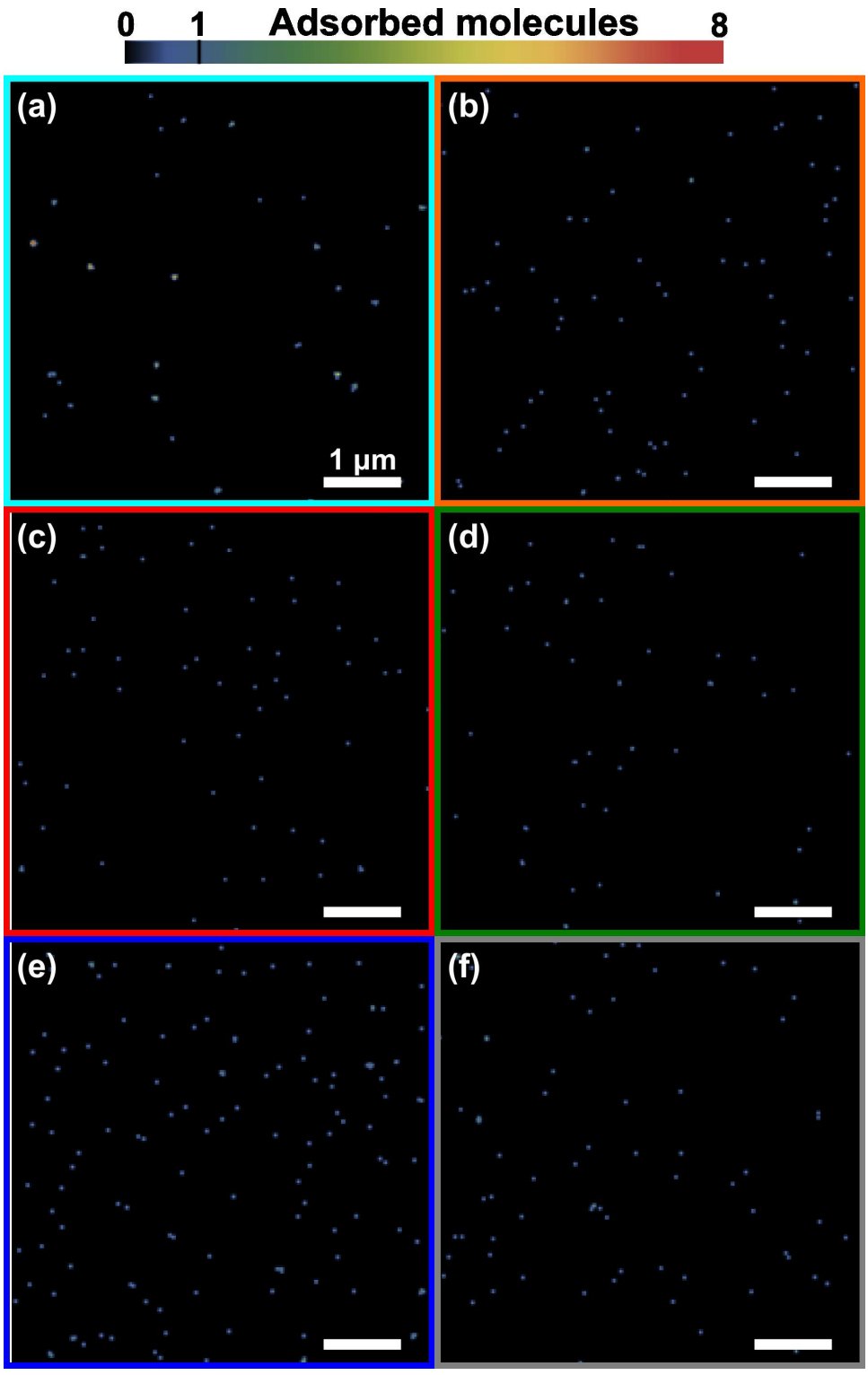

Figure E7: Super-resolution maps of adsorption events for 1,000 IgG adsorption events at high protein concentrations on (a) FS, (b) PEGM/PES, (c) RC, (d) TMS, (e) PVP/PES, and (f) PVAc-PVP/PES. All scale bars represent 1 µm.

E.7 Population heterogeneity at high protein concentrations

Population heterogeneity was also observed on surfaces at higher protein concentrations. On average, molecules – both monomers and oligomers – resided on surfaces for shorter times at higher protein concentrations (see Table E3). A heavy-tailed distribution of mean molecule fluorescence intensities was also observed at high protein concentrations when unlabeled proteins were present (see Figure E8). This suggests that fluorescently-labeled protein oligomers, pre-formed in solution, were present on the surface at both dilute and high protein concentrations.

The population fractions and characteristic residence times identified when fitting the CRTDs of IgG on PVP/PES surface, shown in Figure 5.5, are tabulated in Table E4. For the three populations identified at the dilute and high protein concentrations, both the fractions and the characteristic surface residences times differed. For a given population, the characteristic residence time was shorter at a high protein concentration than at a dilute protein concentration. The fraction of short-lived molecules (population 1) was larger, while the fraction of longer-lived molecules (populations 2 and 3), was smaller at a high protein concentration than at a dilute protein concentration. This suggests both a shift in surface bound populations (e.g. monomer, oligomers, protein orientations, fraction adsorbing to strong sites) as well as a change in protein-surface binding strengths, perhaps due to the presence of other proteins on the surface.

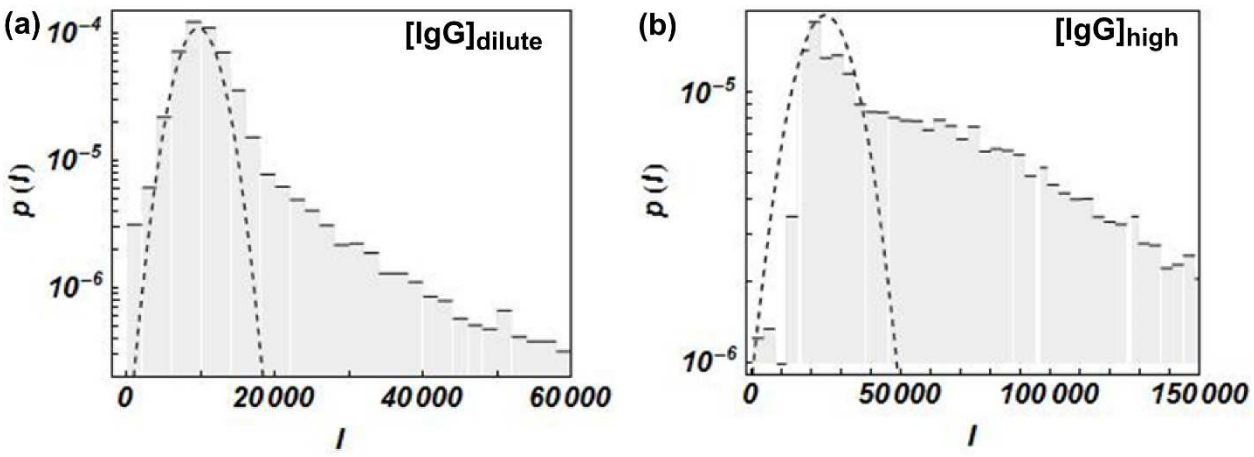

Figure E8: Mean molecular fluorescence intensity distributions of IgG molecules at (a) dilute and (b) high protein concentrations on PVP/PES. Dashed line indicates the normal distribution fit to the first intensity peak (monomers).

Table E4: Fraction and characteristic residence time for each population fit by Equation 1 to CRTDs (shown in Figure 5.5) describing IgG desorption kinetics at dilute and high protein concentrations on PVP/PES. The standard error for each data point is reported in parenthesis and corresponds to the last digit shown.

	[IgG]dilute		**[IgG]high**	
Population	f_i	τ_i (s)	f_i	τ_i (s)
1	0.851(2)	0.489(6)	0.892(2)	0.293(4)
2	0.132(2)	3.23(5)	0.097(1)	2.33(4)
3	0.0171(3)	22.3(2)	0.0109(3)	13.0(1)
Mean		1.22(1)		0.631(7)

E.8 Adsorption event position correlation analysis

A pair correlation function can be used to quantify organization in heterogeneous systems and was used here as an orthogonal method for quantifying surface heterogeneity. If a surface was homogenous, the position of adsorption events would be randomly distributed and uncorrelated. However, surfaces with sites that were visited more times than likely based on simple Poisson probability would show a correlation. A pair radial auto-correlation function, *g(r)*, was used to evaluate the increased probability of finding a second object adsorbed a distance *r* from a given object's adsorption position, as described by:

$$g(r) = \langle \frac{A}{N^2} \sum_{i,j} \delta(\vec{r}_i - \vec{r}_j - \vec{r}) \rangle_{angle} \quad \text{(E1)}$$

where *N* is the number of adsorption events at positions $\vec{r}_i$ for 1 < i < *N* in a total area *A*. We calculated and analyzed pair auto-correlation functions as described by Veatch et al.[2], using their published Matlab package. The pair auto-correlation could be described by:

$$g_{fit}(r) = \left(4\pi\sigma_{loc}^2\rho_{app}\right)^{-1} \exp\left[\frac{-r^2}{4\sigma_{loc}^2}\right] + 1 \qquad \text{(E2)}$$

where σ_{loc} is the resolution for localizing an adsorption site (~50 nm) and ρ_{app} is the apparent density of sites, assuming randomly spatially distributed adsorption sites and that sites could be visited more than once, and that the sampling of sites is well-described by a simple Poisson distribution. We found that the simple Poisson distribution assumption was not valid, and instead a multi-component Poisson distribution fit was used in the Results section to accurately estimate the density of sites. However, the pair auto-correlation analysis was still useful in establishing the existence of the anomalous sites observed on super-resolution adsorption maps and provided a quantitative measure of localization precision.

The pair auto-correlation functions for all protein-surface combinations at dilute concentrations are shown in Figure E9. Figure E9 suggests that the adsorption event locations were correlated at lengths < 300 nm. Fit parameters, described by Equation E2, are shown in Table E5 for the pair auto-correlation functions for all protein-surface combinations. The resolution for localizing an adsorption site fit parameter ranged from 41 nm to 85 nm for different protein-surface combinations. The apparent density of sites nominally followed the inverse trends of heterogeneity where surfaces that had low apparent densities were found to be more heterogeneous (e.g. FS) and surfaces that had high apparent densities were found to be more homogeneous (e.g. PVAc-PVP/PES).

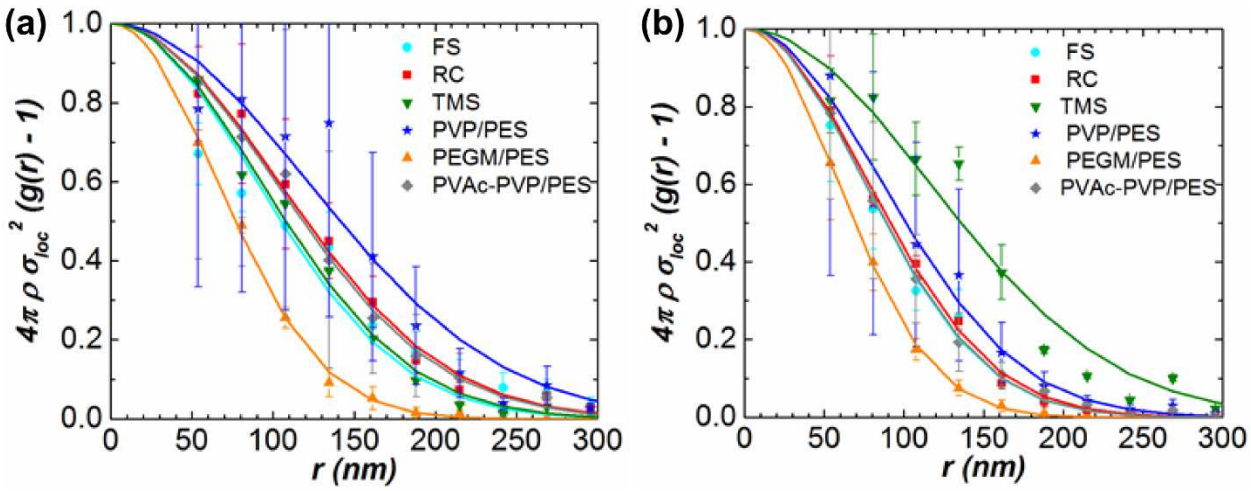

Figure E9: The normalized spatial pair auto-correlation functions for (a) IgG and (b) BSA at dilute protein concentrations, calculated for 1,000 adsorption events for each protein-surface combination. Error bars represent the standard error between the spatial pair auto-correlation functions of different imaged surface areas. The pair auto-correlation functions were normalized by their corresponding fit parameters, tabulated in Table E5.

Table E5: Apparent density (ρ_{app}) and localization resolution (σ_{loc}) fit parameters, described by Equation E2, to the pair-autocorrelation functions show in Figure E9.

		FS	RC	PEGM/PES	PVAc-PVP/ PES	PVP/PES	TMS
$[BSA]_{dilute}$	ρ_{app} x10^{-5}	0.59	1.3	3.1	7.4	4.2	0.60
	σ_{loc} (nm)	53	55	42	53	61	82
$[BSA]_{high}$	ρ_{app} x10^{-5}	1.3	1.2	1.9	17	3.0	0.75
	σ_{loc} (nm)	60	55	48	83	82	79
$[IgG]_{dilute}$	ρ_{app} x10^{-5}	0.28	1.3	2.7	16	1.6	1.2
	σ_{loc} (nm)	63	72	46	71	85	65
$[IgG]_{high}$	ρ_{app} x10^{-5}	0.54	18	15	3.5	20	4.5
	σ_{loc} (nm)	70	51	41	68	69	47

E.9 Power studies showing no photophysical effects

The intensity of laser light can strongly influence the frequency and time a fluorescent molecule may spend in a dark state either temporarily (photoblinking) or permanently (photobleaching).[3] If photobleaching or photoblinking were significant in our system, we expected residence times to be longer at lower power. However, when we varied the laser

power from 100% (6 μW/μm^2) to 50% power, BSA residence times on FS were not statistically different, as shown in Figure E10. For example, the mean characteristic residence times were similar: 1.5 ± 0.3 s and 1.3 ± 0.2 s for 100% and 50% laser power respectively. This indicates that photobleaching and photoblinking do not contribute significantly to the protein interfacial dynamics measured here. This was not surprising as each protein was labeled with multiple fluorescence dyes (see Materials and Methods).

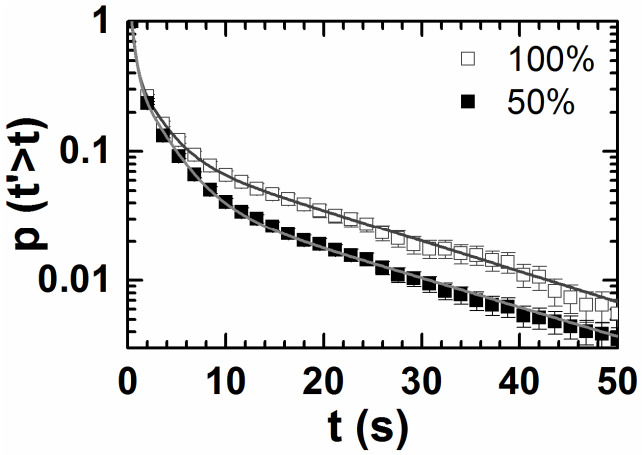

Figure E10: CRTDs for AlexaFluor 555 labeled BSA on FS at a concentration of 10^{-5} mg/mL in PBS for 100% (6 μW/μm^2) and 50% laser power, as indicated.

E.10 Adsorption and desorption fluorescence intensity histograms

We hypothesized that the oligomers observed with fluorescence intensity on the surface at very dilute protein concentrations were pre-formed in solution due to very low protein surface coverage and short residence times. Indeed, SEC revealed that protein oligomers were present in solution (see Figure E4). Therefore we expected a molecule's fluorescence intensity over its residence time to remain fairly constant and to be representative of its oligomerization state. In addition, at very dilute protein concentrations, the average labeled protein surface coverage was very low (i.e. on the order of 0.05 molecules per μm^2). Due to this low protein surface coverage and the fact that protein monomers remained on the surface for short time, the probability of proteins associating on the surface was vanishingly low.

The probability distributions of the fluorescence intensity at initial (immediately after adsorption) and final (immediately before desorption) frames of each molecular trajectory were very similar and indistinguishable from to the mean molecular fluorescence intensity, as shown in Figure E11. This suggests that protein associations at the surface were vanishingly rare and that the mean fluorescence intensity for a given molecular trajectory was a good indicator of a molecule's oligomerization state.

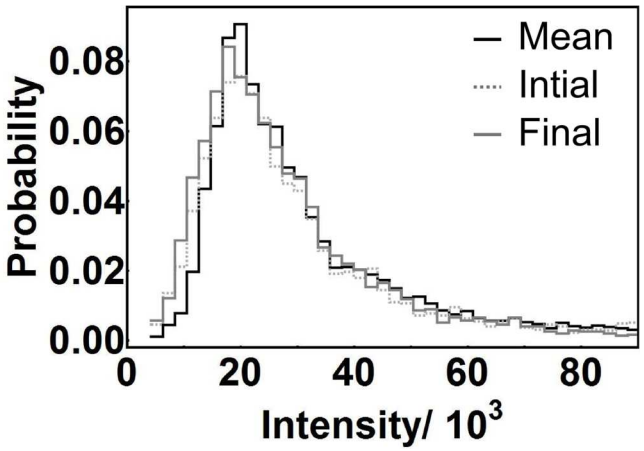

Figure E11: The probability distribution of the initial, mean, and final fluorescence intensities of IgG molecular trajectories on RC at an extremely dilute protein concentration.

E.11 Residence time and site adsorption distributions showing no dependence on tracking radius

We investigated the potential dependence of protein dynamics and adsorption site mapping on tracking radius, which is the maximum possible distance used to link together two center of intensities in subsequent frames to form a single molecular trajectory. Selecting an inappropriate tracking radius can have several important consequences. By selecting too small of a tracking radius, a molecular trajectory may erroneously be divided into separate trajectories due to localization error; this scenario would lead to an overestimation of adsorption events and shorter residence times. In contrast, by selecting too large of a tracking radius, two different molecules may erroneously be linked; this scenario would lead to longer residence times and

reduced adsorption site counts. The likelihood of linking two different molecules is greatly reduced by controlling the surface coverage of fluorescently labeled molecules such that the average distance between adsorbed molecules is much larger than the tracking radius. For our experimental system, in any given frame, molecules were separated by an average distance of 4–17 μm (e.g. one molecule per ~50 μm^2).

Figure E12 shows CRTDs and site adsorption event count probability distributions for IgG on RC where three different tracking radii were used: 2, 4, and 6 pixels, corresponding to 0.54, 1.08, and 1.62 μm. We found that both residence time and adsorption event count distributions were insensitive to the tracking radius. A mean characteristic residence time of 2.1 ± 0.6 s was consistent for all tracking radii considered. Similarly, *h* for 20,000 IgG trajectories on RC were statistically the same with a value of 6 ± 1 x 10^3 for all considered tracking radii. This suggests that by selecting a tracking radius of 4 pixels, we neither split nor erroneously linked molecular trajectories.

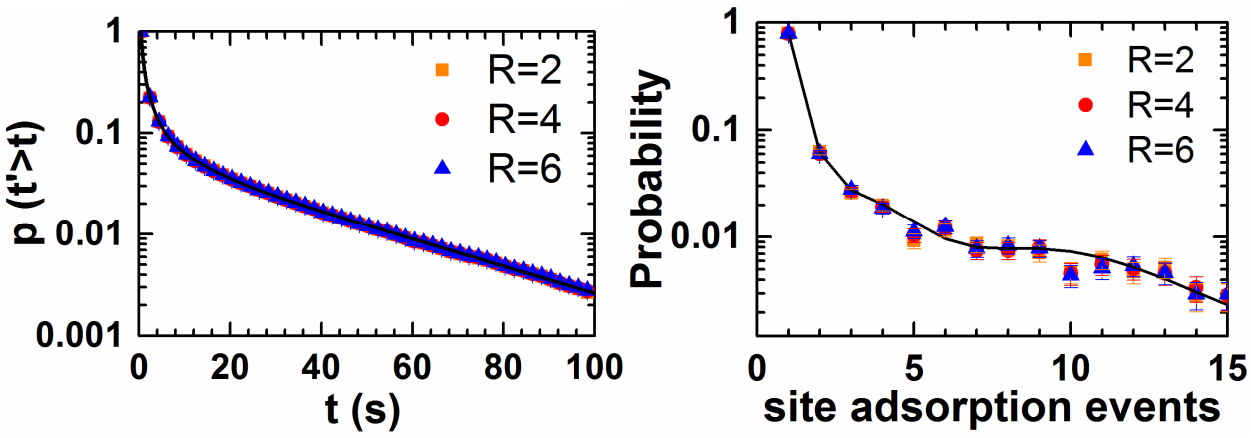

Figure E12: (a) CRTDs at extremely dilute protein concentration of IgG on RC and (b) probability distributions of site adsorption event counts for 20,000 IgG trajectories on RC where a tracking radius (R) of 2, 4, and 6 pixels was used to link diffraction limited spots from frame-to-frame.

E.12 Site adsorption distributions showing no dependence on acquisition time

As a control, several movies were taken with an acquisition time of either 100 ms or 200 ms, capturing single molecule BSA interfacial behavior at a concentration of 10^{-5} mg/mL on FS. As suggested in the Results, an acquisition time of 200 ms limits our ability to observe molecules that remain adsorbed for significantly shorter times than our acquisition time. Therefore, we might expect that site adsorption event count probability distribution and the heterogeneity index, *h*, would vary to some extent with acquisition time. Figure E13 shows that site adsorption event count probability distributions for 1,000 BSA adsorption events on FS were statistically similar for both 100 ms and 200 ms acquisition times. The calculated *h* values from these distributions were 21 ± 5 and 19 ± 6 x10^4 for acquisition times of 100 ms and 200 ms, respectively, and within standard error of each other. This suggests *h* was a fairly robust measurement of the surface site distribution, at least by a twofold decrease in acquisition time.

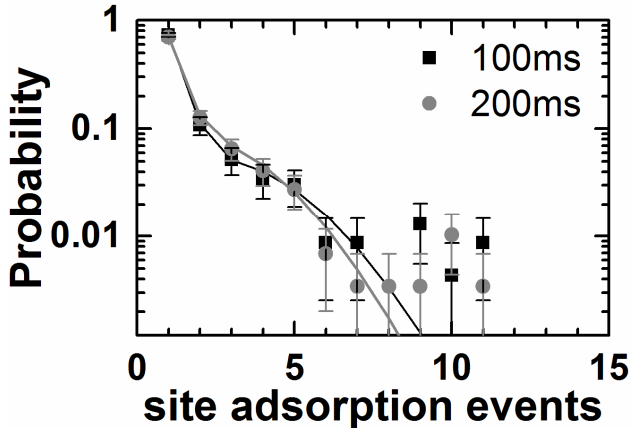

Figure E13: Probability distributions of site adsorption event counts for 1,000 BSA trajectories on FS for movies taken with an acquisition time of either 200 ms (acquisition time used for all experiments) or 100 ms, at a BSA concentration of 10^{-5} mg/mL.

E.13 References

(1) Kontturi, E.; Thüne, P. C.; Niemantsverdriet, J. W. Cellulose Model Surfaces - Simplified Preparation by Spin Coating and Characterization by X-Ray Photoelectron Spectroscopy, Infrared Spectroscopy, and Atomic Force Microscopy. *Langmuir* **2003**, *19*, 5735–5741.

(2) Veatch, S. L.; Machta, B. B.; Shelby, S. A.; Chiang, E. N.; Holowka, D. A.; Baird, B. A. Correlation Functions Quantify Super-Resolution Images and Estimate Apparent Clustering due to Over-Counting. *PLoS One* **2012**, *7*, e31457.

(3) Eggeling, C.; Widengren, J.; Rigler, R.; Seidel, C. A. M. Photobleaching of Fluorescent Dyes under Conditions Used for Single-Molecule Detection: Evidence of Two-Step Photolysis. *Anal. Chem.* **1998**, *70*, 2651–2659.

Appendix F: Chapter 6 Supporting Information

F.1 d_{app} distributions change with concentration

Figure F1 shows the d_{app} distributions of all molecule states on TMS at Fg_A concentrations of 10^{-5}, 10^{-4}, and $2x10^{-4}$ mg/mL. At all [Fg_A], there were two distinct peaks – above and below d_{app} ~1. The relative area, height, and peak positions changed with Fg_A concentration, suggesting some physical change in adsorbed and associating Fg molecules at the interface. In particular, as [Fg_A] increased, the low-d_{app} peak (High-RET state) increased while the high-d_{app} peak (Low-RET state) decreased, consistent with increasing protein-protein associations at higher [Fg_A] on TMS.

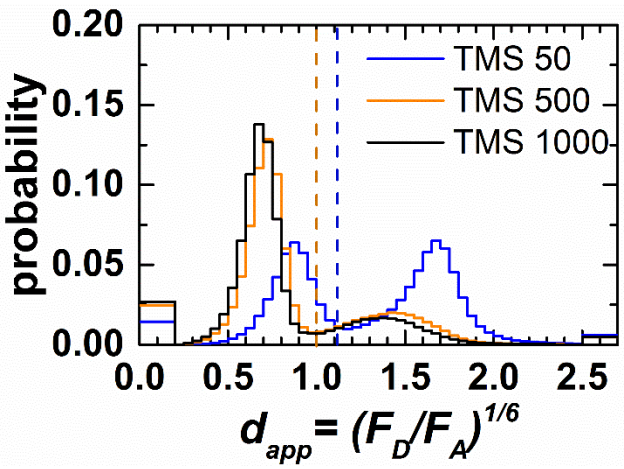

Figure F1: Probability distribution of apparent relative distance, d_{app}, for Fg on TMS at Fg_A concentrations of 10^{-5}, 10^{-4}, and $2x10^{-4}$ mg/mL. d_{app} thresholds between High-RET and Low-RET states are indicated for [Fg_A] of 10^{-5} mg/mL (dark blue) and 10^{-4} mg/mL (orange). A molecule's association state for a given frame was identified as High-RET if d_{app} < RET threshold (associated) or as Low-RET if $d_{app} \geq$ RET threshold (unassociated). The step functions at either end of the distribution represent when either F_D or F_A was less than 0 and d_{app} could not be calculated accurately. The area under each "box" is proportional to the number of association states where either F_D ($0.0 < d_{app} < 0.02$) or F_A ($2.5 < d_{app} < 2.7$) was insignificant such that the total area under the "boxes" and curve integrates to unity.

F.2 Protein surface coverage changes with bulk protein concentration

Protein surface coverage of Fg_D (including Fg_D undergoing both High-RET and Low-RET) could be quantified by averaging the number of molecules present in each movie frame over the course of a movie. The Fg_A surface coverage could then be estimated by multiplying the Fg_D surface coverage by the respective Fg_A:Fg_D ratio, shown in Table S1. Due to our temporal resolution (i.e. acquisition time of 100 ms), this surface coverage may underestimate the total surface coverage. However the values reported below provide a good estimate of the surface coverage of molecules that remain on the surface for at least 100 ms. At a Fg_A concentration of 10^{-5} mg/mL, the apparent surface coverage was 5 times higher on TMS than on OEG. On both OEG and TMS the surface coverage increased with increasing [Fg_A].

Table F1: Fg surface coverage (Γ, μg/m^2) at each [Fg_A] (mg/mL) on TMS and OEG. The values in parentheses represent the standard deviation between movie experiments and correspond to the final digit.

[Fg_A]	Fg_A:Fg_D	Γ_{TMS}	Γ_{OEG}
10^{-5}	500	0. 15(3)	0.032(6)
10^{-4}	5000	2.4(2)	1.9(3)
$2x10^{-4}$	10,000	6(2)	6(2)

F.3 Associating molecules remain on the surface longer than unassociated molecules

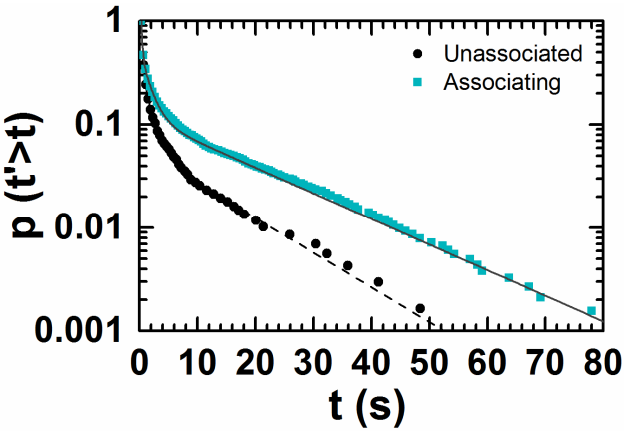

Figure F2: CRTDs of Fg_D molecules that either associated/dissociated (i.e. associating) or remained unassociated (i.e. unassociated) while at the interface, on OEG at [Fg_A] = 10^{-5} mg/mL.

As shown previously for BSA on PEG,[1] Fg_D proteins that dynamically associated (i.e. associating molecules) remained on the surface for longer than Fg_D proteins that remained unassociated for their entire surface trajectory. Figure F2 shows that associating Fg_D proteins were more likely to reside on the surface for long times than unassociated Fg_D proteins on OEG at a Fg_A concentration of 10^{-5} mg/mL. This trend was consistent for all [Fg_A] on both TMS and OEG.

F.4 Residence time and contact time cumulative distributions change with increasing Fg concentration

The cumulative distributions of associating molecule surface residence times and protein association contact times are shown in Figures F3 and F4, respectively. These distributions were fit to a weighted sum of first-order processes, as described previously.[1,2] The mean characteristic surface residence times and characteristic contact times, shown in Figure 6.2 and 6.5 respectively, were calculated from these fit parameters. The mean characteristic surface residence times of associating molecules increased with an increasing Fg_A concentration on TMS but not on OEG, such that associating molecules remained longer on TMS than on OEG at a bulk protein concentration of $2x10^{-4}$ mg/mL. A similar trend, although less pronounced, was observed for all molecular trajectories (both associating and unassociated molecules) as shown in Figure F5.

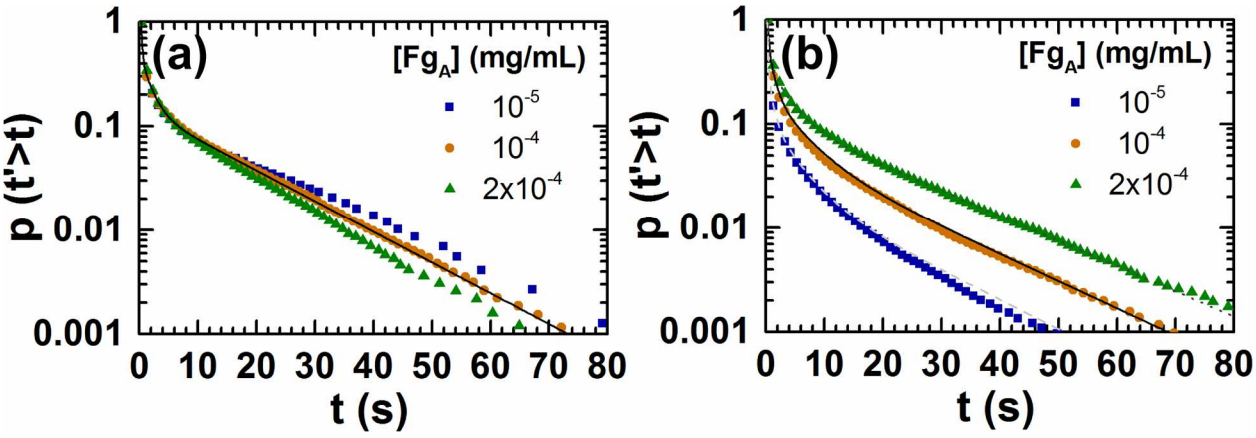

Figure F3: CRTDs of associating molecules (i.e. undergo an association or dissociation while at the interface) for each [Fg_A] considered on (a) OEG and (b) TMS.

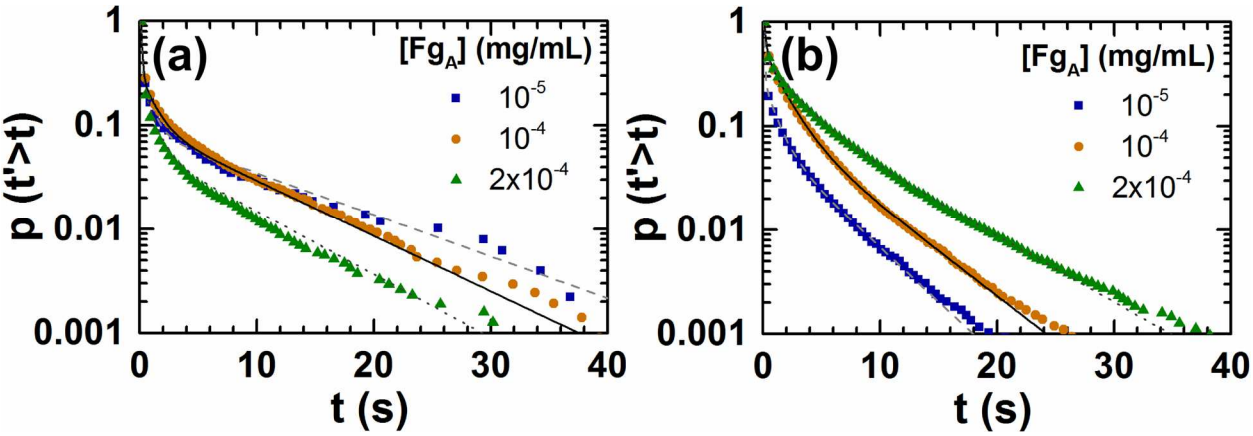

Figure F4: Cumulative contact time distributions for dynamic Fg-Fg associations at each [Fg$_A$] on (a) OEG and (b) TMS.

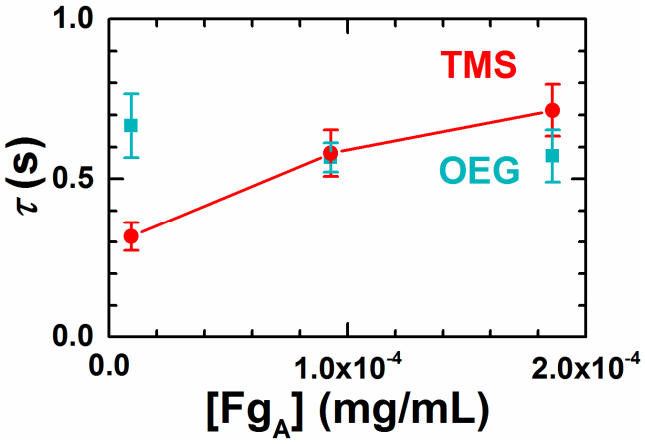

Figure F5: Mean characteristic surface residence times of all Fg$_D$ molecules (e.g. both unassociated and associating molecules) on OEG and TMS for all [Fg$_A$].

F.5 References

(1) Langdon, B. B.; Kastantin, M.; Walder, R.; Schwartz, D. K. Interfacial Protein-Protein Associations. *Biomacromolecules* **2014**, *15*, 66–74.

(2) Kastantin, M.; Langdon, B. B.; Chang, E. L.; Schwartz, D. K. Single-Molecule Resolution of Interfacial Fibrinogen Behavior: Effects of Oligomer Populations and Surface Chemistry. *J. Am. Chem. Soc.* **2011**, *133*, 4975–4983.